JPRS L/10155

2 December 1981

USSR Report

PHYSICS AND MATHEMATICS

(FOUO 10/81)

FBIS FOREIGN BROADCAST INFORMATION SERVICE

NOTE

JPRS publications contain information primarily from foreign newspapers, periodicals and books, but also from news agency transmissions and broadcasts. Materials from foreign-language sources are translated; those from English-language sources are transcribed or reprinted, with the original phrasing and other characteristics retained.

Headlines, editorial reports, and material enclosed in brackets [] are supplied by JPRS. Processing indicators such as [Text] or [Excerpt] in the first line of each item, or following the last line of a brief, indicate how the original information was processed. Where no processing indicator is given, the information was summarized or extracted.

Unfamiliar names rendered phonetically or transliterated are enclosed in parentheses. Words or names preceded by a question mark and enclosed in parentheses were not clear in the original but have been supplied as appropriate in context. Other unattributed parenthetical notes within the body of an item originate with the source. Times within items are as given by source.

The contents of this publication in no way represent the policies, views or attitudes of the U.S. Government.

APPROVED FOR RELEASE: 2007/02/09: CIA-RDP82-00850R000400080009-0

JPRS L/10155

2 December 1981

USSR REPORT

PHYSICS AND MATHEMATICS

(FOUO 10/81)

CONTENTS

LASERS AND MASERS

UDC 621.373.826.038.823

NUMERICAL STUDY OF CO_2 PROCESS LASER WITH CLOSED GASDYNAMIC CYCLE

Moscow KVANTOVAYA ELEKTRONIKA in Russian Vol 8, No 8(110), Aug 81 (manuscript received 8 Sep 80, after revision 23 Feb 81) pp 1656-1662

[Article by V. V. Breyev, A. V. Gubarev, A. V. Kazhidub, A. T. Kukharenko, F. V. Lebedev and V. P. Panchenko, Institute of Atomic Energy imeni I. V. Kurchatov, Moscow]

[Text] The article briefly describes a mathematical model developed by the authors for complex calculation of a CO_2 electric discharge laser including discharge chamber, optical resonator amplifier, radiation focusing system, nozzle, diffuser, coolers, compressor and connecting tubing. A numerical study of a 10 kW CO_2 process laser is done on the basis of the developed set of programs.

The outlook that has been noted in recent years for using CO_2 electric discharge lasers in technology [Ref. 1-5] has brought to the forefront problems of design calculations and optimization of the parameters of such facilities. These problems can now be resolved, as the physical processes occurring in CO_2 electric discharge lasers have been fairly well studied. Methods are also known for engineering calculation of all components of the gasdynamic circuit of the facility: compressor, heat exchangers, tubing and so on.

Ref. 4 gives a detailed description of a mathematical model of a CO_2 electric discharge laser with closed gasdynamic circuit. Our paper discusses the results of an engineering study using this mathematical model of a CO_2 process laser with power of about 10 kW [Ref. 3].

The mathematical model of the electric discharge CO_2 laser includes algorithms for the following calculations:

flow of active medium in external electric field and in radiation field;

multiple-pass unstable amplifier cavity with arbitrary mirror arrangement;

distortions of radiation wavefront by inhomogeneities of the medium;

propagation and focusing of output emission;

pressure losses on different sections of the gasdynamic circuit and its hydraulic and thermal closure.

To describe the flow of active medium in the gas discharge gap and on the section of stimulated emission of light, we have used a quasi-one-dimensional approximation for independent streamtubes, which enables us to get a nonuniform distribution of the gain and density of the medium in accordance with the distribution of the radiation field. The flow in a stream filament is described by the known system of differential equations [Ref. 6]

$$dF/dx=-H, \tag{1}$$

where

$$F=|\rho u;\ \rho u^2+p;\ \rho u\,(\varepsilon+p/\rho+u^2/2);\ \rho uE_1;\ \rho uE_2;\ \rho uE_N|;$$
$$H=|\mu;\ \mu u;\ \mu\,(\varepsilon+p/\rho+u^2/2)+Q_v;\ \mu E_1+p_1;\ \mu E_2+p_2;\ \mu E_N+p_N|.$$

Here $\mu=\rho udA/Adx$, A is the area of a stream filament proportional to the flow section, E_1, E_2, E_N are the energies of the lower and upper vibrational modes of the CO_2 molecule, and of the vibrational mode of nitrogen respectively. The remaining notation is obvious, and the expressions for volumetric sources are given in Ref. 6.

The geometric-optics approximation [Ref. 7] was used to determine the radiation field in a multipass unstable cavity amplifier and the energy characteristics of the laser facility. In doing this calculation it is necessary to assign the radii of curvature of the opaque and output mirrors of the cavity, the dimensions of the output mirror of the cavity, and also the coordinates of the centers of all mirrors and of the output aperture. These data are sufficient for defining the path of rays in the optical system filled with homogeneous medium (with constant value of the index of refraction). The change of intensity of the light wave in this case is

$$R^{-2}d\,(R^2I)/dR=k_yI, \tag{2}$$

where R is the distance from the focus of the spherical wave, I is the intensity of the wave, k_y is the gain of the medium. The formulation of the boundary value problem for equation (2) and algorithm for its solution are described in Ref. 6.

Theoretical studies and estimates have shown that the inhomogeneity observed in CO_2 lasers has a weak distorting effect on the trajectory of rays. This enables us to reduce the problem of determining the wavefront at the output of the optical system to calculation of the phase advance due to the difference in optical paths in homogeneous and inhomogeneous media. The change in the index of refraction determined by the density of the medium is found from the solution of system of equations (1), (2).

In considering comparatively short-focus and low-power systems that are conventionally used in process lasers, nonlinear effects of the light propagation in atmosphere can generally be disregarded. Therefore the distribution of light intensity in the focal plane of the lens is determined by the Kirchhoff integral written for the complex electric field amplitude E(x,y,z) in the paraxial approximation:

$$E(x, y, f) = \frac{k \exp(ikf)}{2\pi i f} \int_{-a}^{a} \int_{-b}^{b} E(\xi, \eta, 0) \exp\left[ik \frac{(x-\xi)^2 + (y-\eta)^2}{2f}\right] d\xi\, d\eta, \quad (3)$$

where $i = \sqrt{-1}$, a and b are the dimensions of the rectangular aperture of the outgoing radiation.

The initial function

$$E(\xi, \eta, 0) = \sqrt{I} \exp[ik\psi + ik(\xi^2+\eta^2)/2f], \quad (4)$$

where $I(\xi,\eta)$, $\psi(\xi,\eta)$ are intensity and phase (eikonal) of the radiation emanating from the optical system. Considering function $E(\xi,\eta,0)$ periodic with respect to ξ and η with periods 2a and 2b respectively, we can use the algorithm of fast Fourier transformation [Ref. 6] to find the intensity distribution in the focal plane.

To check out the mathematical model described in Ref. 6, we calculated a CO_2 laser with closed gasdynamic cycle with test results described in Ref. 2-4. The gasdynamic circuit of this facility includes two parallel channels and a common discharge chamber combined with the optical cavity. In the calculation, consideration was taken of the experimentally determined coefficients of pressure losses in the coolers, and the head characteristics of the compressor. The optical diagram of the laser is shown in Fig. 1a. The four-pass unstable cavity consisted of opaque mirror 1 with radius of curvature $R_1 = 26$ m, three flat rotating mirrors 2-4, feedback mirror 5 with $R_5 = 13$ m, and output flat mirror 6 with rectangular hole of 4.5 x 2.5 cm. The static pressure of the working mixture $N_2:CO_2:H_2O:O_2 = 0.874:0.05:0.006:0.07$ at the inlet to the nozzle was 3.3 kPa, and the temperature at the outlet

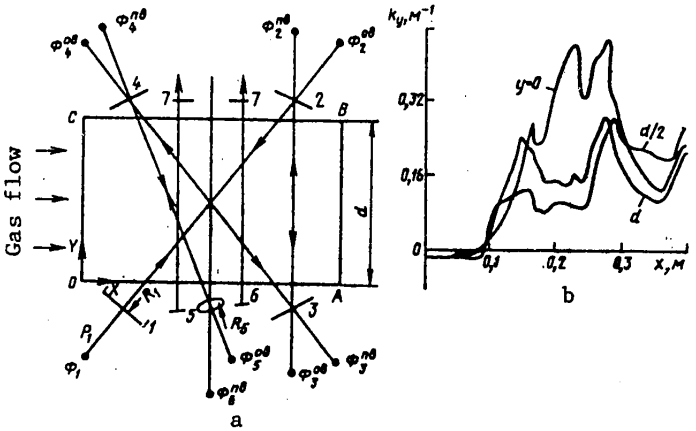

Fig. 1. Optical diagram of laser (a) and the gain behavior lengthwise of the discharge chamber in the midsection and on the ends

from the coolers was 290 K. An electric discharge with fairly uniform energy input over the volume of the discharge chamber was realized on the section from x = 0.8 to

x = 0.38 m. Vibrational efficiency of the discharge based on experimental data [Ref. 3, 8] was taken as equal to 0.85.

For purposes of illustration, Fig. 1b shows the distribution of the calculated gain of the medium along the flow at three levels with respect to the Y axis. We see considerable nonuniformity of the field of k_y. According to calculations at an energy input $N_e = 62.5$ kW (this corresponds to the maximum energy input in the experiment), the flow is accelerated in the discharge chamber by about 40%, and its temperature rises by about 35%. At the output from the zone of stimulated emission, about 28% of N_e remains in vibrational degrees of freedom of CO_2 and N_2 molecules. The maximum nonuniformity of pressure and velocity of the flow in the transverse direction reaches 3% and 2% respectively. This result confirms the admissibility of the filament flow model. Notice should be taken of good agreement of the calculated values of flow velocity and pressure at the output from the lasing zone with the experimental data.

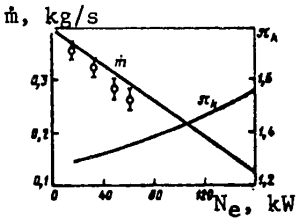

Fig. Gas flow ṁ in the discharge chamber as a function of supplied electric power (o--experiment) and required degree of compression π_K in the compressor as a function of supplied electric power at constant gas flow

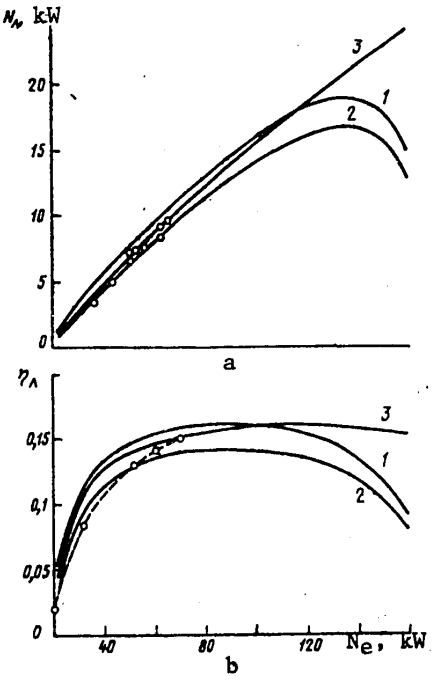

Fig. 3. Emission power (a) and electro-optical efficiency (b) as functions of supplied electric power: gas flow variable (1, 2) and constant (3); coefficient of losses in the mirrors q = 2 (1,3) and 4% (2); o--experiment

Fig. 2 and 3 show the calculated curves for output power N_Λ, electric efficiency of the laser η_Λ, and gas flow through the discharge chamber as functions of the power N_e invested in the discharge. The results of experiment as shown on the same figures agree well with the calculated curves.

The distribution of gas density found in the calculation in the cavity zone enables us to calculate the distribution of the phase of the radiation at the output of the facility (cross section 7-7 on Fig. 1a), and to find the structure of the radiation intensity distribution in the focal spot.

For the electro-optical laser scheme shown in Fig. 1a, at a power of 62.5 kW invested in the discharge the phase difference of the outgoing beam does not exceed 3π. The calculated intensity field in the focal spot of a lens with focal length of f = 50 m is shown in Fig. 4. The broken line shows the intensity distribution for the case of a plane wavefront (without consideration of distortions). In the center of the principal maximum the intensity reaches about 16 kW/cm^2; however, this maximum contains only about 30% of the emission power of the facility. Angular deviation of the light beam from the optical axis (about $2 \cdot 10^{-4}$) is approximately equal to the angular divergence of the radiation with respect to half power level. Under real conditions the radiation divergence was about 10^{-3} [Ref. 2], which was caused by considerable phase distortions in the output windows.

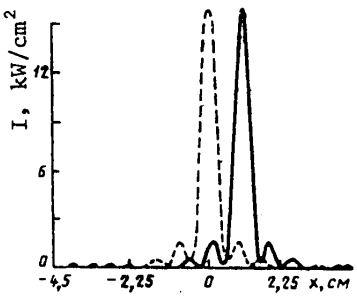

Fig. 4. Radiation intensity distribution in focal cross section for plane (broken line) and distorted (continuous line) wavefronts

Good coincidence of all calculated relations with experiment over a fairly wide range of variation in working conditions of the laser shows adequate description by the mathematical model [Ref. 6] of processes in the CO_2 laser, which provides the basis for applying this model to numerical investigation and optimization of the designs of such facilities.

Let us mention the principal results of the theoretical analysis of the CO_2 process laser [Ref. 3] with optical diagram shown in Fig. 1.

The main pressure losses in the circuit of the facility are due to the hydraulic drag of the coolers (about 50%), the drag of sections with high flow velocity (nozzle, diffuser) and of the discharge chamber (about 20 and 12% respectively). The drag of the discharge chamber increases with increasing energy input.

As the energy input increases on the discharge gap, the flow of the working mixture in the circuit decreases, and at N_e = 120 kW it falls to about one-half.

The change in the coefficient of losses in the mirrors from 2 to 4% (curves 1, 2 on Fig. 3) leads to a reduction in emission power by about 10%.

Stimulated emission of light arises only with a power input of more than 20 kW to the discharge.

As the power invested in the discharge increases, the electro-optical efficiency rises rapidly, and at $N_e \geq 60$ kW it reaches ~15%.

As the power invested in the discharge increases, the radiation power at first rises monotonically, reaching a maximum of 15-19 kW (see curves 1, 2 on Fig. 3) at $N_e \approx 140$ kW, and then drops sharply. The reduction of radiation power at N_e greater than 140 kW is due to the reduction in gas flow (see Fig. 2) and its strong overheating. At constant gas flow through the discharge gap the maximum radiation power reaches about 25 kW at input power of about 200 kW and is limited by gasdynamic suppression.

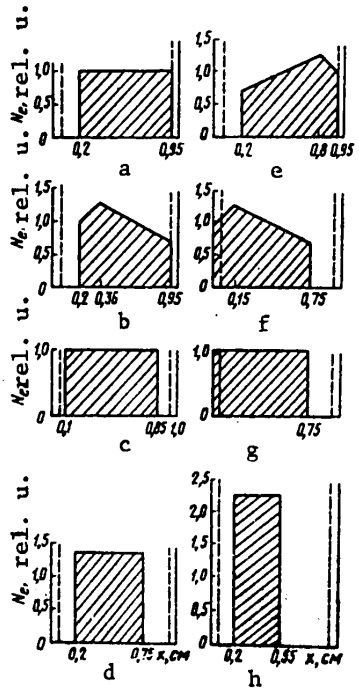

Fig. 5. Influence that the location of the energy input zone has on laser output power (region of energy input is shaded, the broken lines show the extreme limits of the light beams): Output power $N_\Lambda = 10$ (a), 10.6 (b), 11.4 (c), 12.3 (d), 9.6 (e), 13.3 (f, g), and 13.6 kW (h)

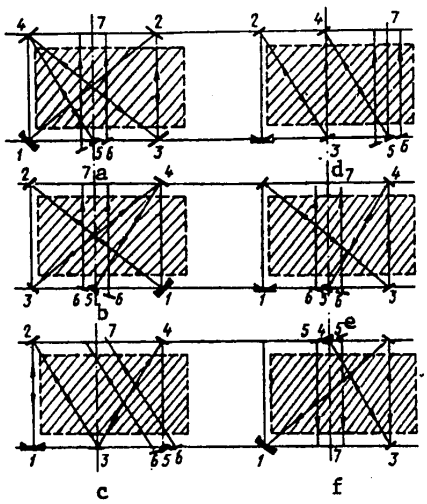

Fig. 6. Influence that location of optical passages has on the output power of the laser (region of energy input is shaded): $N_\Lambda = 10$ (a), 8.5 (b), 10.8 (c), 8.9 (d), 10.5 (e) and 10.7 kW (f)

At constant energy input to the discharge gap ($N_e = 62.5$ kW), a reduction in molar concentration of CO_2 from 5 to 3% is accompanied by a drop in emission power by ~20%. Upon an increase in CO_2 content from 5 to 10% the output emission power at first increases by ~8%, and then monotonically decreases.

Theoretical power of the facility reaches maximum at water vapor concentration of 0.6-1%.

A change in oxygen concentration from ~7 to ~20% has almost no effect on the output radiation power and electro-optical efficiency of the laser. This means that air that has been dried to the necessary moisture concentrations with addition of CO_2 can be recommended for use as a working mixture. However, the final solution of this problem must take consideration of plasma-chemical processes.

The above-described results of the theoretical study have been directed at investigation of a specific CO_2 process laser [Ref. 3]. Obviously most of these results can be obtained experimentally as well. The advantages of mathematical modeling and numerical study show up most completely in solving problmes of design selection of the parameters of the facility as a whole, and in particular in optimization of the electro-optical system of the given facility. Experimental solution of such problems requires large material investments and time.

To illustrate this, let us give the results of calculation of different designs of the electro-optical system for the facility investigated above. It was assumed that the outside overall dimensions of the electro-optical system, its flow section and the joining components are retained unaltered, and coincide with the regular system (see Fig. 1), as does the total energy input to the positive discharge column $N_e = 62.5$ kW. Let us note that these studies together with the development of the methodology took a total of about six man-months, while the machine time of a BESM-6 computer was approximately 10 hours.

Fig. 5 shows some investigated variants of the distribution of energy input in the electro-optical system of the facility. The design of the optical system remained unchanged (see Fig. 1). The situation shown on Fig. 5e was realized under experimental conditions. In this case the output power of the radiation was 9.6 kW (electro-optical efficiency $\eta_A = 15\%$). Change in the form of distribution of the energy input has a weak influence on the output power (see cases a, b, e on Fig. 5). More significant is the upstream shift of the zone of energy input relative to the cavity (cases c, f, g on Fig. 5). The calculations show that an upstream displacement of the energy input zone by 8 cm should lead to an increase in output power by about 30%. A similar result is realized when the length of the discharge zone is shortened due to an increase in specific energy input and when its "center of gravity" is shifted upstream (cases d and h on Fig. 5).

The results of investigation of different designs of the optical system with unchanged distribution of the energy input in the positive column (see Fig. 5a) and cavity magnification are shown on Fig. 6. The resultant data show that the geometry of the cavity passages used in the experiment is near optimum. A tendency can be seen toward an increase of output power as the center of gravity of the radiation field is shifted downstream. Let us also note that when the cavity is located in the lower zone of the energy input, the output power should remain practically unchanged even when the number of cavity passages is limited to three (see Fig. 6f).

The mathematical model of the process laser that was used in this paper does not reflect such important points as the limitation on maximum energy inputs of a stable discharge and the influence of plasma-chemical processes on vibrational kinetics. Nonetheless, the modeling method that has been developed is very useful and can be applied on the stage of design and development of process laser systems.

REFERENCES

1. Hoag, E., Pease, H., Staal, J., Zar, J., APPL. OPTICS, Vol 13, 1974, p 1959.

2. Abil'siitov, G., Artamonov, A. V., Velikhov, Ye. P., Yegorov, Yu. A., Kazhidub, A. V., Lebedev, F. V., Sidorenko, Ye. I., Sumerin, V. V., KVANTOVAYA ELEKTRONIKA, Vol 7, 1980, p 2467.

3. Abil'siitov, G., Antonova, L. I., Artamonov, A. V., Golubev, V. S., Drobyazko, S. V., Yegorov, Yu. A., Katsuro, N. I., Kazhidub, A. V., Lebedev, F. V., Senatorov, Yu. M., Sidorenko, Ye. M., Sumerin, V. V., Turundayevskiy, V. B., Frolov, V. M., KVANTOVAYA ELEKTRONIKA, Vol 6, 1979, p 204.

4. Artamonov, A. V., Yegorov, Yu. A., Kazhidub, A. V., Katsuro, N. I., Lebedev, F. V., Sidorenko, Ye. M., Sumerin, V. V., Frolov, V. M., KVANTOVAYA ELEKTRONIKA, Vol 5, 1978, p 920.

5. Letokhov, V. S., Ustinov, N. D., "Moshchnyye lazery i ikh primeneniye" [Powerful Lasers and Their Applications], Moscow, Sovetskoye radio, 1980.

6. Breyev, V. V., Gubarev, A. V., Kazhidub, A. V., Kukharenko, A. T., Mamzer, A. F., Panchenko, V. P., Rikenglaz, M. M., Preprint, IAE, Moscow 1980, No 3319.

7. Anan'yev, Yu. A., "Opticheskiye rezonatory i problema raskhodimosti lazernogo izlucheniya" [Optical Cavities and the Problem of Divergence of Laser Radiation], Moscow, Nauka, 1979.

8. Artamonov, A. A., Breyev, V. V., Kukharenko, A. T., Samokhin, A. A., "Trudy vtoroy Vsesoyuznoy konferentsii po fizicheskim protsessam v gazovykh OKG" [Proceedings of Second All-Union Conference on Physical Processes in Gas Lasers], Uzhgorod, 1978.

6610
CSO: 1862/14

UDC 621.373.826.038.023

COPPER VAPOR LASER WITH TRANSVERSE DISCHARGE

Moscow KVANTOVAYA ELEKTRONIKA in Russian Vol 8, No 8(110), Aug 81 (manuscript received 11 Nov 80) pp 1686-1696

[Article by A. V. Sokolov and A. V. Sviridov]

[Text] The paper gives the results of a study of a copper vapor laser with radially transverse discharge at pressures up to 1.5 atmospheres. It is shown that when the parasitic inductance of the laser discharge circuit has been sufficiently reduced, high efficiency can be realized. A physical efficiency of 5.3% is attained in the copper vapor laser. It is also shown that the use of vaporizers enables appreciable improvement of the output parameters of a laser with radially transverse discharge.

It is established that circulation of the active Cu-Ne mixture overcomes the restriction imposed on the pumping power by heat release in the active medium of the Cu-laser. Lasing of copper vapor is achieved in a pulsed discharge with hollow cathode. Lasing power was 1.2 W, physical efficiency reached 5%, and the specific energy output was 15 $\mu J/cm^3$.

1. Introduction

The possibility of realizing efficient lasing and attaining economic working conditions in lasers with transverse discharge on vapors of copper and other metals depends to a great extent on the resolution of two important questions.

The first is the question of transferring pumping energy to the active zone of a laser with minimum losses. Studies on optimizing copper vapor lasers were begun in Ref. 1, 2. This paper examines the influence that parasitic inductance in the chain of transfer of pumping energy to the active zone has on laser operation. Results achieved with lasers with transverse and longitudinal discharges are compared with respect to the attained efficiency. The considerable difference between lasers with transverse and longitudinal discharges is due to the great difference in discharge currents. Operation of a laser with transverse discharge requires pumping currents more than an order of magnitude greater than longitudinal discharge currents. Because of this, the influence of the supply inductance is quite appreciable in a laser with transverse discharge.

The second question is investigation of different methods of producing the working mixture based on vaporizing metal. We have examined the following methods: heating the walls of the active zone of the laser by a special heater [Ref. 3] or by the heat released in the electric discharge [Ref. 4]; producing metal vapor by using vaporizers; producing the working mixture by forming a flow of metal vapor and inert gas without entrainment and losses of metal vapor (in contrast to the method used in Ref. 5).

2. Experimental Facility

The research was done on an experimental facility based on a coaxial laser with cylindrical metal electrodes between which a transverse discharge was produced. The discharge zone 40 cm long was bounded by the walls of the outer electrode (anode) 6 cm in diameter and the cathode 2 cm in diameter. The working mixture of the laser consisted of neon and copper vapor [Ref. 6].

The laser was pumped by an oscillator with cable transformer described in Ref. 1. Pulses of 200 ns duration at the base with amplitude of 0.8-2 kV were transferred to the laser cell through cables uniformly distributed between the lead-ins. The output impedance of the pumping oscillator, depending on the number of cables connected to the cell, was 0.15 or 0.4 Ω, and the transformation ratio $n_{tr} = 10$. The excitation pulse recurrence rate was 2-6 kHz. Fig. 1 shows a diagram of connection of the discharge gap to the pumping oscillator and to the sensors for registration of pumping pulses.

The registration sensors for voltage and current pulses were voltage dividers based on low-inductance resistors and a Rogowski loop. Provisions were made for monitoring voltage pulses directly across the electrodes of the discharge gap. To do this, the inner electrode was connected to one of the voltage dividers via a separate high-voltage lead-in (see Fig. 1). This eliminated the voltage drop across the parasitic inductance of the high-voltage lead-in transferring the pumping pulses to the discharge gap, and enabled registration of the true shape and amplitude of the voltage pulse across the laser electrodes. From the sensors, the pulses were sent to a two-beam oscilloscope with nanosecond time resolution, enabling phasing of the current and voltage pulses, as well as the laser light pulse obtained by a coaxial photocell. The mean output luminosity was measured by a calorimeter. The electrode temperature in the discharge zone was measured by an optical micropyrometer and a thermocouple with signal operating a chart recorder.

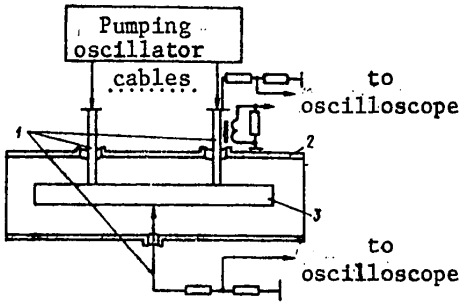

Fig. 1. Diagram of connection of the discharge gap of the coaxial laser to the pumping oscillator and to the pumping pulse registration sensors: 1--high-voltage lead-ins; 2--anode; 3--cathode

3. Influence of Supply Inductance on Laser Efficiency

Because of the large currents that are realized in the discharge of a transverse-discharge laser, it is impossible to disregard the supply inductance, which has

impedance with a large reactance component. The supply inductance is an energy reservoir that has a considerable effect on the fraction of energy released in the plasma resistance in different time intervals of pumping pulse action. Thus the efficiency of a laser on vapors of copper and other metals is intimately related to the processes that take place in the electrical part of the laser, an equivalent circuit being shown in Fig. 2.

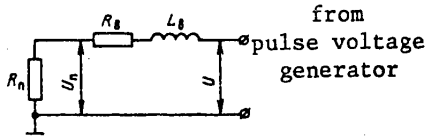

Fig. 2. Equivalent electric circuit of laser chamber: U--voltage across lead-ins of laser chamber; $L_в$--parasitic inductance; $R_в$--lead-in resistance; $R_п$--plasma resistance; $U_п$--voltage across discharge gap of laser chamber

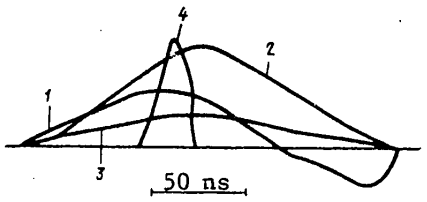

Fig. 3. Typical oscillograms of pulses of voltage across the lead-ins of the laser chamber (1), discharge current (2), voltage across the electrodes (3) and lasing (4)

As has already been stated, the measurement part of the experimental facility enabled recording of oscillograms of the currents and voltages on different parts of this circuit. In this way oscillograms were obtained of the pulses of currents and voltages on the chamber, as well as of the voltages across the plasma resistance. A typical oscillogram of the pumping pulses is shown in Fig. 3. This same figure shows the lasing pulse phased with the current and voltage. Graphic integration was used to determine the energy supplied to the chamber and released across the plasma resistance over any time interval of pulse action.

The equivalent electric circuit of the laser is described by the equation

$$L\frac{di}{dt}+iR_в+iR_п=U. \qquad (1)$$

Multiplication of this equation by idt and integration transforms it to

$$\int Lidi+\int i^2R_в dt+\int i^2R_п dt=\int iUdt. \qquad (2)$$

The resultant equation characterizes the energy balance in the electric circuit of the laser, where $\int iUdt=W_н$ is the energy supplied to the chamber input without consideration of reflections; $\int i^2R_в dt=W_в$ is the energy released across the lead-in resistance; $\int i^2R_п dt=W_п$ is the energy released across the plasma resistance; $\int Lidi=W_L$ is the energy that is stored and returned by the inductance. During the entire pumping pulse, $\int Lidi=0$ in view of the reactive nature of the inductance that stores energy E in the first half of the pulse ($E=Li^2_{max}/2$ at maximum current i_{max}) and returns it to the discharge circuit in the second half of the pulse when $di/dt<0$.

The advisability of accounting for the resistance of the lead-in when examining the electric circuit of the transverse-discharge laser was confirmed. The results of graphic integration of oscillograms of the pulses of current and of voltage across the inlet to the cell and across the plasma resistance showed that the energy released across the resistance of the high-voltage lead-in reaches 30% of the energy supplied to the cell input. The results of calculations of energy losses across

the lead-in resistance as measured by an R-333 DC resistance bridge with shorted electrodes with consideration of the temperature behavior of this resistance showed good agreement with experimental data. The lead-in resistance of the investigated laser was comparable with the output impedance of the pumping oscillator, amounting to ~0.1 Ω with respect to order of magnitude.

Despite the fact that the parasitic inductance in the discharge circuit does not consume energy during a pulse, it has a detrimental effect on lasing. With sufficiently powerful pumping, the lasing pulse is observed in the first half of the excitation pulse. Specifically, during the first half of the pumping current pulse (when $di/dt > 0$), the lead-in inductance takes from the discharge circuit an energy of $Li_{max}^2/2$, which it returns in the second half of the pulse when lasing has terminated, and therefore this energy is expended only on harmful heating of the active mixture. In the given experiments at the maximum attainable currents the inductance took up to 50% of the energy of the first half of the pulse.

Efficiency can be increased by shortening the duration of the pumping pulse before the instant of lasing termination. The difficulty in this method is in the problem of making a pumping oscillator that shapes a pulse with duration of the order of 10 ns, and a laser chamber with parasitic inductance of the order of 1 nH.

Taking consideration of the losses on inductance in the first half of the pumping current, we can get a criterion for determining the permissible parasitic inductance of the laser discharge circuit. In the first half of the pumping pulse, which is taken as triangular for the sake of simplicity, the pumping energy W_C without consideration of losses in the pumping oscillator during commutation, as well as during transfer to and reflection from the cell, is $CU_C^2/4$, where C and U_C are the capacitance and voltage of charging of the cable line. for a reasonable magnitude of losses of ~10% of this energy, we have $CU_C^2/40$. Setting this expression equal to the energy stored by the inductance and equal to $Li_{max}/2$, we get an expression for the permissible inductance:

$$L = CU_C^2/(20i_{max}^2) = W_C/(10i_{max}^2).$$

Using this relation, let us determine the permissible inductance under some real conditions. For example at a pumping energy of 1 J and maximum pumping current pulse amplitude of 10 kA, the inductance in the laser discharge circuit should not exceed 1 nH.

This reasoning implies that when considering the problem of the potentially attainable efficiency of a transverse-discharge metal vapor laser, one should take account of losses on supply inductance and on the lead-in resistance. With consideration of these losses, the efficiency of the laser is

$$\eta = W_{out}/(W_H - Li_{max}^2/2 - W_B),$$

where W_{out} is the lasing pulse energy [Ref. 1]. The efficiency defined in this way enables us to evaluate the potential capabilities of transverse-discharge metal vapor lasers, and to compare them with longitudinal-discharge lasers. It should be noted that in longitudinal-discharge lasers the losses on parasitic inductance and lead-in resistance are insignificant in virtue of the fact that their operation requires pumping currents several orders of magnitude lower than in a transverse

discharge, while the plasma resistance, being tens and even hundreds of ohms, far exceeds the lead-in resistance.

The maximum attainable efficiency of a transverse-discharge laser is 3% [Ref. 7].

In experiments on getting high efficiency in a coaxial laser, a method was used that was suggested in Ref. 1, where it was shown that the physical efficiency of a laser with respect to the energy supplied to the cell increases with a reduction in the voltage across the laser chamber and the output impedance of the pumping oscillator (we reduced the latter to 0.15 Ω). At a voltage of 0.8 kV across the cell, the physical efficiency of the laser reached 2.5%. The pumping energy was determined, as in Ref. 1, by graphic integration of the pulses of current and voltage across the cell.

Such a determination of efficiency does not permit evaluation of the potential capabilities of the investigated laser due to technical difficulties in making a low-inductance laser chamber. Therefore, to determine the efficiency that can be attained with transverse excitation of copper vapor, it is necessary to take consideration of losses in the electric circuit of the laser.

In the experiment under discussion, the lasing pulse was located on the current pulse front, where $di/dt > 0$, and therefore part of the useful energy was released on the inductance. Losses on inductance reached ~50%, which was confirmed by graphic integration of the pulses of current and voltage across the electrodes of the discharge gap carried out up to the instant of lasing termination. Losses on the lead-in resistance were disregarded, as steps were taken in these experiments to reduce this resistance.

Thus the potentially attainable, but apparently not maximum possible efficiency of the coaxial laser (efficiency with respect to energy supplied to the cell after deducting losses on inductance) was 5.3%. The obtained efficiency is almost twice that of a longitudinal-discharge laser, and even greater than that theoretically predicted for excitation of copper vapor in an electric discharge [Ref. 8].

The results show the considerable promise of lasers with transverse discharge of copper vapor, and apparently of other metal vapors.

4. Influence of Methods of Producing the Working Mixture on Laser Efficiency

To increase the practical efficiency of the laser, we must reduce energy expenditures on producing metal vapor in addition to overcoming the difficulties associated with energy losses in the electric pumping circuit. Considered below are various methods of producing the working mixture from the standpoint of increasing practical efficiency and achieving effective stimulated emission of the coaxial laser. These studies were done with the described laser fed from a pumping oscillator with output impedance of 0.4 Ω.

The most widely used method of producing copper vapor in a transverse-discharge laser is heating up the entire electrode zone with special heaters. An external cylindrical heater was used in the laser that we investigated. Provisions were made for controlling the heater temperature by varying its power consumption. This made it possible to establish the required temperature of the wall of the active

zone on which the copper to be vaporized was located irrespective of pumping power. Such a heating method is very convenient in physical research, and extends the range of study as compared with the mode of self-heating due to discharge heat that has been used in work with longitudinal tubes, where it is necessary to change the pumping power associated with wall temperature.

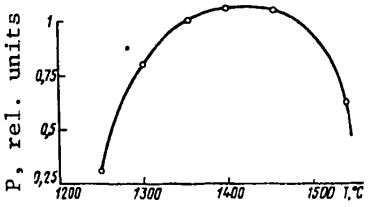

Fig. 4. Laser output power as a function of wall temperature

An investigation of the output power of the coaxial laser as a function of wall temperature of the active zone (Fig. 4) showed that lasing arises at a copper vaporization temperature of 1200-1250°C. As the temperature increases, the output power of the laser rises, reaching a maximum at 1450°C. Then lasing power falls, and stops almost entirely at about 1600°C. At the optimum temperature and a pulse recurrence rate of 3 kHz the laser output power was 10.5 W at a laser efficiency with respect to the energy of the pumping oscillator accumulator of ~1%. The practical efficiency of the laser with consideration of the power expended on heating the electrodes was considerably lower ($\gtrsim$0.1%).

These results show the necessity of looking for ways to reduce the overall electric supply power of the laser. Experiments were done in which the electrodes were heated via the pumping energy. To do this, the energy and recurrence rate of the excitation pulses were increased while simultaneously reducing the heater power. At a pumping pulse recurrence rate of 6 kHz the heater was completely disconnected, and the laser operated in the self-heating mode; however, the wall temperature was below optimum. We were not able to achieve efficient stimulated emission by using the energy released in the discharge to heat the electrodes. The output power was only 1-2 W with yellow emission predominating, whereas a green line was mainly excited at the optimum excitation rate of 3-4 kHz. Apparently effective self-heating can be realized in coaxial tubes of smaller diameter with appropriate heat insulation.

To find the second optimum with respect to neon pressure reported in Ref. 2, experiments were done in which a heater was used to raise the temperature of the entire zone, and the pressure in the cell was reduced from a starting point of 1.5 atm. In view of the instability of laser operation due to breakdowns of the high-voltage lead-in at low pressures, we were unable to detect the second optimum. At the same time, in the range of neon pressures below 5 mm Hg (measured in the cold region of the chamber), breakdown in the lead-in had almost no effect on the stability of the hollow-cathode discharge described below.

Laser operation at low buffer gas pressures or without buffer gas is of particular interest and opens up definite prospects for realization of one of the principal advantages of copper vapor lasers: high lasing pulse recurrence rate. A number of causes have been suggested for the limitation on lasing pulse recurrence rate. Among the most probable is the insufficient rate of the process of deionization of the gas-discharge plasma of the laser in the interpulse period.

To establish the nature of the deionization process in the laser plasma decomposing in the space between pulses, a third auxiliary electrode in the form of a grid

(collector) was inserted into the active zone. This grid had its own separate current lead through which a certain potential could be applied relative to the main electrodes. For constant voltage, the main electrodes were held under ground potential in view of design particulars of the cable transformer of the pumping oscillator. The collector was located at the same distance from anode and cathode. Experiments showed that in the absence of a potential across the collector, the latter had no influence on either the occurrence of the pulse discharge in the chamber or the lasing parameters.

A positive potential was applied to the collector relative to the main electrodes of the laser. In the absence of a pumping pulse, a semi-self-maintained discharge could be set up between the collector and the main electrodes, and monitored from its current-voltage characteristics. At the instant of the pumping pulse, there was a sharp change in the number of charged particles in the discharge gap which collected on the main electrodes and on the collector in the space between pulses during plasma decomposition. The amplitude of the collector current and its shape in different time intervals showed a reduction in the number of charged particles as a result of plasma deionization. The time behavior of the collector current was recorded by a resistor connected in the collector supply circuit; the signal from this resistor was sent to an S1-54 oscilloscope.

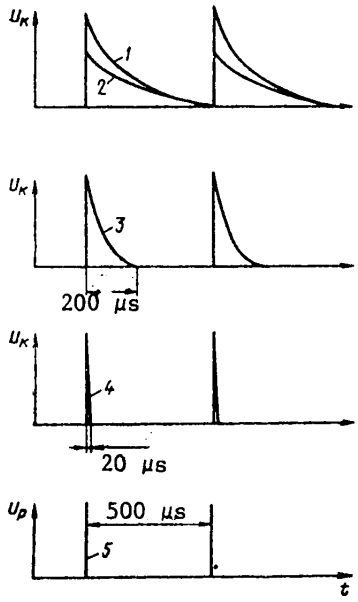

Fig. 5. Behavior of deionization process during pause between pumping pulses (5) for different pressures p_0 of Cu-Ne mixture and voltages U_{acc} across the accumulator (U_K--collector voltage; U_p discharge gap voltage: U_{acc} = 16 (1, 3, 4) and 8 kV (2); p_0 = 1000 (1, 2), 100 (3) and 1-3 mm Hg (4))

Fig. 5 shows time dependences of collector current for different mixture pressures and pumping voltages. They all were obtained at a collector voltage of +300 V, excitation rate of 0.5 kHz and electrode temperature of 1500°C. In the pressure range from 100 mm Hg and up, the collector current remains practically unchanged, and depends only on the pumping voltage (curves 1, 2). Apparently the process of volumetric recombination predominates at these pressures. When the pressure falls below 100 mm Hg, the time behavior of the collector current changes sharply (curves 3, 4). There is an increase in the rate of plasma decomposition. When the pressure of the working mixture decreases to a few mm Hg, processes of charge recombination on the wall as a result of diffusion of charge carriers to the wall of the discharge chamber begin to predominate. The role of volumetric recombination begins to fall off [Ref. 9].

This technique, which was used by gas-discharge classicists in various versions at the dawn of research on recombination phenomena [Ref. 10], enables quantitative determination of parameters of the investigated effects, but on the first stage in this work this problem was not raised, and an express method was needed that would

enable keeping qualitative track of the deionization process in the active zone of the pulse laser during the experiments.

The experiments done with the three-electrode laser show that metal vapor lasers with low pressure of the working mixture may be quite promising. At low pressures (1-10 mm Hg), effective plasma decomposition is possible in the period between excitation pulses due to diffusion of electrons [Ref. 11], ions and metastable atoms to the walls with subsequent deionization of the ions and quenching of the metastable atoms.

We were unable to achieve efficient lasing at low pressure in lasers in which transverse and longitudinal discharges were used. Pressure reduction leads to a reduction in the discharge current, and thus to deterioration of the conditions of excitation. This effect is especially pronounced with cransition to the range of pressures in which we are interested from a few mm Hg to a fraction of this pressure unit, where multiple reduction of the discharge current occurs. Thus the excitation of metal vapor in a laser chamber of about 1 mm Hg in conventional types of discharges (longitudinal and transverse) is ineffective in view of the low electron concentration.

There is a way out of this situation. For pulsed excitation of metal atoms at low pressure it is advisable to use a hollow-cathode discharge [Ref. 10]. The discharge with a hollow cathode is characterized by an anomalous current rise in just the low-pressure region of interest to us at comparatively low voltages applied to the discharge gap. In other words the hollow-cathode discharge most completely satisfies the conditions necessary for metal vapor laser operation.

It should also be emphasized that in view of the possibility of using longitudinal current components for pumping in the hollow cathode, the overall pumping current is slight, perhaps an order of magnitude less than the pumping current in a transverse discharge for the same active volumes. This circumstance relaxes requirements for the supply inductance and thus simplifies the design of the discharge chamber, minimizes inductive losses, and enables high physical efficiency.

Pulse lasing of copper atoms excited in a hollow-cathode discharge has been previously reported in Ref. 12.

The electrode configuration in the investigated laser enabled realization of the hollow-cathode effect and stimulated emission of copper atoms without particular difficulty. To do this, the inner electrode was made as a tube 0.8 cm in diameter and 40 cm long with a slit made in the center. This electrode acted as a hollow cathode. A planar cavity was formed by an opaque mirror with dielectric coating and a glass plate.

Pulsed lasing of copper atoms in the hollow cathode was observed on both characteristic lines: green and yellow at a cathode wall temperature of about 1500°C. At an excitation pulse voltage amplitude across the electrodes of 1.2 kV and pulse recurrence rate of 0.5 kHz, the output power was 100 mW. Increasing the excitation frequency to 4 kHz led to an increase in the mean output power to 1.2 W. Specific energy output was 15 $\mu J/cm^3$ at pumping current in the pulse of about 100 A. The physical efficiency of the laser (calculated with respect to the pumping power absorbed in the plasma without reflections [Ref. 1]) reached 4.8-5%. The effect of

superluminescence was observed in this mode. Increasing the excitation rate was limited by the capabilities of the pumping oscillator, but we are assuming that the optimum lasing frequency is considerably higher and may be tens of kilohertz.

The characteristics obtained in these preliminary experiments are on the level of the best results achieved with copper vapor lasers. All this shows that the hollow-cathode laser has a good outlook for operation with metal vapor.

A considerable percentage of the electric power in operation of transverse-discharge lasers on copper vapor is expended on heating of the active zone from the external heater.

Experiments with vaporizers without additional zone heating enabled a considerable increase in the practical efficiency of the coaxial laser with consideration of power going to the production of copper vapor, and also yielded efficient lasing. In this case the copper vapor source was provided by vaporizers like that described in Ref. 13. The vaporizers were placed in the lower part of the anode at a length of 20 cm. The total area of the molten metal speculum was 6 sq. cm. With optimum excitation, the output power was 8-9 W. The temperature of the metal melted in the vaporizers was more than 1600°C, and the temperature of the electrodes heated by the energy released in the vaporizers and in the discharge reached 1000-1100°C. While raising the temperature in the vaporizers above the indicated value did lead to a further increase in output power, there was a concomitant sharp drop in the service life of the vaporizers because of intensive destruction of heating elements.

Some reduction in laser output power as compared with the case of zone heating from an external source can apparently be attributed to intense condensation of copper vapor on relatively cool electrodes. A confirmation of this assumption is the presence of a considerable copper layer uniformly sputtered over the entire surface of the electrodes, which was observed upon disassembly of the laser cell. The power consumed by the vaporizer heater was reduced by an order of magnitude as compared with the power required for heating the entire zone, and the luminosity of the laser changed insignificantly. This led to an increase in the practical efficiency of the laser, which was about 0.6% (with consideration of the power of the vaporizers).

An investigation was also made of the working conditions of the laser with simultaneous activation of the overall heater and vaporizers. In the authors' opinion, this somewhat increased the copper vapor concentration in the active zone as compared with the laser operating conditions considered above, keeping the wall temperature of the anode close to optimum (1400-1500°C). Results found in the course of these experiments and reflected in Fig. 6 show that increasing the concentration above that corresponding to the optimum temperature leads to an increase in output power. As can be seen from the figure, there is a considerable region where the lasing power in operation with a single heater is 2-3 times lower than the power when the heaters are engaged with retention of temperature on the 1600°C level. The saturation of laser luminosity when working with vaporizers can apparently be attributed to disruption of the temperature conditions of the active zone of the laser upon additional heating of the mixture by the energy released in the vaporizers, which is comparable with the heat from pumping.

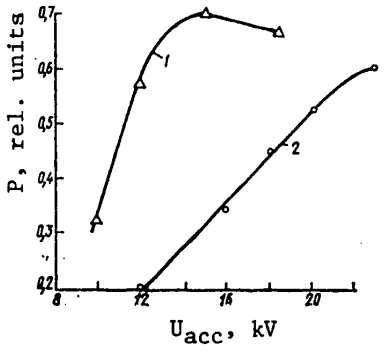

Fig. 6. Laser output power as a function of accumulator voltage with vaporizer (1) and without it (2)

In the authors' opinion, the optimum copper vapor concentration is considerably higher than that corresponding to the optimum temperature of the electrodes of the zone, i. e. higher than 10^{15} cm^{-3}. Therefore the temperature dependence of output power shown in Fig. 4 does not define the region of optimum concentration, but characterizes the change of temperature conditions in the active zone. Although there is an increase in copper vapor concentration as the electrode temperature rises, the gas temperature also rises beyond the limiting value, which may lead to deterioration of lasing conditions. Gas superheating can also explain inefficient laser operation in the self-heating mode, as well as the presence of an optimum pumping power beyond which the lasing power begins to fall. The optimum pumping power referred to the length of the active zone was 40 W/cm.

In addition to gas superheating that leads to metastable states of copper atoms, there may also be other causes leading to deterioration of lasing conditions as there is an increase in the zone temperature, rate and energy of excitation pulses, such as prolonged time of plasma deionization, discharge contraction and so on. Determination of their contribution is a complicated and important problem.

One of the effective ways of cooling the active mixture of gas lasers is circulating the mixture through a closed loop from the active volume to the heat exchanger and back. We did experiments with circulation of the Cu-Ne working mixture due to natural flow of the heated gas in a gravitational field in the direction perpendicular to the optical axis (Fig. 7). The gas heated in the discharge gap entered the heat exchanger, and after cooling was again returned to the active zone. To avoid metal vapor condensation, the temperature of the electrodes and heat exchanger was maintained on a level of 1400-1500°C. The gas heated in the discharge to higher temperatures gave up heat during motion to the relatively cool heat exchanger and electrodes.

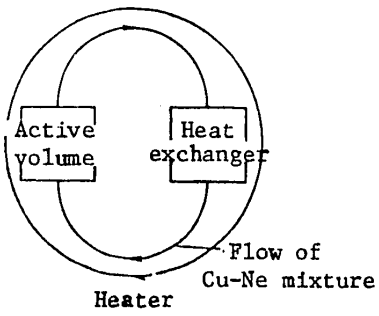

Fig. 7. Diagram of circulation of Cu-Ne working mixture

The use of such a method of circulating the mixture in lasers on copper and other metal vapors is justified by the presence of a high temperature head determined by the difference in temperatures of the gas in the active zone and the heat exchanger, which may be greater than 1000 K, although it is difficult to expect greater gas circulation velocities in view of the technical difficulties of making large vertical dimensions of the laser and its components that are to be heated to high temperatures.

Despite the low velocities of gas flow (of the order of 10 cm/s), which are very difficult to measure and estimate correctly [Ref. 14], the luminosity of the laser

was increased to 15 W instead of 10.5 W (i. e. by a factor of 1.5) as compared to a laser without circulation, all other parameters being equal. There was also an increase in the maximum pumping power, which was about 60 W/cm (Fig. 8).

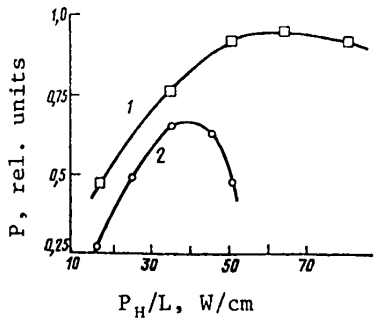

Fig. 8. Output power as a function of linear pumping power with circulation (1) and without it (2)

These experimental studies reinforce the confidence in the advisability of cooling the working mixture of the copper vapor laser, and show that an effective method of doing this may be to circulate the mixture through a closed loop. An appreciable effect should be expected as the velocity of gas circulation is increased. This is an indication of the necessity for further development of this area of metal vapor laser physics.

5. Conclusion

1. In a pulsed transverse-discharge laser at currents of 1-10 kA, and also when the discharge currents are increased to 1 kA in a laser with longitudinal discharge, the influence of parasitic inductances in the discharge circuits and its resistances is quite appreciable, leading to a reduction in the physical efficiency of the laser. A criterion is established for determining the admissible parasitic inductance in the laser discharge circuit.

2. It has been shown that a physical efficiency of 5.3% can be attained in a transverse-discharge laser when the lead-in inductance is minimized.

3. Copper vapor lasing has been accomplished in a hollow-cathode pulsed discharge at low pressures of the mixture and insignificant inductive losses. Physical efficiency reached 5%, and the specific energy output was 15 $\mu J/cm^3$.

4. It has been shown that the insertion of a third electrode for an auxiliary constant semi-self-maintained discharge enables monitoring the the deionization process in the decomposing plasma in the interval between pulses.

5. It has been shown that the use of vaporizers in a transverse-discharge laser makes it possible to raise the practical efficiency to 0.6%.

6. It has been established that circulation of the working mixture overcomes the limitation on pumping power and improves the characteristics of the copper vapor laser.

The results lead us to conclude that the possibilities of the copper vapor laser are far from exhausted, and their study is a topical problem.

REFERENCES

1. Babeyko, Yu. A., Vasil'yev, L. A., Sviridov, A. V., Sokolov, A. V., Tatarintsev, L. V., KVANTOVAYA ELEKTRONIKA, Vol 6, 1979, p 1102.

2. Bokhan, P. A., Shcheglov, V. B., KVANTOVAYA ELEKTRONIKA, Vol 5, 1978, p 381.

3. Walter, W. T., Solimene, N., Piltch, M., IEEE J., Vol QE-2, 1966, p 474.

4. Isayev, A. A., Kazaryan, M. A., Petrash, G. G., PRIBORY I TEKHNIKA EKSPERIMENTA, No 1, 1973, p 188.

5. Russell, G. R., Nerheim, N. M., Pivrotto, T. J., APPL. PHYS. LETTS., Vol 21, 1972, p 565.

6. Babeyko, Yu. A., Vasil'yev, L. A., Sokolov, A. V., Sviridov, A. V., Tatarintsev, L. V., KVANTOVAYA ELEKTRONIKA, Vol 5, 1978, p 2041.

7. Bokhan, P. A., Gerasimov, V. A., KVANTOVAYA ELEKTRONIKA, Vol 6, 1979, p 451.

8. Yeletskiy, A. V., Zemtsov, Yu. K., Rodin, A. V., Starostin, A. N., DOKLADY AKADEMII NAUK SSSR, Vol 220, 1975, p 318.

9. Granovskiy, V. L., RADIOTEKHNIKA I ELEKTRONIKA, No 3, 1966, p 371.

10. Leb, L., "Osnovnyye protsessy elektricheskikh razryadov v gaze" [Principal Processes of Electric Discharges in Gas], Moscow-Leningrad, Gosudartsvennoye izdatel'stvo tekhnicheskoy i teoreticheskoy literatury, 1950.

11. Gabay, S., Smilanski, I., IEEE J., Vol QE-16, No 6, 1980.

12. Fahlen, Theodore, J. APPL. PHYS., Vol 45, 1974, p 4132.

13. Ferrar, C. M., IEEE J., Vol QE-9, 1973, p 856.

14. Harnett and Irvine, eds., "Uspekhi teploperedachi" [Advances in Heat Transfer], Moscow, Mir, 1970.

6610
CSO: 1862/14

UDC 546.27+621.315

PHYSICOCHEMICAL AND ELECTROPHYSICAL PROPERTIES OF HIGH-TEMPERATURE INSULATING CERAMICS FOR ELEMENTAL VAPOR LASERS

Moscow KVANTOVAYA ELEKTRONIKA in Russian Vol 8, No 8(110), Aug 81
(manuscript received 13 Nov 80) pp 1697-1701

[Article by O. I. Buzhinskiy, V. V. Lopatin and V. P. Chernenko, Scientific Research Institute of High Voltages, Tomsk Polytechnical Institute]

[Text] The paper gives the characteristics of high-temperature ceramics that are widely used in the construction of elemental vapor lasers. It is shown that ceramics based on pyrolytic boron nitride have the best characteristics with respect to a set of selected indices.

A facility is described for measuring low-voltage and high-voltage electrophysical characteristics of dielectrics in a variety of gases at pressures of 1-10^5 Pa and temperatures up to 2500 K. The first experimental results are given on high-voltage electrophysical characteristics of pyrolytic boron nitride.

Elemental vapor lasers are currently in wide use as they cover a broad spectral band and have high efficiencies and gains. It would be impossible to increase the efficiency, emission energy and other technical-economic parameters of such lasers without using insulating materials that retain their dielectric properties up to temperatures of 2000-3000 K. The choice of dielectric materials for various structural components is dictated by their temperature conditions, by the complex of physicochemical and electrophysical properties of the material, and also by the characteristics of the medium.

At present, structures capable of operation in weakly aggressive atmospheres (air, nitrogen and commercially pure noble gases at pressures up to 1 kPa) utilize components of high-temperature ceramics based on widely available and fairly well studied oxides and carbides [Ref. 1-3], as well as nitrides that are not yet so widely available [Ref. 4]. The literature contains reliable low-voltage electrophysical characteristics of oxides: volumetric ρ_V and surface ρ_S resistivities, loss tangent $\tan\delta$ and permittivity ε. What we do not have are the high-voltage properties at high temperatures (electric strength E_{br}, surface arcover gradient E_{arc}) which significantly determine the emission characteristics of lasers. And despite the publication of considerable research, we do not even have reliable

low-voltage electrophysical characteristics for nitrides. This is because items made of BN and AlN powders are not series produced, and their properties are determined to a considerable extent by the impurities of the powder, and by the production and sintering process. In addition, the differences between electrophysical characteristics can be explained by the lack of a generally accepted method of measurements at high temperatures. This is particularly important for measuring the electrophysical characteristics of anisotropic polycrystalline materials such as pyrolytic boron nitride.

In this paper a critical analysis is made of the properties of high-temperature ceramics both from data in the literature and as measured by the authors.

Among the large number of high-temperature dielectrics, the best insulating properties are shown by corundum α-Al_2O_3, zirconium dioxide ZrO_2, brokerite BeO. nitrices of aluminum AlN and boron BN (hereafter the α-modifications will be called simply BN and Al_2O_3). Oxides of aluminum and beryllium, nitrides of boron and aluminum are made in the form of powders, and items are produced from them by hot pressing. In recent years [Ref. 5] a technique has been developed for making items from boron nitride by the method of gas-phase deposition: so-called pyrolytic boron nitride (PBN); despite identical chemical composition and microstructure, items made from powdered BN and PBN have different physicochemical and electrophysical characteristics (Table 1, Figure). An advantage of powder materials is the capability of molding "thick-walled" items. PBN can be used to make "thin-walled" (down to 5 mm) items with large overall dimensions and complex shape in the form of plates, tubes, boxes and the like. A distinguishing feature of BN and PBN is anisotropy of their properties in mutually perpendicular directions, which is a consequence of the graphite-like hexagonal lattice. With respect to selected physicochemical properties (see Table 1) and especially with consideration of the temperature dependences of thermophysical and mechanical parameters, the most suitable dielectrics for making items for work at temperatures up to 2000-2500 K are ordinary and pyrolytic boron nitride.

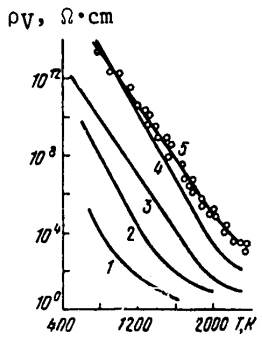

Temperature dependence of volumetric resistivity of ceramics: 1--ZrO [8, 10]; 2--BN [6, 10]; 3--BeO [8]; 4--BN [15]; 5--PBN, from measurement results for 10 specimens

High melting point, slow vaporization, fairly high mechanical strength at high temperatures and a number of other properties enable successful use of these materials in high-temperature devices. PBN has high thermal conductivity and diffusivity in the direction parallel to the plane of deposition, and low values of these parameters in the perpendicular direction. In addition, because of its high thermal diffusivity, PBN has excellent thermal stability: items made from this material can withstand about 100 heat cycles of 300-2000-300 K without cracking or peeling (the experiments were done with nitrogen cooling under a pressure of 100-1000 Pa). The best oxide ceramic, brokerite, withstands 25 such cycles [Ref. 9] (hot-pressed--12 cycles with heating to 1500 K [Ref. 6, 8]). In contrast to other ceramics, PBN is very resistant to heat shocks: in the thermal stability tests, the specimens were heated to 2000 K within 15 minutes.

TABLE 2

T, K	800	1000	1250	1500	1800	2100	2500
ρ_S, Ω	$4 \cdot 10^{14}$	10^{13}	$7 \cdot 10^{9}$	$8 \cdot 10^{7}$	$5 \cdot 10^{6}$	$4 \cdot 10^{4}$	$8 \cdot 10^{3}$

The authors have developed a high-temperature facility for measuring low-voltage (ρ_V, ρ_S, ε, $\tan\delta$) and high-voltage (E_{br}, E_{arc}) electrophysical characteristics of dielectrics. The facility with resistive graphite heater can be used for measurements in a variety of gases at pressures of $1\text{-}10^5$ Pa and a temperature of up to 2500 K. Techniques have been developed for preparing specimens and carrying out measurements of low-voltage and high-voltage characteristics at high temperatures. In measuring the temperature dependence of ρ_V and ρ_S of PBN, we observed the standard technique approved for low temperatures (State Standard GOST 6433.2-71). The electrodes were applied to flat specimens by smearing with grade MPG-8 graphite or by platinum sputtering. The measurements were made with a guard electrode at constant field strength of E = 50 V/mm after settling of the absorption current. The electric strength E_{br} was measured on oscillating pulses with amplitude of up to 40 kV, period of oscillations of 0.18 μs, and logarithmic decrement of 2.

The permittivity of the ceramics is nearly independent of temperature, and the loss tangent increases by about three orders of magnitude when the temperature is increased to 1000 K.

The Figure shows temperature dependences of volumetric resistivity ρ_V for BN and PBN in the direction perpendicular to the plane of pressing (curves 2, 4, 5).

Table 2 summarizes the results of measurements made by the authors of the surface resistivity ρ_S for PBN in the direction parallel to the plane of deposition. Unfortunately, the measurements of ρ_S for BN and PBN [Ref. 6, 8, 11, 15, 21] were made in a two-electrode system, in which a combination of ρ_V and ρ_S is measured rather than each one individually due to the anisotropy of the material. Besides, these papers do not state the voltage and field strength at which the measurements were made. This is apparently one of the reasons for the considerable divergence of the results (for example, see the Figure, curves 2 and 4). It has been established that the function $\rho_V = f(T)$ remains practically unchanged in air, nitrogen, argon and helium in the pressure range of $1\text{-}10^5$ Pa.

The electric strength E_{br} of PBN flat specimens 0.25 mm thick in the temperature range of 800-1900 K was 160-200 kV/mm. The electric strength of PBN under repeated pulse action (multipulse E_{br}) is considerably lower than for a single pulse, the determining factors in reduction of E_{br} being the repetition rate and number of the acting pulses. For example at a rate of 1 Hz and T = 1800 K, E_{br} decreases by 20-30% with breakdown occurring as early as the 100-th pulse.

From our research, we can draw the following conclusions.

1. The literature does not give the high-voltage electrophysical characteristics of high-temperature insulating ceramics.

TABLE 1

Characteristic	PBN	BN	Al_2O_3	AlN	BeO	ZrO_2
Crystal structure	Hexagonal (graphite-like)			Hexagonal (Würtzite)		Tetragonal
Melting point, K	3270 [5]	3270 [6]	2320 [7]	2670 [6]	2720 [7]	2970 [7]
Heat conduction at 1300 K, W/(m·K)	65 — ∥ [5, 20] 2 — ⊥ [5, 21]	27 [6]	6 [8]	8 [6]	30 [8]	2 [8]
Temperature coefficient of linear expansion at 1300 K, 10^{-6} K^{-1}	2,6 — ∥ [5, 19] 42 — ⊥ [21]	0,8 [6]	8,5 [9]	4,8 [6]	9,2 [9]	11,5 [8]
Specific heat at 1300 K, kJ/(kg·K)	1,8—2,5 [5]	2 [10]	1,1 [8]	1,26 [6]	2 [10]	2,7 [10]
Vaporization rate at 2500 K, kg/(cm^2·s)	$4 \cdot 10^{-5}$ [5]	10^{-4} [8, 10]	—	—	10^{-3} [10]	$6 \cdot 10^{-5}$ [10]
Vapor pressure at 2000 K, Pa	10^{-3} [5]	10^{-1} [10]	10^{-2} [10]	10^{-1} [6]	$3 \cdot 10^{-3}$ [10]	—
Tensile strength at 1300 K, N/mm^2		18—[6, 8]				
stretching	49 [5]	4— [6]	78 [13]	177 [12]	34 [9]	—
bending	90 — ∥ [11]	4,9 [6,8]	—	—	128 [9]	—
Oxidizability (mass lost in oxygen stream in 10 hours), g/cm^2	10^{-5} [5]	$8,5 \cdot 10^{-4}$ [6]	—	1% mass converted to Al_2O_3	—	—
Permittivity at 10^6-10^9 Hz	4,0 [11, 21]	4,1—4,5 [6]	10 [7,17]	8,5 [14,6]	7,35 [17]	12,3 [18]
Dielectric losses, $\tan\delta \cdot 10^4$	2—4 [20]	4—10 [17]	5 [7]	0,35—5 [19]	2—5 [7,17]	36—51 [18]

Note: ∥,⊥ is the direction parallel and perpendicular to the plane of deposition.

The mechanical strength of PBN (tensile, bending and compression) at low temperatures is lower than for other ceramics, but at 1000-1400 K it becomes comparable to or even considerably greater than their strength. Table 1 gives the physicochemical characteristics of BN and PBN with density of about 2 g/cm^3 (theoretical density is 2.28 g/cm^3), which should be considered the optimum from the standpoint of both the process of item manufacture and resultant properties. Reducing the density of PBN to 1.7-1.8 g/cm^3 cuts mechanical strength approximately in half [Ref. 11], reduces chemical stability and increases the probability of peeling of items. PBN has higher chemical stability than other ceramics, shows almost no tendency to react with most elements right up to temperatures of 2000-2500 K, does not dissolve in water, and dissolves poorly in acids and alkalis. It is also quite resistant to oxidation [Ref. 5] as the boron oxide (B_2O_3) film that forms on the surface protects it from further oxidation. PBN is easily machined, has fairly high vacuum properties, and forms vacuum-tight seals to titanium and copper by the method of contact-reactive soldering with titanium-containing solders [Ref. 16].

2. The use of ceramics like these in facilities that operate in multipulse conditions requires measurements of the lifetime of insulation.

3. In insulation components that operate at temperatures up to 2000-2500 K, items made from PBN can be unambiguously recommended for use with respect to a number of characteristics. Where thick-walled insulators are necessary, hot-pressed BN, brokerite or aluminum nitride can be used.

REFERENCES

1. Petrash, G. G., "Spravochnik po lazeram" [Laser Handbook], edited by A. M. Prokhorov, Moscow, Sovetskoye radio, Vol 1, 1978, pp 183-197.

2. Isayev, A. A., Petrash, G. G., Kazaryan, M. A., PRIBORY I TEKHNIKA EKSPERIMENTA, No 1, 1973, p 188.

3. Bokhan, P. A., Nikolayev, V. N., Solomonov, V. I., KVANTOVAYA ELEKTRONIKA, Vol 2, 1975, p 159.

4. Buzhinskiy, O. I., Kolganov, A. S., Krysanov, S. I. et al., KVANTOVAYA ELEKTRONIKA, Vol 4, 1979, p 2040.

5. Sharupin, B. N., in: "Khimicheskoye gazofaznoye osazhdeniye tugoplavkikh neorganicheskikh materialov" [Chemical Gas-Phase Deposition of Refractory Inorganic Materials], edited by V. S. Shpak and R. G. Arvabe, Leningrad, 1976, pp 66-101.

6. Samsonov, G. V., "Nitridy" [Nitrides], Kiev, Naukova dumka, 1969.

7. Kikoin, I. K., ed., "Tablitsy fizicheskikh velichin" [Tables of Physical Quantities], Moscow, Atomizdat, 1976.

8. Samsonov, G. V., "Fiziko-khimicheskiye svoystva okislov: spravochnik" [Physicochemical Properties of Oxides: Handbook], Moscow, Metallurgiya, 1978.

9. Belyayev, R. A., "Okis' berilliya" [Beryllium Oxide], Moscow, Atomizdat, 1962.

10. Kotel'nikov, R. B. et al., "Osobotugoplavkiye materialy" [High Refractories], Moscow, Metallurgiya, 1969.

11. Bershadskaya, M. D., ELEKTRONNAYA TEKHNIKA. SERIYA MATERIALY, No 4, 1978, p 68.

12. Libovits, G., "Razrusheniye" [Fracture], Moscow, Mir, 1976, p 7.

13. Lukin, Ye. S., Sysoyev, E. P., Poluboyarinov, D. N., OGNEUPORY, No 12, 1976, p 34.

14. Repkin, Yu. D., OGNEUPORY, No 2, 1965, p 41.

15. Poluboyarinov, D. N., Shishkov, N. V., Kuznetsova, I. G., IZVESTIYA AKADEMII NAUK SSSR: NEORGANICHESKIYE MATERIALY, Vol 3, 1967, p 1828.

16. Batygin, V. N., Kruchinin, V. P., Kylasova, T. M., ELEKTRONNAYA TEKHNIKA, SERIYA ELEKTRONIKA SVCh, No 3, 1977, p 71.

17. Koritskiy, Yu. V., ed., "Spravochnik po elektrotekhnicheskikm materialam" [Handbook on Electronics Materials], Moscow, Energiya, Vol 2, 1974.

18. Tareyev, B. M., Lerner, M. M., "Oksidnaya izolyatsiya" [Oxide Insulation], Moscow, Energiya, 1975.

19. Andreyeva, T. V., Barantseva, I. G., Dubnik, Ye. M., Yupko, V. L., TEPLOFIZIKA VYSOKIKH TEMPERATUR, Vol 2, 1964, p 829.

20. Novikova, N. A., Vlasov, Ye. G., Nepomnyashchiy, L. B., OGNEUPORY, No 10, 1971, p 54.

21. Bershadskaya, M. D., Avetikov, V. G., Sharupin, B. N., ELEKTRONNAYA TEKHNIKA, SERIYA MATERIALY, No 6, 1978, p 61.

6610
CSO: 1862/14

UDC 621.378.33

ENERGY AND SPECTRAL CHARACTERISTICS OF CO GASDYNAMIC LASER WORKING MEDIA

Moscow KVANTOVAYA ELEKTRONIKA in Russian Vol 8, No 8(110), Aug 81
(manuscript received 8 Jan 81) pp 1797-1801

[Article by B. S. Aleksandrov, G. A. Andronov, V. A. Belavin, B. M. Dymshits, Ya. P. Koretskiy and V. F. Sharkov]

[Text] The paper gives the results of measurement of the power and spectral composition of CO gasdynamic laser emission. Good agreement between the results of calculation and experimental data justified the confidence of the mathematical model of the CO gasdynamic laser and of the earlier prediction based on this model of an attainable specific energy output of 50 J/g for a CO gasdynamic laser using a CO-Ar mixture.

Recent years have seen the publication of research dealing with CO gasdynamic lasers. None of them expresses any doubt as to the good outlook and high energy efficiency of this system. Of course, there is a realistic basis for the optimistic prospects of CO gasdynamic lasers: 1) high quantum yield of the CO molecule; 2) the thermal stability of the molecule, and consequently the capability of storing a large amount of vibrational energy; 3) low vibrational-translational relaxation rate. However, the mere fact of a large store of vibrational energy that can be retained during gas flow through a nozzle does not in itself ensure high output characteristics of the laser: the stored energy has still to be converted efficiently to emission.

The efficiency of CO gasdynamic lasers still remains low, which is entirely natural as experiments have been done only on small-scale facilities using shock tubes under conditions that are obviously far from optimum. Suffice it to say that for example the maximum specific energy output that has been experimentally attained is no more than 2.2 J/g for a CO-N_2-Ar mixture [Ref. 1], and 5.4 J/g for a Co-Ar mixture [Ref. 2]. These values are clearly far from the true capabilities of the CO gasdynamic laser. Therefore theoretical predictions of the capabilities and efficiency of this kind of laser should take on particular significance.

Some theoretical research has been done [Ref. 3-5] in which an investigation has been made of kinetic processes in supersonic expanding flows leading to the formation of inverse population in media containing CO, and calculations have been done on the energy and spectral output characteristics of the laser. However, it cannot be said that we have yet achieved unanimity of views on the energy capabilities of

CO gasdynamic lasers. Predictions of the energy efficiency of CO gasdynamic lasers given by various authors differ by about an order of magnitude [Ref. 3-5]. Such a discrepancy of results can be attributed both to the difference in mathematical models used for the calculations, and to incompleteness of information on the kinetic constants appearing in the equations. In this connection, the job of substantiating the confidence of the mathematical model of the CO gasdynamic laser is of particular urgency.

In Ref. 5, the first attempt was made at substantiating the confidence of the mathematical model of a CO gasdynamic laser by comparing experimental and theoretical data. However, this comparison was not sufficiently complete. Comparison of calculated and experimental data at isolated points may be insufficient for the absolute value of lasing power. More convincing would be agreement between several parametric relations, assuming that the calculations were done with the same set of semiempirical constants.

This paper gives the results of a study of spectral and energy characteristics of a CO gasdynamic laser using a more imporved experimental method. The spectral composition of radiation, the most important characteristic of a laser, so far has remained practically uninvestigated for the CO gasdynamic laser. Ref. 1 gives the results of measurement of the relative intensity (weak, moderate, strong) of individual lines; the emission spectrum of the CO gasdynamic laser given in Ref. 5 was recorded by a thermophosphor, i. e. it corresponds to the time-integrated radiation over the entire pulse. The resturcturing of the spectrum that we observed when the experimental conditions were varied has enabled us to refine the theoretical model.

The experimental studies were done on a facility described in Ref. 5. A mixture of CO:Ar = 37:63 was heated and compressed in a shock tube. A supersonic tapered nozzle was used with half-angle of 10° and an interchangeable critical section, enabling variation of the degree of expansion of the nozzle from 200 to 6400. The nozzle diameter in the vicinity of the optical cavity was 200 mm. An external cavity was used, formed by an opaque metal mirror and a semitransparent mirror. Lasing involved about 1/10 of the gas flow close to the axis of the nozzle bounded by the aperture of the windows set at the Brewster angle. Emission power was measured in the standard way: simultaneous measurement of pulse shape and total energy gave the time dependence of power. The duration of the quasi-cw period of stimulated emission was about 1 ms.

An investigation was made of the way that lasing power depends on the transmission factor t of the output mirror of the cavity. Flat dielectric mirrors (t = 0.15 and 0.35) and a germanium plane-parallel plate (t = 0.53) were used as the output mirror. The curve for output radiation power W_{out} as as a function of transmission factor (Fig. 1a) has a maximum in the vicinity of t = 0.15-0.35 for the given specific conditions of the experiment.

The radiation power was also measured as a function of the degree of expansion of the nozzle F/F_{cr} (Fig. 1b). The output mirror with t = 0.15 was used. These results cover a different range of variation in F/F_{cr} (200-800) than in Ref. 3 (400-3600). The level of W_{out} in our research was considerably higher due to the use of a more efficient optical cavity.

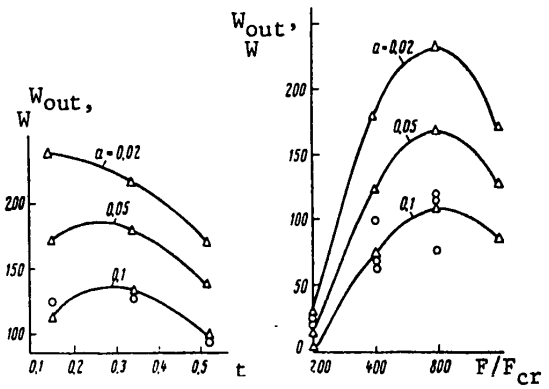

Fig. 1. Emission power as a function of transmission factor t of the output mirror (a) and a function of the degree of expansion of the nozzle F/F_{cr} (b): mixture CO:Ar = 37:63; p_0 = 90 atm; T_0 = 2050 K; o--experiment; Δ--calculation with different values of the loss factor a on one mirror; F/F_{cr} = 800 (a); t = 0.15 (b)

Fig. 1 also shows the results of calculations of the output radiation power of the CO gasdynamic laser for the given conditions. The method of calculation is given in Ref. 5. The calculations were done at different loss factors a on one mirror. It was assumed that the value of a includes not only the losses immediately on the mirror (thermal, diffuse scattering, etc.) that may be determined with satisfactory accuracy, but also possible absorption in the boundary layer where the gas temperature is high and the state is close to equilibrium, losses on the mirrors, losses on inhomogeneities of the medium distributed through the volume and so on. Obviously it is impossible to measure the value of this quantity directly; however, comparison of the results of calculation for different a with experiment gives a satisfactory indirect estimate of a.

In comparing experimental and calculated data, it is also necessary to remember that the cross section of the output window in the experiments had the shape of an ellipse with axes of 30 and 15 mm, as did the working section of the mirror surface, whereas the calculations were done for rectangular mirrors measuring 30 x 10 mm with gaussian field distribution in the direction of gas flow and constant distribution in the perpendicular direction. Clearly under such conditions we cannot expect complete correspondence of values of the output power W_{out} observed in the experiment to the calculated value. The best confirmation of the correctness of the computational method might be agreement of qualitative dependences of W_{out} on various parameters of the experiment.

The calculated behavior of the function $W_{out}(t)$ satisfactorily reproduces the dependence found in the experiment (see Fig. 1a). Obviously there is no question of coincidence of absolute values in the given case since the value of a is arbitrarily chosen, and one can always select a such that absolute values will agree at one point. However, if we consider the fact that the best agreement is observed at a = 0.03-0.1, and examine the results of comparison of the calculated dependence $W_{out}(t)$ with the experimental curve as an indirect method of determining a, then in calculations of other dependences at predetermined a, coincidence of the curves and in particular of absolute quantities is a strong argument in favor of the confidence of the mathematical model and the assumed kinetic constants.

We can see from Fig. 1b that the theoretical model also correctly describes the dependence of W_{out} on the geometric degree of nozzle expansion. It should be taken into consideration that in calculation and experiment, F/F_{cr} increases due to a reduction in F_{cr} while F remains constant, which reduces the gas flow through the

optical cavity. For the given conditions, the calculation, like the experimental data of Ref. 2, gives a maximum value of W_{out} in the vicinity of $F/F_{cr} = 800$. The less abrupt fall-off in experimental values of W_{out} as F/F_{cr} decreases in comparison with the calculated curves can be attributed to the fact that with decreasing F/F_{cr} there is a reduction in the thickness of the boundary layer and in its role in absorption. The results shown in Fig. 1b also confirm the assumption that the loss factor is close to $\alpha = 0.05$-0.10.

The occurrence of the maximum on the curve for $W_{out}(F/F_{cr})$ (see Fig. 1b) accompanied by a reduction in gas flowrate G is due to a monotonic increase in specific energy output W_{out}/G as F/F_{cr} increases in the given interval. This result agrees with the conclusion of Ref. 1 on an increase in efficiency of the CO gasdynamic laser (a quantity that is obviously proportional to the specific energy output) with increasing F/F_{cr} found experimentally.

The spectral measurements were made with a spectrograph with diffraction grating of 200 lines per mm with intensity maximum at 4.3 μm. A diagram of the device is shown in Fig. 2. The collimator objective was a system comprising LiF lens 6 and concave spherical mirror 7. The spectrum was recorded by 10-channel IR receiver 9 with reception area of 3 x 30 mm built up of 10 Ge-Au cells measuring 3 x 3 mm. The IR receiver was operated at the temperature of liquid nitrogen. A wavelength band of 4.7-5.4 μm could be recorded. The parallel laser beam was focused on the reception area of the IR receiver by relative shifting of the mirror and lens in the collimater objective. Wavelength tie-in was with respect to high orders (7-9) of a helium-neon adjustment laser emitting on a wavelength of 0.6328 μm. This same laser was used for alignment of the entire optical system. A diaphragm 4 was placed in front of the collimator objective to reduce radiation intensity.

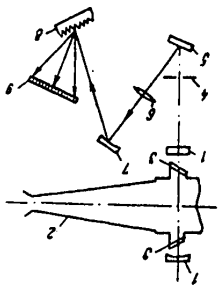

Fig. 2. Diagram of spectrograph:
1--cavity mirrors; 2--nozzle; 3--Brewster windows; 4--diaphragm; 5--flat mirror; 6--LiF lens; 7--concave mirror of collimator objective; 8--diffraction grating; 9--IR radiation receiver

The described system for recording the spectrum, in contrast to the system that we had previously used based on a thermophosphor [Ref. 5], enabled us to record the spectral distribution of emission energy as a function of time.

The random error in tie-in with respect to wavelengths, due mainly to the finite dimensions of the He-Ne laser beam in the plane of the IR receiver we estimate at $\delta\lambda = \pm 4$ cm^{-1} $= \pm 0.01$ μm.

The relative sensitivity of the cells of the IR receiver was calibrated by a heated nichrome filament by focusing the filament image on the reception cells. The relative error of measurement of the signal amplitude from each reception cell according to our estimates was 15-20%.

Measurements were made of the spectral composition of emission of a CO gasdynamic laser on a mixture of CO:Ar = 37:63 at $p = 90$ atm and $T_0 = 2050$ K for nozzles with

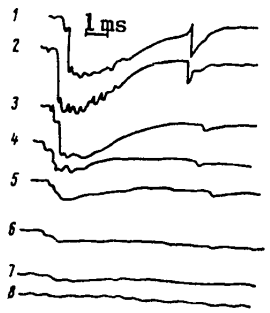

Fig. 3. Oscillograms of signals from IR receiver. Conditions the same as in Fig. 1a: 1) 4.85-4.91 μm; 2) 4.91-4.98 μm; 3) 4.98-5.04 μm; 5) 5.10-5.17 μm; 6) 5.17-5.23 μm; 7) 5.23-5.29 μm; 8) 5.29-5.36 μm

F/F_{cr} = 200, 400, 600 and 800. Fig. 3 shows oscillograms of signals obtained from the IR receiver. It can be seen from the oscillograms that the duration of quasisteady lasing is about 1 ms.

On the whole, the reproducibility of the results should be considered satisfactory: the boundaries of the spectrum and position of the maximum were completely reproduced. The general shape of the envelope curve of the spectrum was also constant from experiment to experiment: a single maximum in the short-wave part of the spectrum and a long declining "tail" in the long-wave part. However, the rate of decline of the tail as well as the ratios of intensities in different parts of the spectrum underwent considerable deviations from experiment to experiment (Fig. 4).

Fig. 5 shows experimental and calculated spectra of radiation for different values of F/F_{cr} at times corresponding to steady-state emission. The intensity of the maximum line in each case

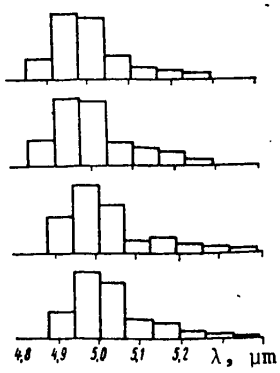

Fig. 4. Results of measurement of the spectrum of a CO gasdynamic laser in series of experiments with fixed conditions: F/F_{cr} = 400

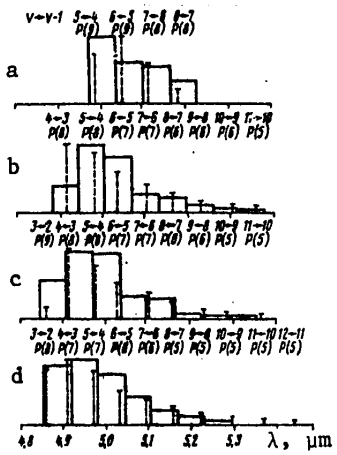

Fig. 5. Experimental and calculated spectrum of CO gasdynamic laser at F/F_{cr} = 200 (a), 400 (b), 600 (c) and 800 (d). Remaining conditions as in Fig. 1a

was taken as equal to unity. Fig. 5 illustrates on the basis of individual examples the degree of agreement between the results of experiments and calculation done at $\alpha = 0.05$.

With a simultaneous increase in F/F_{cr} and the degree of cooling of the gas in the optical cavity, there is an expansion in the overall limits of the spectrum, the main fraction of emission energy is shifted into the short-wave region and there is a transition to lower vibrational transitions. As F/F_{cr} changes from 200 to 800, the gas temperature in the cavity changes from 75 to 40 K. A comparison of calculation and experiments shows that the calculation satisfactorily reproduces the range of wavelengths and the behavior of the spectrum with a change in the degree of expansion. In evaluating the reproducibility of the experiments and comparing them with calculation, it is necessary to consider first of all that the tie-in of crystals recording IR emission to a certain wavelength range was done with accuracy of ±0.01 μm, and secondly that defocusing of the collimator objective of the spectrograph due to the dispersion properties of the lens caused focusing of the spectral lines on the receiver surface in spots of finite dimensions so that some of them could be registered by two adjacent crystals.

In addition to their independent interest, these results have confirmed the confidence of theoretical prediction of the attainable specific energy output of a CO gasdynamic laser based on a mixture of CO-Ar (~50 J/g), which was made in Ref. 5.

REFERENCES

1. McKenzie, R. L., PHYS. FLUIDS, Vol 15, 1972, p 2163.

2. Andronov, G. A., Armer, A. G., Belavin, V. A., Dymshits, B. M., Koretskiy, Ya. P., Sharkov, V. F., KVANTOVAYA ELEKTRONIKA, Vol 4, 1977, p 1799.

3. Kukhto, A. N., TEPLOFIZIKA VYSOKIKH TEMPERATUR, Vol 14, 1976, p 1281.

4. Vasilik, N. Ya., Vakhnenko, V. A., Margolin, A. D., Shmelev, V. M., ZHURNAL PRIKLADNOY MEKHANIKI I TEKHNICHESKOY FIZIKI, No 5, 1978, p 16.

5. Aleksandrov, B. S., Andronov, G. A., Belavin, V. A., Sharkov, V. F., TEPLOFIZIKA VYSOKIKH TEMPERATUR, Vol 16, 1978, p 1112.

6610
CSO: 1862/14

UDC 621.378.33

COPPER ATOM LASER LEVEL EXCITATION EFFICIENCY IN ELECTRIC DISCHARGE

Moscow KVANTOVAYA ELEKTRONIKA in Russian Vol 8, No 8(110), Aug 81
(manuscript received 11 Dec 80) pp 1842-1845

[Article by O. I. Buzhinskiy and M. L. Petrov]

[Text] On the basis of numerical solution of Boltzmann's equation for the energy distribution function of electrons, the authors determine the rate constants of excitation of laser levels, and the electron energy balances in a discharge in a Cu-Ne mixture for different relative compositions corresponding to copper vapor lasers with a heating method of producing copper atoms. It is found that as the relative concentration of copper atoms increases, the region of most effective excitation of laser levels shifts toward larger values of E/N--the ratio of electric field strength in the discharge to the total number of particles in a unit volume. An examination is made of causes for the change in specific energy output at high temperatures in lasers with thermal method of producing copper atoms (heating by the discharge, forced independent heating).

One of the ways to increase energy output in copper vapor lasers is to increase the density of copper atoms in the working volume. However, experiments have shown that energy output increases with rising temperature of the active medium only up to ≅1900 K [Ref. 1]. As temperature rises further, there is even a reduction in energy output [Ref. 2]. On the other hand, when copper atoms are produced by using the mechanism of explosion of conductors, an increase in energy output is observed up to concentrations of $\cong 10^{18}$ cm^{-3} [Ref. 3], which corresponds to "thermal population" temperatures much greater than 2000 K. As yet there has been no explanation for the causes of the difference in specific energy output of a copper vapor laser as a function of copper atom concentration for the thermal population and the explosive mechanism. Therefore it is of interest to determine the electron energy balance in a Cu-Ne discharge on the basis of numerical solution of Boltzmann's equations for the electron distribution function and ascertainment of the rate constants of laser level excitation for different relative compositions of the Cu-Ne mixture, and to analyze the results as a basis for explaining the existing differences in the behavior of specific energy output of copper vapor lasers.

The electron energy distribution function was determined from solution of the isotropic compondnt of the Botzmann's equation:

$$\frac{1}{3}\left(\frac{E}{N}\right)^2\left(\frac{u}{\sum y_j Q_{mj}}\frac{df}{du}\right)+\sum_j \frac{2m}{\mu_j} y_j \frac{d}{du}\left(u^2 Q_{mj} f+\frac{kT}{e}u^2 Q_{mj}\frac{df}{du}\right)+$$

$$+\sum_{i,j} y_j (u+u_{ij})\, f(u+u_{ij})\, Q_{ij}(u+u_{ij}) - uf(u)\sum_{i,j} y_j Q_{ij}(u)=0, \qquad (1)$$

where y_j is the relative concentration of atoms of the j-th type; Q_{mj} is the transport cross section of collision between electrons and atoms; Q_{ji} is the excitation cross section for the i-th level of an atom of j-th type; μ_j is the mass of an atom of the j-th component; u_{ij} is the corresponding loss of electron energy; f is the symmetric component of electron energy distribution.

This equation is valid under conditions of spatial homogeneity and weak anisotropy of the distribution function, where the frequency of elastic collisions of electrons with atoms considerably exceeds the frequency of inelastic collisions. The first term in equation (1) corresponds to the energy acquired by an electron in the field. The second and third terms are the electron energy losses in elastic collisions in the diffusion approximation. The last two terms of the equation describe the losses of energy by the electron in inelastic processes. Equation (1) was numerically solved by using a method developed in Ref. 4. The transport cross section and sixteen cross sections of lower levels of the neon atom were taken into consideration in the calculations. The cross sections of processes of collisions between electrons and neon atoms were taken from Ref. 5. At present there are no reliably measured excitation cross sections for resonant levels of the copper atom. Experimental results found in Ref. 6, 7 differ by an order of magnitude from the results in Ref. 10. Calculation of these cross sections by oscillator strengths [Ref. 8] and by the Bethe formula [Ref. 9] gives values approximately half the level quoted in Ref. 10, and higher than those of Ref. 6, 7. The authors of 10 normalize the results of absolute cross sections of the excitations by a factor of two, holding the relative accuracy of the results to 30%. Our calculations used cross sections of excitation of resonant, metastable levels, as well as the transport cross section of collisions of electrons with copper atoms from Ref. 10 with normalization by a factor of two toward reduction. For the copper atom levels that have allowed transitions to the ground state, the excitation cross sections by electron impact were calculated by the Bethe formula in terms of the oscillator strengths of these transitions [Ref. 9]. In addition to the above-mentioned levels, seven others excited from the ground state of the copper atom were taken into consideration. The ionization cross section of the copper atom was taken from Ref. 11.

After numerical solution of equation (1) and determination of the distribution function $f(\omega)$ of electrons, the following were found:

rate constants of the investigated processes

$$W_{ik}=\left(\frac{2e}{m}\right)^{1/2}\int_0^\infty uQ_{ik}f(u)\,du, \qquad (2)$$

electron drift rate

$$V_{др}=-\left(\frac{2e}{m}\right)^{1/2}\frac{1}{3}\left(\frac{E}{N}\right)\int_0^\infty u\left[\sum y_j Q_{mj}(u)\right]^{-1}\frac{df}{du}\,du \qquad (3)$$

and the relative energy inputs (energy balance) to the various processes

$$z_{ik}=\left(\frac{E}{N}\right)^{-1}\frac{y_{ik}u_{ik}}{V_{др}}W_{ik};\ \sum_{i,k}z_{ik}=1. \tag{4}$$

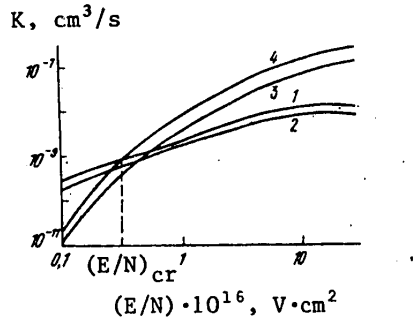

Fig. 1. Constants K as a function of E/N in Cu-Ne mixture at $X = 10^{-2}$: 1, 2--metastable levels of lines 510.6 (1) and 578.2 nm (2); 3, 4--resonant levels of lines 578.2 (3) and 510.6 nm (4)

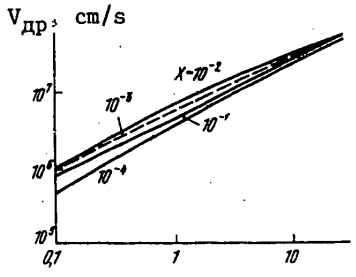

Fig. 2. Electron drift rate in Cu-Ne mixture as a function of E/N

Fig. 1 shows rate constants K for excitation of laser levels of mixture Cu:Ne = 1:100 ≡ X as a function of ratio E/N of electric field strength to the total number of particles in 1 cm^3, and Fig. 2 shows curves of electron drift rate for different relative compositions of the Cu-Ne mixture as a function of parameter E/N. As we can see from Fig. 2, the drift rate increases with increasing concentration of the mixture (or with increasing concentration of copper atoms) from $X = 10^{-4}$ to $X = 10^{-2}$ (at fixed E/N), and then falls at $X = 10^{-1}$.

The specific energy invested in the discharge can be determined from the relation

$$W = Een_eV_{др}, \tag{5}$$

where E is the electric field strength in the discharge, e is the electronic charge, $V_{др}$ is drift rate.

Relation (5) implies that a reduction in drift rate with increasing concentration of copper atoms leads to a reduction in energy input to the discharge at the same values of electron density.

Fig. 3 shows curves for energy balance of electrons in the discharge as a function of E/N for different relative concentrations of the Cu-Ne mixture. As comparative characteristics of the given variants we take the values $(E/N)_{max}$ where the greatest effective energy contribution is made to the resonant levels, and $(E/N)_{cr}$ where the rate constant of excitation of the upper laser level for the green line (510.6 nm) becomes greater than the rate constant of excitation of the metastable level for this same lasing line (see Fig. 1). The results are summarized in the Table, which shows that the quantities $(E/N)_{cr}$ and $(E/N)_{max}$ increase with increasing copper

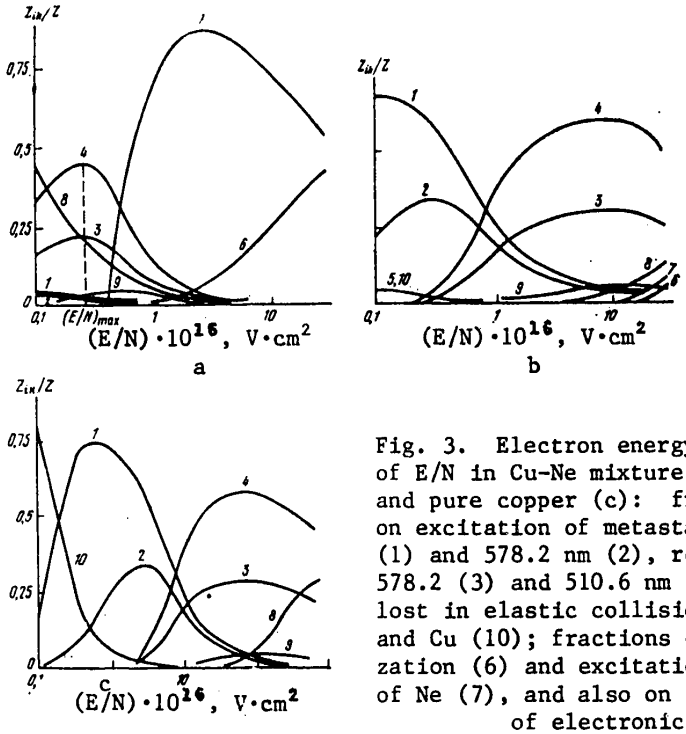

Fig. 3. Electron energy balance as a function of E/N in Cu-Ne mixture at $X = 10^{-4}$ (a), 10^{-1} (b) and pure copper (c): fractions of energy expended on excitation of metastable levels of lines 510.6 (1) and 578.2 nm (2), resonant levels of lines 578.2 (3) and 510.6 nm (4); fractions of energy lost in elastic collisions with atoms of Ne (5) and Cu (10); fractions of energy expended on ionization (6) and excitation of electronic levels of Ne (7), and also on ionization (8) and excitation of electronic levels of Cu (9)

atom concentration. For example $(E/N)_{max}$ is equal to $2\cdot10^{-16}$ and 10^{-15} for $X = 10^{-2}$ and 10^{-1} respectively. Consequently at $X = 10^{-1}$, five times the electric field strength compared with the case of $X = 10^{-2}$ is required to attain values of E/N that maximize the energy expended on excitation of resonant levels at the same density of atoms. Thus, as the temperature of the active medium in copper vapor lasers with neon increases, there is an increase in the requirements for electric field strength as a consequence of the increase in $(E/N)_{cr}$ and $(E/N)_{max}$, and there is also a reduction in the energy input to the discharge due to the decrease in electron drift rate with increasing X. In all probability, it is these factors that lead to an optimum in the relation between specific energy output and temperature of the medium in a copper vapor laser with buffer gas. This effect is not observed in copper vapor lasers without buffer gas. According to calculation of the energy balance of electrons in pure copper (see Fig. 3c), the fraction of energy expended on excitation of resonant levels first increases to values of $E/N \cong 10^{-14}$ V·cm² as the copper atom density increases (at constant voltage across the discharge capacitance in this case, E/N is decreasing),

X	$(E/N)_{cr}\times10^{-16}$, V·cm²	$(E/N)_{max}\times10^{-16}$, V·cm²
10^{-4}	0,04	0,2
10^{-3}	0,08	0,6
10^{-2}	0,25	2
10^{-1}	1,2	10
pure copper	10	80

and then begins to fall, approaching zero at $E/N \cong 10^{-16} V \cdot cm^2$. For example, at a voltage across the discharge gap of ~10 kV and interelectrode spacing of ~2.5 cm, such a value is realized only at a copper atom density of $4 \cdot 10^{19}$ cm^{-3}. Besides, in the case of exploding conductors the atoms are dispersed and the vapor temperature drops, possibly below the temperature corresponding to thermal population of the metastable state, which has been observed experimentally specifically in Ref. 12.

Thus the results of calculations of electron energy balance show that in a discharge in pure copper right up to copper atom densities of $\sim 10^{18}$ cm^{-3}, the upper laser levels can be effectively excited, and the absence of appreciable population of the metastable level is conducive to an increase in the specific energy output in the copper vapor laser at vapor pressure close to the atmospheric level.

Our calculations did not take consideration of many processes responsible for the emission characteristics of the laser. Therefore the results can only be used to estimate the limiting copper concentration in the copper vapor laser.

REFERENCES

1. Buzhinskiy, O. I., Krysanov, S. I., Slivitskiy, A. A., PRIBORY I TEKHNIKA EKSPERIMENTA, No 4, 1979, p 274.
2. Smilanski, J., Kerman, A., Levin, L. A., Rez, G. E., OPTICS COMMS, Vol 25, 1978, p 79.
3. Isakov, I. M., Leonov, A. G., PIS'MA V ZHURNAL TEKHNICHESKOY FIZIKI, Vol 2, 1976, p 865.
4. Sherman, B., J. MATH. ANALYT. APPLIC., Vol 1, 1960, p 342.
5. Pevgov, V. G., candidate's dissertation, Moscow Physicotechnical Institute, 1977.
6. Aleksakhin, I. S., Borovik, A. A., Starodub, V. L., Shafran'osh, ZHURNAL PRIKLADNOY SPEKTROSKOPII, Vol 30, 1979, p 236.
7. Borozdin, V. S., Smirnov, Yu. N., Sharonov, Yu. D., OPTIKA I SPEKTROSKOPIYA, Vol 43, 1977, p 384.
8. Corliss, C., Bosman, W., "Veroyatnosti perekhodov i sil ostsillyatorov" [Probabilities of Transitions and Oscillator Strengths], Moscow, Mir, 1968.
9. Sobel'man, I. I., "Vvedeniye v teoriyu atomnykh spektrov" [Introduction to the Theory of Atomic Spectra], Moscow, Fizmatgiz, 1964.
10. Trajmar, S., Williams, W., Srivastava, S. K., J. PHYS. B., Vol 10, 1977, p 3323.
11. Pavlov, S. I., Rakhovskiy, V. I., ZHURNAL EKSPERIMENTAL'NOY I TEORETICHESKOY FIZIKI, Vol 52, 1967, p 21.
12. Shukhtin, A. M., Mishakov, V. G., Fedotov, G. A., Ganeyev, A. A., OPTIKA I SPEKTROSKOPIYA, Vol 39, 1975, p 785.

6610
CSO: 1862/14

UDC 621.375.82+533.601

ACTIVE MEDIA FOR CO_2 GASDYNAMIC LASERS USING COMBUSTION PRODUCTS OF LOW-NITROGEN FUELS

Moscow KVANTOVAYA ELEKTRONIKA in Russian Vol 8, No 8(110), Aug 81
(manuscript received 18 Dec 80) pp 1846-1849

[Article by N. V. Yevtyukhin, Institute of Chemical Physics, USSR Academy of Sciences, Chernogolovka]

[Text] An experimental study is done on the way that optical gain K_0 depends on stagnation parameters in a CO_2 gasdynamic laser using combustion products of model fuels with low nitrogen content: atomic fraction of N in the composition $\xi_N = 0.4$. The experiments were done in the following ranges of variation in the pressure and temperature of the gas in the prechamber: $p = 4-25$ atm, $T = 1300-2300$ K. It is shown that as the stagnation parameters increase, there is a considerable reduction in the range of working media with $\xi_N = 0.4$ that show active properties. The compositions of combustion products that are characterized by comparatively high values of K_0 are formed when fuel is burned with an excess oxidant ratio different from unity.

1. Introduction

In Ref. 1-3 an experimental and theoretical study was done on the amplification and energy characteristics of multicomponent active media of CO_2 gasdynamic lasers that are produced by burning different fuels with C-, H-, O-, N-elemental composition. These papers determined the major principles governing the behavior of laser characteristics with a change from one composition of combustion products to another for fuels with fixed fraction of N in the composition $\xi_N = 0.6$. A value of $\xi_N = 0.6-0.7$ is typical of compositions produced by diluting nitro compounds and hydrocarbons with air. In this case the concentration of molecular nitrogen in the working medium is approximately 60-75 mol.% [Ref. 4, 5]. To evaluate the effectiveness of using high-enthalpy fuels that contain nitro groups and other nitrogen compounds and are undiluted by nitrogen or air, it is of interest to study the change in the way that the weak-signal gain K_0 depends on composition and stagnation parameters for working media with a lower value of ξ_N in the composition.

This paper gives the results of an experimental study of amplification of resonant emission in multicomponent active media with $\xi_N = 0.4$ done in accordance with the approach and techniques presented in Ref. 1, 4, 6.

2. Method of the Experiment

The experiments were done on a gasdynamic laser with combustion chamber operating in the quasi-cw mode. To produce and study high-temperature laser-active media of predetermined composition and temperature, a method was used that is based on igniting model mixtures of C_2H_2, H_2, CO, O_2, N_2O, O_2 and N_2 under isochronous conditions [Ref. 6]. The combustion products expanded through a flat profiled nozzle with height of the critical cross section of 0.03 cm, degree of expansion of 50, and width of 40 cm. The active media were probed at a distance of 5.3 cm downstream from the critical cross section of the nozzle by a cw CO_2 electric discharge laser operating on transition P18. Processes of combustion and discharge of the gas through the nozzle were monitored by two inductive pressure sensors located in the wall of the combustion chamber (p_1) and preceding the nozzle inlet (p_2).

3. Results of the Experiments and Discussion

The initial data and major results of the experiments are presented in tables 1 and 2 and in figures 1 and 2. Table 1 shows the compositions of ten model fuel mixtures used in the work, initial pressures in the chamber p_H before initiation

TABLE 1

№	Model fuel mixture composition, mole/kg							p_H, atm	$T_{гр}$, K	$T_{гэ}$, K
	C_2H_2	H_2	CO	O_2	N_2O	CO_2	N_2			
1	1,03	—	2,06	16,48	—	—	13,73	4,4	2500	2160
2	1,01	—	3,18	18,71	—	0,86	13,46	4,4	2500	2370
3	1,05	—	3,49	11,20	—	2,82	14,01	4,2	2500	2320
4	1,05	—	3,67	8,13	—	4,81	14,13	4,2	2500	2320
5	1,07	—	2,32	—	8,74	8,38	5,52	4,0	2500	2240
6	1,08	—	7,25	—	7,25	5,68	7,12	4,0	2500	2330
7	1,09	—	12,62	—	6,11	2,57	8,42	4,0	2500	2300
8	1,76	1,64	—	5,76	—	7,82	15,09	4,2	2500	2270
9	1,21	4,80	—	6,02	—	7,20	16,05	4,0	2500	2150
10	—	12,38	—	6,88	—	5,15	18,32	4,6	2500	2280

TABLE 2

№	Main components of equilibrium composition of combustion products, mol.% (T = 1500 K, p = 10 atm)							p_{opt}, atm	T_{opt}, K	K_{0max}, $м^{-1}$
	N_2	CO_2	H_2O	CO	O_2	H_2	NO			
1	43,2	13,0	3,2	—	40,5	—	0,1	10	1670	0,52
2	44,6	20,1	3,3	—	31,8	—	0,1	7,1	1620	0,66
3	46,2	27,7	3,5	—	22,2	—	0,1	6,5	1590	0,62
4	47,9	35,9	3,6	—	12,5	—	0,1	6,0	1570	0,49
5	49,7	44,7	3,7	—	1,8	—	0,1	6,1	1500	0,25
6	47,1	32,4	2,9	17,0	—	0,6	—	7,4	1620	0,64
7	44,0	18,0	1,8	34,8	—	1,5	—	10	1740	0,63
8	49,7	37,3	11,2	—	1,8	—	—	5	1440	0,36
9	49,7	29,8	18,6	—	1,8	—	—	5	1400	0,27
10	49,7	14,9	33,5	—	1,8	—	—	4	1330	0,02

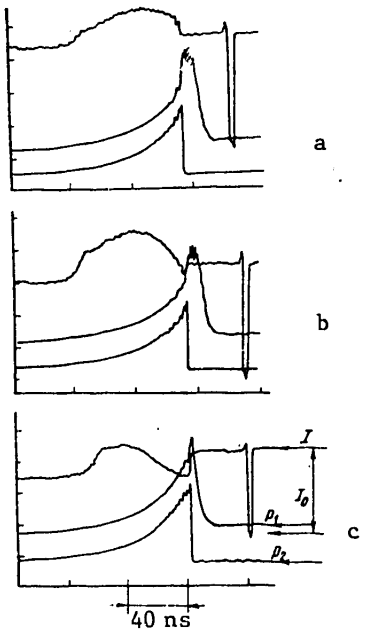

Fig. 1. Recordings showing the change in the probing radiation signal in active media with $\xi_N = 0.4$ for different ratios of CO_2 and O_2 (compositions 1 (a), 3 (b) and 5 (c) of the tables): I_0--zero signal level; p_1, p_2--profiles of signals from pressure sensors in the chamber walls and prenozzle space respectively

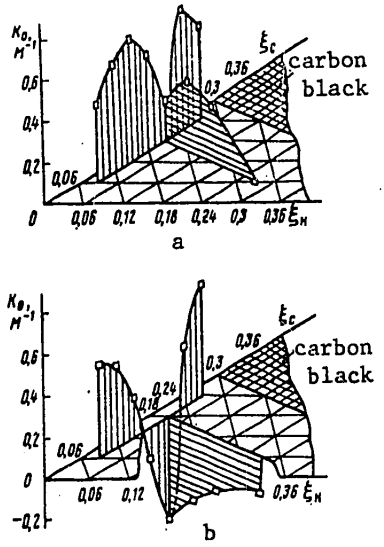

Fig. 2. Optical gain K_0 in CO_2 gasdynamic laser using combustion products as a function of the elemental composition of fuels with relatively low nitrogen content in the composition ($\xi_N = 0.4$): $p = 5$ (a) and 15 atm (b); $T = 1450$ (a) and 1950 K (b)

of the combustion reaction, calculated $T_{гр}$ and average experimental $T_{гэ}$ values of the maximum combustion temperatures. It is clear from Table 1 that the values of $T_{гэ}$ are an average of 7% lower than the calculated values. This systematic deviation is the result of two major factors: heat transfer to the wall, and somewhat premature opening of the diaphragm that separates the combustion chamber from the prenozzle space. The latter factor has a direct influence on the completeness of combustion of the fuel mixtures. However, taking into consideration that the characteristic combustion times in the given case are ≤ 10 ms (see Fig. 1), it should be assumed that the degree of undercombustion decreases considerably during the equalization of perturbations throughout the space in front of the nozzle after the instant of opening of the diaphragm (period of settling to quasi-steady flow).

Table 2 shows the concentrations of major components of equilibrium compositions of the combustion products of the fuel mixtures. These compositions are given for a temperature of 1500 K, which characterizes one of the quasiequilibrium states of the working medium in the chamber preceding the nozzle. Also given there are

the maximum values of gain K_{0max} that were found in the experiments, and the corresponding values of the temperature T_{opt} and pressure p_{opt} in the chamber.

The diagrams of Fig. 2 illustrate the principal trends in the behavior of gain in media with low N_2 content with a transition from relatively low to higher values of stagnation parameters in the prechamber. Here K_0 is plotted as a function of the elemental composition of the model fuel mixtures at fixed values of T and p in the prechamber. The elemental compositions corresponding to the compositions selected for the study are located on two characteristic lines of the diagram: 1) a line on which the atomic fraction of the element H is fixed in the composition $\xi_H = 0.03$ (compositions 1-7 of the tables); 2) a line that corresponds approximately to the stoichiometric proportion of fuel and oxidizer in the model fuel--the line of ternary mixtures N_2-CO_2-H_2O [Ref. 1-3] (compositions 5, 8-10 of the tables). The transition from composition 5 to compositions 8-10 is characterized by an increase in the fraction of water vapor in the combustion products from 3 to 35 mol.% and a simultaneous reduction in carbon dioxide content from 45 to 15 mol.%. In turn, movement along the line $\xi_H = 0.03$ from composition 5 to different sides from the line of ternary mixtures also corresponds to a reduction of CO_2 content in the combustion products, chiefly due to an increase in the concentrations of O_2 or CO. Let us note that on the basis of the results of Ref. 1-3 it can be stated that the behavior of K_0 along the given lines upon the whole determines the relief structure of gain over the entire range of fuel compositions in which we are interested.

Typical recordings showing the behavior of gain in the gasdynamic laser operating in the quasi-cw mode on combustion products of model fuels are given in Fig. 1. The results of processing of these recordings and the way that they are distributed on Fig. 2 show that for high-temperature working media of CO_2 gasdynamic lasers that contain approximately 40-50% N_2 there is much less evidence of the peculiarities noted previously in Ref. 1 in the dependence of K_0 on composition and stagnation parameters. As can be seen from a comparison of the diagrams of Fig. 2, there is an appreciable reduction in the ranges of working compositions with $\xi_N = 0.4$ that show active properties as the stagnation parameters increase. And compositions with the highest values of K_0 are situated farther and farther from the line of ternary mixtures N_2-CO_2-H_2O. Let us note that in our experiments the rms error that characterizes variance of the reproducibility of K_0 is approximately equal to 0.05 m^{-1} on all levels of values of the measured quantity. The result of estimation of the error of measurements of p and T showed that the error in determination of pressure does not exceed 10%, and for pressure--15% of the true value.

Generalizing the experimental data found in Ref. 1 and in this paper, we can conclude that for the entire aggregate of fuel compositions with C-, H-, O-, N-elemental composition that yield a high-temperature medium ($T > 1500$ K) upon combustion with nitrogen composition insufficient for CO_2 gasdynamic lasers ($\xi_N < 0.8$-0.9), preference should be given to compositions both with low hydrogen content ($\xi_H \cong 0.02$-0.06) and with ratio of combustible and oxidative components in the fuel different from the stoichiometric composition. The excess oxidant ratio should differ from unity (to either side) increasingly with decreasing nitrogen concentration in the composition in the fuel mixture and with increasing stagnation parameters.

REFERENCES

1. Yevtyukhin, N. V., Genich, A. P., Yudanov, A. A., Manelis, G. B., KVANTOVAYA ELEKTRONIKA, Vol 5, 1978, p 1013.

2. Genich, A. P., Yevtyukhin, N. V., Kulikov, S. V., Manelis, G. B., Solov'yeva, M. Ye., ZHURNAL PRIKLADNOY MEKHANIKI I TEKHNICHESKOY FIZIKI, No 1, 1979, p 34.

3. Genich, A. P., Kulikov, S. V., Manelis, G. B., ZHURNAL PRIKLADNOY MEKHANIKI I TEKHNICHESKOY FIZIKI, No 4, 1979, p 11.

4. Genich, A. P., Yevtyukhin, N. V., Manelis, G. B., FIZIKA GORENIYA I VZRYVA, No 5, 1975, p 755.

5. Kozlov, G. I., Ivanov, V. N., Korablev, A. S., Selezneva, I. K., ZHURNAL EKSPERIMENTAL'NOY I TEORETICHESKOY FIZIKI, Vol 68, 1975, p 1647.

6. Yevtyukhin, N. V., Genich, A. P., Manelis, G. B., FIZIKA GORENIYA I VZRYVA, No 4, 1978, p 36.

6610
CSO: 1862/14

UDC 541.141.4

SPECTROSCOPY AND PRIMARY PHOTOLYSIS PROCESSES OF IODIDES FOR PHOTODISSOCIATION IODINE LASERS (REVIEW)

Moscow KVANTOVAYA ELEKTRONIKA in Russian Vol 8, No 7(109), Jul 81 (manuscript received 4 Dec 80) pp 1397-1424

[Article by A.M. Pravilov, Leningrad State University imeni A.A. Zhdanov]

[Text] The general laws governing diatomic and polyatomic iodide spectroscopy in the ultraviolet and far ultraviolet regions of the spectrum are treated. The spectroscopic properties are compared with the existing data in the literature on their primary photolysis processes; the major attention in this case is devoted to alkyl iodides and perfluoralkyl iodides. An attempt is made to interpret the observed laws.

Introduction

Lasing was produced for the first time more than 15 years ago based on the transition

$$J\,(^2P_{1/2}) \rightarrow J\,(^2P_{3/2}) + h\nu,\ \lambda = 1315\ \text{нм} \qquad (1)$$

with the photolysis of a number of alkyl iodides and CF_3I in their first absorption bands [1]. Since that time, the power, efficiency and energy throughput of photodissociation iodine lasers (FIL) operating with this transition have been increased considerably; more successful iodides (RI) have been selected: the working materials of photodissociation lasers and the secondary processes which govern the operating efficiency of photodissociation iodine lasers have been studied in considerable detail.

Some of the most important parameters which govern the efficiency of RI usage in photodissociation iodine lasers are the spectral functions of the absolute quantum yields of the formation of $I(^2P_{1/2})$ - I* and $I(^2P_{3/2})$ - I with RI photolysis:

$$RJ + h\nu \nearrow R + J^*,\ \Phi_{J^*}(\lambda); \qquad (2)$$

$$RJ + h\nu \searrow R + J,\ \Phi_J(\lambda) \qquad (2')$$

and the values of the integral quantum yields of these atoms in the first RI absorption band:

$$\Phi_{J^*} = \int_{\lambda_1}^{\lambda_2} \Phi_{J^*}(\lambda)\,\sigma(\lambda)\,d\lambda \Big/ \int_{\lambda_1}^{\lambda_2} \sigma(\lambda)\,d\lambda;$$

$$\Phi_J = \int_{\lambda_1}^{\lambda_2} \Phi_J(\lambda)\,\sigma(\lambda)\,d\lambda \Big/ \int_{\lambda_1}^{\lambda_2} \sigma(\lambda)\,d\lambda,$$

where $\sigma(\lambda)$ is the total RI absorption cross-section; λ_1 and λ_2 are the boundaries of the first absorption band. However, the methods of deriving information on these quantities and the theoretical representations of the RI photodissociation processes have been extremely unsatisfactory right up to the present [2]. For this reason, the selection of the working material for photodissociation iodine lasers has been made empirically.

Despite the definite successes in increasing the efficiency of photodissociation iodine lasers, the question of the choice of the most suitable working materials for lasers of this type, from our point of view, cannot be considered closed, since the limit still has not been reached here. As will be shown below, when predicting the efficiency of various RI reactions, one must first of all take into account the ratio of the reaction rate constants:

$$R + R\,(+M) \rightarrow R_2\,(+M), \tag{3}$$

$$J + R\,(+M) \rightarrow RJ\,(+M), \tag{4}$$

$$J^* + R\,(+M) \rightarrow RJ\,(+M), \tag{5}$$

$$J^* + R \rightarrow J + R \tag{5'}$$

and the quantities Φ_{I^*} and Φ_I. Since the synthesis of the materials and the measurement of the values of Φ_{I^*} and k_3-k_5 for them are expensive and lengthy processes, then for a substantiated and economically expedient selection and synthesis of new RI materials, it is essential to have concepts concerning the spectroscopy of iodides and the mechanism for their photodissociation which are as clear-cut as possible.

Unfortunately, these questions have not been discussed in sufficient detail in the literature and there is only fragmentary information in the original papers of Mulliken [10, 11, 17-21], Goodeve and associates [3], Donohue and Wiesenfeld [4, 5], as well as in the reviews and monographs of [6-9]. It is expedient for this reason to discuss the spectroscopy of iodides and the existing experimental data on their photodissociation processes within the framework of a single review for the purpose of establishing the general governing laws for the quantities $\Phi_{I^*}(\lambda)$ and $\Phi_I(\lambda)$ in the case of RI photodissociation.

The general laws governing the spectroscopy of the triplet state of the molecules are treated in the first section of this review, including diatomic molecules, for the case of a large spin-orbital interaction, as well as some aspects of the theory

of the photodissociation of polyatomic molecules which are relevant to the issue under discussion. The existing experimental data on the processes of iodide photodissociation are compared in the second and third sections with the information on their spectroscopic properties; the treatment runs from simple molecules to complex ones.

1. General Laws Governing Iodide Spectroscopy. The Relationship of the Photodisintegration Mechanism of Molecules to Their Absorption Spectra.

In terms of the Λ-s (or Λ-Σ) coupling [7, p 156; 10, 11], similar to the Russell--Saunders coupling in atoms [12], the ground states of all of the iodides under considerations R'I (R' = H, X is a halogen atom, CH_3 and other organic radicals) are singlet states because of the closed nature of the electron shells in these states (for example, see [7, p 251; 8, p 630]), while the first excited states are triplets. The latter is a consequence of Hund's rule [13, p 81] applied to the ground states of $I(^2P)$ and R = $H(^2S)$, $X(^2P)$, $CH_3(^2A''_2)$, etc. For this reason, for an understanding of iodide spectroscopy we shall briefly consider some of the questions of triplet state molecular spectroscopy, including the case of large spin-orbital interaction. The major question which will be of interest to us here is which factors govern the probability of a radiation transition from the ground state of R'I to states which correlate with the dissociation products of R'I:R' + + I* and R' + I.

As is well known, the probability of an electrical dipole transition from the ground state, described by the total electron wave function Ψ''_{es} per unit of radiation density, to a state described by Ψ'_{es}, is equal to:

$$B = \frac{8\pi^3}{3h^2} |R_e|^2, \tag{6}$$

where

$$R_e = \langle \Psi'_{es} | M_e | \Psi''_{es} \rangle \tag{7}$$

is the electron transition moment; M_e is the dipole moment operator [8, pp 128, 433].

In the case considered here, one of the states in the terms of the Λ-s coupling is a singlet, while the other is a triplet. Consequently, in the absence of spin-orbital interaction, i.e., when Ψ''_{es} and Ψ'_{es} are purely spin states [13, p. 202], the total electron wave function is described by the product of the orbital wave function of Ψ''_e, Ψ'_e, which depends only on the spatial coordinates, by the spin wave function β, which depends on the spin coordinates: $\psi_{es} = \psi_e\beta$. For this reason, because of the orthogonality of the spin functions belonging to different multiplet states, $R_e = 0$ [14, p. 288].

However, in real molecules, the interaction of the spin moment of an electron with the magnetic field which causes its orbital motion leads to the presence of spin-orbital interaction and the concept of a purely spin state is a rather rough approximation. The total electron wave function in this case is not described by the product $\Psi_e\beta$, but has a more complex form $\Psi_{es} = \Psi_e\beta + \chi_{es}$, where χ_{es} depends both on the spatial and the spin coordinates [8, p. 26]. All of this leads to the fact that different multiplet states, if these are permitted by the selection rules, can "interact" and "mix", i.e., their "true" wave functions are

superimpositions of unperturbed wave functions obtained in a zero approximation (without taking spin-orbital interaction into account). In a first approximation, without taking electron-vibration interaction into account, which plays a lesser role in the case under discussion here than spin-orbital interaction, the true wave function of a triplet state (in terms of the Λ-s coupling) is:

$$^3\Psi^r_{es} = {}^3\Psi^{0r}_{es} + \sum_k \frac{\langle {}^1\Psi^0_{esk} | H_{sl} | {}^3\Psi^{0r}_{es} \rangle}{E^0_3 - E^0_{1k}} \Psi^0_{esk}, \tag{8}$$

while for the singlet state:

$$^1\Psi_{es} = {}^1\Psi^0_{es} + \sum_m \sum_{r=-1}^{1} \frac{\langle {}^3\Psi^{0r}_{esm} | H_{sl} | {}^1\Psi^{0}_{es} \rangle}{E^0_1 - E^0_{3m}} {}^3\Psi^{0r}_{esm}, \tag{9}$$

where $^1\psi^0_{es}$ and $^3\psi^{0r}_{esm}$ are the total electron wave functions of the "unperturbed" singlet and triplet states (r = -1, 0, 1); E^0_{1k} and E^0_m are their energies; H_{sl} is the spin-orbital interaction operator; the summing is carried out with respect to the k-th singlet and m-th triplet states [13, p. 218; 14, p.292]. A precise calculation of the operator H_{sl} is not feasible, even when neglecting the interaction of the spin moment of the i-th electron with the orbital moment of the j-th electron:

$$H_{sl} = \frac{\hbar}{4m^2c^2} \cdot \sigma (\text{grad } V \times p) \tag{10}$$

(Here, σ and p are spin and orbital moment operators; V is the potential at the point where the electron is located). In some cases, for example, for a hydrogen atom, this operator can be precisely calculated; the value of the spin-orbital splitting in the triplet state, which characterizes the amount of spin-orbital interaction E_{sl}, is proportional to z^4/n^3 in this case, where z is the nuclear charge and n is the principal quantum number [13, p. 206; 15]. We will note that in other fields also, the sharp dependence of the spin-orbital interaction on the nuclear charge and distance of the electrons from heavy nuclei is preserved. In calculating H_{sl} in molecules, for example, McClure's approximation of the central field can be used [13, p. 207; 16].

However, for the following treatment, the only fact of importance to us is that because of the complete symmetry of H_{sl} in the point group of symmetry of the molecule, including both the spatial and spin coordinates [13, p. 226], the correction terms in (8, 9) are other than zero if $^1\psi^0_{esk}$ and $^3\psi^{0r}_{es}$ or $^3\psi^{0r}_{esm}$ and $^1\psi^0_{es}$ belong to the same types of symmetry (irreducible representations) in the given point group. For equation (8) this means that at least one of the

direct product components of the irreducible representations of the electron orbital and spin wave functions of the r-th component of the triplet state should match the irreducible representation of at least one of the orbital wave functions of the singlet states, or what is the same thing, there should be the following fully symmetrical representation in the expansion of the direct product of the irreducible representations of the total electron wave function of the triplet state and of at least one of the k singlet states [8, p 27; 13, p 226]:

$$\Gamma_{1_{\Psi_{es}^{0k}}} \times \Gamma_{3_{\Psi_e^0}} \times \Gamma_{3_{\beta^0}} = \Gamma_i + \cdots \tag{11}$$

(the irreducible representation of the singlet state spin function is completely symmetrical).

A similar result is obtained for equation (9) if:

$$\Gamma_{1_{\Psi_e^0}} \times \Gamma_{3_{\Psi_{em}^0}} \times \Gamma_{3_{\beta^0}} = \Gamma_i + \cdots \tag{11'}$$

The classification of electron motion in a molecule according to types of symmetry in the case of a large spin-orbital interaction depends on the molecule geometry, the nuclear charge, etc., and for this reason, it is necessary to become familiar with the classification of various types of coupling in molecules for the group theory analysis of equations (7) - (11) in the case where the electron states are described in terms of the Λ-s coupling.

The spectroscopy of diatomic molecules with large spin-orbital interaction (including diatomic halogens) has been developed primarily in the works of Mulliken [10, 11, 17-21] (also see [22-25]).

As is well known, in the case of spin-orbital interaction in even one of the atoms incorporated in a molecule, the axial electrical field, if it exists in the molecule, may not break the coupling of the orbital moment I of an electron to spin moment s. In this case, the total electron moment of momentum $\boldsymbol{j} = \boldsymbol{l} + \mathrm{s}$ precesses about the axis of the diatomic molecule Z, and only a quantum number corresponding to the projection Ω of the total moment of momentum $\boldsymbol{J} = \sum_i \boldsymbol{j}_i$ onto the Z axis is a "good" quantum number. The projections of the total orbital moments of momentum $\boldsymbol{L} = \sum_i \boldsymbol{l}_i$ and the spin of the molecule $S = \sum_i s_i$ onto the Z axis (Λ and Σ respectively) become meaningless: the corresponding quantum numbers Λ and S also become meaningless along with them. This rough description of the coupling of the moments in a diatomic molecule in the presence of strong spin-orbital interaction corresponds to Hund's case C [7, p 165; 10].

Mulliken treated several variants of cases of Hund's C coupling in a series of papers.

Case "C with close nuclei" [11, 17]. Because of the closeness of the nuclei, the axial electrical field component is small, the precession of the orbital moment about the Z axis is weak and L, S, J_a (J in the atom) and Ω are "good" quantum numbers (admittedly, the first three are not completely so). This case has no direct bearing on the following presentation.

Ω-ω coupling [11, 18, 21, 24]. If the molecule can be represented as a charged core, characterized by quantum numbers Λ_c, Σ_c and Ω_c with an electron sufficiently

remote from it (so that the interaction is weak), then the state of the molecule can be described by considering the projections of the orbital and spin moments of the core and this electron on the internuclear axis. For example, for the Rydberg states of diatomic molecules R'I, where R' = H(^{2}S), X(^{2}P), the electron configuration of the valence shell has the form [18]:

$$R'J\left[\left(\sigma^2\pi_R^4\pi^3\right)^2\Pi_{3/2}\sigma^*\right]_{2,1}, \tag{12}$$

$$R'J\left[\left(\sigma^2\pi_R^4\pi^3\right)^2\Pi_{1/2}\sigma^*\right]_{0,1}; \tag{13}$$

and the electron configuration I_2 in this case is:

$$J_2\left[\left(\sigma_g^2\pi_u^3\pi_g^4\right)^2\Pi_{3/2u}\sigma_g^*\right]_{2,1u}, \tag{14}$$

$$J_2\left[\left(\sigma_g^2\pi_u^3\pi_g^4\right)^2\Pi_{1/2u}\sigma_g^*\right]_{0,1u} \tag{15}$$

(The configuration of the $R'J^+$ ion is written in the parentheses). The state R'J is characterized in this case by the quantum numbers S_c, Λ_c, Σ_c and Ω_c, $\Omega = \Omega_{c\pm1/2}$; the spin quantum number of the molecule has no meaning. The states of the molecule having identical quantum numbers $\Lambda = \Lambda_c$ and Ω, and naturally also the parity g, u and the properties with respect to reflection in the plane passing through the Z(+,-) axis, the same type of symmetry, they "mix" and "are repelled". In other words, the "true" wave functions, i.e., those obtained in a sufficiently good approximation, of the states belonging to the same type of symmetry are the linear combination of "old" unperturbed states. This applies in particular to the $^3\Pi_1$ and $^1\Pi$ states (in terms of the Λ-s bond) of heteroatomic molecules. For this reason, as compared to the case of the Λ-s bond, the intensity of the $^1\Pi \leftarrow X^1\Sigma^+$ transition falls off, while that of the transition $^3\Pi_1 \leftarrow X^1\Sigma^+$ increases. The fact that the R'I states described by configurations (12)-(15) form doublet pairs $^3\Pi_0$, $^1\Pi$ and $^3\Pi_1$, $^3\Pi_2$ (in terms of the Λ-s bond) with an energy interval between these pairs on the order of the spin-orbital interaction energy $E_{s\ell}$, equal in this case to $\Delta E_{^2\Pi_{3/2},\ ^2\Pi_{1/2}}$, is also significant in this case; the splitting in the doublet is on the order of the singlet-triplet splitting energy $\Delta E_{^3\Pi,^1\Pi}$, which is a great deal smaller here than $E_{s\ell}$ (Figure 1).

Case "C with distant nuclei", type I, type II. [11, 17, 21, 23, 24]. If the interatomic spacing in the molecule is sufficiently great, while the dissociation energy is small (for example, I_2), then the spin-orbital coupling in the atoms comprising the molecule can be preserved because of the axially molecular field and the total moment of the atom J_a does not become meaningless. In this case, the electron state of the molecule is characterized by only one of the quantum numbers Ω (Ω is the sum of the projections of J_{a1} and J_{a2} onto the Z axis); the quantum numbers Λ, S and Σ are meaningless. Naturally, the properties of

symmetry (g, u; +, -) are preserved. Mulliken breaks the "C with distant nuclei" case down into "C, type I" and "C, type II". In the first case, the states with same type of symmetry belonging to different molecular configurations, but which are formed from identical atomic configurations or having the same types of symmetry within the framework of the Λ-s coupling "interact" and "mix"; in the second case, states formed from different atomic configurations and not having the same types of symmetry within the framework of the Λ-s coupling can interact. We will consider the details of these coupling types in the discussion of the I_2 molecule; we will only note here that in the case of the "C, type I, type II" coupling, the $^3\Pi_0$ state splits into $^3\Pi_0^+$ and $^3\Pi_0^-$ (0^+ and 0^- in terms of the "C" coupling) and there is a change in the mutual arrangement of $^3\Pi_2$, $^3\Pi$, $^3\Pi_0^+$, $^3\Pi_0^-$ and $^1\Pi$ (in terms of the Λ-s coupling; 2, 1, 0^+, 0^- and 1 in terms of the "C" coupling) as compared to the Ω-ω coupling because of the interaction of these states with higher states.

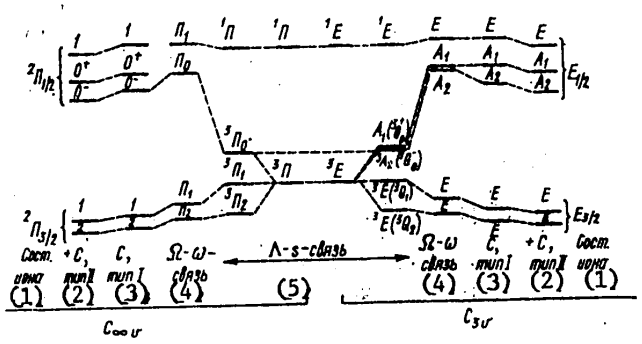

Figure 1. The mutual arrangement of the molecular energy levels for an electron configuration of $\sigma^2\pi^4\pi^3\sigma^1\ ^{1,3}\Pi$ (symmetry group $C_{\infty v}$) and $\ldots e^3a_1^{1,3}E(C_{3v})$ for the case of large and small spin-orbital interactions (based on the data of [8, p.348; 24, 43]). The positioning of the levels is approximate; the spin-orbital interaction increases in strength from the center towards the edges.

Key: 1. Ion state;
2. C, type II;
3. C, type I;
4. Ω-ω coupling;
5. Λ-s coupling.

It is also important for us that in the case of the "C, type I, type II" coupling, the possibilities are increased for the "interaction" of states, since of the quantum numbers, only Ω has any meaning.

Thus, the difference in the Ω-ω and "C, type I type II" couplings reduces to a different classification of the electron states, and consequently, to different prohibitions on "mixing", as well as to a different mutual arrangement of these states. What this leads to will be seen in the review of the spectroscopy and photochemsitry of specific iodide molecules. We will only note here that the various bond types can be realized not only in different molecules, but in different states of the same molecule or in one state of a molecule, but with different interatomic spacings [24].

To estimate the probability of a radiation transition in various R'I molecules, it is necessary to first of all establish what type of coupling describes the given molecule in the Franck-Condon transition region or (when considering polyatomic molecules), which of the types of couplings of diatomic molecules is most suited to the description of the R'-I coupling in this molecule. One must further establish which states can "mix" with states entrained in the radiation transition, and to estimate, or if possible, calculate the effect of this "mixing".

As will be shown below, the consideration of just this aspect of the photodissociation process is insufficient to describe the photodecomposition of R'I and estimate the quantities Φ_{I*} and Φ_I. Nonadiabatic processes of state interaction are also of great importance, where these states correlate with R' + I* and R' + I in the Franck-Condon transition region as well as in the case of large values of r_{C-I}, i.e., processes, the influence of which can be manifest when the R' radicals and the I, I* atoms break up (see below for the theory of semicollisions).

The theory of photodisintegration of polyatomic molecules has as yet been quite poorly developed. In principle, any such theory should answer three interrelated groups of questions which to some extent apply to the topic under discussion:

1. How do the spectral functions of the total or partial absorption cross-sections of a molecule depend on its photodisintegration mechanism; what information can be derived from these spectra? How is a molecule absorption spectrum to be resolved into partial cross-sections corresponding to a transition to molecular states which disintegrate via one channel or another?

2. How does the probability of molecular disintegration via any channel in the presence of nonadiabatic processes of state interaction of the molecule depend on the photon energy?

3. What should the distributions of the photodissociation products of a molecule be via a given channel in terms of the kinetic energy, vibrational-rotational excitation of polyatomic photofragments, and the angular distribution of the dispersal of all the photofragments with the absorption of a light quantum of any energy throughout the entire absorption spectrum of this molecule?

The approaches to the solution of these problems which have been developed at the present time do not make it possible to resolve them even in the case of the photodissociation of triatomic molecules. Some of the literature known to us has

been devoted to attempts to obtain answers to the first of the questions considered here. A critical analysis of this literature does not come within the scope of our task, and for this reaon we will discuss only its applicability to the study of iodide photochemistry.

As is well known, the absorption spectrum of a diatomic molecule in the case where it corresponds to a transition to the repulsion branch of the upper state or to a purely repulsive state is approximated quite well by a gaussian distribution or a gaussian distribution corrected by a frequency factor [7; p. 282]. Since the first absorption band of alkyl iodides and perfluoralkyl iodides likewise has a bell-shaped form, while their photodissociation process is basically described by reactions (2) and (2'), it seems enticing to employ the diatomic approximation (assuming the mass of R to be concentrated in a point and neglecting the vibrational-rotational excitation of R) to describe the photodissociation of these molecules and to resolve their absorption spectrum into partial cross-sections corresponding to the dissociation of these molecules via the channels (2) and (2') [3]. However, this model is too rough; naturally, it cannot yield any information on the vibrational-rotational excitation of the R radical. The limited nature of its application to polyatomic molecules also follows, if only from the fact that in the case of certain properties of the upper repulsive states, at least of linear triatomic ABC molecules, the vibrational excitation of the AB radical

$$ABC + h\nu \rightarrow AB^* + C \qquad (16)$$

can lead to oscillations in the ABC absorption spectrum [27, 28]. It is therefore not surprising that no successful attempts to apply the diatomic model to the photodissociation processes of polyatomic RI molecules have been described in the literature, as far as we know.

As far as the second of the questions under consideration is concerned, there have been successful attempts to calculate the relative yield of photodissociation products in the presence of nonadiabatic processes for the photodissociation of diatomic molecules [29-31]. We shall touch upon this question later in the discussion of the photodecomposition processes for IX, X = F, Cl, Br.

A discussion of the techniques of calculating the vibrational-rotational excitation and angular distribution of the dispersal of the photo fragments with the photodissociation of the molecules does not come within the scope of this review, since we are directly interested here only in the spectral functions of the absolute quantum yields of the atoms in the case of molecular photodissociation. We will note only that neither the quasidiatomic model (for example, see [32]) nor the "semicollision" model (for example, see [33]) provides satisfactory agreement with the experimental data on vibrational excitation of R' in the case of photodissociation for even ICN [33, 34], not to mention CH_3I [32]. Satisfactory qualitative agreement between theory and experiment has been obtained only in the more precise models of the photodissociation of linear triatomic molecules, in

particular, ICN [35-37]. One can become familiar with the various computational models for the photo fragment excitation energy, for example, in [26, 37-39].

We shall now discuss how the general governing laws for iodide spectroscopy we considered above are manifest in specific diatomic molecules; this will aid us in the discussion of questions concerning polyatomic iodides.

2. The Photochemistry of Diatomic Iodides

An enormous amount of literature has been devoted to the study of the spectroscopic properties of diatomic iodides, especially I_2. However, we will be interested here only in those papers which deal with the photodisintegration processes of iodides, i.e., the processes of photodissociation and predissociation.

Hydrogen iodide HI [11- 21, 40, p. 159; 41-51]. The absorption spectra of hydrogen iodide were studied in [41-44, 50, 51]; quantitative data for the spectral region of $\lambda < 200$ nm, according to the data available to us, were obtained only in [44]. The photochemistry of HI and DI has been poorly studied, and the only more or less reliable data that we have are for only a few wavelengths in A band (see the Table).

The spectroscopy of HI in the first absorption band was discussed in detail for the first time by Mulliken [11, 21]; essentially no substantial changes have taken place in the interpretation of this band since that time (see, for example [49]). Mulliken demonstrated that the type of coupling and the mutual arrangement of the first excited states in the HI molecule should be described by means of Ω-ω coupling, possibly with a slight addition of "C, type I" coupling [11]. Consequently, the first exicted states of HI should comprise two groups of doublets $^3\Pi_2$, $^3\Pi_1$ and $^3\Pi_0$ $^1\Pi$ (see Figure 1). Transitions from the ground state of HI ($X\ ^1\Sigma^+$) to state $^3\Pi_1$, $^1\Pi$ should be observed, where the intensity of the latter transition should "be pumped across" to the $^3\Pi_1 \leftarrow X^1\Sigma^+$ transition; if there is actually a slight addition of "C, type I" coupling, then the transition $^3\Pi_0^+ \leftarrow$ $\leftarrow X\ ^1\Sigma^+$ should be observed ($0^+ \leftarrow 0^+$ in terms of the "C" coupling) as a consequence of the "mixing" of these states with higher states of this same symmetry type (see [11, 51]). The latest experimental data have completely confirmed this interpretation. The resolution of the HI absorption spectrum in partial cross-sections, corresponding to transitions to the $^3\Pi_1$, $^3\Pi_0$ and $^1\Pi$ states, carried out by Wilson and his coworkers based on experimental data on the values of Φ_I^* $\Phi_I^*(\lambda)[\Phi_I^*(\lambda) + \Phi_I(\lambda)]$ at $\lambda = 254$, 266 and 279 nm confirmed Mulliken's predictions of both the mutual arrangement of potential energy curves for these states and (qualitatively) the intensities of the radiation transitions to these states [21, 49] (Figures 2, 3; see the Table).

The photochemistry of HI and DI at $\lambda < 254$ nm and 214 nm respectively, if the erroneous data of Martin et al. is not considered [47, 49], according to the information we have, has not been studied at all; it is only known that some of the rotational lines in their absorption spectra are predissociated [43]. Transitions to Rydberg states are observed in this region of the spectrum, starting with the B band [50] ($\lambda_{max} = 180$ nm), where these states converge to the doublet components of the HI^+ ion ($^2\Pi_{3/2}$ and $^2\Pi_{1/2}$). An interpretation and analysis of

Experimental Data on Iodide Photochemistry

Экспериментальные данные по фотохимии йодидов

R·J	$\Phi_{J\cdot}(\lambda)$	$\Phi_{J\cdot}(\lambda)+\Phi_J(\lambda)$	$\frac{\Phi_{J\cdot}(\lambda)}{\Phi_{J\cdot}(\lambda)+\Phi_J(\lambda)}$	λ, нм nm	Φ_J	$\frac{\Phi_{J\cdot}}{\Phi_{J\cdot}+\Phi_J}$	References Ссылка, примечание Remarks
1	2	3	4	5	6	7	8
HJ	—	—	0,55±0,25 0,36±0,05 0,11±0,14	253,7 266,2 279 >200 >200		<0,2 <0,1	[46] [49] [48] [45]* [4,5]*
J_2	~0	0,94—0,3	~1 0,5—0,0	266,2 501—624 483,5—533			[57,58] (1) [56] на основании [55,59] (в присутствии 350—500 мм рт. ст. He, Xe)
JCN		possibly	0,6—0,3 возможно, 0,4 <0,05 0,5±0,1	266—280 266 >200 >200			[37] [31] [74]* [78]*
CH_3J	$0,90^{+0,1}_{-0,2}$	1,0—0,1 ≥0,99	~0,77 0,75—0,20	254 266,2 300—244 >200 >200 >200 185; 254 147		0,92±0,02 0,76±0,08 0,88±0,04	[117, 119] [32] [112] [4,5]* [108]* [106]* [122] [116]
C_2H_5J	0,79±0,08	0,99±0,01		254 >200		0,69±0,05	[119] [4,5]*
C_3H_7J	0,78±0,08	0,99±0,01		254 >200		0,67±0,04	[118] [4,5]*

Key: 1. Based on [55, 59] (in the presence of 350 to 500 mm Hg He, Xe).

Table, continued:

1	2	3	4	5	6	7	8
CH_3CHJCH_3	0,4±0,2	0,90±0,02		254 >200		<0,1	[118] [4,5]*
C_4H_9J	0,67±0,07	0,99±0,01		254 >200		0,82±0,04	[118] [4,5]*
$CH_3CHJC_2H_5$	0,80±0,08	0,89±0,03		254 >200		<0,1	[119] [4,5]*
$(CH_3)_2CHCH_2J$	0,75±0,07	0,99±0,01		254 >200		0,69±0,04	[119] [4,5]*
$(CH_3)_3CJ$				>200		<0,1	[4,5]*
CD_3J				>200		⩾0,99	[4,5]*
CH_3J	$1_{-0,3}$ 1,0—0,8 0,0±0,1	$1_{-0,1}$ 1,0—0,93 1,0—0,0		254 315—235 265 >200 >200 180—155	$0,94^{+0,07}_{-0,09}$	$0,98^{+0,02}_{-0,09}$ 0,91±0,005 0,91±0,03 0,91±0,09	[117] [2] [111] [4,5]* [106]* [88,120]
C_2F_5J	1,0—0,74	1,0—0,92		315—235 >200 >200	$0,94^{+0,06}_{-0,07}$	$0,96^{+0,04}_{-0,09}$ 0,93±0,02 >0,98	[2] [106]* [4,5]*
C_3F_7J	1,0—0,78 0,1±0,1	1,0—0,95 0,77—0,0	0,978±0,02	315—235 265 >200 >200 180—155	0,86±0,07	$0,88^{+0,02}_{-0,09}$ >0,99 0,995±0,005	[2,110] [111] [4,5]* [106]* [88,120]

Table, continued:

Продолжение таблицы

1	2	3	4	5	6	7	8
CF_3CFJCF_3	1,00—0,34 0,0+0,1	1,00—0,93 0,90—0,0		315—235 >200 >200 180—155	0,51±0,05	0,52+0,09 0,90±0,02 0,93±0,03	[2,110] [4,5]* [106]* [88,120]
C_4F_9J				>200		0,99±0,01	[106]*
$(CF_3)_3CJ$	0,47—0,30	1,00—0,89	0,877±0,013	315—245 265	0,39±0,04	0,40±0,04	[89] [111]
$C_5F_{11}J$	1,0—0,8	—		305—255	—	—	[89]
$(CF_3)_2CFC_2F_4J$	0,70—0,66	1,0—0,92		305—245			[89]
$C_6F_{13}J$				>200		0,99±0,01	[107]*
$CF_3OC_2F_4J$	1,0—0,95 0,0+0,1	1,0—0,94 0,8—0,4		315—235 180—155	$0,98^{+0,02}_{-0,07}$	$0,99^{+0,01}_{-0,07}$	[2,110] [88,120]
CH_3COJ	~0			266			[137]
GeH_3J				>200		0,56	[135]*
HgJ_2	1,0—0,0			320—265			[67]**

* Данные несопоставимы (см. текст).
** Данные, по-видимому, завышены на 20% (см. текст).

* The data are not comparable (see the text);

** The data are apparently overstated by 20 percent (see the text).

APPROVED FOR RELEASE: 2007/02/09: CIA-RDP82-00850R000400080009-0

FOR OFFICIAL USE ONLY

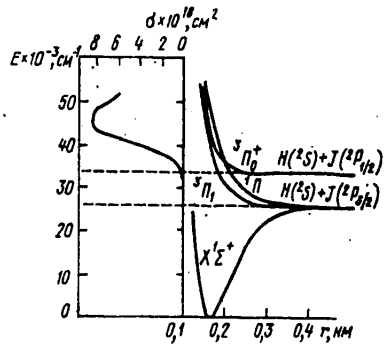

Figure 2. The absorption spectra and the calculated potential curves for HI [49].

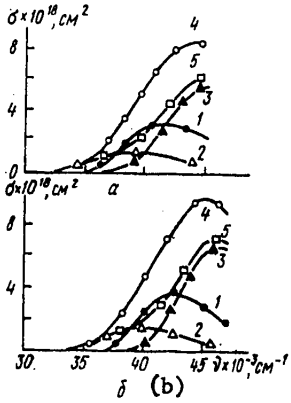

Figure 3. The total (4) and partial absorption cross-sections of HI (a) and DI (b) in the spectral region $\lambda > 214$ nm, corresponding to transitions to the state $^3\Pi_0^+$ (1), $^3\Pi_1$ (2) and $^1\Pi$ (3); 5 is the sum of 2 and 3 [49].

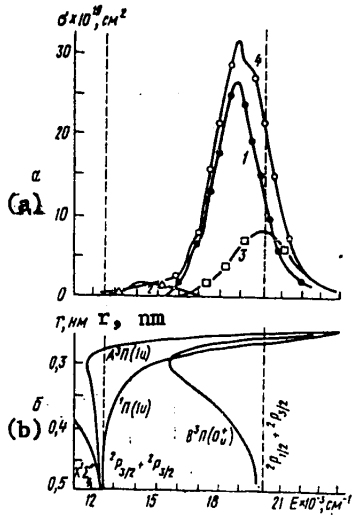

Figure 4. The total (4) and partial absorption cross-sections of I_2 in the spectral region $\lambda > 400$ nm, corresponding to transitions to the states $^3\Pi_{0u}^+$ (1), $^3\Pi_{1u}$ (2), $^1\Pi_u$ (3) (a) and a schematic of the levels of I_2 (b) [24, 61].

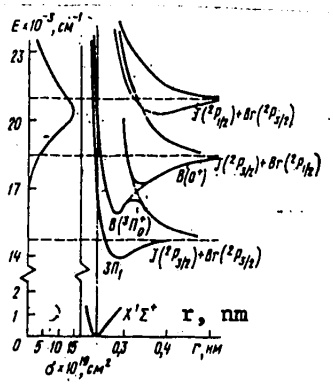

Figure 5. The absorption spectrum and potential energy curves of IBr (based on the data of [29, 67]).

the vibrational-rotational structure in the 42.5 - 180 nm region were made in [43, 51], and also presented there are the spectroscopic constants of the observed electron states. We will note that the nature of the HI absorption spectrum in the 220 - 190 nm spectral region is altogether unclear.

Molecular iodine [21, 23, 24, 40, p 147, 181; 52-62]. As has already been mentioned, considerable research has been devoted to the study of molecular iodine spectroscopy (for a bibliography of the early literature, for example, see [23, 24]). However, only those aspects of I_2 spectroscopy and photochemistry which have a bearing on polyatomic iodides will be of interest to us here.

The absorption spectra of I_2 have been studied, for example, in [52-54] (also see [23, 24]). There is sufficiently reliable data on the photochemistry of I_2 for certain wavelengths in the region $\lambda \geq 266$ nm in [55-59]. Based on these data, the I_2 absorption spectra in the visible and IR regions were resolved into partial cross-sections in [54], where these cross-sections correspond to transitions to lower excited states with a configuration of $\sigma_g^2\pi_u^4\pi_g^3\sigma_g^1$ -- 2431 1 u ($^3\Pi_{1u}$), 0_u^+ ($^3\Pi_{0u}^+$) 1 u ($^1\Pi_u$) (Figure 4). Of these states, only 0_u^+ correlates with I + I*, being a coupling state, in contrast to the similar state of HI ($^3\Pi_0^+$). There is a detailed expansion in [60] which was made on the basis of magnetic circular dichroism spectra with measurements in a solution of I_2 in hexane. A comparison of the data shown in Figure 3 and 4 shows that for I_2 as compared to HI, the contribution of the transition to a state which correlates with I + I* is significantly higher in the initial absorption bands. Simple calculations performed by Mulliken [21, 23], assuming the feasibility of "C, type I + type II" coupling, demonstrated that this effect is due primarily to the "mixing" of the singlet ground state (within the framework of Λ-s coupling) 2440 $X0_g^+$ ($^1\Sigma_g^+$) with the "triplet" state of 2441 0_g^+ ($^3\Pi_{0g}^+$) lying 4.1 eV above it (this is the "C, type I" "mixing" effect, since the data on the state correlate with identical configurations of iodine atoms $p^5 \cdot p^5$). This effect is also due to a certain extent to the "contribution" to the "triplet" state 2431 0_u^+ of the "singlet" ion state 1441 0_u^+ ($^1\Sigma_u^+$), which is realized through the "triplet" 1342 0_u^+ ($^3\Pi_u^+$) state, i.e., the 1441 0_u^+ "mixes" with the 1342 0_u^+, while this "new" state mixes with the 2431 0_u^+. This is an effect within the framework of the "C, type II" coupling, since the 1441 0_u^+ and 2431 0_u^+ states have different types of symmetry within the Λ-s coupling framework, and moreover, are formed from different iodine atom configurations (the 1441 0_u^+ and 1342 0_u^+ states correlate with $I^+ + I^-$ ions, the $p^4 \cdot p^6$ configuration).

Thus, we see that the presence of "C, type I, type II" coupling leads to "mixing" of the "singlet and "triplet" states of symmetry $0_{u,g}^+$ in I_2 and an increase in the value of Φ_{I*} as compared to the case of Ω-ω coupling.

A review and bibliography of literature devoted to the study of absorption and fluorescence with the exicitation of vapors in the ultraviolet and far ultraviolet regions of the spectrum can be found in [23, 62].

The interhalogens IF, ICl, IBr [18, 24, 29, 31, 63-70]. Just as for the I_2 molecule, the probability of a transition to the BO^+ ($^3\Pi_0^+$) in the first absorption band of the interhalogens is significantly higher than the probability of a

transition to the state A1 ($^3\Pi_1$) [18, 24, 63, 64]. Thus, there is apparently "C" coupling in IX molecules (X = F, Cl, Br). Unfortunately, IX spectroscopy and photochemistry have been studied unsatisfactorily in the second and subsequent bands, and it is therefore difficult to establish the energy and electron configuration of the states which perturb the B state.

The photodisintigration products of ICl and IBr in the first absorption band should be I + X or I + X*; in a zero order approximation, the coupling A1 and repulsive 0^+ states correlate with the first pair, and the coupling state $B0^+$ ($^3\Pi_0^+$) correlates with the second (Figure 5). In the IF molecule, the $B0^+$ state correlates with I* + F [65, 66]; the authors of [67] suppose that yet another state can converge to I + Br* for the IBr molecule (see Figure 5).

However, here the nonintersection rule is manifest and in the IBr absorption spectrum, for example, there is a system of bands corresponding to the transition to a "new adiabatic" coupling state $B'0^+$. At the same time, in the case of absorption in a continuum, corresponding to the transition $B0^+ \leftarrow X0^+$, the major photodissociation channel is (17), and not (17'):

$$JBr(X0^+) + h\nu \nearrow J + Br^*, \quad (17)$$

$$\searrow J + Br, \quad (17')$$

as follows from the nonintersection rule. This effect is well explained both semiclassically (within the framework of the Landau-Zener model [29]) and quantum mechanically [30]; the calculations are in excellent agreement with experimental data [31, 64]. No states have been detected experimentally which correlate with I* + X or I* + X*; according to the data of [67], with the photodisintegration of IBr, $\Phi_{I^*}(\lambda) < 10^{-4}$ in the region $\lambda > 300$ nm. In the opinion of the authors of [67], the reasons for this can be either the small relative values of the Franck-Condon coefficients or the "repulsion" of states which converge to I* + Br and I + Br* (see Figure 5). At room temperature in the gas phase, along with the vapors of ICl and IBr, there are always I_2, Cl_2 or Br_2 which are in thermodynamic equilibrium with IX (the IF molecule is generally chemically unstable [65]), and for this reason it is difficult to obtain quantitative data on the absorption spectra of IX. We do not have such information on the ultraviolet and far ultraviolet regions of the spectrum, and can mention only the papers [68-70] in which the absorption spectra of ICl and IBr are graphed, and the Rydberg bands are referenced to them.

3. The Photochemistry of Polyatomic Iodides

The major goal of this review is to consider the spectroscopy and photochemistry of polyatomic iodides, primarily alkyl iodides and perfluoralkyl iodides, since it is specifically these which are the working materials of photodissociation iodine lasers. Along with the presentation of the experimental data, we will

devote as much attention as possible to attempts to tie together the spectroscopic and photochemical data so as to understand the factors which govern the value of Φ_{I^*} with the photodissociation of various RI's. The treatment of diatomic iodide spectroscopy and photochemistry presented above, as we shall see, will be very useful in this case.

Cyanogen iodide ICN [28, 33, 34, 71-81]. A rather large quantity of both experimental [34, 71-79] and especially theoretical [28, 33, 35-37, 76, 77, 80, 81] literature has been devoted to the study of ICN spectroscopy and photochemistry. The theoretical interest is due to the relative "simplicity" of analyzing the photodisintegration processes of a linear triatomic molecule in the presence of a certain quantity of experimental data on the vibrational-rotational excitation of the CN radical, which is formed with the photodissociation of ICN in a rather wide spectral range. Least well known of all is the spectral function $\Phi_{I^*}(\lambda)$ with the photodissociation of ICN, which is not surprising if one considers the difficulties which arise with the quantitative recording of these atoms. Reviews of the latest achievements in the study of ICN are found, for example, in [37, 76, 77, 79].

It is well known that with the absorption of a photon in the first absorption band of ICN (λ = 290 to 220 nm), transitions are made to two states (both 0^+ in terms of the "C" coupling [37]). One of them (a linear one) correlates with CN ($X\ ^2\Sigma^+$) + I*, and the other (bent or linear, but predissociated through the bent one) correlates with CN ($X\ ^2\Sigma^+$) + I (see the Table) [34]. At λ = 266 nm, approximately 99 percent of the CN radicals ($X\ ^2\Sigma^+$) are formed primarily in the vibrational state. The quantum $\Phi_{I^*}(\lambda)$ has been measured sufficiently reliably only for $\lambda \geq 266$ nm (see the reference to the private correspondence from Baranovskiy and MacDonald in [37]): $\Phi_{I^*}(\lambda) = 0.6 - 0.3$ at λ = 266 - 280 nm. An analysis of the reasons for the observed distribution of partial cross-sections in the A band is extremely difficult because of the sparse information on ICN spectroscopy. Recent calculations show satisfactory agreement with experimental data on the spectral functions of vibrational excitation of CN radicals, but are either not completely satisfactory or unsatisfactory as regards the spectral functions $\Phi_{I^*}(\lambda)$ and CN rotational excitation (for example, see [37]). The photochemistry of ICN in the far ultraviolet spectrum has been studied, for example, in [76, 79] and the absorption spectra in [71-74, 79] (Figure 6).

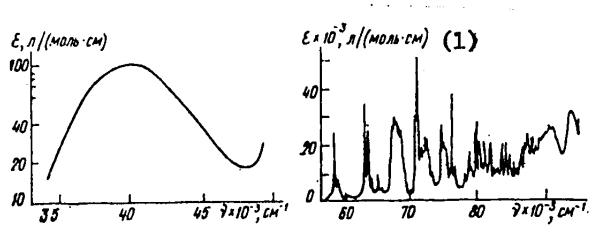

Figure 6. The absorption spectrum of ICN [34].

Key: 1. 1/(mole · cm).

Alkyl iodides and perfluoralkyl iodides. RI spectroscopy. [2, 3, 8, 9, 19, 20, 82 - 103]. The spectroscopy of alkyl iodides and (to a lesser extent) perfluoroalkyl iodides has been studied rather well at the present time. The absorption spectra of numerous compounds have been measured [2, 82-89] (see references to other papers in [83, 88]) and the vibrational structure and association of bands in the absorption spectrum in the far ultraviolet region of the spectrum have been analyzed for CH_3I, CD_3I [90-92], C_2H_5I [93] and CF_3I [94] (also see [8, pp. 132, 536, 540; 95, 96].

Data on the bond lengths and the sizes of the valence angles in RI are given in [97-98] and the spectroscopic constants of the ground and excited states of RI are given in [8, pp. 634, 639; 90, 93, 99-102].

The configuration of the ground state of CH_3I (and CF_3I), according to the data of Mulliken [19], without taking into account the electrons of the inner shells of the iodine atom, has the form: $(1s_C)^2[sa_1]^2\ (5s_Ia_1)^2\ [\pi e]^4\ [\sigma a_1]^2\ (5\ p\pi_I e)^4\ {}^1A_1$ (the noncoupling electrons are given in the parentheses, while the ones in brackets are coupling electrons), where $[sa_1]$, $[\pi e]$ and $[\sigma a_1]$ extend over the entire molecule, but $[\pi e]$ is practically completely localized while $[sa_1]$ is partly localized at the CH_3 radical. The C-I coupling is provided for the greatest part by the $[\sigma a_1]$ orbital with the slight addition of the $[sa_1]$ orbital. Absorption of CH_3I, at least up to the first ionization potential (taking spin-orbital splitting into account) inclusively, is due to the transport of the one of noncoupling electrons from the $(5\ p\pi_I\ e)$ orbital, the major contribution to which is made by the $5p_x$ and $5p_y$ electrons of the iodine atom, to higher orbitals. Mulliken has convincingly demonstrated that in the first absorption band of CH_3I there is the transition $\ldots (5\ p\pi_I e)^3\ [\sigma a_1^*]^{1,3}E \leftarrow \ldots (5\ p\pi_I\ e)^4\ {}^1A_1$, where $[\sigma a_1^*]$ is the antibonding orbital[19, 20], in which case, just as for other iodides, the state ^3E is split into $E + E + A_1^* + A_2$ because of the strong spin-orbital interaction, of which, only A* correlates with $CH_3 + I^*$. The nature and similarity of the initial absorption bands of the various alkyl iodides and perfluoroalkyl iodides (Figure 7) [83-86, 88-89] allow for the assumption that the $^{1,3}E$ states are repulsive, while the $[\sigma a_1^*]$ orbital is localized near the C-I bond. These circumstances allowed Mulliken to classify the lower excited states of these molecules as components of Q complex [19] ^1Q, $^3Q_0$, $^3Q_1$ and $^3Q_2$, similar to the $^3\Pi$, $^3\Pi_0$, $^3\Pi_1$ and $^3\Pi_2$ states of diatomic molecules (see Figure 1). Mulliken came to the conclusion based on an analysis of the data of Porret and Goodeve [3] that the most intense shortwave component of the first absorption band of CH_3I corresponds to a transition to the $^3Q_0$ state [20], so that the type of coupling in CH_3I is similar to "C, type I, type II" coupling in diatomic molecules.

The absorption spectrum of CH_3I in the far ultraviolet region of the spectrum has been studied quite well [82, 90-92, 95, 96]. In a spectral range of $\lambda > 130$ nm, it consists of intense bands which fall in the Rydberg series, superimposed on the continuum, where these bands converge to the first two states of the CH_3I ion formed with the separation of the $5\ p\pi_I$ electron $\ldots (5\ p\pi_I\ e)^3$ CH_3I^+ $(E_{3/2}, E_{1/2})$ (ionization potentials of 9.49 and 10.11 eV respectively [95]). The first terms of these series form the well-known B, C, D, etc. bands of CH_3I and correspond to transitions to states just as for the A-states, with

configurations of ... $(5\ p\pi_I\ e)^3\ (n\sigma a_1)^{3,1}$ E, where n = 6, 7, ... 0 - 0 transition to the B state (type E symmetry), corresponding to the $^3\Pi_2$ state with a linear configuration, occurs at 203.13 nm; in the C state (E, $^3\Pi$) - at 201.16 nm; in the D sate (E, $^1\Pi$) - at 183.07 nm) [90]. There are also transitions to the (A_1, A_2, $^3\Pi_0$) states and the 0 - $0_{\tilde{\nu}}$ transition at λ = 185.05 nm (see Figure 7). The difference in the energies of C and D states and all subsequent pairs of similar states with identical values n, which converge to different states of the ion $E_{3/2}$, $E_{1/2}$, is approximately constant and close to the value of spin-orbital splitting in CH_3I^+ ≈ 4,900 cm^{-1}) [8, p. 538; 83, 84, 90]. We will note that there is also similar effect in other iodides (for example, see [83, 84]). The intensities of the strongest vibrational bands in these transitions have the following ratio: ≈ 44 ($^3\Pi_2$): 500 ($^3\Pi_1$): ≈ 30 ($^3\Pi_0^{\pm}$): 540 ($^1\Pi$) [90]. A similar intensity distribution in similar transitions occurs in HI: 0.01 ($^3\Pi_2$): 1 ($^3\Pi_1$): 0.1 ($^3\Pi_0$): 2.4 ($^1\Pi$) for the 0 - 0 transitions [43]. All of this is evidence of the closeness of the nature of the coupling in the Rydberg states of CH_3I to the Ω-ω coupling in diatomic iodides, with a slight tendency towards a "C" type coupling (see section 1).

Transitions to states which are closer to the CH_3I^+ ($E_{3/2}$, $E_{1/2}$) ion states are placed in the Rydberg series, which, as a comparison of the absorption spectra of CH_3I and Xe has shown, correspond to the transition of 5 $p_{x,y}$ electrons of the iodine atom not only in the ns-orbital, as at lower photon energies, but also in the nd and even the np orbitals [83, 91, 104]. The continuum in the far infrared region of the spectrum for CH_3I and other alkyl and perfluoralkyl iodides, as Boschi and Salahub propose [83, 84], is due to the absorption of radiation by the C-C and C-H bonds (this does not contradict our data [88]).

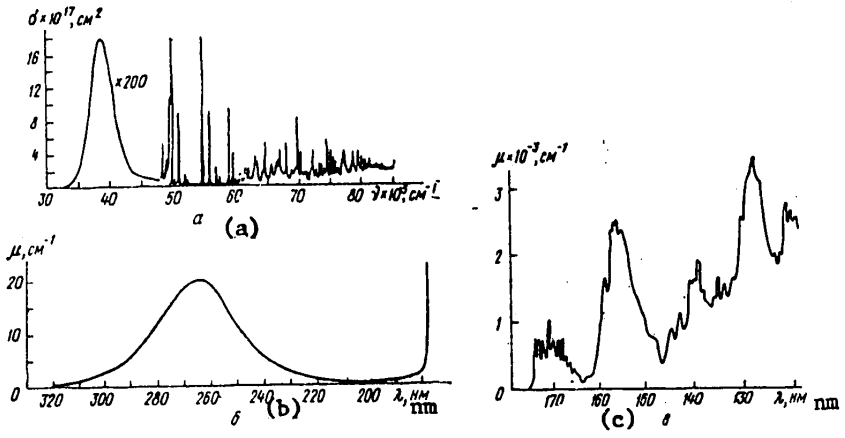

Figure 7. The absorption spectra of CH_3I (a) [82] and CF_3I (b, c) [88].

The absorption spectrum of C_2H_5I in the far ultraviolet, which is similar in nature to the absorption spectrum of CH_3I, has been much more poorly studied because of the vibrational-rotational structure which is considerably richer than that of CH_3I. Assignment of some of the transitions in the first terms of the Rydberg series of C_2H_5I ($\lambda > 175$ nm) though has been done successfully [8, p 553; 83, 93]. We will note that as compared to CH_3I in ethyl iodide, the relative intensity of the transitions to states similar to the $^3\Pi_2$ and $^3\Pi_0^+$ of the HI molecule is significantly higher, something which in the opinion of the authors of [93] is due to the delocalization of the nonbonding electron of the iodine atom and the reduction of the symmetry from C_{3v} down to C_s.

According to data available to us, an analysis of the vibrational structure and the assignment of the bands in the absorption spectrum of CF_3I in the region of $\lambda >$ > 130 nm were most completely carried out by Sutcliffe and Walsh [94]. In their opinion, this spectrum is similar to the CH_3I absorption spectrum. The B-band ($\lambda =$ = 174 nm) apparently corresponds to the C-band of CH_3I, i.e., is due to the transition to the $E(^3\Pi_1)$ state; the C-band is complex and is due, in all probability, to transitions to states A_1 and $E(^3\Pi_0^+, {}^1\Pi)$. The relative intensity of the transitions to these states is unknown because of the impossibility of resolving the vibrational structure of the C-band; to all apparent extents, the relative probability of a transition to a state similar to the A_1 state in CH_3I is higher in CF_3I [94]. Just as for CH_3I, these and the subsequent bands fall in the Rydberg series [83, 84].

An analysis of the vibrational structure and the assignment of the absorption bands of the more complex alkyl iodides and their perfluoro analogs have not been carried out because of the fact that the vibrational-rotational structure cannot be resolved [83, 84, 88]. There is all the reason to assume that the nature of the absorption spectrum of these compounds is similar to CH_3I.

Procedures for studying primary iodide photolysis processes [2, 5, 32, 67, 88, 106--120]. The rather high deactivation rate, the relatively low excitation energy of I* and the forbidden nature of the transition (1) (the radiation lifetime of iodine atoms is $\tau_{I*} \simeq 0.1$ sec [104, 105]) makes it very difficult to obtain quantitative information on the values of $\Phi_{I*}(\lambda)$ with the photolysis of RI. Obtaining sufficiently large monochromatic radiation fluxes in the ultraviolet and far ultraviolet regions of the spectrum is a complex task, and for this reason, a considerable portion of the data on the values of Φ_{I*} and the reaction rate constants with the participation of I* has been obtained at the present time by kinetic spectroscopy techniques with flash photolysis of RI in a broad spectral range ($\lambda > 200$ nm) [4-6, 106-108]. The incorrectness of this approach to the study of photoprocesses has been discussed in detail in a paper by the author on the technique for the measurement of the quantum yields of photoprocesses [109] (also see [88, 110]). The reason for the incorrectness consists of the following. If the quantum yield of I* atoms, for example, is measured in a wide spectral range, $\lambda_1 - \lambda_2$, then only a certain value can be measured:

$$\Phi_J^{изм} = \int_{\lambda_1}^{\lambda_2} \Phi_{J*}(\lambda)\, I_{погл}(\lambda)\, d\lambda \Big/ \int_{\lambda_1}^{\lambda_2} I_{погл}(\lambda)\, d\lambda,$$

where $I_{absorp.}(\lambda) = I_{погл}(\lambda) = I_0(\lambda)\{1 - \exp[-\sigma_{RJ}(\lambda) n_{RJ} l]\}$ is the spectral function of the radiation absorbed by the RI molecule; $\sigma_{RI}(\lambda)$ is the spectral function

of the absorption cross-section; n_{RI} is the concentration of RI; l is the cell length. The integral absolute quantrum yield of the I* atoms in the range $\lambda_1 - \lambda_2$ is

$$\Phi_{J^*} = \int_{\lambda_1}^{\lambda_2} \sigma_{J^*}(\lambda)\, d\lambda \Big/ \int_{\lambda_1}^{\lambda_2} \sigma_{RJ}(\lambda)\, d\lambda \quad (\sigma_{J^*}(\lambda) = \Phi_{J^*}(\lambda)\, \sigma_{RJ}(\lambda))$$

which is equal to $\Phi_{I^*}^{meas}$ only if in the region $\lambda_1 - \lambda_2$, $\Phi_{I^*}(\lambda)$ = const., or the measurements are made for the case of an optically thin RI layer and a constant spectral composition of the light source ($I_0(\lambda)$ = const.). It is practically impossible to realize the latter condition with flash photolysis of iodides in the 320 to 230 nm range. For this reason, the data obtained in [4-6, 106-108] for $\Phi_{I^*}(\lambda \neq 1$ or 0 throughout the entire A band are not comparable and are meaningful only for the experimental conditions realized in this literature. This remark also fully applies to papers [45, 74, 78] (see the Table).

Kinetic spectroscopy of photodissociation fragments [32], a unique kinetic method developed in [111] as well as the optical-acoustical effect [112] have also been used to study RI photodissociation processes; results of measuring $\Phi_{I^*}(\lambda)$ were recently published for the photolysis of HgI_2, obtained by observing I* luminescence with the photolysis of HgI_2 by the radiation of dye lasers [67]. We will also mention papers [113] (the resolution of the CH_3I absorption spectra into partial cross-sections by means of magnetic circular dichroism) and [114] (the measurement of the angular distribution of RI photodissociation fragments). Information on the value of $C_{I^*}(\lambda) + \Phi_I(\lambda)$ and a 0 photodissociation channel of RI, different from (2) and (2'), was also obtained by classical photochemical techniques (for example, see [115, 116]).

Work has been underway for a number of years in our laboratory of the photon studies department of the Scientific Research Institute of Physics at Leningrad State University on the study of spectral functions of the absolute quantum yields of the photodissociation channels for RI into R + I*, R + I, etc. [2, 88, 89, 110, 117-120]. The method which we have developed numbers among one of the variants of the classical technique of [109], in which the yield of atoms and radicals is measured based on the output of stable photolysis products from mixtures of the compounds being studied with acceptors of these particles and with other gases and vapors. The essence of the technique used by us is set forth in detail in [2] (also see [88, 118]). The basis for it is the strong difference (no less than a factor of 10^4 times [2]) in the reaction rates of the I* and I atoms with nitrosyl chloride:

$$I^* + NCCl \rightarrow NO + ICl \quad (18)$$

$$I + NCCl \rightarrow NO + ICl \quad (19)$$

and the presenc of activation energy in the reactions of R with NOCl:

$$R + NOCl \rightarrow NO + RCl \quad (20)$$

By thermalizing the hot radicals formed in the photolysis process with the introduction of a thermalizer for the M radicals, for example, CO_2 molecules, and bringing the intesity of the radiation absorbed by the iodine, $I_{h\nu}$ up to levels on the order of 10^{14} quanta/(cm^3 · sec), conditions can be created in the photolysis of an RI-NOCl-M mixture where only the I* atoms react with the NOCl, while the I and R are expended in the following reactions:

$$2I + M \rightarrow I_2 + M \quad (21)$$

$$R + ICl \rightarrow RCl + I \quad (22)$$

as well as (3) and (4). The absolute quantum yield of NO ($\Phi_{NO}(\lambda)$) under these conditions is equal to $\Phi_{I*}(\lambda)$.

In the case where R is poorly thermalized or the reaction rate constant (3) is small ($\leq 10^{-12}$ cm^3/sec), any alkene (for example, H-butylene [2, 89, 117, 118]) is introduced into the system being studied to prevent reaction (20), or the photolysis is carried out in the presence of small quantities of I_2 and ICl. The sum of the absolute quantum yields of the I* and I atoms is measured by means of photolysis of the RI - NOCl mixture under conditions where all of the iodine atoms and radicals formed in the primary photolysis processes of the RI react with the NOCl, and in this case, $\Phi_{I*}(\lambda) + \Phi_I(\lambda) = (1/2)\Phi_{NO}^{max}(\lambda)$ [2, 117], or when studying the photolysis of an RI-NO-M mixture, in this case, $\Phi_{I*}(\lambda) + \Phi_I(\lambda) = 2\Phi_{I_2}^{max}(\lambda)$ [2, 88]. The absolute quantum yields of RI photodissociation processes which differ from (2) and (2') are measured by means of the photolysis of a mixture RI - I_2 - M based on the yield of stable photodissociation products or the interaction of the radicals with I_2 [88, 118, 119] (see below).

Primary RI photolysis processes. There is very little information on the primary photolysis processes of RI, and for this reason, practically all of the existing experimental data will be cited and briefly discussed below (see the table).

CH_3I, ultraviolet spectrum [4, 5, 32, 106, 108, 112-117, 119, 122]. Experimental data on the values of $\Phi_{I*}(\lambda)$, $\Phi_I(\lambda)$, Φ_{I*} and Φ_I or their ratios were obtained in [4, 5, 32, 106, 108, 112, 117, 119] (see the table). Unfortunately, the data on the quantities $\Phi_{I*}(\lambda)/[\Phi_{I*}(\lambda) + \Phi_I(\lambda)]$ were given in [32, 112] without indicating the measurement precision. The reliability of the data obtained in [4, 5, 106, 108] has already been discussed; one can only add that a comparison of the operating conditions of the flash lamps in [4, 5] and [121] make it possible to assume that the radiation spectrum of the lamp used in [4, 5] is apparently different from the radiation spectrum of an absolute black body. The maximum in the radiation spectrum of this lamp possibly occurred at $\lambda < 250$ nm. In this case, the disparity in the data of [4, 5, 32] will be even greater. We shall note the earlier work of Porret and Goodeve [3] as well as recent results in resolving the absorption spectrum of CH_3I into partial cross-sections corresponding to transitions to states, which in an adiabatic approximation should dissociate via channels (2) and (2') (Figure 8) [113]. However, it is impossible from these data to derive the

spectral function $\Phi_{I^*}(\lambda)$, since the state which dissociates into $CH_3 + I$ is located in the region of the Franck-Condon transition above the $^3Q_0$ state which dissociates into $CH_3 + I^*$. Nonadiabatic processes are possible in the dissociation of these states where these processes are capable of substantially changing the form of these partial cross-sections in the case where they are obtained on the basis of a study of the photodissociation processes. It is possible therefore that the data cited in [112, 113] differ markedly.

In the first absorption band with small yields ($< 10^{-3}$), the following photodissociation processes apparently take place [115, 116, 122]:

$$CH_3J + h\nu \nearrow CHJ + H_2, \quad (23)$$

$$\searrow {}^{1,3}CH_2 + HJ. \quad (24)$$

CH_3I, the far ultraviolet region of the spectrum [107, 116, 122]. The photochemistry in the far ultraviolet portion of the spectrum has been studied extremely poorly. It has been shown that in the spectral region $\lambda > 140$ nm, the main primary CH_3I photolysis process is dissociation into $CH_3 + I$ (I*) (the value of $\Phi_{I^*}(\lambda)$ is unknown), and the probability of photodissociation into $CH_I + H_2$ [sic] or $CH_2 + HI$ is less than 0.01.

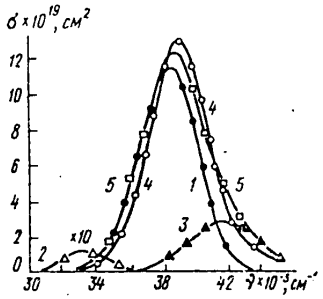

Figure 8. The partial cross-sections of CH_3I, corresponding to transitions to the states $^3Q_0$ (1), $^3Q_1$ (2) and ^1Q (3); the total absorption cross-section (from experiment) (4); $\sigma = \Sigma\sigma_i$ (5) [113] (see the text).

Other alkyl iodides, the ultraviolet portion of the spectrum [4, 5, 32, 106, 118, 119]. The data obtained for C_2H_5I - $(CH_3)_2CHCH_2I$ on the quantities $\Phi_{I^*}(\lambda)$, $\Phi_I(\lambda)$ and their ratios are presented in the table. As has already been noted, the primary iodide photolysis processes can occur via channels other than (2) or (2'); for example, for C_4H_9I, this is [119]:

$$C_4H_9J + h\nu \nearrow C_4H_8 + HJ, \ \varphi(\lambda) = (1{,}1 \pm 0{,}3) \cdot 10^{-2}, \quad (25)$$

$$\searrow C_3H_8 + CHJ, \ (3 \pm 1) \cdot 10^{-4}. \quad (26)$$

The values of the quantum yields of these processes are given in [11, 119]. Here, we will only note that the most probable of these reactions is the regrouping of RI* with the splitting off of the HI molecule:

$$RJ + h\nu \rightarrow RJ^* \rightarrow (R{-}H) + HJ. \qquad (27)$$

The absolute quantum yield of these processes, $\phi(\lambda)$, when λ = 254 nm varies from 0.008 ($(CH_3)_2CHCH_2I$) to 0.1 (CH_3CHICH_3). To all apparent extents, this regrouping is accomplished when R and the I atom fly apart as a consequence of the excitation of strong deformational vibrations in the H - C - I group.

An increase in the length of the C - C chain in RI leads to a monotonic increase in the value of $C_{I^*}(\lambda)$, λ = 254 nm. However, it is a complex matter to interpret these data, since they were obtained for a single photon energy.

Vibrationally excited radicals, which are formed with the photodissociation of RI, can either decay via a monomolecular mechanism, or react with the I_2 molecule [118, 119], for example:

$$C_4H_9^* \rightarrow \begin{cases} C_4H_8 + H, & (28) \\ C_3H_6 + CH_3, & (28') \\ C_2H_4 + C_2H_5; & (28'') \end{cases}$$

$$C_4H_9^* + J_2 \rightarrow \begin{cases} C_4H_8 + HJ + J, & (29) \\ C_3H_6 + CH_3J + J, & (29') \\ C_2H_4 + C_2H_5J + J. & (29'') \end{cases}$$

If meachanism (28) obtains, then the lifetime of vibrationally excited radicals for R = C_3H_7 and CH_3CHCH_3, for example, exceed one microsecond and 80 nanaseconds respectively [118].

The primary photolysis processes of alkyl iodides, other than CH3I, have not been studied in the far ultraviolet region of the spectrum, as far as we know.

Perfluoroalkyl iodides, the ultraviolet spectrum [2, 4, 5, 89, 104, 110, 111, 117]. The primary photolysis processes of perfluoralkyl iodides (RFI), widely used in photodissociation iodine lasers, have been studied throughout the entire first absorption band of λ = 315 to 235 nm [2, 89, 110]. The spectral functions $\Phi_{I^*}(\lambda)$ and $\Phi_{I^*}(\lambda) + \Phi_I(\lambda)$ have been obtained; the spectral functions of the partial RFI absorption cross-sections corresponding to transitions to states which dissociate into RF + I*, RF + I($\sigma_{I^*}(\lambda)$, $\sigma_I(\lambda)$) and via other channels, as well as the integral quantum yields Φ_{I^*}, $\Phi_{I^*} + \Phi_I$, the oscillator strengths f_{I^*} and f_I and the

energies for vertical transitions to these states; attempts were also made to interpret the observed relationships.

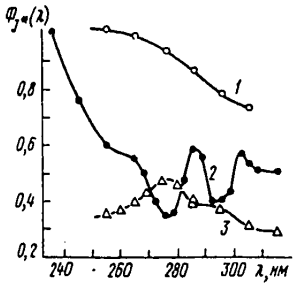

Figure 9. The spectral functions $\Phi_{I^*}(\lambda)$ for the photolysis of C_2F_5I (1), CF_3CFICF_3 (2) and $(CF_3)_3CI$ (3) [2, 89].

The values of $\Phi_{I^*}(\lambda)$ in the first absorption band of unbranched RFI's with a terminal position of the I atom (we shall call them "linear"), vary continuously in a range of 1.0 to 0.8 (for example, C_2F_5I in Figure 9); an increase in the length of the C - C chain leads to a shift in the minimum of this function to the region of the maximum of the total absorption cross-section. The corresponding cross-sections have a bell-shape (for example, C_2F_5I in Figure 10); with an increase in the length of the C - C chain, the difference in the energies of the photons, ΔE, corresponding to the maxima of these bands decrease and the value of Φ_{I^*} decreases from 0.94 (CF_3I) down to 0.86 - 0.89 (C_3F_7I, $C_5F_{11}I$) (see the table). The spectral functions $\Phi_{I^*}(\lambda)$, $\Phi_I(\lambda)$ and the corresponding curves of $\sigma_{I^*}(\lambda)$ and $\sigma_I(\lambda)$ with the photodissociation of branched RFI's or molecules without a terminal position of the I atom have a somewhat different form. It is as if the $\Phi_{I^*}(\lambda)$ curve for $(CF_3)_3CI$ is "inverted" with respect to "linear" RFI's and has small singularities; for CF_3CFICF_3, these curves have an oscillating nature (see Figures 9, 10); in both of these cases, the values of Φ_{I^*} are substantially smaller than for the "linear" compounds.

As has already been noted, it is impossible to compare the data obtained in [4, 5, 106] directly with the data obtained in our laboratory. However, as analysis demonstrates, the values of $\Phi_{I^*}^{meas}/(\Phi_{I^*} + \Phi_I)$, computed on the basis of the spectral functions $\Phi_{I^*}(\lambda)$ obtained by us and the possible radiation spectrum of the pulsed source used in [4, 5], especially if one takes into account the contribution of the reactions of I atoms with the radicals (which were not considered by the authors of [4, 5], and which should increase the value of $\Phi_{I^*}^{meas}$, especially with the photolysis of CF_3CFICF_3, see [2]), should be close to the values obtained in [4, 5]. The analysis of the data of [106] is difficult because of the inadequacy of the information on the conditions under which they were obtained. The results of papers [2, 89, 111] for RFI $\neq (CF_3)_3CI$ are close to each other. One of the probable reasons which can partially explain the observed divergence in the values of $\Phi_{I^*}(\lambda)/[\Phi_{I^*}(\lambda) + \Phi_I(\lambda)]$, $\lambda = 265$ nm, as was shown in [89], consists in the possibility of chemiluminescence being present in the process of radical recombination with the I* atoms, $\lambda \leq 1{,}315$ nm; such processes occur in the condensed phase at low temperatures [123, 124].

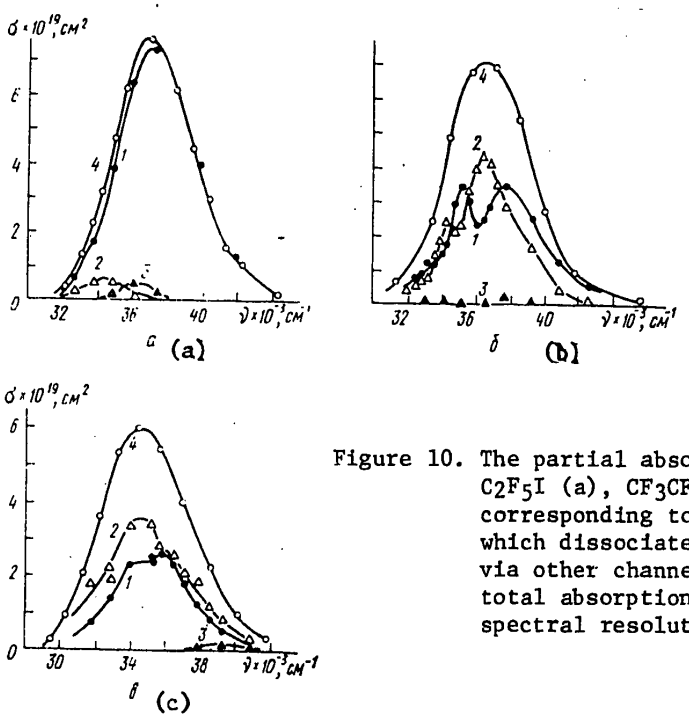

Figure 10. The partial absorption cross-sections of C_2F_5I (a), CF_3CFICF_3 (b) and $(CF_3)_3CI$ (c) corresponding to transitions to states which dissociate into R + I* (1), R + I (2), via other channels (3), as well as the total absorption cross-section (4). The spectral resolution is approximately 4 nm.

Perfluoroalkyl iodides, the far ultraviolet region of the spectrum. [88, 120]. As far as we know, the photochemistry of RFI in the far ultraviolet has been studied only in [88, 120]. In the first (B) and second (C) far UV absorption bands of CF_3I, C_3F_7I, CF_3CFICF_3, $\Phi_{I^*}(\lambda) = 0.0 \div 0.1$, in the B band, $\Phi_I(\lambda) \simeq 1$ (CF_3I); 0.77 (C_3F_7I); 0.9 (CF_3CFICF_3), in the C band for RFI $\neq CF_3I$, only the breaking of the C - C chain occurs with the formation of the CF_3 radical ($\phi^{meas} = 0.1 - 0.14$ (C_3F_7IO; 0.3 - 0.1 (CF_3CFICF_3)). The excited states of RFI, which are formed with the absorption of a light quantum in the C band, have a probability on the order of 0.9 of undergoing nonradiative processes which lead to deactivation of RFI*l*.

The interpretation of RI photochemistry, the ultraviolet region of the spectrum. [2, 5, 89]. The explanation of the general laws governing the primary photolysis processes of iodides, especially in the first absorption band, are of definite interest from our point of view. If the relationship between the spectroscopic properties and the primary photolysis processes of RI are understood, then one can predict the value of Φ_{I^*} with the photodissociation of iodides which have not yet been studied or have not been synthesized at all and which for some reason are of promise for use in photodissociation iodine lasers. The lack of reliable quantitative information on the spectral functions $\Phi_{I^*}(\lambda)$ and $\Phi_I(\lambda)$ as well as the complexity of the object have until recently not permitted the reliable determination beforehand of which factors - molecule symmetry, ionization potential of the radical R, as the authors of [4, 5] assume, or which other factors determine the probability of transitions to states which dissociate into R + I* and R + I. An analysis of the general laws governing the spectroscopy of triplet states, including the case of large spin-orbital interaction, and the manifestations of these

laws in diatomic molecules, an analysis of which was given above, should aid to some extent in understanding this question.

As was shown in the first section of this review, in the case of weak spin-orbital interaction in CH_3X molecules (X is a halogen atom), the transition to a state which correlates with $CH_3 + X$ ($^2P_{1/2}$) in their first absorption band should have a very low probability, since this state is a triplet. Strong spin-orbital interaction with CH_3I and CF_3I, which is due to the presence of a heavy iodine atom in these molecules, can lead and actually does lead to a mixing of this "triplet" state with the "singlet" or ground "singlet" state with the "triplet" ones (see (8) and (9)). It is only necessary that this "mixing" be permitted by the selection rules (see (11) and (12)) and be sufficiently "strong". It is therefore useful to analyze the types of coupling which are realized in RI molecules, something which should make it possible to classify the excited states of RI and correctly apply the selection rules. Their formal application (especially within the framework of Λ-s coupling) neither in symmetry group C_{3v} (CH_3I, CF_3I) nor, even more, in the C_s (C_2H_5I and possibly, C_2F_5I) and C_1 (other RI's) is altogether fruitful, since is does not provide an explanation of the large value of $\Phi_I^*(\lambda)$ with the photolysis of these compounds. This leads to the thought that during RI photodissociation, processes which occur near the C - I bond are quite significant; consequently, the application of the description of bond types which are realized in diatomic iodides can be justified for RI molecules.

Experiments show that in the CF_3I molecule, the value of Φ_I^* is close to unity, i.e. the probability of a transition to the $^3Q_0$ state (according to Mulliken) is much greater than to $^3Q_1$ (the ^1Q state, according to Mulliken, falls in the higher energy region, see Figure 1). The value of the energy difference, ΔE, of vertical transitions to states which dissociate into $CF_3 + I^*$ and $CF_3 + I$ in the region of the Franck-Condon transition is also high in this molecule. An increase in the length of the C - C chain leads to a reduction in ΔE and Φ_I^* [2, 89]. The analysis carried out in [2] demonstrated that three questions must be answered for the interpretation of these laws:

1. Why is $f_{I^*} >> f_I$ in CF_3I?
2. Why does $\Delta E \to 0$ in "linear" RFI's with an increase in the C - C chain?
3. Why does the value of Φ_I^* decrease when $\Delta E \to 0$?

A rather precise quantum chemical calculation is necessary to answer the first question. However, based on the material presented above, it appears to us that one can state certain concepts of the factors which govern the large value of Φ_I^* in the photolysis of CF_3I as well as concerning the electron states of CF_3I, the "mixing" of which with the "unperturbed" $^3Q_0$ and X states must be taken into account within the framework of the given calculation.

The type of coupling in the states under discussion for the CH_3I molecules, and moreso for the CF_3I molecules which are incorporated in the Q-complex of Mulliken, is undoubtedly close to the "C" type coupling of diatomic molecules. We shall ascertain which "triplet" states, both in symmetry group $C_{\infty v}$, and possible in group C_{3v} can be mixed in with the ground "singlet" state ($X^1\Sigma^+$, $C_{\infty v}$; $\tilde{X}\ ^1A_1$, C_{3v}) and

which "singlet" states can mix with the discussed "triplet" $^3Q_0$ ($^3\Pi_0^+$, $^3A_1$, symbols in terms of the Λ-s coupling). It is useful in this case to take into account the laws governing "C, type I" coupling (see sections 1 and 2 of this review).

The mixing of the $^3Q_2$, $^3Q_1$ and ^1Q states included in the Q-complex either with the ground or with the $^3Q_0$ states cannot explain, from our point of view, the observed effect. In fact, the mixing of the ground state (0^+, A_1 in the case of a strong spin-orbital interaction) with the $^3Q_2$ (2, E) state is forbidden in the $C_{\infty v}$ group, and is permitted with the $^3Q_1$ state (1, E) when the electron-vibrational or electron-rotational interaction is taken into account [8, p 472]. The conclusion can be drawn, however, from an analysis of the factors which govern the size of Φ_{I*} during the photolysis of I_2 (see [23] and section 2 of this review) that because of the large energy gap between the states $^3Q_1$ and X ($3.6 \cdot 10^4$ cm^{-1} [2]), this "complex" interaction can hardly provide for the observed effect (see (8) and (9)). If mixing of the $^3Q_0^+$ and ^1Q states did occur, then the latter would be manifest in the CF_3I absorption spectrum, however, this state has not been detected in the expansion of the CF_3I absorption spectrum into partial cross-sections [2].

It remains to be hypothesized that the large value of Φ_{I*} with the photolysis of CF_3I is due to the "interaction" of one or more Rydberg states (apparently, the lowest ones) with $^3Q_0^-$, or $^3Q_0^+$ with the ground state of CF_3I. Apparently, a similar effect takes place in the CH_3I molecule. The absorption cross-sections in these states are considerably higher (by a factor of 10^2) than the in Q-complex states (see Figure 7), so that even their weak "admixing" can provide for the observed effect. To all apparent extents, it is primarily necessary in the calculations to take into account the "triplet" $A_1(0^+)$ state, which is incorporated in the group of Rydberg states, converging to the $E_{1/2}$ ion state. It is possible that the value of Φ_{I*} with the photodissociation CF_3I [2, 112] which is greater than for CH_3I, is related to the higher probability of a transition to this state in CF_3I (see above, and [90, 94]).

The second and third questions which come up in the interpretation of the observed change in the value of Φ_{I*} in a number of RFI's have been treated in detail [2, 89]. As has already been noted, the value of the spin-orbital splitting between the terms of the Rydberg series with identical principal quantum numbers n, which converge to different RI^+ ion states, with a sufficient degree of precision is independent of n, the kind of RI and is approximately equal to 0.6 eV. This effect occurs because of the small influence of a Rydberg electron on the value of the spin-orbital splitting, due primarily to the unpaired $5p^x$ or $5p^y$ electron which remains close to the iodine atom [2]. The hypothesis has been advanced that the value of ΔE in the Q complex is determined by how much this nonbonding ($5p\pi_I e$)-electron that becomes an antibonding [σ*]-orbital, neutralizes the spin density of the remaining nonbinding electron, i.e., what portion of the time it is close to the iodine atom. Calculations of the electron density distribution and the contribution of various atomic orbitals to the RFI molecular orbitals, including the contribution of the $5p_x$ and $5p_y$ orbitals to the molecular [σ*] orbital, which were made by the MO LKAO [molecular orbital, linear combination of atomic orbitals] SSP [not further defined] technique in a semi-empirical CNDO/BU [not further defined] variant, confirmed this hypothesis [2]. In fact, the value of ΔE is smaller, the greater the amount of time this nonbinding electron, which is incorporated in the [σ*]-orbital, is located close to the iodine atom.

The relative change in the oscillator strengths of the transition to the $^3Q_0^+$ and $^3Q_1$ (0^+ and 1) state correlates well with the value of ΔE, and as the analysis of [2] demonstrated, can be explained by the "repumping of oscillator strength" from a state with a greater f to a state with a lesser f. The "interaction" of these states in the presence of electron-vibrational or (and) electron-rotational interaction because of their closeness ($\Delta E \approx 10^3$ cm^{-1} [2]) can be rather strong (see (8), (9) and [8, p. 472]). The given explanation is in good agreement with the small change in the oscillator strength for the A-band, the weak change in the mutual arrangement of this and subsequent absorption bands and the length of the C--I bond in RFI molecules with a change in the kind of radical [2, 97, 98]. The presence of oscillation of the partial absorption cross-sections in the CF_3CFICF_3 molecule [2] (see Figure 10b), and possibly, $(CF_3)_3CJ$ [89] (see Figure 10c) is likewise quite well explained within the framework of this model, taking into account the strong interaction ("repulsion") of the surfaces of the $^3Q_0^+$ and $^3Q_1$ states in the region of the Franck-Condon transition [2, 85].

In a number of "linear" RFI's, CF_3I - $C_5F_{11}I$, the quantity ΔE does not fall below 800 cm^{-1}, and correspondingly, $\Phi_{I^*} \geq 0.86$. Considering the anticipated slight change in the values of valence angles and lengths of the bonds [97, 98], there is no basis for expecting a marked increase in Φ_{I^*} with a further increase in the length of the C - C chain in RFI.

The branching of the RFI molecule or the rearrangement of the iodine atom, as a rule, leads to a decrease in the quantity Φ_{I^*}, something which is apparently due to a change in the nature of the [σ^*] orbital because of the F atoms which are spatially close together [2, 89].

It is interesting to note that all of the RFI molecules which have been considered, even $(CF_3)_3CI$ ($\Phi_{I^*} = 0.39$) are good working substances for photodissociation iodine lasers [2, 86, 89. 111, 125]. A comparison of the lasing characteristics and the reaction rate constants (3) - (5) for these iodides (see the bibliography on rate constants [2]), which was made in [89], shows that these reactions play a very important role in the lasing characteristics of RFI in the case of weak pumping. The calculation of the specific energy throughput as a function of Φ_{I^*} which was done in [89] for CF_3I and $(CF_3)_3CI$ confirms this conclusion.

Other iodides. [2, 67, 84, 114, 126-138]. Papers in which quantitative data is presented for the spectroscopy and primary processes of the photolysis of other iodides, including organic iodides, are not very numerous. The absorption spectra of HgI_2 have been measured [67], as well as the spectra of partially fluorine substituted alkyl iodides [84], iodine substituted unsaturated compounds with a double bond [84, 126-130], with a triple bond [131], methylene iodide, iodoform and carbon tetraiodide [132-134] (in [133, 134], the measurements were made in solutions and in [126], the information is of a qualitative nature). The absorption spectra of $CF_3OC_2F_4I$ has also been measured [88]. A detailed bibliography of the earlier works is contained in [84] (also see [133, 134]).

Information on the primary photolysis processes of these compounds is also found in [2, 88, 114, 127, 128, 132, 135-138]. We shall briefly consider the most important data presented in the given papers.

Mercury iodide HgI_2. [67]. The spectral function $\Phi_I^*(\lambda)$ with HgI_2 photolysis is given in a recent paper [67] (see the table). Absolute calibration with respect to the quantum yield was accomplished at λ = 275 nm in this work using the data of [5]: $\Phi_{I^*} \geq C_3F_7I$). Since $\Phi_I^*(\lambda) = 0.80$ with the photolysis of C_3F_7I, λ = = 275 nm, we consider the data given in [67] to be overstated by 20 percent.

$CF_3OC_2F_4I$. [2, 88, 110, 120]. This compound has the greatest value of $\Phi_I^*(\lambda)$ = = 0.98 of the substances studied in our laboratory (see the table). Based on what has been presented, it is not difficult to relate this fact to the presence of an oxygen atom in the C - C chain, where the atom has a greater similarity to an electron [139], something which should "pull" the [λ^*] orbital away from the iodine atom [2]. The photochemistry of $CF_3OC_2F_4I$ in the far ultraviolet region of the spectrum was studied in [88].

Acetyl iodide CH_3COI, perfluoroacetyl iodide CF_3COI [137, 138]. It has been shown by means of kinetic spectroscopy of photodissociation fragments that the absorption of a photon having an energy corresponding to λ = 266 nm by the CH_3COI molecule leads to its dissociation into CH_3CO^* and an I atom (the yield of I* atoms is close to zero), and the lifetime of the hot CH_3CO^* radicals is on the order of picoseconds; they decay into CH_3 + CO [137]. The first state in the photodissociation of CF_3COI is similar to that of [138], however, the lifetime of CF_3CO^* is very much greater (1 msec); there is no data in [138] on the value of $\Phi_I^*(\lambda)$ with the photolysis of CF_3COI, λ = 266 nm.

GeH_3I. [135]. The photodissociation processes of GeH_3I were studied in the first absorption band with excitation in a broad spectral range, and therefore, for the reasons presented above, the data obtained will not be discussed here (see the table).

Vinyl iodide C_2H_3I [128]. The major photodissociation processes which have been studied are:

$$C_2H_3J + h\nu \nearrow C_2H_3 + J, \quad (30)$$

$$\searrow C_2H_2 + HJ, \quad (30')$$

where $\phi_{30'}/\phi_{30}$ = 0.14 (313 nm) and 0.20 (254 nm); $\phi_{30'} + \phi_{30} < 1$. The value of $\Phi_I^*(\lambda)$ is unknown.

Methylene iodide CH_2I_2, iodoform, CHI_3. [132]. The main photodissociation channel of CH_2I_2 and CHI_3 in the 250 - 350 nm region is:

$$R'J + h\nu \rightarrow (R'—J) + J\ (J^*). \quad (31)$$

The excited states of CH_2I_2 which are populated with the absorption of a photon, belonging to the spectral region indicated above, have a B_1 symmetry; CHI_3 - E.

Iodine substituted aromatic compounds. There is information on the lifetimes and types of symmetry of the first excited states of some of these compounds in [114, 136].

Conclusion

The treatment of the general laws governing the spectroscopy and photochemsitry of iodides presented in this review make it possible to conclude that a type of coupling is realized in the initial excited states of alkyl iodides and their perfluoro analogs which is close to "C" type coupling of diatomic molecules, with the presence of interaction between states which dissociate into R + I* and R + I, which leads to a reduction in the quantity Φ_{I^*} with an increase in the interaction. The size of this effect can be estimated if the RI geometry is known or can be predicted with sufficient precision. The unbranched molecules of perfluoroalkyl iodides with a terminal position of the iodine atoms have a value of Φ_{I^*} in a range of 1.0 to 0.86; changing the position of the iodine atom or the branching of the iodides in the molecules which have been studied leads to a reduction in the value Φ_{I^*}. Apparently the other classes of compounds treated in this paper hold little promise for use in iodine photodissociation lasers.

In conclusion, the author would like to thank V.S. Ivanov and Ye.P. Smirnov for their useful discussions.

BIBLIOGRAPHY

1. J.V.V. Kasper, G.S. Pimentel, APPL. PHYS. LETTS., 5, 231 (1964).

2. V.S. Ivanov, A.S. Kozlov, A.M. Pravilov, Ye.P. Smirnov, KVANTOVAYA ELEKTRONIKA [QUANTUM ELECTRONICS], 7, 993 (1980).

3. D. Porret, C.F. Goodeve, PROC. ROY. SOC., A165, 31 (1938).

4. T. Donohue, J.R. Wiesenfeld, CHEM. PHYS. LETTS., 33, 176 (1975).

5. T. Donohue, J.R. Wiesenfeld, J. CHEM. PHYS., 63, 3130 (1975).

6. R.J. Donovan, D. Husain, ADV. PHOTOCHEM., 8, 1 (1974).

7. G. Gertsberg, "Spektry i stroyeniye dvukhatomnykh molekul" ["The Spectra and Structure of Diatomic Molecules"], Moscow, GITTL Publishers, 1949.

8. G. Gertsberg, "Elektronnyye spektry i stroyeniye mnogoatomnykh molekul" ["The Electron Spectral and Structure of Polyatomic Molecules"], Moscow, Mir Publishers, 1969.

9. A.B. Nikol'skiy, OPTIKA I SPEKTROSKOPIYA [OPTICS AND SPECTROSCOPY], 29, 1,049, (1971).

10. R.S. Mulliken, REV. MOD. PHYS., 2, 60 (1930).

11. R.S. Mulliken, PHYS. REV., 47, 413 (1935).

12. S.E. Frish, "Opticheskiye spektry atomov" ["Optical Spectra of Atoms"], Moscow, Fizmatgiz Publishers, 1963, p 212.

13. S. Mak-Glinn, T. Adzumi, M. Kinosita, "Molekulyarnaya spektroskopiya tripletnogo sostoyaniya" ["Triplet State Molecular Spectroscopy"], Moscow, Mir Publishers, 1968.

14. R.Khokhshtrasser, "Molekulyarnyye aspekty simmetrii" ["Molecular Aspects of Symmetry"], Moscow, Mir Publishers, 1968.

15. E.V. Shpol'skiy, "Atomnaya fizika" ["Atomic Physics"], Moscow, Nauka Publishers, 1974, Vol 2, p 301.

16. D.S. McClure, J. CHEM. PHYS., 17, 665 (1949).

17. R.S. Mulliken, REV. MOD. PHYS., 3, 89 (1931).

18. R.S. Mulliken, PHYS. REV. 46. 549 (1934).

19. R.S. Mulliken, J. CHEM. PHYS., 3, 506 (1935).

20. R.S. Mulliken, J. CHEM. PHYS., 8, 382 (1940).

21. R.S. Mulliken, PHYS. REV., 57, 500 (1940).

22. J.H. Van Vleck, PHYS. REV., 40, 568 (1932).

23. R.S. Mulliken, J. CHEM. PHYS., 55. 288 (1971).

24. J.A. Coxon, "Molecular Spectroscopy", Vol. I, Chem. Soc. (L), 1973, p 1.

25. R.S. Mulliken, ANN. REV. PHYS. CHEM., 29, 1, (1978).

26. W.M. Gelbart, ANN. REV. PHYS. CHEM., 28, 323 (1977).

27. R.T. Pack, J. CHEM. PHYS., 65, 4765 (1976).

28. J.A. Beswick, J. Jortner, CHEM. PHYS., 24, 1 (1977).

29. M.S. Child, MOL. PHYS., 32, 1495 (1976).

30. M.S. Child, R. Lefebvre, CHEM. PHYS. LETTS., 55, 213 (1978).

31. M.S. De Vries, N.J.A. Van Veen, A.D. De Vries, CHEM. PHYS. LETTS., 56, 15 (1978).

32. S.J. Riley, K.R. Wilson, FAR. DISC. CHEM. SOC., 53, 132 (1972).

33. K.E. Holdy, L.C. Klotz, K.R. Wilson, J. CHEM. PHYS., 52, 132 (1972).

34. J.H. Ling, K.R. Wilson, J. CHEM. PHYS., 63, 101 (1975).

35. M.D. Morse, K.F. Freed, Y.B. Band, CHEM. PHYS. LETTS., 44, 125 (1976).

36. H. Halavee, M. Shapiro, CHEM. PHYS., 21, 105 (1977).

37. M.D. Morse, K.F. Freed, Y.B. Band, J. CHEM. PHYS., 70, 3620 (1979).

38. Y.B. Band, M.D. Morse, K.F. Freed, J. CHEM. PHYS., 68, 2702 (1978).

39. E.J. Heller, J. CHEM. PHYS., 68, 2066 (1978).

40. J. Calvert, J. Pitts, "Fotokhimiya" ["Photochemistry"], Moscow, Mir Publishers, 1968.

41. C.F. Goodeve, A.W.C. Taylor, PROC. ROY. SOC. (L), A154, 181 (1936).

42. J.F. Ogilvie, TRANS. FARADAY SOC., 67, 2205 (1971).

43. S.G. Tilford, M.L. Ginter, A.M. Bass, J. MOL. SPECTROSC., 34, 327.

44. J. Romand, ANN. PHYS. (Paris), 4, 527 (1949).

45. R.J. Donovan, D. Husain, TRANS. FARADAY SOC., 62, 1050 (1966).

46. P. Cadman, J.C. Polanyi, J. Smith, J. CHEM. PHYS., 69, 14 (1967).

47. L.E. Compton, R.M. Martin, J. PHYS. CHEM., 73, 3474, (1969).

48. G.A. Oldershaw, D.A. Porret, A. Smith, J. CHEM. SOC. FAR. TRANS., I, 68, 2218 (1972).

49. R.D. Clear, S.J. Riley, K.R. Wilson, J. CHEM. PHYS., 63, 1340 (1975).

50. W.C. Price, PROC. ROY. SOC. (L), A167, 216 (1938).

51. M.L. Ginter, S.G. Tilford, A.M. Bass, J. MOL. SPECTROSC., 57, 271 (1975).

52. E. Rabinovich, W.C. Wood, TRANS. FARADAY SOC., 32, 540 (1936).

53. J.A. Myer, J.A. R. Samson, J. CHEM. PHYS., 52, 716 (1970).

54. J. Tellinghuisen, J. CHEM. PHYS., 57, 2821 (1973).

55. J.I. Steinfeld, J.D. Campbell, N.A. Weiss, J. MOL. SPECTROSC., 28, 204 (1969).

56. L. Brewer, J. Tellingshuisen, J. CHEM. PHYS., 56, 3929 (1972).

57. R.J. Oldman, R.K. Sander, K.R. Wilson, J. CHEM. PHYS., 54, 4127 (1971).

58. R.D. Clear, K.R. Wilson, J. MOL. SPECTROSC., 47, 39 (1973).

59. T.W. Broadbent, A.B. Callear, J. CHEM. SOC. FAR. TRANS. II, 68. 1367 (1972).

60. M. Brith, O. Schepp, P. Stephens, CHEM. PHYS. LETTS., 26, 549 (1974).

61. J.B. Tellinghuisen, "Coloques Internationaux, Aussoi 1977" ["International Colloquium, Aussoi, 1977"], Paris, 1977, p 317.

62. H. Hemmati, G.J. Collins, CHEM. PHYS. LETTS., 67, 5, (1979).

63. W.G. Brown, G.E. Gibson, PHYS. REV., 40, 529 (1932).

64. A.B. Petersen, I.W. Smith, CHEM. PHYS., 30, 407 (1978).

65. M.A.A. Clyne, S.I. McDermid, J. CHEM. SOC. FAR. TRANS. II, 74, 1644 (1978).

66. M.A.A. Clyne, S.I. McDermid, J. CHEM. SOC. FAR. TRANS. II, 72, 2252 (1976).

67. S.L. Baughcum, H. Hoffman, S.R. Leone, D.J. Nesbitt, FAR. DISC. CHEM. SOC., 67, 306 (1979).

68. R.J. Donovan, P.J. Robertson, SPECTROSCOP. LETTS., 5, 28 (1972).

69. R.J. Donovan, P.J. Robertson, SPECTROSCOP. LETTS., 5, 361 (1972).

70. P. Venkateswarlu, CAN. J. PHYS., 53, 812 (1975).

71. G.W. King, A.W. Richardson, J. MOL. SPECTROSC., 21, 339 (1966).

72. G.W. Kind, A.W. Richardson, J. MOL. SPECTROSC., 21, 353 (1966).

73. J.A. Myer, J.A.R. Samson, J. CHEM. PHYS., 52, 266 (1970).

74. R.J. Donovan, J.R. Konstantos, J. PHOTOCHEM., 1, 75 (1972).

75. A.D. Baranowski, J.R. McDonald, CHEM. PHYS. LETTS., 45, 172 (1977).

76. M.N. K. Ashfold, J.P. Simons, J. CHEM. SOC. FAR. TRANS. II, 73, 858 (1977).

77. M.J. Sabety-Dzvonik, R.J. Gody, J. CHEM. PHYS., 66, 125 (1977).

78. S.T. Amimoto, J.R. Wiesenfeld, R.H. Young, CHEM. PHYS. LETTS., 65, 402 (1979).

79. G.A. West, M.J. Berry, CHEM. PHYS. LETTS., 56, 423 (1978).

80. J.W. Rabalais, J.M. McDonald, V. Scherr, S.P. McGlynn, CHEM. REV., 71, 73 (1971).

81. O. Atabeck, R. Lefebvre, CHEM. PHYS. LETTS., 52, 29 (1977).

82. R.N. Haszeldine, J. CHEM. SOC., 43, 1764 (1953).

83. R.A. Boschi, D.R. Salahub, MOL. PHYS., 24, 289 (1972).

84. R.A. Boschi, D.R. Salahub, MOL. PHYS., 24, 735 (1972).

85. K. Hohla, K.L. Kompa, Z. NATURF., 27a, 938 (1972).

86. G.A. Skorobogatov, V.G. Seleznev, B.N. Maksimov, O.N. Slesar', ZhTF [JOURNAL OF TECHNICAL PHYSICS], 45, 2454 (1975).

87. V.Yu. Zalesskiy, I.L. Yachnev, OPTIKA I SPEKTROSKOPIYA [OPTICS AND SPECTROSCOPY], 43, 438 (1977).

88. A.M. Pravilov, F.I. Vilesov, V.A. Yelokhin, V.S. Ivanov, A.S. Kozlov, KVANTOVAYA ELEKTRONIKA, 5, 618 (1978).

89. A.S. Kozlov, A.M. Pravilov, KHIMIYA VYSOKIKH ENERGIY [HIGH ENERGY CHEMISTRY], 15, No 6 (1981).

90. W.S. Felps, P. Hochmann, P. Brint, S.P. McGlynn, J. MOL. SPECTROSC., 59, 355 (1976).

91. W.T. Want, W.S. Felps, G.L. Findley, A.R.P. Rau, S.P. McGlynn, J. CHEM. PHYS., 67, 3940 (1977).

92. J.D. Scott, W.S. Felps, S.P. McGlynn, NUCL. INSTR. METHODS, 152, 231 (1978).

93. N.L. Baker, B.R. Russel, J. MOL. SPECTROSC., 69, 211 (1978).

94. L.H. Sutcliffe, A.D. Walsh, TRANS. FARADAY SOC., 57, 873 (1961).

95. W.C. Price, J. CHEM. PHYS., 4, 539 (1936).

96. R.S. Mulliken, E. Teller, PHYS. REV., 61, 277 (1942).

97. A.L. Andreassen, S.H. Bauer, J. CHEM. PHYS., 56, 3802 (1972).

98. L.V. Vilkov, V.S. Mastryukov, N.I. Sadova, "Opredeleniye geometricheskogo stroyeniya svobodnykh molekul" ["The Determination of the Geometric Structure of Free Molecules"], Leningrad, Khimiya Publishers, 1978, p 125.

99. G.A. Gowder, S. Ali, J. MOLEC. STRUCT. 25, 377 (1975).

100. G.A. Gowder, S. Ali, J. MOLEC. STRUCT. 30, 181 (1976).

101. J.C. Cummings, R.E. Palmer, D.P. Aeschilman, OPTICS COMMUNS., 27, 455 (1978).

102. G.A. Gowder, J. MOL. SPECTROSC., 48, 467 (1979).

103. D.R. Salahub, R.A. Boschi, in "Chemical Spectroscopy and Photochemistry in the VUV", Dordrecht-Boston, 1974, p. 191.

104. F.J. Comes, S. Pionteck, BERICHTE BUNSENGES. PHYS. CHEM., 81, 219 (1977).

105. F.J. Comes, S. Pionteck, CHEM. PHYS. LETTS., 58, 616 (1978).

106. G.A. Skorobogatov, V.G. Seleznev, O.N. Slesar', V.M. Tret'yak, "Tezisy dokl. III Vsesoyuz. soveshch. po fotokhimii" ["Abstracts of Papers of the Third All-Union Conference on Photochemistry"], Rostov-na-Donu, 8 - 11 June 1977, p 234.

107. M.R. Levy, J.P. Simons, J. CHEM. SOC. FAR. TRANS. II, 71, 561 (1975).

108. R.E. Palmer, T.D. Padrick, J. CHEM. PHYS., 64, 2051 (1976).

109. A.M. Pravilov, KHIMIYA VYSOKIKH ENERGIY, 15, No 4 (1981).

110. A.M. Pravilov, A.S. Kozlov, F.I. Vilesov, KVANTOVAYA ELEKTRONIKA, 5, 1161 (1978).

111. L.S. Yershov, V.Yu. Zalesskiy, V.I. Sokolov, KVANTOVAYA ELEKTRONIKA, 5, 865 (1978).

112. T.F. Hunter, K.S. Kristjansson, CHEM. PHYS. LETTS., 58, 291 (1978).

113. A. Gedanken, M.D. Rowe, CHEM. PHYS. LETTS., 34, 39 (1975).

114. M. Dzvonik, J. Yang, R. Bersohn, J. CHEM. PHYS., 61, 4408 (1974).

115. Tsao-Chi-Wing, J.W.A Root, J. CHEM. PHYS., 76, 308 (1972).

116. C.C. Chou, P. Angelberger, F.S. Rowland, J. PHYS. CHEM., 75, 2536 (1971).

117. A.M. Pravilov, L.G. Karpov, L.G. Smirnova, F.I. Vilesov, KHIMIYA VYSOKIKH ENERGIY, 7, 335 (1973).

118. L.G. Karpov, A.M. Pravilov, F.I. Vilesov, KHIMIYA VYSOKIKH ENERGIY, 8, 489 (1974)

119. L.G. Karpov, A.M. Pravilov, F.I. Vilesov, KVANTOVAYA ELEKTRONIKA, 4, 822, (1977).

120. L.G. Karpov, A.M. Pravilov, F.I. Vilesov, KVANTOVAYA ELEKTRONIKA, 4, 889, (1977),

121. Yu.G. Basov, S.L. Boldyrev, L.I. Larionov, A.S. Doynikov, G.Ye. Tsvilyuk, KVANTOVAYA ELEKTRONIKA, 2, 1840 (1975).

122. G.A. Tacacs, J.E. Willard, J. PHYS. CHEM., 81, 1343 (1977).

123. L.E. Brus, V.E. Bondybey, CHEM. PHYS. LETTS., 36, 252 (1975).

124. L.E. Brus. V.E. Bondybey, J. CHEM. PHYS., 65, 71 (1976).

125. V. Yu. Zalesskiy, A.M. Kokushkin, KVANTOVAYA ELEKTRONIKA, 3, 1501 (1976).

126. R.F. Schoufele, L. Goodman, TRANS. FARADAY SOC., 61, 597 (1965).

127. R.C. Neuman, Jr., J. ORG. CHEM., 31, 1852 (1965).

128. S. Yamashita, S. Noguchi, T. Hayakawa, BULL. CHEM. SOC. JAPAN, 45, 659 (1972).

129. C. Sandorfy, in "Chemical Spectroscopy and Photochemistry in VUV", Dordrecht-Boston, 1974, p 174.

130. J. Schander, B.R. Russel, J. MOL. SPECTROSC., 65, 379 (1977).

131. D.R. Salahub, R.A. Boschi, CHEM. PHYS. LETTS., 16, 320 (1972).

132. M. Kawasaki, S.J. Lee, R. Bersohn., J. CHEM. PHYS., 63, 809 (1975).

133. M. Ito, P.S. Kuang, E.M. Kosower, TRANS. FARADAY SOC., 57, 1662 (1961).

134. K. Kimura, S. Nakagura, SPECTROCHIMICA ACTA, 17, 166 (1961).

135. R.J. Donovan, C. Fotakis, H.M. Gillespie, J. PHOTOCHEM., 6, 133 (1976).

136. M. Kawasaki, S.J. Lee, R. Bersohn, J. CHEM. PHYS., 66, 2674 (1977).

137. P.M. Kroger, S.J. Riley, J. CHEM. PHYS., 67, 4483 (1977).

138. P.M. Kroger, S.J. Riley, J. CHEM. PHYS., 70, 3863 (1979).

139. "Energii razryva khimicheskikh svyazey, potentsialy ionizatsii i srodstvo k elektronu" ["Chemical Bond Rupture Energies, Ionization Potentials and Electron Affinity"], Handbook edited by A. P. Kondrat'yev, Moscow, Nauka Publishers, 1974.

8225
CSO: 1862/252

UDC 621.373.826.038.823

TUNABLE CARBON MONOXIDE LASER

Moscow KVANTOVAYA ELEKTRONIKA in Russian Vol 8, No 7 (109), Jul 81
(manuscript received 19 Nov 80) pp 1540-1550

[Paper by V.I. Masychev, V.G. Plotnichenko and V.K. Sysoyev, Physics Institute imeni P.N. Lebedev of the USSR Academy of Sciences, Moscow]

[Text] The spectral and energy (power) characteristics of a sealed carbon monoxide laser with selective and nonselective optical resonators were studied. A diffraction grating with 100 lines/mm and a blaze angle of 30 degrees was used to make the selective resonator, which served as the input element of the laser. The radiation spectrum of the tunable CO laser contained 90 emission lines in a range of 1,626 to 1,910 cm^{-1} with a power of 10 mW to 1.36 W. In the case of the nonselective resonator, 36 emission lines were obtained with an integral power of about 13 W.

1. Introduction

Several new experimental techniques such as calorimetry, interferometry, polarimetry, photoacoustical spectroscopy, etc. have recently been proposed for the study of the optical losses in highly transparent solid-state materials used in high power laser equipment as well as in fiber optic devices [1, 2]. Their high sensitivity (on the order of 10^{-5} - 10^{-7} cm^{-1}) is achieved primarily through the use of high power radiation sources (usually from 0.1 to 100 W).

The solid-state or gas lasers employed for this purpose usually emit either one wavelength [3, 4] or several wavelengths simultaneously [5]. This substantially limits the capabilities of the methods enumerated above, since spectral measurements of the absorption and scattering coefficients in the materials being studied are needed to obtain information on the kind, quantity and form of inclusion impurities, which lead to additional optical losses.

It is necessary that the radiation source provide for the following for the spectral measurements of optical losses in highly transparent solid-state materials:

--The capability of tuning the emission wavelength in a maximally wide spectral range;

--The capability of selectively segregating a rather narrow spectral range from the entire tuning range (the width of the band singled out should be less than the absorption bandwidth of impurities, which in solid state materials at room temperature usually exceeds several cm^{-1});

--The capability of obtaining maximum emission power over the entire tuning range;

--Minimum emission power fluctuations ($\approx$ 1 %) over the measurement time (usually from several seconds to several minutes).

In the central infrared spectrum (from 2 to 15 μm), in which it is anticipated that optical losses will reach a level of 10^{-6} - 10^{-9} cm^{-1}, a figure which is several orders of magnitude lower than in the materials based on quartz glass [6, 7], where HF (2.7 μm), DF (3.8 μm), CO (5.5 μm) and CO_2 (10.6 μm) lasers in principle can be used as such sources.

The 4 - 7 μm band is of major interest, in which both the minimum of the internal optical losses and a minimum of the material dispersion for many IR materials occur [8, 9]. This band can be almost completely covered by a carbon monoxide laser, which makes it possible to obtain an emission of more than 270 lines with intervals from hundredths to several cm^{-1} [10].

The task proposed in this work was the design of a tunable CO laser suitable for the measurement of optical losses in solid-state material. The studies made of its spectral and energy (power) characteristics are of independent scientific and practical interest in view of the presence of a rather limited quantity of literature devoted to tunable carbon monoxide lasers.

2. The Structural Design of the Tunable CO Laser and the Parameters of the Selective Element

The tunable CO laser was designed around the industrial LG-22-CO laser (CO variant). The gas discharge tube of the indicated laser was fabricated from molybdenum glass. The length of the discharge portion of the tube was 125 cm and the internal diameter was 15 mm. A completely reflective internal mirror with a radius of curvature of 3 m was secured to one of the end faces of the tube, where this mirror was aligned during the assembly of the tube. The output face of the tube was covered with a gallium arsenide window, which was sealed to the face at the Brewster angle. The working composition of the gas discharge tube was a mixture of CO-He-N_2-He gases at an overall pressure of about 19.5 mm Hg.

The discharge was excited by direct current and cooled by a water flow. The temperature of the cooling water was 12 to 14 °C and the water rate of flow did not usually exceed 5 to 6 l/min.

A glass diffraction grating with an aluminum reflective coating having 100 lines/mm and a blaze angle of 30° was used for the selection of the vibrational-rotational transitions. The grating was set up in an autocollimating mode and was the output element of the optical resonator. The choice of such a grating configuration was due primarily to the specific structural design features of the laser gas discharge tube, which had, as was indicated above, a completely reflective mirror internal to the vacuum. A second order interference echelette was used for feedback (k = 2).

The emission from the resonator was brought out through zero (k = 0) and first (k = 1) orders at angles of 0 and -33° respectively to the normal of the grating, which is in good agreement with the calculated value of the angles obtained from the formula of a diffraction grating operating in an autocollimating mode. A linearly polarized plane wave with an electrical vector perpendicular to the lines of the grating (perpendicular E polarization) fell on the grating.

The dispersion resolution in a spectral range of 5.2 to 6.2 μm was $\Delta\nu$ = 2.2 to 2.75 cm^{-1} for the given optical resonator configuration (radius of curvature of the mirrors of R_1 = 3 m and $R_2 = \infty$; a spacing between them of 160 cm) and the grating parameters (k = 2, N = 100 lines/mm). In this case, the grating makes it possible in principle to single out one vibrational-rotational component of any of the P-bands. On the other hand, since the energy levels of the CO molecule are almost equidistant, then because of the overlap of various P-bands, CO lasers emit frequencies which are close, the interval between which can be less than 0.01 cm^{-1} [11]. For this reason, several emission lines could fall together in the spectral range $\Delta\nu$ resolved by the grating being used.

It is necessary to know such parameters of the diffraction grating as the intensity distribution in the working orders and the overall optical losses for the entire spectral range in order to optimize the output parameters of the created laser. The measurement of these parameters was made using the configuration shown in Figure 1a.

The laser beam (in this case, one of the beams), brought out from the resonator, is again reflected to diffraction grating 1 by means of rotating mirror 2. In this case, the direction of the radiation reflected from the mirror is close to the direction of the diffracted radiation of the gradient used for feedback. After falling on the grating, the beam is again diffracted in directions which are determined by the grating parameters. By measuring the power of the diffracted radiation, T_0, P_1, P_2 and the power of the radiation incident on the mirror P'_Σ (or, as it turned out, the power P^0_Σ which is equal to it), one can determine the reflection factors in the k-th order of R_k and the overall diffraction grating losses γ as a function of the frequency of the incident laser emission (and consequently, also as a function of the angle of incidence of the radiation on the grating ϕ reckoned from the normal to its surface):

$$R_k = P_k/P'_\Sigma;\quad \gamma = \left(P'_\Sigma - \sum_k P_k\right)/P'_\Sigma.$$

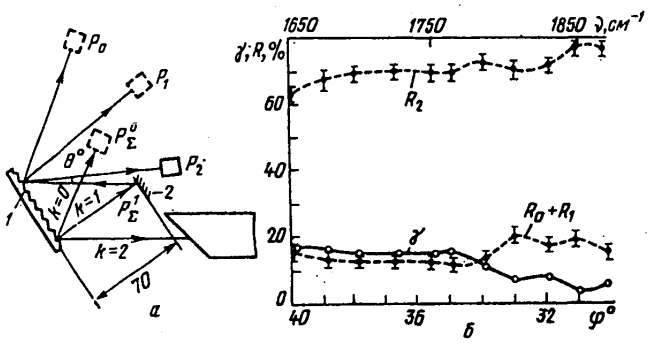

Figure 1. The configuration for the measurements of the reflection factors R_k in various spectral orders and the optical losses γ of the diffraction grating (a) and the spectral characteristics of these quantities (b).

The measured functions of $R_k(\nu)$ and $\gamma(\nu)$ for the grating used in this work are shown in Figure 1b. As the measurements have shown, the intensity distributions of the diffracted radiation in the zero and first orders proved to be practically the same.

3. A Study of the Spectral and Energy Characteristics of a Tunable CO Laser.

An overall schematic of the experimental set-up for the study of the spectral and energy characteristics of the laser which was created is shown in Figure 2.

The emission from laser 1, after being reflected from rotating mirror 2, was modulated by mechanical chopper 3 and split by means of light dividing plate 4 into two parts, each of which was directed into the appropriate measurement channel.

One part of the laser radiation was focused by KCl lens, 5, on the input slot of the infrared monochromator of an IKS-29 spectrophotometer (6), after which it was fed to Ge:Au photodetector 7. The electrical signal from the photodetector was recorded by a KSP-4 autorecorder (9) following amplifier U2-8 (8). In the alignment of the readout circuitry, its operation was visually monitored by means of the S1-48B oscilloscope 10.

The other part of the radiation, intended for monitoring the stability of the emission power during laser operation, fell on radiation detector 11, the signal from which was amplified in 12 and recorded by autorecorder 13. To reduce the thermal and mechanical drifts of the optical resonator, and consequently also the power and frequency of the emission, the laser being studied was rigidly secured on a special vibration resistant stand, made of invar.

A calibrated IMO-2N meter, 14, was used for the absolute measurements of the laser emission power.

The monochromator and resulting laser emission spectra were calibrated based on the absorption spectra of H_2O vapors in the atmosphere, prerecorded on a type FTS-14 Fourier-spectrometer with a spectral resolution of 0.1 cm^{-1}. The monochromator provided a spectral resolution of the recorded laser emission spectra of no worse than 0.5 cm^{-1}.

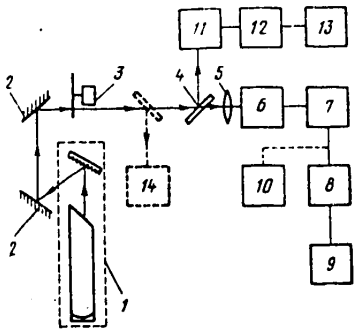

Figure 2. Schematic of the experimental set-up.

The frequencies of the vibrational-rotational transitions observed in the experiments and their identification which we made in accordance with [10, 12, 13] are given in Table 1. As can be seen from the Table, the emission spectrum of the sealed CO laser corresponded to transitions of the P-branch of the ground electron state $X'\Sigma^+$ of the CO molecule between the vibrational levels $v \rightarrow v - 1$ from $19 \rightarrow 18$ to $7 \rightarrow 6$ with rotational quantum numbers of $J - 1 \rightarrow J$ from 9 to 23. The laser emission spectrum was recorded at discharge parameters corresponding to the maximum emission power for all vibrational-rotational transitions, i.e., for the operation of the device with a nonselective optical resonator. The discharge current was 18 mA and the voltage across the tube was about 8 KV.

The lasing region of the laser with the grating encompassed a spectral range of 1,626 to 1,910 cm^{-1} (6.15 to 5.23 μm) in which 90 vibrational-rotational transitions were observed. The emission power for the strong lines amounted to from 100 to 940 mW. We will note that the emission powers shown in Table 1 represent the sum of the resonator output powers in the zero and first interference orders of the diffraction grating.

An analysis of Figure 1b and Table 1 shows that the relatively low emission powers in a range of 1,650 to 1,750 cm^{-1} are undoubtedly related to the large optical losses in the diffraction grating which run up to 15 - 17 percent. As was shown in [15], the optical losses of a resonator can have a substantial impact on the emission power of CO lasers, which have relatively low gains at the emission lines.

It should be noted that when tuning the selective resonator, it was possible to have lasing both at one and at several transitions simultaneously. The vibrational-rotational transitions at which simultaneous lasing was observed are noted in Table 1 with the curly braces. It is characteristic that with emissions at two and more transitions simultaneously, the difference between the rotational quantum numbers $|\Delta J| = |J''_v - J''_{v-1}|$ remained constant when tuning the diffraction grating and was equal to -6.

TABLE 1

Emission Lines and Their Power in a CO Laser with a Diffraction Grating

Line Номер линии Number	Wavelength Длина волны ν, $см^{-1}$ cm-1	(A) Обозначение линий $v' \rightarrow v''$	$P(J'')$	Мощность излучения P, мВт (B) (C) при $I_p = 18$ мА	при $I_p = I_{opt}$	(D) opt, мА
1	2	3	4	5	6	7
1	1626,17	19→18	P (15)	0	30	13
2	1631,73	18→17	P (20)	0	18	7
3	1639,49	18→17	P (18)	1	24	12
4	1643,26	18→17	P (17)	1	16	11
5	1650,81	18→17	P (15)	14	60	10
6	1658,23	18→17	P (13)	0	40	12
7	1660,17	17→16	P (19)	20	56	13
8	1664,06	17→16	P (18)	76	94	14
9	1667,91	17→16	P (17)	96	116	14
10	1671,75	17→16	P (16)	20	80	10
11	1679,29	17→16	P (14)	226	250	14
12	1686,71	17→16	P (12)	4	64	10
13	1688,74	16→15	P (18)	93	205	14
14	1696,50	16→15	P (16)	54	76	14
15	1704,13	16→15	P (14)	60	68	22
16	1705,61	15→14	P (20)	70	80	14
17	1707,89	16→15	P (13)	0	10	6
	1707,89	16→15	P (13)	160	260	14
18	1709,59	15→14	P (19)	166	260	22
19	1711,62	16→15	P (12)	50	100	10
20	1713,56	15→14	P (18)	300	320	16
21	1721,39	15→14	P (16)	220	230	16
22	1725,23	15→14	P (15)	450	460	10
23	1726,33	14→13	P (21)	160	200	25
24	1729,06	15→14	P (14)	400	400	18
25	1732,85	15→14	P (13)	116	130	12
26	1736,62	15→14	P (12)	100	150	16
27	1738,40	14→13	P (18)	750	750	18
28	1742,37	14→13	P (17)	560	560	18
29	1746,30	14→13	P (16)	340	340	18
30	1747,04	13→12	P (22)	16	16	18
31	1750,20	14→13	P (15)	550	550	18
32	1754,07	14→13	P (14)	440	500	14
33	1755,27	13→12	P (20)	540	580	25
34	1757,90	14→13	P (13)	180	260	10
35	1759,34	13→12	P (19)	640	660	20
	1759,34	13→12	P (19)	100	140	24
36	1763,36	13→12	P (18)	620	620	18
37	1765,50	14→13	P (11)	30	40	14
38	1767,36	13→12	P (17)	10	30	14
39	1767,76	12→11	P (23)	540	540	18
40	1775,26	13→12	P (15)	560	600	16
41	1779,16	13→12	P (14)	164	180	20
42	1780,23	12→11	P (20)	350	400	25
43	1783,02	13→12	P (13)	200	250	10
44	1784,33	12→11	P (19)	600	620	20
45	1786,64	13→12	P (12)	0	20	14
	1786,64	13→12	P (12)	100	120	10
46	1788,40	12→11	P (18)	350	350	18
47	1796,43	12→11	P (16)	200	260	10
48	1796,94	11→10	P (22)	320	400	25
49	1800,40	12→11	P (15)	520	540	14
50	1801,13	11→10	P (21)	560	600	20

TABLE 1, continued:

1	2	3	4	5	6	7
51	1804,28	12→11	P (14)	340	380	25
52	1805,29	11→10	P (20)	750	750	18
53	1808,35	12→11	P (13)	0	100	8
	1808,35	12→11	P (13)	200	260	14
54	1809,41	11→10	P (19)	860	920	20
55	1812,02	12→11	P (12)	0	80	16
	1812,03	12→11	P (12)	140	140	18
56	1813,50	11→10	P (18)	700	900	25
57	1815,81	12→11	P (11)	452	452	18
58	1817,56	11→10	P (17)	628	628	18
	1817,56	11→10	P (17)	1260	1360	22
59	1821,60	11→10	P (16)	150	240	22
60	1821,99	10→9	P (22)	500	520	22
61	1823,41	12→11	P (9)	100	300	26
62	1825,61	11→10	P (15)	300	350	14
63	1826,21	10→9	P (21)	720	740	25
64	1829,59	11→10	P (14)	42	50	19
65	1830,40	10→9	P (20)	174	180	19
66	1833,51	11→10	P (13)	320	320	18
67	1834,57	10→9	P (19)	940	940	18
68	1842,80	10→9	P (17)	880	900	22
69	1846,87	10→9	P (16)	80	150	25
70	1847,11	9→8	P (22)	1040	1080	22
71	1850,91	10→9	P (15)	350	400	20
72	1851,38	9→8	P (21)	750	760	22
73	1854,91	10→9	P (14)	240	240	18
74	1855,61	9→8	P (20)	700	740	25
75	1858,91	10→9	P (13)	40	60	14
76	1859,80	9→8	P (19)	240	240	18
77	1863,98	9→8	P (18)	380	420	25
78	1868,12	9→8	P (17)	110	110	18
79	1872,21	9→8	P (16)	420	440	20
80	1876,30	9→8	P (15)	210	210	18
81	1876,63	8→7	P (21)	270	280	22
82	1880,33	9→8	P (14)	60	80	12
83	1880,90	8→7	P (20)	180	180	18
84	1885,13	8→7	P (19)	340	360	22
85	1889,34	8→7	P (18)	28	28	18
86	1893,52	8→7	P (17)	180	180	18
87	1897,66	8→7	P (16)	52	54	15
88	1901,74	8→7	P (15)	42	44	22
89	1906,25	7→6	P (20)	22	24	9
90	1910,51	7→6	P (19)	36	40	15

Key:

A. Designation of the lines;
B. Emission power, P, MW;
C. At I_p = 18 mA;
D. At $I_p = I_{opt}$.

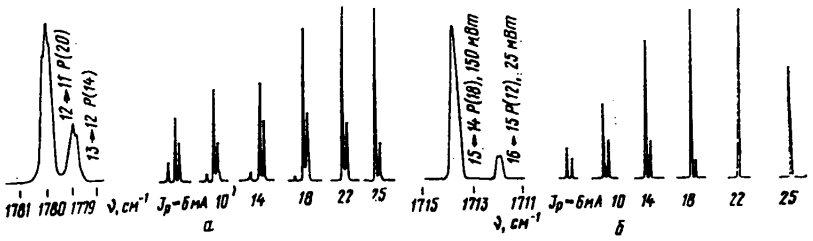

Figure 3. The relationship between the intensities of some emission lines with a change in the discharge current.

Thus, if lasing occurred at the 1,854.91 cm^{-1} line (the 10 → 9 P transition (14)), then the 1,855.61 cm^{-1} line was also observed at the same time (the 9 → 8 P transition (20)). If lasing with three lines was realized simultaneously, for example, at frequencies of 1,823.41, 1,825.61 and 1,826.21 cm^{-1}, belonging to three different bands (12 → 11, 11 → 10 and 10 → 9), then the law indicated above was also preserved ($|\Delta J| = |J''_{v+1} - J''_v| = |J''_v - J''_{v-1}| = 6$).

It should also be noted that with simultaneous lasing with two or more transitions, the ratio between the intensities of the lines and the number of them depended substantially on the angular adjustment of the echelette. This is apparently related to the difference in the spectral-selective losses of the optical resonator at various inclination angles of the grating. For this reason, in the case of simultaneous lasing with several transitions, the diffraction grating was fine-tuned to obtain the maximum total power with the minimum number of transitions (usually two) with the minimum frequency spacing between them (less than the spectral resolution of the selective element).

Additionally, attempts were made in the experiments to obtain the maximum emission powers at each of the lines through the optimization of the discharge current. The maximum emission powers obtained in this case for each line and the optimal discharge currents are given in the right side columns of Table 1. With a change in the discharge current, the ratio between the line intensities, as a rule, varied considerably, and in a number of cases, the weakest of the generated lines was successfully suppressed (Figure 3). The curves for the emission power are shown in Figure 4 as a function of the discharge current for certain lines.

The typical emission power instability of the CO laser with a diffraction grating which was studied here, recorded following preheating of the device for 1.5 to 2 hours, usually did not exceed 5 percent over 5 to 10 minutes.

4. A Comparison of the Emission Spectra of CO Laser with Selective and Nonselective Resonators

It is of interest to compare the emission spectra of a carbon monoxide laser with selective and nonselective resonators.

In the case of operation without selection of the vibrational-rotational transitions, the diffraction grating was replaced with a flat semitransparent mirror with a multilayer dielectric coating. The reflection factor of the mirror was 87 to 90 percent in a range of 1,650 to 1,950 cm^{-1}.

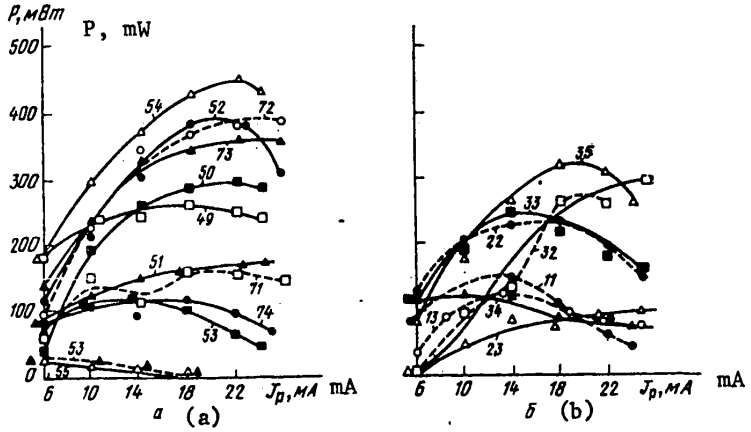

Figure 4. The emission power of a laser with a selective resonator as a function of discharge current. The numbers of the lines are taken from Table 1.

The frequencies, identification and emission power of the vibrational-rotational transitions observed in the experiments are given in Table 2. As can be seen from the Table, up to 36 transitions were observed which belong to the $v \rightarrow v - 1$ vibratrational bands from 19 → 18 to 7 → 6 in a range of 1,626 - 1,914 cm^{-1}. The integral emission power, measured with the IMO-2N detector, amounted to about 13 W, and in this case, the most intense lines had a power of more than 1 W. We will note that the laser emission spectra were usually recorded after heating the device for 1.5 to 2 hours at discharge parameters which correspond to the maximum integral emission power. The discharge current in this case amounted to 18 mA, the voltage across the gas discharge tube was 8 KV and the water rate of flow (at a temperature of 12 to 14 °C) was about 6 liters/min.

TABLE 2

Emission Lines and Their Power in a CO Laser with a Nonselective Resonator

Line Number Номер линии	Wavelength Длина волны ν, $см^{-1}$ cm^{-1}	Обозначение линий Designation of the Lines $v' \rightarrow v''$	$P(J'')$	Emission Power, Мощность излучения, мВт mW
1	1626,17	19→18	P (15)	14
2	1639,45	18→17	P (18)	10
3	1650,81	18→17	P (15)	7
4	1664,06	17→16	P (18)	84
5	1667,91	17→16	P (17)	18
6	1688,74	16→15	P (18)	2
7	1692,65	16→15	P (17)	213
8	1709,59	15→14	P (19)	170
9	1713,57	15→14	P (18)	86
10	1721,39	15→14	P (16)	75
11	1738,70	14→13	P (18)	274
12	1742,37	14→13	P (17)	212
13	1755,27	13→12	P (20)	128
14	1759,34	13→12	P (19)	187
15	1763,36	13→12	P (18)	553
16	1780,23	12→11	P (20)	34
17	1784,33	12→11	P (19)	1038
18	1788,40	12→11	P (18)	1101
19	1805,25	11→10	P (20)	1223
20	1809,41	11→10	P (19)	295
21	1813,50	11→10	P (18)	2
22	1817,56	11→10	P (17)	69
23	1821,99	10→9	P (22)	372
24	1826,21	10→9	P (21)	1124
25	1834,57	10→9	P (19)	423
26	1842,80	10→9	P (17)	270
27	1846,89	10→9	P (16)	626
28	1850,91	10→9	P (15)	1146
29	1854,91	10→9	P (14)	355
30	1872,21	9→8	P (16)	1524
31	1876,30	9→8	P (15)	335
32	1880,33	9→8	P (14)	296
33	1893,52	8→7	P (17)	661
34	1897,66	8→7	P (16)	18
35	1901,74	8→7	P (15)	53
36	1914,77	7→6	P (18)	2

It is interesting to compare the results obtained with the results of the known literature on transition selection with sealed CO lasers with a diffraction grating, in particular, with paper [14].

The emission spectrum of the laser studied here proved to be considerably wider than in paper [14], in which there were no transitions belonging to the vibrational bands 19 → 18, 18 → 17 and 17 → 16 in the low frequency band and 8 → 7 and 7 → 6 in the high frequency band. Moreover, the overall number of lines segregated in [14] was considerably smaller than in the laser we studied (36 and 90

transitions respectively). The latter remark is also justified for a nonselective optical resonator: 23 transitions in paper [14] and 36 transitions in this paper. The maximum laser emission power densities we obtained were likewise higher than in [14] (1.36 and 0.2 W respectively), despite the considerable diffraction grating losses, which reached 15 to 17 percent in the low frequency of the spectrum. Apparently, these differences are related to the substantial difference in the ratio of the components of the working mixture, and primarily to the lack of oxygen in the working mixture of the device studied here.

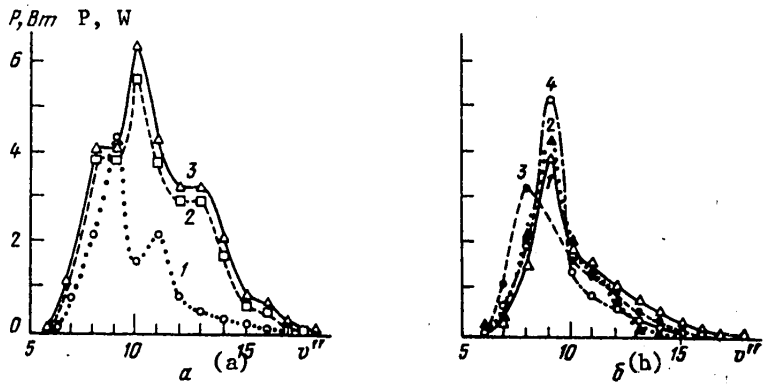

Figure 5. The contributions of individual vibrational transitions to the output power of a CO laser as a function of the number of the lower vibrational level.

Key: a. Nonselective resonator, J_p = 18 mA (1); selective resonator, J_p = 18 mA (2) and J_{opt} (3);

b. Nonselective resonator; the alignment settings of mirrors 1 - 4 correspond to the columns of Table 4.

Now, if on analogy with the results of paper [14], the powers of the groups of lines corresponding to different vibrational bands are summed, then the power distribution in the vibrational-rotational emission bands of laser with selective and nonselective resonators can have several maxima (Figure 5a, Table 3). We will also note that the power distribution in the groups of lines corresponding to the different vibrational bands in a laser with a nonselective resonator depend substantially on the alignment of its mirrors. As can be seen from Figure 5b and Table 4, for the four emission spectra taken sequentially with the same preliminary alignment of the output mirror, the power distribution in the groups of lines proved to be substantially different, however, in this case, the integral emission power of the laser changed insignificantly. This is in good agreement with what was noted previously in paper [15] as regards the high stability of the integral emission power of CO lasers, despite the relatively great fluctuations in the emission power for each of the emission transitions.

TABLE 3

Vibrational Transitions and Their Powers in a CO Laser with Selective and Nonselective Resonators

Line Number Номер линии	(1) Номер нижнего колебательного уровня	(2) Неселективный резонатор P, мВт	(3) Селективный резонатор	
			P, мВт mW	P (J_{opt}), мВт mW
1	7→6	2	58	64
2	8→7	732	1092	1126
3	9→8	2135	3910	4080
4	10→9	4386	3924	4110
5	11→10	1589	5890	6518
6	12→11	2173	3792	4242
7	13→12	868	2950	3196
8	14→13	486	3010	3200
9	15→14	331	1822	2030
10	16→15	215	510	714
11	17→16	102	442	660
12	18→17	17	16	158
13	19→18	14	0	30

Key: 1. Number of the lower vibrational level;
2. Nonselective resonator, P, mW;
3. Selective resonator.

TABLE 4

Vibrational Transitions and Their Powers in a CO Laser with Four Different Mirror Settings

Line Number Номер линии	(A) Номер нижнего колебательного уровня	(B) Мощность излучения, мВт			
		№ 1	№ 2	№ 3	№ 4
1	7 → 6	19	133	5	53
2	8 → 7	530	523	1 123	539
3	9 → 8	1 657	2 022	3 038	1 898
4	10 → 9	3 895	4 370	2 365	5 045
5	11 → 10	1 707	1 778	1 480	1 386
6	12 → 11	1 362	1 272	1 170	851
7	13 → 12	1 008	877	907	679
8	14 → 13	775	281	466	421
9	15 → 14	453	278	326	272
10	16 → 15	296	187	209	168
11	17 → 16	121	104	108	88
12	18 → 17	19	0	14	0
13	19 → 18	30	0	0	25
(C) Суммарная мощность излучения		11 872	11 820	12 274	11 432

Key: A. Number of the lower vibrational level;
B. Emission power, mW;
C. Total emission power.

We demonstrated the possibility of utilizing the laser described here for the measurement of optical losses in highly transparant solid-state materials with the example of calorometric measurements of the bulk and surface absorption coefficients in monocrystals and in a TlCl optical ceramic, the results of which are given in paper [16].

BIBLIOGRAPHY

1. L.H. Skolnik, "Optical Properties of Highly Transparent Solids", Ed. S.S. Mitre, B. Bendow, Plenum Press, 1975, p. 405.

2. A. Hordvik, APPL. OPTICS, 16. 2828 (1977).

3. D.A. Pinnow, T.C. Rich, APPL. OPTICS, 12, 984 (1973).

4. S.D. Allen, J.A. Harrington, APPL. OPTICS, 17, 1679 (1978).

5. V.G. Artyushenko, Ye.M. Dianov, L.V. Zhukova, F.N. Kozlov, V.N. Masychev, Ye.G. Morozov, V.G. Plotnichenko, KVANTOVAYA ELEKTRONIKA, 6, 646 (1979).

6. H. Osanai, T. Shioda, T. Moriyama, S. Araki, M. Horiguchi, T. Izawa, H. Takata, ELECTRON. LETTS., 12, 549 (1976).

7. T. Izawa, N. Shibata, A. Takeda, APPL. PHYS. LETTS., 31, 33 (1977).

8. L.G. VanUitert, S.H. Wemple, APPL. PHYS. LETTS., 33, 57 (1978).

9. C.H.L. Goodman, SOLID STATE AND ELECTRON DEVICES, 2 (5), 129 (1978).

10. R.M. Dale, M. Herman, J.W.C. Johus, A.R.W. McKellar, S. Nagler, I.K.M. Strathy, CAN. J. PHYS., 57, 677 (1979).

11. R.B. Dennis, H.A. Mackenzie, G. McCleccand, F.H. Hamza, OPT. AND LASER TECHNOL., 10, 221 (1976).

12. "Spravochnik fizicheskikh velichin" ["Handbook of Physical Quantities"], edited by I.K. Kikoin, Moscow, Atomizdat, 1976, p 720.

13. "Spravochnik po lazeram" ["Laser Handbook"], edited by A.M. Prokhorov, Moscow, Sov. Radio Publishers, 1978, p 108.

14. V.P. Avtonomov, M.V. Zavertayev, Yu.A. Kochetkov, N.N. Ochkin, N.N. Sobolev, KVANTOVAYA ELEKTRONIKA, 6, 1556 (1976).

15. V.S. Aleynikov, V.N. Masyche, KVANTOVAYA ELEKTRONIKA, 6, 1556 (1976).

16. Ye.M. Dianov, V.I. Masychev, V.G. Plotnichenko, V.K. Sysoyev, KVANTOVAYA ELEKTRONIKA, 7, 1342 (1980).

8225
CSO: 1862/252

UDC 621.373.826.038.825.3

EFFICIENCY OF Li-Nd-La PHOSPHATE GLASS LASER IN LOW PUMPING POWER RANGE: FREE-RUNNING OPERATION

Moscow KVANTOVAYA ELEKTRONIKA in Russian, Vol 8, No 7 (109), Jul 81 (manuscript received 23 Dec 80) pp 1598-1600

[B.I. Denker, N.N. Il'ichev, G.V. Maksimova, A.A. Malyutin, V.V. Osiko and P.P. Pashinin, Physics Institute imeni P.N. Lebedev of the USSR Academy of Sciences, Moscow]

Free running operation of a laser using concentrated Li-Nd-La phosphate glass was studied in a pumping energy range of 1 to 15 J. A laser efficiency of 2.9 percent was obtained at a pumping energy of 14.5 J. The internal losses of the resonator are estimated and the ultimately attainable efficiency is determined. Laser operation was studied in one-shot and pulse repetition modes right up to a frequency of 25 Hz.

Free-running oscillation was optimized and studied in [3] for a pumping range of 20 to 100 J for concentrated Li-Nd-La phosphate glass (KNFS [CPG] [1, 2]). The results obtained in [3], as well as in [4], show that in the small pumping energy range (less than 20 J), the parameters of CPG laser can be rather high. Obtaining the maximum efficiencies in this pumping range is especially important from the viewpoint of increasing the pulse repetition rate in neodymium glass lasers.

This paper, which is a continuation of [3], is devoted to the optimization of the free-running mode of a CPJ laser for one-shot and repeating pulses in a pumping energy range of 1 to 15 J, where primary attention has been devoted to the question of the efficiency of pumping energy converstion to the inverted population, which is of importance in laser design. This parameter also primarily governs the utlimately attainable efficiency of the lasers.

The studies were performed with cylindrical active elements (AE) with dimensions of 6.3 mm in diameter by 100 mm long made of CPG with an Nd^{3+} ion concentration of $8 \cdot 10^{20}$ cm^{-3}. To strengthen the laser, the side surface of the active element was etched to a depth of $\approx$ 100 μm. The end face surfaces were not transilluminated.

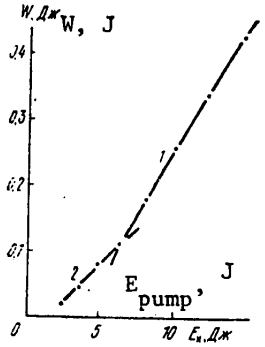

Figure 1. The output energy as a function of the pumping energy for mirrors with reflection factors of R = 83 %, r = 5 m (1) and R = 96.5 %, r = = 3 m (2).

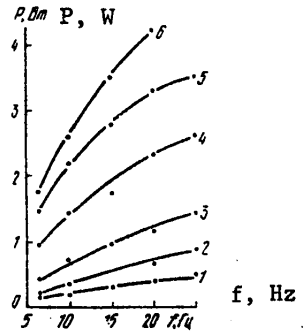

Figure 2. The average output power as a function of frequency for a pumping energy of 2.6 J/pulse (1), 3.6 J/pulse (2), 4.9 J/pulse (3), 8.1 J/pulse (4), 10 J/pulse (5) and 12 J/pulse (6); R = 96.5% (1-3) and 83% (4-6).

The pumping was accomplished with a Xe lamp (gas pressure of about 800 mm Hg) with discharge dimensions of 4 mm in diameter by 60 mm long. The illumination source was a quartz monoblock 40 mm in diameter by 60 mm long with a silver coating, cooled with distilled water. The discharge circuit of the pulse tube was formed by a 20 μFd capacitor and an inductance of 33 mHy. A slaved arc mode with a current of about 0.7 amps was employed.

The laser emission energy in a one-shot pulse mode is shown in Figure 1 as a function of the pumping energy for two values of the reflection factor of the output mirror: 83 and 96.5%. It should be noted that the utilization of a slaved arc made it possible to obtain a gain in the output energy (for example, with a pumping energy of 10 J, a gain by a factor 1.7). It can be seen from Figure 1 that with 10 J pumping, the effeciency is 2.6%. The threshold pumping when the denser of the mirrors was used amounted to 1 J.

The results of measurements of the lasing characteristics of a CPG laser operating in a pulse-periodic mode are shown in Figure 2. The family of curves is plotted which show the average emission power as a function of the pulse repetition rates. The pumping energy is fixed along each curve.

Of the greatest interest here are the results obtained for high pulse repetition rates. Thus, at a frequency of 20 Hz and with an average pumping power of 240 W, an average output power of 4.2 W was obtained (efficiency of 1.75%). In the region of low pumping energies (2.6 J/pulse), the average output power was 0.5 W at a repetition rate of 25 Hz (efficiency of 0.77%). In an almost fully enclosed resonator with the same frequency and a pumping energy per pulse of 1.2 J, the average emission power (in one direction) was 3.3 mW.

It should also be noted that the emission energy with pumping of 10 J/pulse for a frequency of 25 Hz is only 40% less than the energy obtained in the one-shot pulse mode (see Figure 1). Preliminary investigations showed that the major reason for this reduction is the thermo-optical distortions of the active element during its pumping, which can be extremely effectively compensated for fixed operating modes.

The internal resonator losses can be determined from the slopes of the curves plotted in Figure 1 [5], as well as the ultimately possible differential laser efficiency (i.e., the laser efficiency in the absence of internal resonator losses). An expression was used for this which relates the lasing energy W to the parameters of the resonator, the active medium and the pumping energy E_H for a free running laser. We shall write this function for a four-level medium [6], taking into account the finite pumping pulse width, assuming it has a rectangular waveform:

$$W = \frac{\eta |\ln R|}{\varkappa - \ln R} E_H - E_0 \left(1 + \frac{T}{\tau}\right), \tag{1}$$

where R is the output mirror reflection factor; κ is the internal resonator losses; T is the pumping pulse width; τ is the lifetime of the upper lasing level; η is the efficiency of pumping energy conversion to the inverse population; $E_0 = \omega S|\ln R|/2\sigma$; σ is the lasing transition cross-section; S is the cross-sectional area of the active element; ω is the lasing quantum energy. Included in κ are the losses due to absorption and light scattering in the resonator elements, as well as diffraction losses and losses related to inaccuracy in aligning the resonator. In particular, if only the absorption losses are considered, then $\kappa = 2\gamma l$, where γ is the coefficient of absorption in the active element at the lasing wavelength; l is the length of the active element.

Formula (1) is quite well observed where the threshold is sufficiently exceeded and where the lasing pulse width practically matches the pumping pulse width. When a sufficient amount of experimental data is available, this expression can be used to find a number of laser parameters: κ, η, E_0 and even R. The latter is necessary when interference effects between the end faces of the active element and the resonator mirrors have a strong impact on the effective transparency of the output mirror.

From the differential laser efficiency

$$\eta_d = \frac{dW}{dE_H} = \eta \frac{|\ln R|}{\varkappa - \ln R} \tag{2}$$

using two experimental curves for $W(E_H)$ for different R_a and R_b, one can find κ and η. Thus, designating $x = \eta_a/\eta_b$, $y = \ln R_a/\ln R_b$, and assuming that κ does not depend on R, we derive the following from (2):

$$\varkappa=(x-1)\,|\ln R_a|/(y-x). \qquad (3)$$

The quantity y can be found as the ratio $W_a(0)/W_b(0)$, extending the function $W(E_H)$ until it interesects the axis of the output energy on the side of its negative values.

We have the following for our experimental data from (1) and (2) (see Figure 1): $\kappa = 0.04 \pm 0.024$ and $\eta = 5 \pm 1.2$ %. (The effective reflection factors taking into account the influence of the end face of the active element were used in the calculations).

Thus, an inverstigation of the lasing characteristics of a CPG laser in a pumping energy range of 1 to 15 J has shown that a CPG active element of a comparatively small diameter (6.3 mm) efficiently intercepts the pumping radiation (η = 5%). A CPG laser also has a rather high efficiency in a pulse-periodic mode, right up to a repetition rate of 25 Hz.

The low internal losses of the resonator attest to the rather high optical quality of the CPG active element. The numerical values of κ and η can be utilized in the design of lasers operating not only in a free running mode, but also in a Q-switched mode.

BIBLIOGRAPHY

1. S.Kh. Batygov, Yu.K. Voron'ko, B.I. Denker, A.A. Zlenko, A.Ya. Karasik, G.K. Maksimova, V.B. Neustruyev, V.V. Osiko, V.A. Sychugov, I.A. Shcherbakov, Yu. S. Kuz'minov, KVANTOVAYA ELEKTRONIKA, 3, 2243 (1976).

2. Yu.K. Voron'ko, B.I. Denker, A.A. Zlenko, A.Ya. Karasik, Yu.S. Kuz'minov, G.V. Maksimova, V.V. Osiko, A.M. Prokhorov, V.V. Sychugov, G.P. Shipulo, I.A. Shcherbakov, DAN SSSR [REPORTS OF THE USSR ACADEMY OF SCIENCES], 227, 75 (1976).

3. A.G. Avanesov, Yu.G. Basov, V.M. Garmash, B.I. Denker, N.N. Il'ichev, G.V. Maksimova, V.V. Osiko, A.A. Malyutin, P.O. Pashinin, A.M. Prokhorov, V.V. Sychev, KVANTOVAYA ELEKTRONIKA, 7, 1,120 (1980).

4. A.G. Avanesov, I.V. Vasil'yev, Yu.K. Voron'ko, B.I. Denker, S.V. Zinov'yev, A.S. Kuznetsov, V.V. Osiko, P.P. Pashinin, A.M. Prokhorov, A.A. Semenov, KVANTOVAYA ELEKTRONIKA, 6, 1,586 (1979).

5. Yu.A. Anan'yev, A.A. Mak, B.M. Sedov, ZhETF [JOURNAL OF EXPERIMENTAL AND THEORETICAL PHYSICS], 48, 7 (1965).

6. A.A. Mak, Yu.A. Anan'yev, B.A. Yermakov, UFN [PROGRESS IN THE PHYSICAL SCIENCES], 92, 373 (1967).

8225
CSO: 1862/252

UDC 621.373.826

REQUIREMENTS PLACED ON PUMPING X-RAY LASER WITH IONIZATION SOURCE

Moscow KVANTOVAYA ELEKTRONIKA in Russian Vol 8, No 7 (109), Jul 81 (manuscript received 28 May 81) pp 1606-1607

[Paper by F.V. Bunkin, V.I. Derzhiyev and S.I. Yakovlenko, Physics Institute imeni P.N. Lebedev of the USSR Academy of Sciences, Moscow]

[Text] It is shown that when pumping a medium with an atomic number of $Z \approx 30$ using shortwave electromagnetic radiation with a wavelength of $\gamma_{pump} \lesssim 0.1$ nm and an intensity of $\approx (10^{15} - 10^{16}$ W/cm^2 over a time of $c_{pump} \gtrsim 30$ nsec, it is possible in principle to achieve lasing with the $n_i = 5.4 \rightarrow n_f = 3$ transitions between hydrogen-like states of multicharged ions ($\lambda_{las} \approx 1$-2 nm). The active medium can be produced during the irradiation, for example, using a copper or brass wire with a length of $l \approx 1$ m and an initial radius of $r_0 \lesssim 0.3$ mm.

As is well known [1], § 16), the recombinational nonequilibrium of a plasma can be maintained in the steady-state by an external ionizing source (for example, an electron beam or short wave electromagnetic radiation), where the conditions for lasing can be realized directly in the medium during the action of the ionizing source. Such a situation has been treated in considerable detail for visible band plasma lasers, however, for the shortwave band ($\lambda_{las} < 50$ nm), only pumping has been discussed for which the energy input and the electron cooling are substantially separated in time. This is explained by the lack of laboratory sources of ionizing radiation with a flux adequate for pumping transitions in the shortwave band. We shall estimate the requirements placed on the ionizing X-ray radiation flux necessary to achieve lasing in the 1-2 nm range in this paper, considering the "exotic" sources of [2].

We shall base our work on the well known scheme [3, 1] for the population inversion of hydrogen-like levels of c = 5, 4, 3. Inversion occurs with the $n_i = 5.4 \rightarrow n_f = 3$ transition as a result of the fact that the lower levels n_f go through a radiation decay faster than the upper levels n_i. We shall not consider inversion relative to the $n_f = 2$ level because of the reabsorption of the radiation of the $2 \rightarrow 1$ transitions and the $1 \rightarrow 2$ pumping by fast secondary electrons (see [1], § 16). The transitions $n_i = 5.4 \rightarrow n_f = 3$ have $\lambda_{las} \approx 1 - 2$ nm for a nuclear charge of $Z \approx 30$. For example, for Z = 26 (iron), $\lambda_{43} = 2.77$ nm and

λ_{53} = 1.9 nm; for Z = 29 (copper), λ_{43} = 2.23 nm and λ_{53} = 1.52 nm; for Z = 30 (zinc), λ_{43} = 2.08 nm and λ_{53} = 1.42 nm. The ionizaton potentials $J_Z = 13.6\ Z^2$ eV for the H-like ions of these elements are J_{Fe} = 9.2 KeV, J_{Cu} = 11.4 KeV and J_{Zn} = 12.2 KeV. It is necessary to steady-state pumping that the pumping quantum energy $h\omega_{pump}$ be greater than J_Z. This corresponds to a pumping wavelength λ_{pump} of 0.1 nm and an effective source temperature of $T_s \gtrsim 10$ KeV.

In order that an inversion be realzed with the $n_i = 5,4 \rightarrow n_f = 3$, the plasma electron concentration and temperature should be comparatively low (see Figures 5 and 3 in [1]): N_e (5-10) $\cdot\ 10^{11}\ Z^7\ cm^{-3} \simeq 10^{22}\ cm^{-3}$, T_e (1-2) Z^2 eV $\simeq$ 1-2 KeV. If the medium is a solid in the initial state, for example, a brass wire with a radius of r_0 = 0.3 nm, then the dispersal of the electron concentration from $N_{e0} \simeq \simeq Z \cdot 10^{22}\ cm^{-3} \simeq 3 \cdot 10^{23}\ cm^{-3}$ to $N_e \simeq 10^{22}\ cm^{-3}$ with a velocity of $v_T \simeq \sqrt{2T_e/am_p} \simeq \simeq \sqrt{T_e/n_pZ} \simeq 0.5 \cdot 10^7$ cm/sec (A $\simeq$ 2Z, $m_p = 1.6 \cdot 10^{-24}$ g) occurs in a time of:

$$t_{dispersal} = (r_0/v_T)(N_{e0}/N_e) \simeq 30 \text{ nsec.}$$

The time that the hard pumping source acts t_{pump} should exceed the time for dispersal to the requisite electron concentration: $t_{pump} \simeq t_{dis}$. We will note that in the case of pumping due to thermal ionization and subsequent cooling [1], the pumping time is not limited on the downside, but rather from above ($t_{pump} < < t_{dis}$).

The threshold ionizing radiation intensity I_{pump}, given the condition that the number of ionization and recombination events are equal, is related to the threshold gain κ_π by the following formula:

$$\kappa_\pi \simeq (\lambda^2_{las}/16\Delta\omega)(N_{Z-1}\sigma_{pic}I_{pump}/h\omega_{pump}),$$

where $\Delta\omega$ is the effective line width; σ_{pic} is the photoionization cross-section of the Z - 1 ion; $N_{Z-1} \simeq N_Z \simeq N_e/Z \simeq 3 \cdot 10^{20}\ cm^{-1}$.

Working from a wire length of $l \simeq$ 1m, we set $\kappa_\pi \simeq 10/l \simeq 0.1\ cm^{-1}$. By taking the Stark line width, with a slight excess in the following form:

$$\Delta\omega = 11\ \frac{\hbar}{m_e}\left(n_f^2 - n_i^2\right)\left(\frac{N_e}{Z}\right)^{2/3} \sim \begin{cases} 5 \cdot 10^{18}\ s^{-1} \text{ for } 4 \rightarrow 3, \\ 10^{18}\ c^{-1} \text{ для } 5 \rightarrow 3, \end{cases}$$

We obtain the conditions:

$$\sigma_{\Phi\pi}\frac{I_н}{\hbar\omega_н} > \begin{cases} 5 \cdot 10_8\ c^{-1} \text{ для } 4 \rightarrow 3\ (Z = 30), \\ 3 \cdot 10^9\ c^{-1} \text{ для } 5 \rightarrow 3\ (Z = 30). \end{cases}$$

For the case of $\sigma_{pic} \approx 10^{-21}$ cm^2, $\omega_{pump} \approx 10$ KeV $\approx 1.6 \cdot 10^{-15}$ J, we have the condition of $I_{pump} 10^{15}$ W/cm^2 for the $4 \rightarrow 3$ transition and $I_{pump} 5 \cdot 10^{15}$ W/cm^2 for $5 \rightarrow 3$ ($Z = 30$). Such an intensity at a distance of about one meter from the pumping source corresponds to the liberation of 10^{14} J over 50 nsec, if more than 10 % of the energy is contained in the hard radiation. The divergence of the laser emission in this case should amount to $\phi = v_T t_{dis}/l \approx 10^{-3}$ rad.

The estimates presented here show that lasing can occur at a wavelength of $\lambda_{las} \approx 1.4$ nm, something which was mentioned in paper [2], (the $5 \rightarrow 3$ transition in zinc is closest to the indicated wavelength, see above). However, the information contained in paper [2] is completely inadequate both for assessing the reliability of the experiment itself and for attempting to interpret it more specifically. On the other hand, the consideration of the dynamics of forced plasma dispersal with the action of high power electromagnetic radiation, similar to that carried out in papers [4, 5], takes on additional interest because of that presented above.

BIBLIOGRAPHY

1. L.I. Gudzenko, S.I. Yakovlenko, "Plazmennyye lazery" ["Plasma Lasers"], Moscow, Atomizdat Publishers, 1978.

2. C. Robinson, Jr., AVIATION WEEK SPACE TECHN., 114, No. 8, 25 (1981).

3. B.F. Gordiyets, L.I. Gudzenko, L.A. Shelepin, ZHURN. PRIKL. TEKH. I TEKHN. FIZ. [JOURNAL OF APPLIED ENGINEERING AND TECHNICAL PHYSICS], 5, 115 (1966).

4. V.I. Derzhiyev, V.S. Marchenko, S.I. Yakovlenko, PIS'MA V ZhTF [LETTERS TO THE JOURNAL OF TECHNICAL PHYSICS], 6, 605 (1980).

5. A.G. Zhidkov, V.S. Marchenko, "Preprint IAE-3389" ["Institute of Nuclear Energy Preprint No. 3389"], Moscow, 1981.

8225
CSO: 1862/252

UDC 532

DYNAMICS OF HYDROELASTOPLASTIC SYSTEMS

Kiev DINAMIKA GIDROUPRUGOPLASTICHESKIKH SISTEM in Russian 1981 (signed to press 2 Feb 81) pp 2-10

[Annotation, editor's message, preface and table of contents from book "Dynamics of Hydroelastoplastic Systems", by Sh. U. Galiyev, Institute of Strength Problems, UkSSR Academy of Sciences, Izdatel'stvo "Naukova dumka", 276 pages]

[Text] The book deals with mathematical formulation of the problem of nonlinear interaction of solid deformable and liquid media, development of algorithms and numerical investigation of the response of complex hydroelastoplastic systems to explosion in water. A solution is given for a broad class of applied problems. Major emphasis is on studying the influence that other than one-dimensional cavitation, as well as geometric and physical nonlinearities of shells have on unsteady interaction of media; another topic emphasized is calculation of the three-dimensional stress-strain state of cylinders under the action of hydraulic impact. The developed algorithms are shown to be workable, and the principles that govern unsteady nonlinear processes arising in hydroelastoplastic systems are described.

For scientists, engineers and technicians dealing with problems of the mechanics of continuous media, dynamic strength of structural components and high-strain rate metalworking.

Figures 143, tables 17, references 199.

Editor's Message

A considerable number of works have dealt with the problem of unsteady interaction of deformable solids with a liquid. Most have been based on assumptions permitting linearization of the initial equations in whole or in part. Usually the simplest structural components immersed in an infinite fluid are considered, and analytical methods are mainly used in the solution.

The present monograph outlines a theory of nonlinear interaction of deformable bodies with a liquid. The author considers all major nonlinear effects that influence the dynamic strength of components interfacing with the liquid, and in this way considerably extends the range of problems covered by theory. The main new feature of the developed approach is that of accounting for other than one-dimensional cavitation in the liquid, which is principally what has determined

the originality of the proposed research techniques and the results. In addition to nonlinear factors that influence unsteady behavior of multiphase systems comprising a solid deformable body and a liquid, consideration is taken in the solution of the problems of boundedness of the liquid volume, the products of explosion expanding in the liquid, and three-dimensionality of the stressed and strained state of the obstacle.

The book gives a complete presentation of the specifics of the problem of hydroelastoplasticity and the place that it occupies in the mechanics of continuous media. Based on solution of specific problems, the most significant factors are revealed that influence unsteady processes in hydroelastoplastic systems, and their interplay with changes in parameters is demonstrated. The results enable preliminary evaluation of the influence that various nonlinear effects have on the strength of a structural element, and provide a sound basis for disregarding secondary effects. The method of finite differences is used in solving the problems.

The principal conclusions of the work and accuracy of results are confirmed by a large number of calculations done with a variety of grids and computation algorithms, as well as models of interacting media.

The book is structured around original material obtained by the author personnaly, makes an appreciable contribution to the mechanics of continuous media and dynamic strength of structures, and will merit favor by scientists and specialists working with problems in this field of mechanics.

Academician G. S. Pisarenko,
UkSSR Academy of Sciences

Preface

Oscillations and movements of structural elements in a liquid are accompanied by hydrodynamic loading that frequently is considerably dependent on the amount of deformation, which depends in turn on hydrodynamic pressure. Calculation of such structures involves the necessity of simultaneous solution of equations that describe the motion of the liquid and solid deformable media. Therefore the theory of interaction between structures and liquid as component parts contains both hydrodynamics and mechanics of a solid deformable body, and also the conditions on the contact surface of the media. Problems of interaction are considered in a number of previous works.

Of considerable interest are problems of unsteady interaction between deformable solids and liquid. The calculation of dynamic strength of thin-walled and thick-walled structures in contact with a liquid (the hull of ships, pipelines, underwater structures, boilers in electric power plants and so on), as well as the theoretical study of the shape alteration of bodies that are worked by liquid or located in a flow of liquid, reduce to problems of this category. Unsteady processes give rise to complex wave processes in the liquid and deformed body, often with accompanying physically and geometrically nonlinear properties of the interacting media. The pattern of interaction is non-one-dimensional, the contact surface of the media is deformed, giving rise to difficulties in formulation of the conditions of joining on this surface. Because of the complexity of accounting for these nonlinear

factors, until recently problems of interaction have been solved on the basis of the following simplifying assumptions: 1) ideal liquid in motion without eddies; acoustic approximation valid; 2) no cavitation in the liquid; 3) material of obstacle conforms to Hooke law; 4) boundary conditions on the contact surface of the media can be written without consideration of deformation of the surface. Of all the possible nonlinearities, the geometric nonlinearity of the obstacle has been taken into consideration in some cases. Many problems of interaction of an underwater wave with obstacles that are important for practice have been solved in such a formulation. However, the results are valid in a limited range of variation of the load, geometry and material of the deformable body.

In the general case, the given assumptions may not be satisfied. The class of problems that require consideration of the nonlinear properties of the interacting media is constantly growing due both to the increase in requirements for strength of present-day supporting members and structures, and to the increasing use of high-energy unsteady technological processes. For this reason, recent years have seen research in which interaction problems are solved with consideration of the corresponding nonlinear phenomena in the contacting media.

Journal articles have used a variety of approaches to the problems and the methods of solving them, which has been an impediment to familiarity with the problem of nonlinear interaction as a whole, and to analysis of the influence that different nonlinear factors have on the behavior of a structural element. Inadequate attention is given to the influence that cavitation in a liquid has on the process of interaction. This can be attributed to the fact that motion of a medium in cavitation zones is not described by classical equations of hydrodynamics, as well as to the fact that the boundaries of cavitation zones in the liquid are not known at every instant. At the same time, even in the late forties it was noted that it is important to account for cavitation as a factor that determines the destructive action of underwater explosions.

In addition to the given assumptions that allow use of mainly linear equations, it is further assumed in calculations that obstacles can be treated as plates or shells. Such an approach needs refinement for thick-walled bodies in the case of short pulses close to regions of rapid shape change or points of attachment of the body. This explains the interest that has arisen in the interaction of underwater waves with three-dimensional bodies.

A previous work has made an attempt at systematic presentation of the nonlinear theory of interaction of a liquid with deformable bodies. In addition, the same work analyzes the influence of various nonlinear factors on interaction of underwater waves with obstacles, and presents the results of numerical calculations for thin-walled and thick-walled bodies. Despite isolated inadequacies, this paper, published in 1977 [Ref. 32] aroused the interest of specialists [Ref. 25] and was published in English translation in the United States in 1980 [Ref. 175].

Our book is a further development of the monograph of Ref. 32. It presents a nonlinear theory of interaction of deformable bodies with a liquid, accounting for all major nonlinear phenomena in unsteady interaction between a liquid and obstacles. Component parts of the theory are new models of a cavitating liquid with regard to the fact that a real liquid does not work well on tension. The first

model is based on the assumption that zones of destruction (cavitation) in rarefaction waves can be approximately modeled by some continuous medium in which pressure is constant. In the second model the speed of sound in a mixture of liquid and gas bubbles filling a region of destruction in the liquid is taken as a constant quantity much less than the speed of sound in the intact liquid or gaseous medium. The problem of calculating the interaction of pressure waves with obstacles with regard to cavitation in the general three-dimensional model is formulated as a new class of problems of mathematical physics.

Most of the book deals with solving topical problems. Equations that describe the motion of liquid and deformable obstacles are numerically integrated by a finite-difference method. The behavior of thin-walled and thick-walled structural elements in an underwater explosion is studied as well as the arisal and development of cavitation accompanying wave processes in a liquid. It is shown that different kinds of nonlinearities have different kinds of influence on thin-walled obstacles. The geometric nonlinearity of an obstacle shows up only during flexures that exceed its thickness. Nonlinear terms in the conditions on the interface between media have less influence on interaction. Accounting for plastic properties enables determination of the residual change in shape of an obstacle.

An expanded description is given of algorithms used in the calculations for solving the unsteady three-dimensional problem of hydroelasticity for thick-walled structural elements of cylindrical shape. Emphasis is placed on analysis of the strength of structures, and on investigation of the diffraction of elastic waves at corner points, stiffener ribs and joinings between components.

In constructing the theory, the author has used relatively "simple" models of the interacting media: the liquid is taken as inviscid both inside and outside of cavitation zones, plastic properties of the body are accounted for by the theory of flow with isotropic strengthening. On the one hand, this is due to the fact that the exactness of the models used for the media is not the same. Obviously it does not make sense to improve the accuracy of equations defining the plastic flow of material when the accuracy of theories used for the cavitating liquid has not been fully determined. On the other hand, the use of complicated models (plastic behavior of the obstacle material, gas-liquid mixture in cavitation zones, and so on) is difficult in many cases because of a lack of experimentally definable parameters. Finally, the author has aimed at simplicity in formulating the problem, feeling that simple models (where they are successful) often contain the germ of what is typical of the physics of the problem. Indeed, it is the "simplicity" of the models used that has enabled solution of a broad range of heretofore unformulated problems of interaction of the given complex media. Let us note that the behavior of each of them in high-speed processes has only recently come under investigation.

The problem of interaction is considered as a problem of investigation of the behavior of systems with parameters whose time and space distribution is unknown and is to be found during solution. The inadequate coverage of this class of problems has made it necessary to develop nonstandard solution algorithms that enable calculation of the motion of cavitation zones in a liquid, plastic zones in a solid and on the interface between media in space.

Considerable attention is given to investigation of accuracy of the results. In some cases, an approach is used that is based on reducing (fractionating) the spacing of a grid. However, for complicated problems this approach is limited by the capabilities of the computer. Besides, it answers the question of the accuracy of solution of the formulated problem, but not the question of correspondence of the results to actual processes, and because of the novelty of the given problems, this correspondence is very important. Therefore, in verifying the results, more extensive use is made of calculations in accordance with different models of cavitating and ideal liquids, the solid deformable body, and the process of interaction. We assume that agreement of results found by different approximate theories (in the solution of particular problems they get progressively more complicated) is the most weighty proof of their objectivity. Theoretical results are compared with data of experiments. It is shown that the proposed approximate models of a cavitating liquid are completely satisfactory from the standpoint of problems of unsteady interaction of deformable bodies with a liquid. At the same time, differences between some results is an indication of the need for improving the theory and the direction of future research.

The book examines a complex of problems that arise in calculations of the strength and stiffness of structural elements to the action of underwater pressure waves. The algorithms developed are general to some extent. They may be of use both in the solution of problems of hydrodynamics and solid-state mechanics, and in the application of other numerical methods, such as the finite element method, to the calculation of hydroelastoplastic systems. The results can provide sounder preliminary estimates of the influence that various nonlinearities have on the interaction process, and can also serve as a basis for a variety of simplifying assumptions in formulation of problems. The list of references cites papers that have had an influence on the writing of this book.

The author thanks Academician V. V. Novozhilov of the USSR Academy of Sciences, professors A. K. Pertsev, V. V. Matveyev, L. I. Slepyan, R. I. Nigmatullin, R. F. Ganiyev and U. K. Nigul for constructive comments on the manuscript. The author is especially grateful to Academician G. S. Pisarenko of the UkSSR Academy of Sciences for interest in the work, and for assistance in defining the aim and nature of the research.

Contents page

6610
CSO: 1862/262

UDC 537.53

CALCULATING ENERGY CHARACTERISTICS OF ELECTRON-BEAM CONTROLLED CO PROCESS LASER WITH TURBOCOMPRESSOR COOLING

Moscow DOKLADY AKADEMII NAUK SSSR in Russian Vol 259, No 5, 1981 (manuscript received 21 Apr 81) pp 1094-1098

[Article by Academician N. G. Basov, Ye. P. Glotov, V. A. Danilychev, A. M. Soroka, E. M. Urin and V. I. Yugov, Physics Institute imeni P. N. Lebedev, USSR Academy of Sciences, Moscow]

[Text] Electron-beam controlled (EBC) CO_2 lasers are currently in wide use in technological applications [Ref. 1]. Ref. 2 demonstrated the feasibility of a considerable increase in the specific power output and efficiency of EBC-CO_2 laser emission by cooling the lasing mixture to temperatures of T ~ 170-200 K, and proposed an arrangement of turbocompressor cooling in which a gas refrigeration engine is realized on the working laser mixture. Of even more promise is the use of this arrangement in EBC lasers using carbon monoxide; these lasers, in contrast to CO_2 lasers, can in principle operate effectively only with cooling of the gas mixture to cryogenic temperatures of ~100 K [Ref. 3].

At the present time, a lasing efficiency $\eta_\Phi > 60\%$ has been experimentally attained on an EBC-CO laser [Ref. 4]. At the same time, cooling of the laser mixture to cryogenic temperatures requires large energy expenditures, which can appreciably reduce the technical efficiency η_T, the major characteristic of process lasers. However, the active medium of the CO laser is fundamentally different from that of the CO_2 laser in that during the lasing process the vibrational energy remaining in the working medium as a consequence of the difference of η_Φ from unity is not nearly instantaneously converted to heat, but remains stored for some time on vibrational levels. This peculiarity together with considerably greater quantum efficiency (~95% instead of ~47%) leads to a situation where the fraction of pumping energy that is converted to heat during excitation is extermely low (~10%) in the working temperature range as compared with the analogous quantity for the CO_2 laser medium (~80-90%). As a result, the effective specific heat of the CO laser mixture $c_{ef} = c_p/\delta_T$ is nearly an order of magnitude greater than that of the CO_2 laser (c_p is the specific heat at constant pressure, δ_T is the fraction of pumping energy expended on heating the gas). Another important peculiarity of the working medium of CO lasers at low temperatures ($T \lesssim 200$ K) is that the energy stored on vibrational levels is dissipated due to spontaneous emission rather than due to collisional relaxation. As a consequence, it is possible to attain high technical efficiency of the CO laser despite the need of intense cooling of the laser mixture.

In this paper, the authors calculate the energy characteristics of an EBC CO laser with turbocompressor cooling.

1. The equations that describe changes in gasdynamic and optical characteristics of the laser medium in a rectangular active volume take the form

$$(1)\quad \rho u = \rho_0 u_0, \quad \rho u \frac{du}{dx} + \frac{dp}{dx} = 0, \quad p = \frac{R}{\mu}\rho T, \quad \frac{d}{dx}\left[\rho u\left(c_p T + \frac{u^2}{2}\right)\right] = \delta_T Q,$$

$$\frac{d}{dx}(uw) = \eta_{ef} Q - Q_* - Q_{cв},$$

where ρ, u, γ, μ, p are the density, velocity, adiabatic exponent, molecular weight and pressure of the laser mixture; Q is the specific pumping power, the "zero" subscript refers to the input to the active volume. Let us note that the quantity δ_T in optimum mixtures does not exceed 10-15%. This is due to the fact that the pumping efficiency η_{ef} (the fraction of energy expended on vibrational excitation of CO, N_2) reaches 90-95%, while the energy expended on heating due to anharmonicity of the molecules in V-V exhcanges, as well as due to V-T relaxation at $T \lesssim 200$ K is extremely small. $Q_{cв}$ is the specific energy of radiation, w is the vibrational energy of a unit of volume, Q_* is specific power of relaxation losses--power lost due to spontaneous emission and V-T relaxation.

The dependence $Q_*(\rho, T)$ is determined by the dynamics of the change in populations of vibrational levels of CO and the characteristics of the cavity. To determine this dependence, numerical solutions were found for rate equations with consideration of the populations of 30 levels of the CO molecule [Ref. 5]. Fig. 1a shows the calculated dependences of specific lasing power on time at different temperatures for a mixture of $CO_2:N_2:He = 1:2:3$ at density $\rho_0 = 1/3$ amagat unit and specific

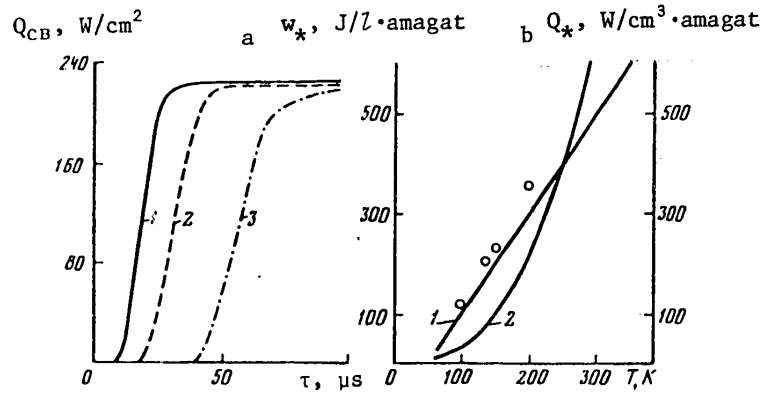

Fig. 1. a--calculated time dependences of specific lasing power at different temperatures (T = 60 (1), 100 (2) and 200 K (3)) for density of a laser mixture of CO_2: N_2:He = 1:2:3 of $\rho_0 = 1/3$ amagat unit, specific pumping power Q = 300 W/cm^3 and threshold gain of $k = 5 \cdot 10^{-4}$ cm^{-1}; b--threshold pumping energy w_* (1) and steady-state power of relaxation losses Q_* (2) as functions of laser mixture temperature. Points show the results of experiments from Ref. 3

pumping power of $Q_0 = 300$ W/cm^3 (threshold gain $k = 5 \cdot 10^{-4}$ cm^{-1}). The density and temperature of the mixture were held constant over the extent of the entire calculation, giving the universal curves shown in Fig. 1b for threshold pumping energy w_* and steady-state power of relaxation losses Q_* corresponding to the flat sections of curves 1, 2, 3 on Fig. 1a as functions of laser mixture temperature. Threshold pumping energy is a linear function of density of the mixture, which is in good agreement with experiment [Ref. 3]. Fig. 1b also shows experimental points for the dependence of w_*/ρ (normalized to normal gas density) on temperature of the laser mixture [Ref. 3]. The experimental points lie somewhat higher than the calculated curve. This is due to heating of the gas before the instant of lasing onset, so that the observed threshold pumping energy corresponds to a temperature higher than the initial temperature.

An important distinguishing feature of the CO laser is that even at normal gas density, V-T relaxation becomes the decisive process of losses only at temperatures higher than room level. At $T \leqslant 200$ K the loss power is determined by the rate of spontaneous decay of vibrational levels [Ref. 5]. Consequently at relatively low temperatures the power of relaxation losses is proportional to ρ.

In an electroionization discharge at constant beam current density, the specific pumping power increases with increasing gas density more strongly than linearly: $Q \sim \rho f(\rho)$ ($f(\rho) \equiv 1$ in the sticking mode and $f(\rho) = \sqrt{\rho}$ in the recombination mode). Therefore in the CO EBC laser it is advisable to increase the pressure of the mixture, enabling not only a reduction in overall dimensions of the facility, but also more efficient use of the advantages of the electroionization discharge. On the other hand in the case of a continuous-wave CO_2 laser the Q_* is determined by V-T processes, and increases with increasing gas density more strongly than the pumping power ($Q_* \sim \rho^2$) [Ref. 2].

Integrating the systems of equations of gas dynamics and the balance of vibrational energy with accuracy to $O(M^2)$ (in present-day EBC lasers $M^2 \lesssim 0.1$), we can get an expression for the physical efficiency of an EBC CO laser

$$(2) \quad \eta_\Phi = \bar{\eta}_{ef} - \delta_T \frac{(\gamma-1)T_0 w_*(T_K)}{\gamma(T_K - T_0)p_0} - \delta_T \left[\frac{\gamma}{\gamma-1} c_p \rho_0 u_0 \left(T_K - T_0\right)\right]^{-1} \int_0^l Q_*(x)\,dx,$$

where $\bar{\eta}_{ef}$ is the pumping efficiency averaged over the entire volume of the active medium, $w_*(T_K)$ is the threshold pumping energy corresponding to the final temperature, T_K is the vibrational energy of a unit of volume carried out of the active volume; l is the length of the active region along the flow corresponding to heating of the mixture to T_K. In the sticking mode the value of l is determined from the relation

$$(3) \quad l = \frac{\gamma}{\gamma-1} \frac{u_0 p_0}{\sigma_T Q_0} \ln \frac{T_K}{T_0},$$

where Q_0 is the specific pumping power at the input to the electroionization discharge.

In this paper calculations of the energy characteristics of EBC CO lasers were done for three pumping powers: $Q_0 = 100$, 300, 1000 W/(cm^3·amagat).

In connection with the fact that gas density in the heating process falls off ($p = \text{const}$, $\rho_K = \rho_0 T_0/T_K$), the working voltages should decrease as the energy input increases to prevent breakdown. This leads to a reduction of pumping power at predetermined beam current density and, what is more significant, to a reduction in the efficiency of pumping of vibrational levels. However, in the mixture under consideration with a change of E/p by 2-2.5 times the quantity η_{ef} remains practically constant and fairly high, $\eta_{ef} \gtrsim 0.9$ [Ref. 5]. Therefore conditions were calculated under which the gas is superheated by no more than a factor of 2.5.

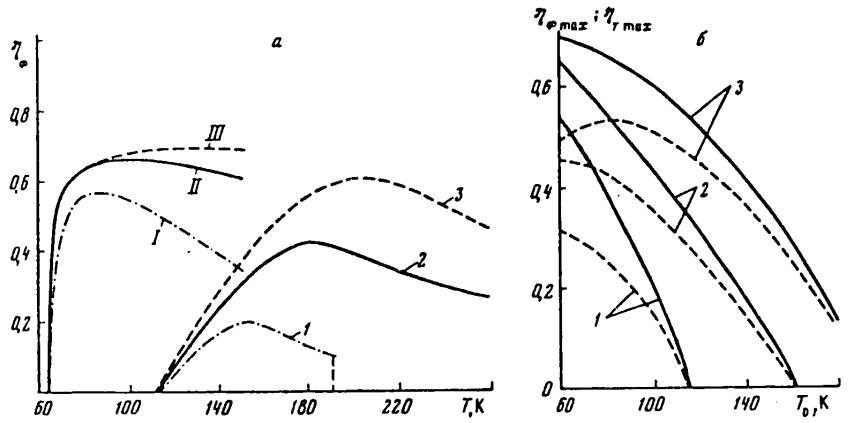

Fig. 2. a--dependence of efficiency η_Φ on the final temperature of the laser mixture at initial temperatures T = 60 (I, II, III) and 100 K (1, 2, 3). The fraction of energy input going to heat $\delta_T = 0.1$; b--T_0-maximum physical efficiency $\eta_{\Phi\ max}$ (solid curves) and technical efficiency $\eta_{T\ max}$ (broken curves) as functions of initial temperature in the case of turbocompressor cooling. The temperature of the mixture at the output from the heat exchanger $T_X = 320$ K; $\xi_K = \xi_T = 1$

Fig. 2a shows curves for the physical efficiency as a function of energy input ($\delta_T = 0.1 = \text{const}$) at different pumping powers and initial temperatures T = 60 K (I, II, III) and 100 K (1, 2, 3). The initial rise in η_Φ is due to excess of the energy input over the threshold (see second term in (2)), while the drop with a further increase in energy input is due to the abrupt increase in the power of relaxation losses Q_* as temperature increases (see Fig. 1b). It can be seen that as the pumping power Q_0 increases, the maximum value of η_Φ rises and corresponds to large energy inputs. For example at initial temperature T = 100 K, $Q_0 = 1$ kW/(cm^3·amagat), the maximum value of η_Φ corresponds to heating of the laser plasma by $\Delta T = 93$ K.

The solid curves on Fig. 2b show the maximum value of η_Φ as a function of the initial temperature of the mixture at different values of Q_0. As the specific pumping power increases, the value of T_0 at which lasing stops increases; however, even at $Q_0 = 300$ W/(cm^3·amagat) this temperature is only 160 K.

2. The problem comes up of getting low temperatures at the input to the active medium of the EBC CO laser by a method with maximum technological feasibility and

minimum possible energy expenditures. The most optimum method of handling this job is to use an arrangement of turbocompressor cooling of the laser mixture [Ref. 2] in which the mixture after the discharge chamber enters a compressor where it is compressed by a factor of Π_K (the degree of compression), and then a heat exchanger where due to the high density and difference of temperatures with the cooling agent it is effectively cooled to a temperature T_X higher than room level, and finally it enters a turbine where, in doing work it is adiabatically cooled to the required temperature T_0. Realization of the refrigeration cycle within the laser facility, i. e. cooling the gas to a temperature lower than the coolant, requires additional energy expenditures, leading to a reduction in technical efficiency. Additional energy expenditures on cooling are associated only with the part of the energy input that goes to heating of the gas. Therefore it is extremely important to select mixtures, temperatures and pumping conditions such that the quantity δ_T will be minimum. As noted above, in the EBC CO laser at $T \lesssim 200$ K relaxation losses are due to spontaneous de-excitation, and consequently do not lead to volumetric gas heating. Besides, the threshold pumping energy w_* that remains in vibrational degrees of freedom is also dissipated mainly due to de-excitation rather than V-T processes, and consequently does not heat the mixture.

The expression for technical efficiency of the EBC CO laser with turbocompressor cooling takes the form

$$(4) \quad \eta_T = \eta_\Phi \Big/ \left[1 + \delta_T \left(\frac{T_X}{T_0} - 1\right) \frac{T_K/\zeta_K - T_0\zeta_T}{T_K - T_0}\right],$$

where T_X is the temperature of the mixture at the output from the heat exchanger; ζ_K, ζ_T are the degrees of adiabaticity of the compressor and turbine. In existing aircraft engines ζ_K, and especially ζ_T are close to unity [Ref. 6]. In the case of an ideal compressor and turbine ($\zeta_K = \zeta_T = 1$), relation (4) takes the form

$$(5) \quad \eta_T = \frac{\eta_\Phi}{1 + \delta_T(T_X/T_0 - 1)}.$$

It can be seen that for completely adiabatic compressor and turbine, and predetermined T_0, the optimum value of T_K from the standpoint of η_T is the same as for η_Φ, since they differ only by a constant factor. On the other hand, in the case of $\zeta_K < 1$, $\zeta_T < 1$ the optimum T_K are different for maxima of η_Φ and η_T.

On Fig. 2b the broken lines show the maximum values of $\eta_{T\,max}$ as a function of T_0 for an ideal turbine and compressor and a value of $T_X = 320$ K. The existence of a maximum on curve 3 is due to the fact that the reduction in expenditures of energy on turbocompressor cooling at low initial temperatures is more rapid with rising T_0 than is the reduction in η_Φ. At comparatively high pumping power $Q_0 =$ 1 kW/(cm^3·amagat) the optimum initial temperature is $T_0 \cong 90$ K and the calculated technical efficiency is greater than 50%.

3. Thus the cw EBC CO process laser with turbocompressor cooling has a number of advantages over analogous carbon dioxide lasers: high technical efficiency (up to 50%) due to a considerably lower percentage of the energy input going to heating of the mixture at low temperatures $T \lesssim 200$ K and the use of an optimum system for

obtaining cryogenic temperatures T ~ 100 K; the possibility of reducing the overall dimensions of the facility through an increase in working pressure due to linear rather than square-law dependence of the power of relaxation losses on the density of the laser mixture at low temperatures.

REFERENCES

1. Basov, N. G., Belenov, E. M. et al., USPEKHI FIZICHESKIKH NAUK, Vol 114, 1974, p 113; Hoag, E., Pease, H. et al., J. APPL. OPT., Vol 13, 1974, p 1959; Basov, N. G., Babayev, I. K. et al., KVANTOVAYA ELEKTRONIKA, Vol 6, 1979, p 772.

2. Basov, N. G., Glotov, Ye. P. et al., Ibid., Vol 7, 1980, p 1067.

3. Basov, N. G., Danilychev, V. A. et al., TRUDY FIZICHESKOGO INSTITUTA IMENI P. N. LEBEDEVA, Vol 116, 1980, p 98.

4. Mann, M. M., Rice, D. K., IEEE, QE, Vol 10, 1974, p 682.

5. Vtorova, N. Ye., Dolinina, V. I. et al., TRUDY FIZICHESKOGO INSTITUTA IMENI P. N. LEBEDEVA, Vol 116, 1980, p 7.

6. Maslennikov, M. M., Shal'man, Yu. I., "Aviatsionnyye gazoturbinnyye dvigateli" [Aircraft Gas Turbine Engines], Moscow, Mashinostroyeniye, 1975.

6610
CSO: 1862/3

UDC 621.373.826

THEORETICAL STUDY OF WAVEFRONT REVERSAL EFFICIENCY IN INVERTED CARBON DIOXIDE

Moscow IZVESTIYA AKADEMII NAUK SSSR: SERIYA FIZICHESKAYA in Russian Vol 45, No 8, Aug 81 pp 1412-1416

[Article by L. A. Vasil'yev, M. G. Galushkin, A. M. Seregin and N. V. Cheburkin]

[Text] The phenomenon of wavefront reversal during degenerate four-wave interaction in amplifying media has been theoretically studied in Ref. 1, where the qualitative patterns of this process were determined on the basis of a steady-state two-level model of the laser system. However, in the experiment of Ref. 2, wavefront reversal was realized in laser media with relaxation properties described by an unsteady multilevel model. Therefore it is of interest to consider wavefront reversal in amplifying media based on complete consideration of the kinetics of the specific laser medium for optimizing conversion parameters under conditions close to those of the experiment.

This paper analyzes wavefront reversal during degenerate four-wave interaction in the amplifying medium of an electron-beam-controlled CO_2 laser. The initial equation that describes this process is written in the form

$$\Delta E+k^2E+ik\alpha(|\mathscr{E}|^2)E=0, \qquad (1)$$

where $\alpha(|\mathscr{E}^2|)$ is the nonlinear gain for intensity, $\mathscr{E}$ is amplitude that is slow compared with the period of the oscillations.

It is assumed relative to the pulses of the reference waves and the inverted radiation that the characteristic time scale of their variation is considerably greater than the time taken by light to cover the distance in the nonlinear medium where wavefront reversal occurs. This condition is usually satisfied in the experiment. We assume that the reference waves are planar waves

$$E_1=\tfrac{1}{2}(A_1(t)e^{i(\omega t-k_1r)}+\text{к.с.}), \quad E_2=\tfrac{1}{2}(A_2(t)e^{i(\omega t-k_2r)}+\text{к.с.}),$$

[к.с. is the complex conjugate] with intensity much less than the wave being reversed (E_3) and the wave that has been reversed (E_4). We will consider the most general case of wavefront reversal during degenerate four-wave interaction where it is realized within the cavity. Therefore the amplitudes of the reference waves are functions of time.

In accordance with condition $\Delta E \ll E_0$, where $\Delta E=E_3+E_4$, $E_0=E_1+E_2$, we have the relation

$$\alpha=\alpha(|\mathscr{E}_0|^2)+\delta\alpha. \qquad (2)$$

Here $\delta\alpha$ is the variation of the gain due to variation of field intensity $\delta|E|^2 = E_0^*\Delta E + E_0\Delta E^*$ as a consequence of the waves in the medium that are being and have been reversed. The dependence of gain α on field intensity is determined from the kinetic equations. In the thermodynamic approximation model based on introducing partial vibrational temperatures, the kinetics of the CO_2 laser for each mode of vibrations of CO_2 and N_2 molecules is described by the following system of equations [Ref. 3]:

$$\frac{\partial\varepsilon_2}{\partial t}=f_2(\varepsilon_2,\varepsilon_3,I)=\frac{P}{\mu}\left[-3D+\sum_m\gamma_m K_{2m}(\varepsilon_{2T}-\varepsilon_2)\right]+ \\ +\frac{2\alpha I}{\mu\gamma_1 k(\Theta_3-\Theta_1)N}+\frac{2p_1+p_2}{\mu}, \qquad (3)$$

$$\frac{\partial\varepsilon_3}{\partial t}=f_3(\varepsilon_2,\varepsilon_3,\varepsilon_4,I)=P[D-\gamma_2K_{12}(\varepsilon_3-\varepsilon_4)]-\frac{\alpha I}{\gamma_1 Nk(\Theta_3-\Theta_1)}+p_3, \qquad (4)$$

$$\frac{\partial\varepsilon_4}{\partial t}=f_4(\varepsilon_3,\varepsilon_4)=P[\gamma_1K_{12}(\varepsilon_3-\varepsilon_4)+\gamma_3K_{23}(\varepsilon_{3T}-\varepsilon_4)]+p_4, \qquad (5)$$

$$\frac{dT}{dt}=(\gamma-1)\gamma_1\Theta_2\left[\sum_m\gamma_m K_{2m}(\varepsilon_2-\varepsilon_{2T})-\frac{3\Theta_2-\Theta_3}{\Theta_2}\sum_m\gamma_m K_{3m}(\varepsilon_3-\varepsilon_{30})\right], \qquad (6)$$

$$\frac{dI}{dt}=c\alpha I-\frac{I}{\tau_p}, \qquad (7)$$

where

$$D=\sum_m\gamma_m K_{3m}\frac{(1-\beta_2)^3}{8(1-\beta_3)}\left\{\frac{\beta_3}{\beta_2}\varepsilon_2^3(1+\varepsilon_3)-\varepsilon_3(2+\varepsilon_3)^3\right\},$$

$$\beta_i=\exp\{\Theta_i/T\}.$$

Here ε_i is the average number of vibrational quanta per molecule in the corresponding vibrational modes; the subscript i = 4, 3, 2 refers to vibrational levels of N_2, antisymmetric and deformational modes of vibrations of CO_2 respectively; P, T are the pressure and temperature of the gas; γ_m are the mole fractions of components CO_2, N_2 and He in the mixture; $\Theta_1 = 1980$ K, $\Theta_2 = 960$ K, $\Theta_3 = 3360$ K;

$$\mu=\frac{3\varepsilon_2^2+6\varepsilon_2+2}{2(1+\varepsilon_2)^2}, \quad Nk=\frac{P}{T}, \quad p_i=jE\frac{\delta_i}{\gamma_i Nk\Theta_i},$$

j, E are the current density and electric field strength in the discharge, δ_i is the relative fraction of pumping power expended on the ν_i-mode, I is intensity of laser radiation, γ is the adiabatic exponent of the gas, ε_{iT} is the equilibrium number of quanta in the modes.

For the gain we can write the expression

$$\alpha=4{,}27\cdot10^{2}\gamma_{CO_2}(2j+1)\left(\exp\left\{-\frac{\Theta_2}{T_2}-\frac{0{,}556j(j-1)}{kT}\right\}-\right.$$
$$\left.-\exp\left\{-\frac{\Theta_1}{T_1}-\frac{0{,}556j(j+1)}{kT}\right\}\right)T^{-3/2}(\gamma_{CO_2}+0{,}73\gamma_{N_2}+0{,}64\gamma_{H_2}+0{,}383\gamma_{H_2O})^{-1}, \quad (8)$$

where

$$T_2=\Theta_2\ln^{-1}\left(\frac{1+\varepsilon_2}{\varepsilon_2}\right),\quad T_1=\Theta_1\ln^{-1}\left(\frac{1+\varepsilon_1}{\varepsilon_1}\right).$$

According to (8), we have the following relation for gain variation

$$\delta\alpha\approx\frac{\partial\alpha}{\partial\varepsilon_2}\delta\varepsilon_2+\frac{\partial\alpha}{\partial\varepsilon_3}\delta\varepsilon_3. \quad (9)$$

Here variations $\delta\varepsilon_2$ and $\delta\varepsilon_3$ are caused by the variation of intensity, which we write in the form

$$\delta I=\tfrac{1}{2}\sigma(A_{1M}e^{-ik_1r}+A_{2M}e^{-ik_2r})\varphi_0^{1/2}(t)[A_3^*(z,t)e^{ikz}+A_4^*(z,t)e^{-ikz}]+\text{к. с.},$$

[к.с. is the complex conjugate] where $\sigma = c/4\pi$, $\phi_0(t)$ is the shape of time pulses of the reference waves.

Calculating the variations of the left and right members of equations (3)-(5), we find expressions for functions $\delta\varepsilon_2$ and $\delta\varepsilon_3$. We seek the solution of the resultant equations in the form

$$\delta\varepsilon_j=\varepsilon_{j1}\frac{\sigma}{2}(A_{1M}e^{-ik_1r}+A_{2M}e^{-ik_2r})e^{ikz}+\varepsilon_{j2}'\frac{\sigma}{2}(A_{1M}e^{-ik_1r}+A_{2m}e^{-ik_2r})e^{-ikz}+\text{к. с.} \quad (10)$$

As a result, we get the following system of equations

$$\frac{\partial\varepsilon_{j1}'}{\partial t}=\frac{\partial f_j}{\partial\varepsilon_2}\varepsilon_{21}'+\frac{\partial f_j}{\partial\varepsilon_3}\varepsilon_{31}'+\frac{\partial f_j}{\partial\varepsilon_4}\varepsilon_{41}'+\frac{\partial f_j}{\partial I}\varphi_0^{1/2}(t)A_3^*(z,t),$$
$$\frac{\partial\varepsilon_{j2}'}{\partial t}=\frac{\partial f_j}{\partial\varepsilon_2}\varepsilon_{22}'+\frac{\partial f_j}{\partial\varepsilon_3}\varepsilon_{32}'+\frac{\partial f_j}{\partial\varepsilon_4}\varepsilon_{42}'+\frac{\partial f_j}{\partial I}\varphi_0^{1/2}(t)A_4^*(z,t). \quad (11)$$

With consideration of (2), (9), we define the solution of equation (1) in the form $E = E_1 + E_2 + E_3 + E_4$ and, using conventional methods of nonlinear optics [Ref. 1, 4], we get equations for the slow amplitudes of the reversed wave and the wave to be reversed:

$$\frac{\partial A_3}{\partial z}=\frac{1}{2}\left(\alpha+\frac{1}{2}\alpha_1''^*(I_1+I_2)\varphi_0^{1/2}(t)+\alpha_2'(I_1I_2)^{1/2}\varphi_0(t)\right),$$
$$-\frac{\partial A_4}{\partial z}=\frac{1}{2}\left(\alpha+\frac{1}{2}\alpha_2''^*(I_1+I_2)\varphi_0^{1/2}(t)+\alpha_1'(I_1I_2)^{1/2}\varphi_0(t)\right), \quad (12)$$

where I_1, I_2 are the maximum intensities of the reference waves during the pulse,

$$\alpha_1' = \frac{\partial \alpha}{\partial \varepsilon_2} \varepsilon_{21}' + \frac{\partial \alpha}{\partial \varepsilon_3} \varepsilon_{31}', \quad \alpha_2' = \frac{\partial \alpha}{\partial \varepsilon_2} \varepsilon_{22}' + \frac{\partial \alpha}{\partial \varepsilon_3} \varepsilon_{32}'.$$

Thus the solution of the problem of determining the phase-adjoint reflectivity has been reduced to system of equations (11) and (12), in which the time-dependent coefficients are found from equations (3)-(7). If amplitudes $A_3(z,t)$ and $A_4(z,t)$ can be expressed in the form

$$A_3(z,t) = \varphi_0^{1/2}(t) A_3(z), \quad A_4(z,t) = \varphi_4^{1/2}(t) A_4(z), \tag{13}$$

then we can easily find an analytical solution of equations (12) that contains parameters determined from numerical solution of equations (11). The functions $A_3^*(z,t)$ and $A_4^*(z,t)$ are replaced by $\phi_3(t)$ and $\phi_4(t)$ respectively. Here $\phi_3(t)$ and $\phi_4(t)$ are the pulse shapes of the wave being reversed and the wave that has been reversed. The solution found by this method implies that relations (13) hold at small values of the phase-adjoint reflectivity R. For this case, which is fairly typical in experiments, we find an expression for R:

$$R \approx \frac{1}{4} \frac{\varphi_0(t)}{\varphi_3(t)} \left(\frac{\partial \alpha}{\partial \varepsilon_2} \varepsilon_{21}' + \frac{\partial \alpha}{\partial \varepsilon_3} \varepsilon_{31}' \right)^2 I_1 I_2 L^2. \tag{14}$$

We calculated the phase-adjoint reflectivity assuming that condition (13) is met. Equations (3)-(7) and (11) were numerically solved by computer, the pulse shape of the signal to be reversed being taken as coincident with that of the reference wave. Fig. 1 shows curves for the phase-adjoint reflectivity as a function of the

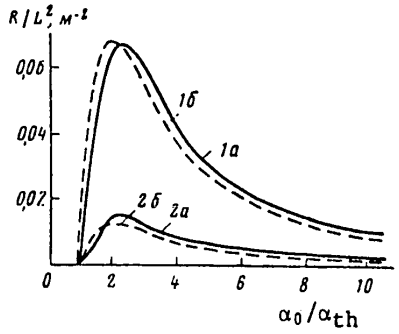

Fig. 1

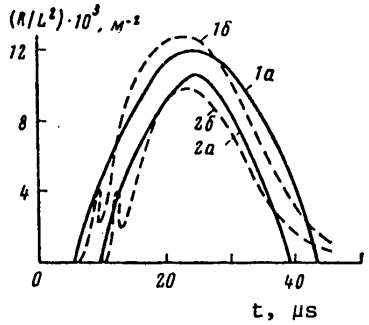

Fig. 2

Fig. 1. Maximum phase-adjoint reflectivity during the pulse as function of maximum excess over the threshold for gas mixture CO_2:N_2:He. Curves 1--composition 1:2:3, $jE = 2 \cdot 10^4$ W·cm^{-3}; curves 2--composition 1:5:4, $jE = 5 \cdot 10^3$ W·cm^{-3} (a--calculation by formula (18), b--computer calculation)

Fig. 2. Phase-adjoint reflectivity as a function of time for mixture CO_2:N_2:He = 1:5:4, $jE = 5 \cdot 10^3$ W·cm^{-3} at various threshold values of α: 1--$\alpha_{th} = 0.387$ m^{-1}; 2--$\alpha_{th} = 0.58$ m^{-1} (a--calculation by formula (18), b--computer calculation)

maximum excess over the threshold during the pulse for two values of the weak-signal gain. Fig. 2 shows values of the phase-adjoint reflectivity calculated by formula (14) as a function of time. Calculation shows that for predetermined pumping there is an optimum excess over the threshold equal to the double value, where R reaches its maximum. Besides, the effectiveness of wavefront reversal increases with increasing pumping level, i. e. with a rise in the weak-signal gain.

Now let us compare the results with approximate calculation based on the following expression for the gain:

$$\alpha \approx \frac{\alpha_0(t) I_н(t)}{I_н(t)+I(t)}, \tag{15}$$

where $\alpha_0(t)$ is the weak-signal gain, $I_H(t)$ is the saturation parameter.

If the gain is an explicit function of intensity I, then the analytical solution of initial equation (1) is found in the form

$$\begin{aligned} A_3^*(z) &= \frac{A_3^*(0)\,[w\cos w(z-L)+0{,}5\beta(I)\sin w(z-L)]}{w\cos wL+0{,}5\beta(I)\sin wL} \\ A_4(z) &= -\frac{1}{2}\frac{\partial\alpha}{\partial I}(I_1I_2)^{1/2}\frac{A_3^*(0)\sin w(z-L)}{w\cos wL+0{,}5\beta(I)\sin wL}. \end{aligned} \tag{16}$$

From (16), we get the following formula for the phase-adjoint reflectivity

$$R=\frac{1}{4}\left(\frac{\partial\alpha}{\partial I}\right)^2\frac{I_1I_2\sin^2 wL}{(w\cos wL-\beta(I)\sin wL)^2}, \tag{17}$$

where

$$w=\frac{1}{2}\left[\left(\frac{\partial\alpha}{\partial I}\right)^2 I_1I_2+\beta^2(I)\right]^{1/2},\quad \beta(I)=\alpha(I)+\frac{1}{2}\frac{\partial\alpha}{\partial I}(I_1+I_2).$$

Allowing for (15), the parameter $\partial\alpha/\partial I$ can be reduced to the form

$$\frac{\partial\alpha}{\partial I}=-\frac{\alpha}{I}\left(1-\frac{\alpha}{\alpha_0}\right)$$

which is convenient for the intracavity method of wavefront reversal where the value of α is known in the steady-state lasing mode. Besides, in the case of wavefront reversal within the cavity, $\frac{1}{2}(I_1 + I_2) = I$, $I_1I_2 \cong I^2$, and therefore the phase-adjoint reflectivity is determined by only three parameters: $\alpha_0(t)$, α, L.

In the approximation of $wL \ll 1$, which has already been used in deriving formula (14), expression (17) takes the form

$$R\approx\left[\frac{1}{2}\alpha L\left(1-\frac{\alpha}{\alpha_0(t)}\right)\right]^2$$

This implies that at a given α_0, the phase-adjoint reflectivity is maximum at $\alpha = 0.5\alpha_0$, which corresponds to double excess over the threshold.

Fig. 1 and 2 show the values of R calculated from (17). It can be seen that in the steady-state lasing mode the results of calculations by formulas (14) and (17) show good agreement.

In conclusion we point out that the method of calculating wavefront reversal during degenerate four-wave interaction developed in this paper can be used to determine major conversion parameters. The calculations given here show that depending on the requirements of the problem, we can optimize the process of wavefront reversal during degenerate four-wave interaction in a laser medium with relaxation properties described by kinetic equations.

REFERENCES

1. Abrams, R. L., Lind, R. S., OPT. LETTS, Vol 2, 1978, p 94.

2. Fisher, R. A., Feldman, B. J., OPT. LETTS, Vol 4, 1979, p 140.

3. Biryukov, A. S., TRUDY FIZICHESKOGO INSTITUTA AKADEMII NAUK SSSR, Vol 83, 1975, p 12.

4. Yariv, A., Pepper, D. M., OPT. LETTS, Vol 1, 1977, p 16.

6610
CSO: 8144/0101-B

UDC 621.378.325

0.5 GW ELECTRON-BEAM EXCITED XeCl LASER

Leningrad ZHURNAL TEKHNICHESKOY FIZIKI in Russian Vol 51, No 6, Jun 81 (manuscript received 24 Jun 80) pp 1323-1325

[Article by V. A. Adamovich, V. Yu. Baranov, Yu. B. Smakovskiy and A. P. Strel'tsov]

[Text] High efficiencies, short wavelengths, and the capability for converting excimer laser emission to pulses with duration of ~10^{-9} s by using stimulated Raman scattering for applications in laser-driven fusion experiments [Ref. 1] are the factors responsible for the recent upsurge of interest in lasers of this type.

Previous research has resulted in lasing energies of the order of 100 J or more and efficiencies of about 10% (see survey of Ref. 2) with excitation of KrF* lasers by an electron beam or an electron-beam controlled discharge. Lasing pulse duration was 0.5-1 μs. Ref. 3 gives the results of investigations of the KrF* laser under conditions of excitation of 2-7 MW/cm^3, demonstrating high efficiency of intense pumping.

Recent results [Ref. 4, 5] show that a laser based on the XeCl* molecule may have output parameters just as high as the KrF* lasers. And the capability of prolonged operation without significant changes in its characteristics gives it certain advantages in the pulse-periodic mode.

This paper gives the results of studies of an excimer laser using an Ar/Xe/CCl_4 mixture excited by an electron beam with duration of ~25 ns.

The experiments were done on a facility described in Ref. 6. An electron beam with electron energy of ~350 keV was coupled via an aluminum foil 50 μm thick into the stainless steel lasing chamber. The output window of the accelerator measured 4.5 x 26 cm, and the geometric transparency of the beam extraction system was 75%. The beam current density was measured by a Faraday cup. The experiments were done on a mixture of CCl_4/Xe/Ar = 1/12.5/1000. The pressure in the laser chamber was varied from 1 to 4 atm. The laser cavity was formed by an aluminum-coated flat mirror 8.5 cm in diameter and a plane-parallel lithium fluoride plate. The distance between mirrors was 40 cm.

Lasing energy was measured by a calorimeter. A coaxial FK-2 cell with time resolution of 018 ns and a 6LOR-04 oscilloscope with 1.2 GHz band were used to record emission pulse shape. The emission spectrum was taken by the STE-1 spectrograph.

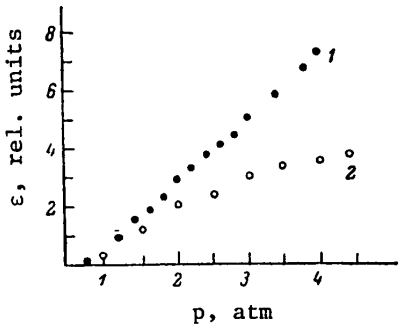

Fig. 1

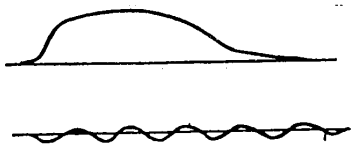

Fig. 2

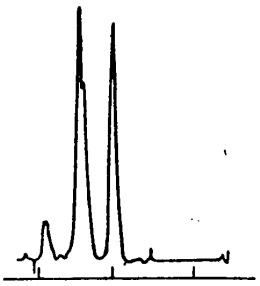

Fig. 3

Fig. 1 shows the radiation energy as a function of pressure of the mixture $CCl_4/Xe/Ar = 1/12.5/1000$. At electron current density of about 110 A/cm^2, the energy increases linearly throughout the investigated pressure range (Fig. 1, *1*). When the beam current density is reduced to half (about 65 A/cm^2), the energy dependence differs from linear (Fig. 1, *2*), which is apparently due to an increase in the influence of quenching collisions as pumping intensity decreases. Let us note that at a current density of about 25 A/cm^2 the lasing threshold was not reached for the above-mentioned mixture and cavity.

The emission pulse shape (Fig. 2, time mark 100 MHz) copies the shape of the beam current pulse. It can be seen from this oscillogram that lasing is steady-state, which appreciably simplifies analysis of systems of this kind.

The distribution of emission energy over the cross section of the output window in the case of planar cavity geometry corresponds to the distribution of electron beam energy losses in the mixture [Ref. 7]. Lengthwise of beam propagation, this distribution is described by the expression $\varepsilon(z) = \varepsilon(0)(1 - z/z_0)$, where z is distance from the foil, $\varepsilon(0)$ are the specific losses near the foil as determined by the formula $\varepsilon(0) = 2.9Bpjv$, B is the stopping power of the mixture, p is pressure, j is current density of the beam, the coefficient 2.9 accounts for electron scattering in the foil. The quantity z_0 in our experiments was 7.5 cm for a pressure of 3 atm. Let us note that such a distribution of invested energy correlates with our previous measurements of beam current density distribution.

Maximum lasing energy was attained on a mixture of 1/40/2000. At pressure of 3.5 atm this energy was ~10 J, and the power was ~0.5 GW. This is the first time that such power has been reached with the XeCl* laser. Average specific energy output was ~7.5 J/*l* at efficiency of ~6% relative to the energy invested in the gas. The emission energy on IR transitions of Xe* [Ref. 8] under the conditions of the experiment did not exceed 40 mJ.

Fig. 3 shows a densitometer reading of the radiation spectrum of the XeCl* laser from which it can be seen that lasing takes place on three lines corresponding to vibrational transitions (0→1), (0→2) and (0→3) of band B→X. The lasing intensity on the first two transitions is about the same. The lasing linewidth is 0.3 Å and is weakly dependent on pressure in the range of 1-4 atm.

The laser divergence in our experiments was ~$4 \cdot 10^{-3}$. Unstable cavities must be used to improve divergence.

Thus the results of these experiments show that pumping by an intense electron beam is one of the most efficient methods of exciting high-pressure excimer lasers. Bilateral input of the electron beam is advisable to improve pumping homogeneity of large-aperture lasers.

In conclusion the authors thank D. D. Malyuta for constructive discussions, V. I. Rozanova for assistance in processing the spectrograms and Yu. I. Abramenko for taking part in the experiments.

REFERENCES

1. Murray, J. R., Goldhar, J., Eimerl, D., Szoke, A., IEEE J. QUANTUM ELECTRON., Vol QE-15, 1979, p 342.

2. Rokni, M., Mangano, J. A., Jarob, J. H., Hsia, J. C., IEEE J. QUANTUM ELECTRON., Vol QE-14, 1978, p 464.

3. Tisone, G. C., Patterson, E. L., Rice, J. K., APPL. PHYS. LETT, Vol 35(6), 1979, p 437.

4. Rothe, D. T., West, J. B., Bhaumik, M. L., IEEE J. QUANTUM ELECTRON., Vol QE-15, 1979, p 314.

5. Bichkov, Yu., Gorbatenko, A. I., Losev, V. F., Mesyats, G. A., Tarasenko, V. F., OPTICS COMM., Vol 30, 1979, p 224.

6. Adamovich, V. A., Baranov, V. Yu., Smakovskiy, Yu. B., Strel'tsov, A. P., KVANTOVAYA ELEKTRONIKA, Vol 5, 1978, p 918.

7. Long, W. H., Bradford, R. S., IEEE J. QUANTUM ELECTRON., Vol QE-15, 1979, p 327.

8. Newman, L. A., DeTemple, T. A., APPL. PHYS. LETT, Vol 27, 1975, p 678.

6610
CSO: 8144/0101-C

DYNAMIC COMPENSATION OF IODINE LASER OPTICAL INHOMOGENEITIES

Leningrad ZHURNAL TEKHNICHESKOY FIZIKI in Russian Vol 51, No 8, Aug 81 (manuscript received 19 Sep 80) pp 1764-1765

[Article by Yu. V. Dolgopolov, S. B. Kormer, S. M. Kulikov, V. M. Murugov, S. M. Pevnyy, A. V. Ryadkov and S. A. Sukharev]

[Text] More and more attention is currently being given to the possibility of using the effect of wavefront reversal to compensate for optical inhomogeneities of laser media and to guide radiation to a target [Ref. 1-4] in laser-driven fusion facilities.

Since results found in Ref. 5-7 have shown the good outlook of iodine lasers for laser-driven fusion, we have investigated [Ref. 3] the conditions of wavefront reversal in induced Mandelstam-Brillouin scattering, and dynamic compensation of optical inhomogeneities of an iodine laser [Ref. 6, 8, 9]. This paper gives subsequent experimental results on dynamic compensation of optical inhomogeneities of a laser medium based on C_3F_7I in a two-stage scheme investigated in Ref. 3, 10 for interstage decoupling.

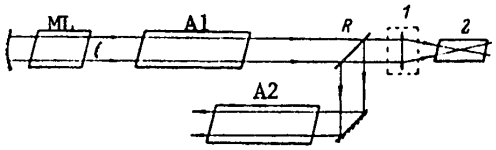

Fig. 1

A laser with unstable telescopic cavity was used as the master laser (Fig. 1) for shaping a reference emission beam with good spatial coherence and small divergence. Induced Mandelstam-Brillouin scattering was achieved by focusing (1) radiation into cell 2 containing SF_6 compressed to 30 atmospheres. The Stokes frequency shift with induced Mandelstam-Brillouin scattering in SF_6 is $\delta\nu_S = 0.006$ cm^{-1} [Ref. 4], and therefore the luminescence linewidth of the amplifiers was increased to $\Delta\nu_{amp} = 0.032$ cm^{-1} by adding buffer gas for more effective amplification of the Stokes signal. To eliminate the influence of reflected Mandelstam-Brillouin radiation on operation of the master laser [Ref. 11], the amplification linewidth of the active medium of the master laser was reduced by selecting the pressure of the

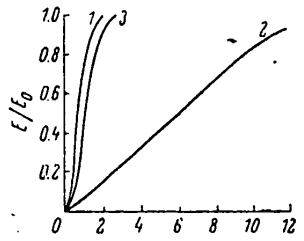

Fig. 2

mixture so that $\Delta\nu_{ML}/2 \lesssim \delta\nu_s$. In addition, the transmission of the beam-splitter mirror was correspondingly chosen.

Emission energy at the output of A2 reached $E_{out} = 470$ J, which is 60-70% of the stored energy. Fig. 2 shows the experimentally determined distributions of energy with respect to angle at the output of ML (1), A1 (2) and A2 (3). Reference emission divergence of $\theta_{ML} = 6 \cdot 10^{-5}$ rad (at the half-energy level) after passage through amplifier A1 increased to $\theta_{A1} = 6 \cdot 10^{-4}$ rad due to the influence of optical inhomogeneities. At the output of A2, divergence decreased to $\theta_{A2} = 1 \cdot 10^{-4}$ rad. Thus, the inaccuracy of dynamic compensation did not exceed $\Delta\theta = 4 \cdot 10^{-5}$ rad. This corresponds in the main to the inaccuracy of coincidence of the refraction index profiles of laser media, which is $\delta(\nabla n) \sim 2 \cdot 10^{-7}$ cm^{-1} [Ref. 9].

The results show the possibility of effective dynamic compensation of optical inhomogeneities of an iodine laser by a Mandelstam-Brillouin mirror.

REFERENCES

1. Nosach, O. Yu., Popovichev, V. I., Ragul'skiy, V. V., Fayzullov, F. S., PIS'MA V ZHURNAL EKSPERIMENTAL'NOY I TEORETICHESKOY FIZIKI, Vol 16, 1972, p 617.

2. Kruzhilin, Yu. I., KVANTOVAYA ELEKTRONIKA, Vol 5, 1978, p 625.

3. Dolgopolov, Yu. V., Komarevskiy, V. A., Kormer, S. B. et al., ZHURNAL EKSPERIMENTAL'NOY I TEORETICHESKOY FIZIKI, Vol 76, 1979, p 908.

4. Yefimkov, V. F., Zubarev, I. G., Kotov, A. V. et al., ZHURNAL EKSPERIMENTAL'NOY I TEORETICHESKOY FIZIKI, Vol 77, 1979, p 526.

5. Brederlov, G., Fill, Ye., Kholl, K., Fol'k, V., Vitte, K. Y., KVANTOVAYA ELEKTRONIKA, Vol 3, 1976, p 906.

6. Basov, N. G., Zuyev, V. S., Katulin, V. A. et al., KVANTOVAYA ELEKTRONIKA, Vol 6, 1979, p 311.

7. Belotserkovets, A. V., Gaydash, V. A., Kirillov, G. A. et al., PIS'MA V ZHURNAL TEKHNICHESKOY FIZIKI, Vol 5, 1979, p 204.

8. Belousova, I. M., Danilov, O. B., Sinitsyn, I. A., Spiridonov, V. V., ZHURNAL EKSPERIMENTAL'NOY I TEORETICHESKOY FIZIKI, Vol 58, 1970, p 1481.

9. Zykov, L. I., Kirillov, G. A., Kormer, S. B. et al., KVANTOVAYA ELEKTRONIKA, Vol 2, 1975, p 123.

10. Kormer, S. B., Kulikov, S. M., Nikolayev, V. D. et al., PIS'MA V ZHURNAL TEKHNICHESKOY FIZIKI, Vol 5, 1979, p 213.

11. Anan'yev, Yu. A., Goryachkin, D. A., Svenitskaya, N. A., Petrova, I. M., KVANTOVAYA ELEKTRONIKA, Vol 6, 1979, p 1773

6610
CSO: 8144/1935

PLASMA PHYSICS

POSSIBLE MECHANISM OF INSTABILITY OF GLOW DISCHARGE ARISING AFTER PULSE ACTION OF EXTERNAL IONIZER

Leningrad PIS'MA V ZHURNAL TEKHNICHESKOY FIZIKI in Russian Vol 7, No 15, 12 Aug 81 (manuscript received 8 Apr 81) pp 911-914

[Article by A. S. Kovalev, A. T. Rakhimov, N. V. Suyetin and V. A. Feoktistov, Scientific Research Institute of Nuclear Physics, Moscow State University imeni M. V. Lomonosov]

[Text] The semi-self-maintained gas discharge has recently been attracting the attention of researchers in connection with the possibility of maintaining burning of such discharges in dense media. However, after a certain time has elapsed, ionization instability develops in semi-self-maintained discharges, the discharge contracts, and arcing begins [Ref. 1]. Breakdown of the gas-discharge gap may take place both during the action of an ionizing pulse [Ref. 1] and after its completion [Ref. 2-4]; in Ref. 4, instability develops after times considerably exceeding the characteristic recombination time.

It was shown in Ref. 3 that Joule heating of the gas and its displacement cannot explain the effect of breakdown that develops after disconnection of the external ionizer. The same conclusion is reached in Ref. 4, where the energy contributed to the discharge was so small that it could not lead to appreciable reduction of gas density.

In the present paper we turn our attention to the fact that the phenomenon of breakdown of the gas-discharge gap after disconnection of the source of external ionization can be satisfactorily explained by taking account of processes of associative ionization of vibrationally excited nitrogen molecules [Ref. 6]. Associative ionizational instability may develop after times much longer than the characteristic time of plasma recombination [Ref. 7].

Let us use the analytical theory of establishing the distribution function with respect to vibrational levels of diatomic molecules developed in Ref. 8 to determine the nature of pumping in the experiments of Ref. 4. According to Ref. 8, the characteristic time of establishment of the quasisteady distribution of molecules with respect to vibrational levels is determined from the expression $t_x \cong v^{**}/2\nu c$, where v^{**} is the number of the vibrational level on which V-T processes begin to predominate over V-V exchange; $\nu = 4\Delta E \delta_{V-V}^{-3} Q_{10} T^{-1}$, ΔE is the energy of anharmonicity, T is translational temperature, δ_{V-T} is the inverse radius of V-T

relaxation, Q_{10} is the parameter of V-V exchange; $c = (W\eta_v/E_1\nu)^{1/2}$, W is pumping power per molecule; η_v is the fraction of power expended on excitation of vibrations, E_1 is the energy of the first vibrational quantum. For the parameters of Ref. 4, $t_x \cong 10^{-3}$ s, and the time of action of the pumping pulse $t_p \cong 25$ μs, i. e. $t_p \ll t_x$. This means that pumping was pulsed, and for subsequent analysis it is important to know only the integral of the input energy. Then the distribution function of the molecules with respect to vibrational levels [f(v,t)] in the approximation of resonant V-V exchange for constant vibrational temperature is described by the formula [Ref. 8]:

$$f(v,t) = (2vt)^{-1}[(12h_0vt)^{1/4}/(v+1)^{1/2} - 1], \quad (1)$$

where v is the number of the vibrational level, n_0 is the average number of quanta generated during pumping per molecule.

The process of associative ionization can begin if the population on some threshold level v_i (for nitrogen $v_i = 32$ [Ref. 8]) is non-zero. From expression (1) we can estimate this time

$$t_1 = \frac{v_i^2}{12n_0v}. \quad (2)$$

After $t > t_1$, the electron concentration is determined from the following equation:

$$\frac{dn_e}{dt} = S - \beta n_e^2, \quad (3)$$

where $S = k_i N^2 [\int_{v_i}^{v_m} f(v,t)\, dv]^2$; $k_i = 3.5 \cdot 10^{-15} \exp\left(-\frac{1160}{T}\right)$ [Ref. 6] is the constant of associative ionization, N is the concentration of N_2 molecules; β is the recombination coefficient; $v_m = \min\{v^{**}; (12n_0vt)^{1/2}\}$. Using expressions (1) and (3), let us determine the time of increase (t_m) in the rate of electron production due to associative ionization to its maximum, assuming that in this time $v^{**} \gg (12n_0vt)^{1/2}$,

$$t_m = \frac{4v_i^2}{3n_0v}. \quad (4)$$

From (3) we can find the electron concentration after time t_m, assuming that $t_m \gg 1/\beta n_e$:

$$n_e = \frac{3}{8}\frac{Nn_0}{v_i}\sqrt{k_i/\beta}. \quad (5)$$

Let us make estimates for $N \cong 2 \cdot 10^{19}$ cm^{-3}, $n_0 = 0.03$, $v_i = 32$, $\beta \cong 10^{-7}$ cm^3 s^{-1}, which corresponds to the experiment of Ref. 4. In this case, $n_e \cong 2 \cdot 10^{11}$ cm^{-3}, i. e. the shielding of the applied voltage by layers near the electrode is small, and within $t_m \cong 300$ μs after disconnection of the external source, current will flow once more, which agrees satisfactorily with the experiment of Ref. 4. Let us note that flow of the current to be registered requires that the pumping level n_0 must be sufficient for producing an electron concentration such that shielding by electrode layers is not complete. In addition, the pumping level must ensure the

condition $v^{**} > v_i$. Since k_i is an exponential function of T, n_e and t_m are also sharply dependent on the temperature of the medium; therefore the given effect may be absent at low temperatures.

We can see from (4) and (2) that $t_m \gg t_b$, i. e. we can assume quasi-steady pumping of vibrational levels of the molecules of the medium by current that arises due to associative ionization processes. Therefore after a certain transient process the electron concentration will be described by the following equations [Ref. 7]:

$$\frac{dn_e}{dt} = k_i N^2 \left(\int_{v_i}^{n^{**}} \frac{c}{v+1}\, dv \right)^2 - \beta n_e^2 . \qquad (6)$$

As implied by Ref. 7, in this case associative ionizational instability should develop, which leads to breakdown of the gas-discharge gap.

Thus for the case of pulsed pumping we have described a mechanism of development of considerable electron concentration and breakdown in times that are longer by a considerable factor than the characteristic recombination time. The case where establishment of the distribution function of molecules with respect to vibrational levels is commensurate with the duration of external pumping, while instability develops on the decomposing phase, was considered in Ref. 9 with consideration of processes of step-by-step ionization, vibrational kinetics and Joule heating.

In addition, let us note that the process of plasma decomposition is determined not only by the recombination time, but also by the time of decomposition of layers near the electrode. The redistribution of electric fields in the gap may have a considerable effect on the electrical density of the medium [Ref. 10]. However, numerical analysis is needed to explain the dynamics of independent ionization in the plasma on the decomposition stage. We will be giving the results of such numerical calculations in a later paper.

REFERENCES

1. Velikhov, Ye. P., Pis'mennyy, V. D., Rakhimov, A. T., USPEKHI FIZICHESKIKH NAUK, Vol 122, No 3, 1977, p 419.

2. Bychkov, Yu. I., Genkin, S. A., Korolev, Yu. D., Kreyndel', Yu. Ye., Mesyats, G. A., Filonov, A. G., ZHURNAL EKSPERIMENTAL'NOY I TEORETICHESKOY FIZIKI, Vol 66, No 2, 1974, p 622.

3. Kostylev, A. A., Londer, Ya. I., Terent'yev, A. P., Ul'yanov, K. N., Fedorov, V. A., TEPLOFIZIKA VYSOKIKH TEMPERATUR, Vol 17, No 6, 1979, p 1167.

4. Gurevich, D. B., Kanatenko, M. A., Podmoshenskiy, I. V., FIZIKA PLAZMY, Vol 5, No 6, 1979, p 1359.

5. Aleksandrov, N. L., Konchakov, A. M., Son E. Ye., FIZIKA PLAZMY, Vol 4, No 1, 1978, p 169.

6. Polak, L. S., Sergeyev, I. A., Slovetskiy, D. I., TEPLOFIZIKA VYSOKIKH TEMPERATUR, Vol 15 No 1, 1977, p 15.

7. Zhdanok, S. A., Napartovich, A. P., Starostin, A. N., PIS'MA V ZHURNAL TEKHNICHESKOY FIZIKI, Vol 5, No 3, 1979, p 155.

8. Zhdanok, S. A., Napartovich, A. P., Starostin, A. N., ZHURNAL EKSPERIMENTAL'NOY I TEORETICHESKOY FIZIKI, Vol 76, No 1, 1979, p 130.

9. Baiadze, K. V., Vetsko, V. M., Zhdanok, S. A., Napartovich, A. P., Starostin, A. N., DOKLADY AKADEMII NAUK SSSR, Vol 249, No 4, 1979, p 832.

10. Feoktistov, V. A., ZHURNAL PRIKLADNOY MEKHANIKI I TEKHNICHESKOY FIZIKI, Vol 5, 1977, p 41.

6610
CSO: 1862/4

PARTICULARS OF OPTICAL DISCHARGE SLOW BURNING INITIATION IN AIR ON OPTICAL BREAKDOWN INOCULATION PLASMA

Leningrad PIS'MA V ZHURNAL TEKHNICHESKOY FIZIKI in Russian Vol 7, No 15, 12 Aug 81 (signed to press 21 Jul 81, manuscript received 6 May 81) pp 897-900

[Article by I. A. Bufetov, A. M. Prokhorov, V. B. Fëdorov and V. K. Fomin, Physics Institute imeni P. N. Lebedev, USSR Academy of Sciences, Moscow]

[Text] In Ref. 1, 2 on investigation of optical discharge in the slow-burning mode, the authors observed formation and prolonged existence (~1 ms) of a break in the plasma column at the point of discharge initiation when laser breakdown of air was used to produce the inoculating plasma. It is shown in the present paper that formation of the break is due to onset of a cool gas flow directed perpendicular to the laser beam that maintains the optical discharge.

Since the observed velocities of the slow burning front are of the order of 10 m/s, the motion of gas at the same or higher velocity in the discharge region may have a considerable effect on the conditions of propagation. Therefore we did experiments to detect and study the motion of air upon relaxation of the cloud of heated gas that is formed as a result of laser breakdown. Air breakdown was achieved by focusing ($f = 22$ cm) the emission pulse ($E = 1$ J, $\tau = 40$ ns) of a Q-switched neodymium laser. Motion of the heated gas was registered by the Töpler schlieren technique. It was found that by time $t \sim 30$ μs after the breakdown, a cool air jet is formed that moves along the axis of the heated zone toward the laser with initial velocity of 150-200 m/s. Jet diameter is about 1.5 mm. The jet arises as a result of asymmetric compression of the hot gas after expansion is completed. Upon passage of the jet through the entire heated zone with dimension of ~1 cm, its velocity at $t \cong 80$ μs decreases sharply to ~10 m/s, and then damps out within a time of about 1 ms; the cool gas flow expands on the beam axis to a diameter of 0.5 cm. At the same time, the hot gas region acquires the shape of a vortex ring whose axis coincides with that of the laser beam. The rate of increase in the outer radius of the ring decreases from 20 m/s at $t \cong 100$ μs to 2 m/s at $t = 1$ ms.

An investigation was made of the influence of the observed gas motion in the region of the laser spark that initiates the discharge on development of slow optical combustion. A Q-switched laser with the above-mentioned parameters was used to produce an inoculating plasma in a weakly focused beam of a millisecond pulsed neodymium laser with power of up to 2 MW maintaining the discharge. The laser beams are mutually perpendicular in the region of intersection [see Ref. 3]. If

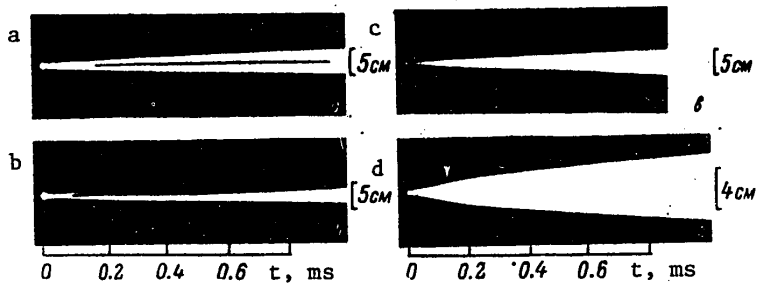

Fig. 1. Continuous slit scan of optical discharge plasma luminescence in the mode of slow combustion. The direction of observation is perpendicular to the initiating and maintaining laser beams. The camera slit is located along the axis of the millisecond laser, with beam directed from the top down on the figure; a) ignition on the axis of beam with diameter d = 4 mm; b) ignition on axis of beam with d = 4 mm, unilateral pickup; c) ignition at 3 mm from axis of beam with d = 4 mm; d) ignition on axis of beam with d = 10 mm, the arrow denoting the instant of an abrupt change in velocity.

the point of focusing of the igniting radiation was situated on the axis of a maintaining beam with diameter of 4 mm, formation of a break in the plasma column at the point of discharge initiation was observed just as in Ref. 1, 2 (Fig. 1a). Formation and reclosure of this break is completely explained by the arisal and subsequent damping of a flow of cool air directed along the axis of the maintaining beam. As it has high velocity, this flow carries plasma out of the beam in the vicinity of initiation and prevents propagation of the discharge into this region. In analogous geometry of the experiment it was also possible to observe "unilateral pickup" of slow burning (Fig. 1b): on one side of the cold air stream the inoculating plasma is completely carried out of the beam as a consequence of some asymmetry of the hydrodynamic motion, and on the other side there is pickup of the discharge. But because of the presence of the cool gas flow, the discharge does not cross the ignition point for a time of the order of 1 ms. In a subsequent experiment with displacement of the ignition point 3 mm to the side from the beam of the millisecond laser, the most intense part of the gas flow is on the outside of the maintaining beam; a nonluminescent region does not form (Fig. 1c). Finally, with focusing of initiating radiation on the axis of a large-diameter maintaining beam (beam diameter of the order of the dimensions of the inoculating plasma), the nonluminescent region occupies only part of the beam diameter. No break in the plasma column is observed when photographed from the side (Fig. 1d). On the other hand, observation along the direction counter to the beam maintaining the discharge in an analogous experiment shows (Fig. 2) that a luminescent ring is formed upon pickup of the inoculating plasma. The central part of the ring corresponds to the region of cool air flow. The symmetry of the ring is lost when its diameter goes beyond that of the beam of the maintaining plasma. The shape of the plasma column thereafter begins to approach a cylinder (Fig. 2, frame 3) [photo not reproduced]. At the same time, there is an abrupt reduction in the velocity of

plasma propagation: from 80 m/s, the rate of increase in the outer radius of the plasma ring, to 40 m/s, the rate of propagation of the planar front (Fig. 1d). The time coincidence of these two values (the change in discharge symmetry and the abrupt reduction in its propagation velocity) is evidence of the change in the gasdynamic mode of propagation of the combustion front as the combustion wave goes out to the lateral surface of the laser beam that maintains the discharge.

The results may serve as a basis for optimizing conditions of forced initiation of slow combustion of optical discharges by optical breakdown. Let us note also that the particulars of laser ignition considered in this paper explain the failure of the attempt in Ref. 4 to initiate a discharge by gas breakdown with a giant pulse, and the requirement for minimizing the energy of the initiating pulse to ensure discharge ignition in Ref. 5. The fact is that under the conditions of sharp focusing of the maintaining beam typical of Ref. 4 and 5, the inoculating plasma may simply be completely carried off by the cool gas flow from the region with high intensity of the radiation that maintains the discharge.

REFERENCES

1. Bufetov, I. A., Prokhorov, A. M., Fedorov, V. B., Fomin, V. K., PIS'MA V ZHURNAL EKSPERIMENTAL'NOY I TEORETICHESKOY FIZIKI, Vol 32, 1980, p 281.

2. Bufetov, I. A., Prokhorov, A. M., Fedorov, V. B., Fomin, V. K., KVANTOVAYA ELEKTRONIKA, Vol 8, 1981, p 751.

3. Bufetov, I. A., Fedorov, V. B., Fomin, V. K., KRATKIYE SOOBSHCHENIYA PO FIZIKE, FIAN, No 10, 1980, p 21.

4. Mul'chenko, B. F., Rayzer, Yu. P., Epshteyn, V. A., ZHURNAL EKSPERIMENTAL'-NOY I TEORETICHESKOY FIZIKI, Vol 59, 1970, p 1975.

5. Franzen, D. F., J. APPL. PHYS., Vol 44, 1973, p 1727.

6610
CSO: 1862/4

UDC 533.951

INTERACTION OF STRONG ELECTROMAGNETIC WAVES WITH COLLISIONLESS PLASMA

Gor'kiy VZAIMODEYSTVIYE SIL'NYKH ELEKTROMAGNITNYKH VOLN S BESSTOLKNOVITEL'NOY PLAZMOY in Russian 1980 (signed to press 7 Jul 80) pp 2-5, 212-214

[Annotation, editor's message and abstracts from book "Interaction of Strong Electromagnetic Waves With Plasma", edited by Doctor of Physical and Mathematical Sciences A. G. Litvak, Institute of Applied Physics, USSR Academy of Sciences, 500 copies, 214 pages]

[Text] The collection contains survey articles dealing with one of the urgent problems of plasma physics: theoretical and experimental investigation of strong Langmuir turbulence excited in a dense collisionless plasma by intense radiation.

An investigation is made of problems of the theory of modulation instability of Langmuir oscillations, the dynamics of strong Langmuir turbulence, and self-stress of radiation in a homogeneous plasma, deformation of the density profile and resonant absorption of strong electromagnetic waves in an inhomogeneous plasma. The results of theoretical research are supplemented by a survey of model microwave experiments on the action of electromagnetic waves on an isotropic plasma.

The materials of the collection may be of interest to an extensive class of specialists dealing with the interaction of electromagnetic radiation with matter, as well as nonlinear effects in the laboratory and in cosmic plasma.

Editor's Message

The problem of interaction of strong electromagnetic waves with plasma is among the problems of plasma physics being most actively researched. The interest in this problem is dictated primarily by the varied applications associated with rf and laser heating of plasma, with research on laser-driven inertial fusion reactions. Of no less importance is the fundamental significance of this problem, since interaction of intense radiation with plasma is accompanied by arisal of some fundamental nonlinear phenomena such as parametric plasma instabilities, deformation of the plasma density profile under the action of pondermotive force, formation of self-consistent distributions of plasma and field--cavitons--excitation of strong plasma turbulence, generation of flows of fast particles and quasisteady magnetic fields and so on. These effects must be studied for many other divisions of plasma physics as well.

This collection is devoted to one of the key questions of the problem of interaction of intense electromagnetic waves with plasma: investigation of processes of resonant excitation of Langmuir oscillations by electromagnetic radiation, resulting in strong Langmuir turbulence and collisionless absorption of powerful radiation.

Most of the content of the collection is made up of solicited survey articles on the theory of resonant interaction of radiation with plasma. These articles can be conditionally divided into two groups. The first includes two surveys dealing with the theory of modulation instability of Langmuir oscillations and strong Langmuir turbulence in a homogeneous plasma. The results of these works are valid for describing processes in a smoothly inhomogeneous plasma in the field of an S-polarized electromagnetic wave as well.

The second group includes three works in which an examination is made of the influence of nonlinear effects on excitation of Langmuir oscillations by the field of a p-polarized electromagnetic wave obliquely incident on an inhomogeneous plasma layer. The first of the articles considers steady-state nonlinear models of interaction, the second examines the dynamics of interaction in an external quasistatic r-f field, and the third investigates the dynamics of resonant interaction of an electromagnetic wave with an extended plasma layer.

The specifics of the investigated problem are associated with the fact that in most cases of practical interest it is impossible to use the well developed apparatus of the theory of weak plasma turbulence since nonlinearity leads to considerable distortion of the dispersion characteristics of plasma oscillations. Besides, as the plasma interacts with coherent radiation, nonlinear processes frequently have a dynamic nature so that it is necessary to deal with investigation of dynamic partial differential equations. All the theoretical papers presented are based on a unified physical approach that turns away from investigation of a system of equations of a collisionless plasma toward examination of comparatively simple physical models described by equations of the field and quasihydrodynamics of the plasma averaged with respect to the period of r-f oscillations. The complexity of the problem is apparently the reason for the fact that despite a common approach in some the articles of the collection in the examination of certain physical models, assumptions are made that are contradictory to some extent, and also the evaluation of rigor and substantiation of fundamentally important statements is sometimes subjective. Considering that more complicated models have to be used to get closer in viewpoints, and especially to determine the conditions of applicability of specific results, the editorial staff has decided not to try to reach full "reconciliation" of factions, and has even welcomed the argumentative trend of some papers. We hope that this will enable the reader to get a more complete idea not only of the advances that have been made in studying the problem, but also of the existing difficulties and contradictions.

Although a rather large number of surveys and even monographs have been published heretofore dealing with the description of experiments on interaction of electromagnetic waves with plasma, we have also deemed it advisable to supplement the theoretical articles in a special way with an attempt to formulate the results of model microwave experiments of the greatest importance for construction of a general physical picture of interaction.

A. G. Litvak

UDC 533.951

STRONG LANGMUIR TURBULENCE AND ITS MACROSCOPIC CONSEQUENCES

[Abstract of article by Galeyev, A. A., Sagdeyev, R. Z., Shapiro, V. D. and Shevchenko, V. I.]

[Text] An examination is made of the theory of strong turbulence based on the concept of collapse of Langmuir waves as a mechanism of pumping short-wave oscillations. A theory of quasi-steady turbulence is developed, assuming that the energy of Langmuir waves excited by an external source is transferred to the region of strong Landau damping as a consequence of collapse. The turbulence spectrum is determined, and the effective collision frequency is calculated that characterizes the rate of absorption of energy of the external source. The authors discuss the macroscopic consequences of the collapse of Langmuir waves upon absorption of an electromagnetic wave in the vicinity of plasma resonance and in application to relaxation of electron beams. Figures 9, references 43.

UDC 533.951

MODULATION INSTABILITY OF LANGMUIR OSCILLATIONS IN THE FIELD OF AN ELECTROMAGNETIC WAVE

[Abstract of article by Litvak, A. G. and Frayman, G. M.]

[Text] The survey presents existing notions on strong Langmuir turbulence excited in a homogeneous plasma by a monochromatic electromagnetic wave. A systematic examination is made of substantiation of model equations that describe Langmuir oscillations in an external field, one-dimensional models of the nonlinear stage of modulation instability, collapse of inhomogeneous Langmuir cavitons, macroscopic characteristics of strong turbulence, and self-stress of the electromagnetic wave. Figures 5, references 41.

UDC 533.951

DENSITY JUMP OF PLASMA IN FIELD OF A STRONG ELECTROMAGNETIC WAVE, AND ITS INFLUENCE ON THE EFFICIENCY OF RESONANT ABSORPTION

[Abstract of article by Gil'denburg, V. B.]

[Text] A systematic exposition is given of the theory of steady-state nonlinear deformation of the resonant region of an inhomogeneous plasma in the field of a strong electromagnetic wave. On the basis of quasi-static models, the author determines the conditions of onset, parameters and structure of a stepwise self-consistent transition of field and density through the plasma resonance surface. An investigation is made of the influence that such a transition has on the efficiency of processes of collisional absorption and wave transformation in an inhomogeneous plasma. The paper gives the results of numerical calculation of flat-layered plasma-field structures formed by a strong p-polarized wave. Figures 8, references 41.

UDC 533.951

DYNAMICS OF INTERACTION OF R-F FIELD WITH INHOMOGENEOUS PLASMA AND ACCELERATION OF PARTICLES IN PLASMA RESONANCE REGION

[Abstract of article by Kovrizhnykh, L. M. and Sakharov, A. S.]

[Text] It is shown within the framework of the homogeneous pumping field model that under conditions where the r-f pressure of a self-consistent field plays an appreciable part in the resonance region, the solution goes out to the state of quasiperiodic generation of peaks of Langmuir oscillations and ion density cavities (cavitons). On the initial stage of development of the process, the electrons are accelerated chiefly in the direction of reduction of plasma density, and then upon formation of cavitons there are two-sided overswings of the accelerated electrons. Estimates are found for the energy of accelerated ions in a strong pumping field, where an appreciable part is played by effects associated with electronic nonlinearity. Figures 12, references 47.

UDC 533.951

DYNAMICS OF PARAMETRIC PLASMA TURBULENCE

[Abstract of article by Andreyev, N. Ye., Silin, V. P. and Stenchikov, G. L.]

[Text] A numerical study is done on the dynamics of nonlinear interaction of a ρ-polarized wave with an inhomogeneous plasma. The initial self-consistent homogeneous system of equations takes consideration of the influence of pondermotive force on hydrodynamic plasma flow and quasilinear relaxation of the electron velocity distribution function. The authors explain the dynamics of the change in plasma density and absorption of electromagnetic field energy by the plasma and the nature of the velocity distribution of electrons. An examination is made of the generation of the second harmonic of radiation. It is found that there are two qualitatively different modes of interaction that depend on the plasma flow velocity gradient in the vicinity of the critical density. Figures 11, references 32.

UDC 533.951

EXPERIMENTAL INVESTIGATION OF RESONANT INTERACTION OF INTENSE ELECTROMAGNETIC WAVES WITH ISOTROPIC PLASMA

[Abstract of article by Brodskiy, Yu. Ya., Gol'tsman, V. L., Litvak, A. G. and Nechuyev, S. I.]

[Text] The paper gives a brief overview of existing model experiments for the purpose of formulating conclusions of importance to construction of a theory of interaction of strong electromagnetic waves with isotropic plasma. In the first part an analysis is made of the results of known quasistatic experiments on investigation of the structure and dynamics of an elementary cell of interaction--the caviton. The second part gives information on nonlinear processes that has been

obtained on the basis of the authors' measurements of the integral characteristics of transmitted and reflected electromagnetic waves and plasma oscillations, and energy functions of electron distribution. Figures 16, references 29.

6610
CSO: 1862/269

UDC 621.378.325

INFLUENCE OF LASER EMISSION WAVELENGTH ON PLASMA FORMATION THRESHOLD WITH IRRADIATION OF OPAQUE MATERIALS

Moscow KVANTOVAYA ELEKTRONIKA in Russian Vol 8, No 7(109), Jul 81 (manuscript received 11 Nov 80) pp 1582-1584

[Paper by Ye. A. Berchenko, A.V. Koshkin, A.P. Sobolev and B.T. Fedyushin]

[Text] A large number of experimental results for plasma formation thresholds is analyzed for the case where opaque materials are irradiated with laser radiation. An empirical equation is derived which makes it possible to predict the moment of plasma formation for a wide range of irradiation conditions. Questions of the impact of laser emission wavelength on the "flare" process and the precision of predictions of the moment of plasma formation are discussed.

An attempt is made in this paper to analyze literature devoted to the theoretical and experimental study of the process of plasma formation with the irradiation of an opaque barrier by a laser. In the modern theoretical "flare" model of laser radiation absorption [1], the following physical factors are taken into account: the reflection of radiation from the barrier; heat sinking into the barrier; the change in the optical and thermodynamic characteristics of the irradiated material as a function of temperature; fusion and vaporization of the material of the barrier; gas dynamic processes upon dispersal of vapor and ambient atmosphere; temperature nonuniformity within the vapors (the possibility of a break between the electron temperature and the heavy particle temperature); ionization kinetics; the actual laser emission power density as a function of time.

However, it is known that model [1] does not provide for satisfactory agreement with experimental results, because of which, the opinion was advanced concerning the possible influence on the "flare" process of some effects [2-4] which were not taken into account [1], such as electron emission from the barrier, anomalous heating of surface defects, amplification of the wave field close to defects as well as when reflected from the barrier and effects related to overheating of the melt of the barrier material (dielectrification of the metal and explosive disintegration of the metastable liquid).

Moreover, the reflective and thermodynamic properties of matter at high temperatures are not sufficnelty well known, something which in turn leads to marked errors in theoretical predictions. One way or another, an adequate "flare" absorption model should include an accounting for the considerable number of physical

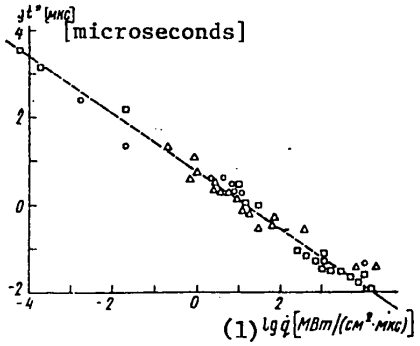

Figure 1. Plasma formation delay as a function of the rate of rise in the laser emission power density for the first (squares), second (trinagles) and third (circles) groups of experiments (see the text).

Key: 1. Log($\dot{q}$) [MW/(cm^2 · μsec)].

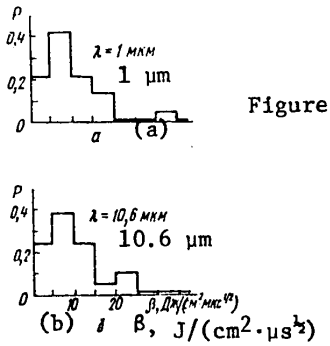

Figure 2. Histograms of the probability density of the quantity $\beta = \varepsilon^*/\sqrt{t^*}$ with the irradiation of a metal barrier.

effects and be extraordinarily voluminous (to the extent necessary). Because of this, we have undertaken an attempt to establish the laws governing the plasma formation process based on an analysis of experimental data.

For practical purposes, the question of the time of absorption "flare" development, t*, for various irradiation conditions is of special interest. All of the experiments considered by us were broken down into three groups: 1) A metal target (as a rule, aluminum), λ = 10.6 μm; 2) Metal target, $\lambda \approx 1$ μm; 3) A target made of a dielectric (glass fiber reinforced plastic), $\lambda \approx 1$ μm. Such differences in the formulation of the experiment as the pressure and kind of ambient gas, the dimater of the irradiation spot, etc., were not taken into account within the scope of each group of experiments. The permissibility of this simplification follows, for example, the results of [5]. Subsequent analysis also demonstrated that the influence of these factors does not exceed the scatter in the experimental data, related primarily to the space-time inhomogeneity of the irradiation, the natural difference in the properties of the samples being irradiated, the multiplicity of experimental techniques as well as a certain ambiguity in the concept of "plasma formation" itself.

To simplify the procedure for taking into account the actual timewise form of a laser pulse, only those experiments were selected in which the absorption "flare" occurred at the leading edge of the pulse for close to its maximum. In this case, the form of the pulse can be described by a single parameter - the characteristic rate of rise of the emission flux density $\dot{q} = q_m/\tau$, where q_m is the maximum value of the emission flux density; τ is the rise time of the laser pulse. Thus, the

plasma formation delay time, other conditions being equal, will depend only on the rate of rise in the emission flux density: $p^* = t^*(\dot{q})$. Experimental values [2, 5 - 19] of t^* are shown in Figure 1 as a function of $\dot{q}$ for all three groups of experiments. These data are satisfactorily described by the empirical formula:

$$t^* = 7q^{-2/3}, \qquad (1)$$

where t^* is in microseconds while $\dot{q}$ is in $MW/(cm^2 \cdot \mu sec)$. The curve of (1) is shown in Figure 1 with the dashed line.

This formula can be qualitatively interpreted as the time for heating the surface of the target up to a certain fixed temperature as a function of $\dot{q}$, assuming that the emission flux density rises linearly [20].

Having this interpretation in mind, as well as the approximate relationship between the energy density at the target, the temperature of the surface and the point in time, which follows from heat conductivity theory, formula (1) can be generalized for the case of an arbitrary laser pulse shape:

$$\varepsilon^*/\sqrt{t^*} \simeq \beta = 10 \text{ J/cm}^2 \cdot \mu\text{sec}^{1/2} \qquad (2)$$

where $\varepsilon^* = \int_0^{t^*} q(t)\,dt$ is the emission energy density at the target at the moment of plasma formation. Expression (2) is to be treated as an equation for the quantity t^*.

The aggregate of experiments considered here was subjected to statistical processing to estimate the precision of (2) as well as to determine the plasma formation threshold as a function of the wavelength of the acting radiation. Histograms of the distribution function (probability density) of the quantity for laser emission wavelength of $\lambda \simeq 1$ and 10.6 μm (aluminum as the barrier material) are shown in Figure 2. It follows from these graphs that for both wavelengths, the maximum value of the distribution function corresponds to a value of $\beta = 7.5$. For a wavelength of $\lambda \simeq 1$ μm, the mathematical mean value is $\bar{\beta} = 9.9$, while the dispersion (mean square deviation) is $\sigma = 6.6$. For the radiation of a CO_2 laser, these quantities are $\bar{\beta} = 9.6$ and $\sigma = 6$ respectively.

Thus, the analysis of the experimental data performed here does not allow us to talk of a marked difference in the plasma formation threshold for wavelengths of $\lambda \simeq 1$ and 10.6 μm.

BIBLIOGRAPHY

1. I.E. Markovich, A.P. Golub', I.V. Nemchinov, A.I. Petrukhin, Yu.Ye. Pleshanov, "Deponir. VINITI" ["Manuscript Deposited in the All-Union Institute of Scientific and Technical Information"], No. 3300-79 (1979).

2. C.T. Walters, R.N. Barnes, R.E. Beverly III, J. APPL. PHYS., 47, 2937 (1978).

3. V.A. Batanov, F.V. Bunkin, A.M. Prokhorov, V.B. Fedorov, ZhETF [JOURNAL OF EXPERIMENTAL AND THEORETICAL PHYSICS], 63, 586 (1972)..

4. B.M. Kozlov, A.A. Samokhin, A.B. Uspenskiy, KVANTOVAYA ELEKTRONIKA, 4, 524, (1977).

5. N.N. Kozlova, "Kand. Diss. MFTI" ["Candidate Dissertation, Moscow Engineering Physics Institute"], Moscow, 1975.

6. P.D. Thomas, AIAA J., 13, 1279 (1975).

7. A.N. Pirri, AIAA J., 15, 83 (1977).

8. W.E. Maher, R.B. Hall, J. APPL. PHYS., 46, 761 (1975).

9. V.A. Boyko, V.A. Danilychev, V.D. Zvorykin, N.V. Kholin, L.Yu. Chugunov, KVANTOVAYA ELEKTRONIKA, 3, 1,955 (1976).

10. V.P. Ageyev, A.I. Barchukov, F.V. Bunkin, V.I. Konov, S.B. Puzhayev, A.S. Silenok, N.I. Chapliyev, KVANTOVAYA ELEKTRONIKA, 6, 78 (1979).

11. V.P. Ageyev, A.I. Barchukov, F.V. Bunkin, V.I. Konov, S.M. Metev, A.S. Silenok, N.I. Chapliyev, IZVESTIYA VUZOV SSSR, SER. FIZIKA [PROCEEDINGS OF THE USSR HIGHER EDUCATIONAL INSTITUTES, PHYSICS SERIES], No. 11, 34 (1977).

12. V.A. Boyko, V.A. Danilychev, V.V. Vladimirov, B.N. Duvanov, V.D. Zvorykin, I.V. Kholin, PIS'MA V ZhTF [LETTERS TO THE JOURNAL OF TECHNICAL PHYSICS], 4, 1,373 (1978).

13. A.V. Bessarab, V.M. Romanov, V.A. Samylin, A.I. Funtikov, ZhTF [JOURNAL OF TECHNICAL PHYSICS], 48, 1,751 (1978).

14. A.V. Bessarab, V.N. Novikov, D.V. Pavlov, A.I. Funtikov, ZhTF, 50, 886 (1980).

15. N.N. Kozlova, A.I. Petrukhin, V.A. Sulyayev, KVANTOVAYA ELEKTRONIKA, 2, 1,390, (1975).

16. Ye.A. Berchenko, A.P. Sobolev, B.T. Fedyushin, KVANTOVAYA ELEKTRONIKA, 6, 1,546, (1979).

17. A.I. Korotchenko, A.A. Samokhin, A.B. Uspenskiy, KVANTOVAYA ELEKTRONIKA, 6, 210 (1979).

18. A.A. Bakeyev, B.A. Barikhin, V.V. Borovkov, L.A. Vasil'yev, L.I. Nikolashina, A.I. Pavlovskiy, N.V. Prokopenko, L.V. Sukhanov, A.I. Fedosimov, V.I. Yakovlev, KVANTOVAYA ELEKTRONIKA, 7, 349 (1980).

19. I.E. Markovich, A.I. Petrukhin, Yu.Ye. Pleshanov, V.A. Rybakov, "Tezisy dokl. IV Vsesoyuz. soveshchaniya po nerezonansnomu vzaimodeystviyu opticheskogo izlucheniya s veshchestvom" ["Abstracts of Reports of the Fourth All-Union Conference on Nonresonant Interaction of Optical Radiation with Matter"], Leningrad, 1978, p 276.

20. J. Radi, "Deystviye moshchnogo lazernogo izlucheniya" ["The Action of High Power Laser Radiation"], Moscow, Mir Publishers, 1974.

8225
CSO: 1862/252

UDC 621.373.826

THEORY OF STEADY OPTICAL GAS BREAKDOWN CLOSE TO METAL SURFACE

Moscow KVANTOVAYA ELEKTRONIKA in Russian Vol 8, No 7(109), Jul 81 (manuscript received 1 Nov 80) pp 1485-1490

[Paper by A.A. Vedenov, G.G. Gladush and A.N. Yavokhin, Institute of Nuclear Power imeni I.V. Kurchatov, Moscow]

[Text] The causes of the formation of a plasma flare close to the surface of metals are studied theoretically in this paper for light power densities on the order of 1 MW/cm^2 (low threshold breakdown). It is demonstrated that the physical nature of this phenomenon can be similar to the ignition of chemical combustion reactions by a hot surface. The breakdown takes place because of thermal ionization of the metal vapors, although the vaporization of the material is insignificant in this case. The effect of diffusion and overheating of the electrons on the amount of the threshold power density is analyzed.

1. It is well known that the laser radiation power density at which a plasma appears above a target surface can be several orders of magnitude less than the breakdown threshold of the pure gases, in the atmosphere of which the laser interaction takes place [1 - 4]. The presence of a plasma can become the decisive factor in the interaction of the radiation and the matter, since it can both strongly shield the surface [2] and promote the radiation heating of the material [5]. The phenomenon of low threshold breakdown has not yet been uniquely theoretically explained. Thermal breakdown is studied in this paper as one of the possible reasons for the formation of a plasma at the surface of a solid.

In the case of a low incident radiation power density q, the ambient gas of the medium is heated by virtue of the thermal conductivity from the surface of the absorbing target. The essence of thermal breakdown consists in the fact that at a radiation density which exceeds a certain critical value, q_π [q_p], the gas is heated up to such a high temperature that its further heating then becomes possible because of the intense thermal ionization, with subsequent direct absorption of the laser beam energy. Such a breakdown mechanism was used in paper [6] to analyze the interaction of a radiation pulse with a metal, where vaporization is significant, while the heating of the vapors took place with the

formation of an intense shock wave. For large values of q, this approach yielded good agreement with experimental data on the surface shielding time. In the quasi-steady-state case, where the pressure in the gas volume has time to equalize, depending on the power density and the external pressure, two interaction variants are possible. The vapors of the material can either slowly diffuse from the focal spot into the ambient gas, or can displace it, forming a steady-state jet. A theoretical analysis of optical breakdown in these cases was reported in [7]. The results of analytical and numerical study of the first of the indicated variants are presented below.

2. Although the occurrence of a plasma flare is a nonsteady-state process, we shall initially treat steady-state problems, since the breakdown phenomenon can be treated mathematically as the transition from one steady-state to another.

We shall assume that the laser beam is focused on the surface of the material in a spot of radius R. In the absence of a well developed vaporization mode, the energy carried away by the material vapors is small, and for this reason, the temperature in the spot is governed by the thermal conductivity of the target: $T_0 = \alpha qR/\kappa_m$ where κ_m and α are the thermal conductivity and absorption coefficients of the target material. At a distance remote from the spot, the gas temperature falls off, as with increasing distance from a point source: proportional to r^{-1}. It will be seen from the following that breakdown occurs at a distance from the target which is considerably less than the radius of the focal spot R. For this reason, one can disregard side losses and limit oneself to the spherically symmetrical or plane case.

To ascertain the main laws governing the phenomenon, we shall initially consider the simplest case of an equilibrium isotemperature medium. In the steady-state case, the temperature of this medium is determined by the energy balance equation:

$$-\frac{\partial}{\partial r}\varkappa r^2\frac{\partial T}{\partial r} = (2-\alpha)K(T, N)qR^2;$$
$$K(T, N) = \frac{4\pi e^2 \bar{v}_e \sigma_{ea}}{cm\omega^2}\left(\frac{2\pi m}{\hbar}\right)^{3/4} pN^{1/2}(kT)^{-1/4}\exp\left(-\frac{I}{2kT}\right); \quad (1)$$
$$N = N_s(T_0);\ T(R) = T_0;\ T(\infty) = 0,$$

where N_s is the equilibrium vapor density; p is the pressure of the ambient medium; I is the gas ionization potential; ω is the laser radiation frequency; σ_{ea}, $\bar{v}_e$, m and e are the scattering cross-section, the thermal velocity, mass and charge of an electron; κ is the heat conductivity coefficient of the gas medium. The fact that the light absorption coefficient K is due to electron scattering at neutral particles (for a CO_2 laser) is taken into account in (1). The density of the metal vapors which diffuse from the target and the temperature fall off at a characteristic distance on the order of R. The absorption factor K, in view of the sharp dependence on T, falls off over a significantly shorter distance, and for this reason, the vapor concentration N can be taken as constant.

We shall assume for simplicity that κ does not depend on temperature; then, by introducing the dimensionless variables $\theta = (T/T_0 - 1)I/2T_0$, $\xi = r/R$ and expanding the exponent close to T_0 [9], we derive the following from (1):

$$\frac{2}{\xi}\frac{\partial\theta}{\partial\xi}+\frac{\partial^2\theta}{\partial\xi^2}=-\frac{D}{\xi^2}e^{\theta};$$
$$\theta(1)=0;\ \theta(\infty)=-I/2T_0;$$
$$D=\frac{qR^2K(T_0)}{\varkappa T_0}\frac{I}{2T_0}(2-\alpha). \qquad (2)$$

Equation (2) is not integrated, but considering the fact that breakdown occurs close to the surface (at a distance of $\xi = D^{-1/2} << 1$), one can shift over to a plane geometry. In this case, the problem reduces to a problem of asymmetrical ignition or ignition by a hot surface [9]. Zel'dovich's condition for ignition has the form:

$$D>{}^1/_8(I/2T_0)^2. \qquad (3)$$

In making the transition to dimensionless variables, we obtain the condition for the quantity q at which breakdown occurs:

$$q_n=\frac{1}{2}(\lambda+I)\frac{\varkappa_M}{\alpha R}\ln^{-1}\frac{32fq^*R^2}{\varkappa I};$$
$$f=\frac{4\pi e^2\bar{v}_e\sigma_{e,a}}{cm\omega^2}\left(\frac{2\pi m}{h}\right)^{3/4}pN_0^{1/2}(kT)^{-1/4}. \qquad (4)$$

where λ is the heat of vaporization; N_0 is the coefficient in the expression $N_s = N_0 \cdot \exp(-\lambda/kT)$, which depends on the material; $q^* \approx 1$ MW/cm^2.

It can be seen from (4) that the breakdown flux density basically depends on the properties of the target material: the thermal conductivity, the absorption factor, the vaporization energy and the ionization potential of the vapor atoms. The properties of the surrounding gas and its pressure have a weak influence on the breakdown threshold. The influence of the light frequency should be manifest in the absorption factor. Estimates based on formula (4) for difficultly fusible metals, for example, for tungsten, yield $q_p \approx 1$ MW/cm^2, which is close to that observed in experiments [4]. However, the surface temperature T_π [T_p] at which breakdown occurs is more important in this approach. It is essential that the pressure of the saturated vapors of the material, which depends sharply on the temperature of the surface, does not exceed the ambient gas pressure. Otherwise, as was stated in section 1, a hydrodynamic outflow of the vapor will appear and the governing laws will be different. According to estimates, the transition temperature is $T_p^* \approx 5{,}000$ to $6{,}000$ °K, and for this reason, even for difficultly fusible materials, T_p is close to the boiling point T_k (for W, $T_k \approx 5{,}800$ °K). Consequently, it is necessary to calculate T_p more precisely.

Because of this, equation (1) was solved with variable coefficients. The metal vapor density was calculated by means of the diffusion equation:

$$\frac{1}{r^2}\frac{\partial}{\partial r}Dr^2\frac{\partial N}{\partial r}=0;$$
$$N(R)=N_s(T_0);\quad N(\infty)=0, \tag{5}$$

where D is the diffusion coefficient, which depends on temperature.

System (1) and (5) was solved by a plotting technique. Various distribution profiles of the temperature T and the metal vapor density were established as a function of the power density q. Curves for T as a function of the radius are shown in Figure 1 for nitrogen at p = 3 atm and for tungsten. The thermal physical constants expressed as a function of temperature were taken from [10], α = 5 percent. Initially, the curve T(r) is close to r^{-1}. At a certain value, $q = q_p$, the temperature profile ceases to be monotonically declining, the value of $\partial T/\partial r$ at the surface of the metal increases with time and becomes positive, while a temperature maximum appears close to the surface and the temperature subsequently rises rapidly. Thus, a thermal breakdown of the gas occurs in the laser beam at $q = q_p$. The curves for q_p and T_p are plotted in Figure 2 as a function of the ambient nitrogen gas pressure. The curve for the boiling point is also plotted in the same graph as a function of pressure [10]. It can be seen that the curve for T_p for a pressure above atmospheric runs below the boiling point curve. Thus, for tungsten-nitrogen vapor, an equilibrium thermal breakdown in the target vapors is possible. Since the thermal-physical coefficients of nitrogen and air are close, these results can also apply to air. As follows from [11], the burning of tungsten in air takes a course through a surface oxidation reaction. The heat of the reaction is liberated at the solid surface. Since the ionization potential of tungsten oxide, WO_3 (11.7 eV), is higher than the ionization potential of tungsten vapors (8 eV), then the breakdown temperature T_p, taking the combustion reaction into account, apparently does not decrease. The threshold light power density is reduced in this case by virtue of the combustion power, which is difficult to estimate under the conditions because of the lack of data on the reaction rates at high temperatures. In principle, an equilibrium thermal breakdown can also occur for other difficultly fusible materials, for example, molybdenum, titanium and tantalum.

Since the ionization potential of the metal atoms is markedly less than the ionization potential of the ambient gas, despite the fact that the density of of the metal vapors is usually substantially lower than the ambient gas density, thermal ionization of just the vapors governs the conductivity of the medium and consequently, the absorption factor. The contribution of the ambient gas is small. Estimates based on formula (4) for air assuming that the latter consists of the easily ionized compound NO (overstated conductivity) yield a value for the breakdown temperature which exceeds the boiling point of tungsten. A numerical solution of equation (1) for an air pressure of 1 - 3 atm, taking into account the radiation absorption factor by air where the radiation is at a wavelength of 10.6 μm [2],

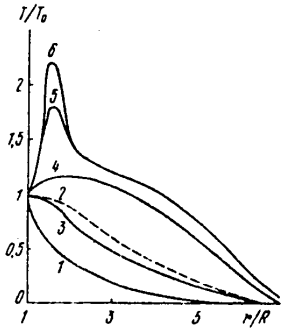

Figure 1. Gas temperature distribution as a function of the radius, T_0 = 5,400 °K.

Key: 1. Initial distribution;
2. Steady-state distribution at $q \leq q_p$;
3-6. The distribution of T(r) for $q \geq q_p$; t/τ = 0.1 (3), 0.2 (4), 0.3 (5) and 0.301 (6); τ = 54 msec and q_p = 0.9 MW/cm^2.

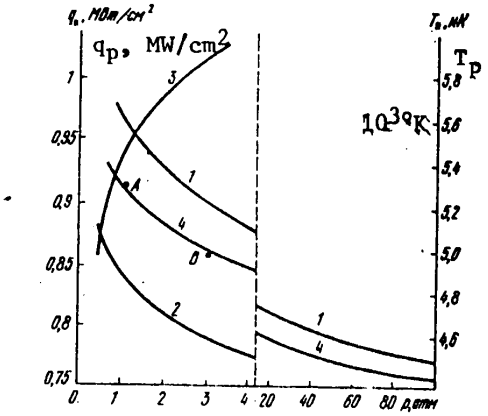

Figure 2. The breakdown power density q_p and the surface temperature T_p as a function of the external pressure.

Key: 1. Nitrogen;
2. The functions specified by formula (4);
3. The boiling point of tungsten as a function of pressure;
4. Nitrogen, taking into account $T_e > T$, points A and B were calculated taking plasma diffusion into account.

yielded a breakdown temperature of 12,000 °K, something which is knowingly higher than the boiling point of any material. This indicates the unreal nature of the presuppositions of [13] and the erroneous conclusions of paper [14], where it is proposed that a low threshold laser breakdown be explained by the thermal breakdown of pure air.

3. It was assumed above that the plasma is in a state of local thermodynamic equilibrium, where the temperature of the electrons T_e is equal to the gas temperature. Since the radiation energy is absorbed by the electrons, and the latter give up heat to the gas as a consequence of elastic and inelastic collisions, then it is possible, generally speaking, for the electron gas to overheat. The latter is extremely important, since the plasma density depends strongly on the temperature of the electrons. These effects can be taken into account by means of thermal balance equations for the electrons and heavy particles:

$$-\frac{1}{r^2}\frac{\partial}{\partial r}\varkappa_e r^2\frac{\partial T_e}{\partial r}=\frac{R^2}{r^2}Kq-\frac{3m\delta}{M}n_s k(T_e-T)\bar{\nu}_e(N_\Sigma\sigma_y+n_s\sigma_k); \tag{6a}$$

$$-\frac{1}{r^2}\frac{\partial}{\partial r}\varkappa r^2\frac{\partial T}{\partial r}=\frac{3m\delta}{M}n_s k(T_e-T)\bar{\nu}_e(N_\Sigma\sigma_y+n_s\sigma_k);$$

$$n_s=\left(\frac{mkT_e}{2\pi\hbar^2}\right)^{3/4}\sqrt{N}\exp\left(-\frac{I}{2kT_e}\right);\quad N_\Sigma=N+N_{cp}, \tag{6b}$$

where σ_k is the coulomb cross-section; δ is the inelastic loss coefficient; $\kappa_e = \nu_e n_f/3\ (N_\Sigma\sigma_y + n_s\sigma_k)$ is the coefficient of electron heat conductivity. Adding (6a) and (6b), and considering the fact that for the given conditions $\kappa_e < \kappa$, we obtain equation (1), in which, however, the absorption factor depends on the electron temperature T_e. The size of the latter is determined by equation (6a). In the absence of electron thermal conductivity, T_e will be maximal:

$$T_e = T + \frac{4\pi e^2 M R^2}{3kcm^2\omega^2\delta r^2}q. \tag{7}$$

It can be seen from (7) that for molecular gases, for example nitrogen, the electron temperature exceeds the gas temperature by the small amount of $\approx$ 300 °K (for $q \approx 1$ MW/cm^2, r = R, δ = 15 [15]). By substituting (7) in (1), one can, as is done for example, in MHD generators with a nonequilibrium plasma [51], take the impact of electron heating on the plasma conductivity into account, and consequently, its impact on the breakdown threshold. Curve 4 in Figure 2 was plotted taking this effect into account. It can be seen that the influence of nonequilibrium is small for molecular gases. In reality, the heating will be even less for molecular gases, since in prebreakdown modes, the frequency of coulomb collisions is on the order of the elastic collisions and much greater than the inverse energy time $3m\delta\nu_y/M$. This leads to more efficient energy transfer from the electrons to the vibrational molecular degrees of freedom and the gas temperature.

In atomic gases, the break in the temperature of the electrons can prove to be substantial. For example, for Ar, in accordance with (7), $T_e - T \approx 6{,}000$ °K. However, the electron thermal conductivity will be significant at atmospheric pressure. Dor this reason, it is necessary to solve (6a) and (6b) simultaneously to find T_e and T. At high pressures (p > 20 atm), the electron thermal conductivity becomes small, and for this reason, the influence of electron heating can be taken into account just as for the case of a molecular gas. Calculations based on (1) and (7) yield a breakdown temperature in Argon at a tungsten surface substantially lower than for nitrogen: $T_p \approx 3{,}800$ °K. Such a low value of the temperature also makes it possible to use this approach for less difficultly fusible materials. For example, T_p = 3,050 °K for steel at p = 15 atm. Thus, the breakdown power density depends on the properties of both the target material and the ambient gas.

4. It was stated at the outset of this paper that the thermal breakdown was analyzed for the simplest case: the case of an equilibrium plasma, where the electron concentration is determined by Saha's formula. Because of the large

spatial gradients for some parameters of the problem, the plasma losses due to diffusion from the surface of the metal into the gas can play a part. This correspondingly reduces the concentration of electrons close to the metal, but nonetheless increases far away from the metal and promotes light absorption in a wider range as compared to the equilibrium case. At atmospheric pressure, as estimates for N_2 show, the diffusion ion flux is comparable to a Saha-Langmuir flow. With an increase in the gas pressure, the relative role of the diffusion losses decreases and the plasma concentration at the cathode becomes close to an equilibrium concentration. The condition of ionization equilibrium in the volume is governed by the diffusion recombination length $l_r = [D_a/(\beta n^2)]^{1/2}$, where β is the recombination coefficient. For the given conditions (higher plasma densities), step ionization and recombination processes play the decisive role [16], which, generally speaking, depend on the individual properties of the ionizing atoms. It is difficult to consider calculations reliable which utilize a general expression for β, which does not depend on the kind of matter [16]. The corresponding estimates for atmospheric pressure yield a value of l_r on the order of 0.1 mm, which does not exceed the size of the focal spot R, but is comparable to the characteristic dimension over which the plasma concentration falls, For this reason, diffusion could have an influence on breakdown, generally speaking, though as numerical calculations have demonstrated, this influence is small.

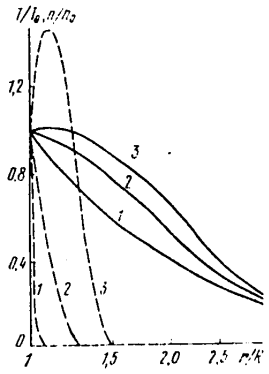

Figure 3. The temperature distribution (solid lines) and density (dashed lines) of a plasma in nitrogen where p = 3 atm, T_0 = = 5,400 °K, q_p = 0.9 MW/cm^2, τ = 0.58 msec; t/τ = 0 (1), 0.51 (2) and 1.5 (3).

To take diffusion into account, the plasma balance equation,

$$-\frac{1}{r^2}\frac{\partial}{\partial r} D_a r^2 \frac{\partial n}{\partial r} = \beta n_s^2 n \left(1 - \frac{n^2}{n_s^2}\right); \qquad (8)$$

$$n(R) = n_s(T(R)); \quad n(\infty) = 0; \quad \beta = 5e^{10}/m^{1/2}(kT)^{9/4}$$

was solved simultaneously with the heat balance equation for the gas (1). The plasma density (1) is determined from (8), Calculations for p = 1 and 3 atm, of

nitrogen yielded a T_p which practically matched the values calculated for an equilibrium plasma (see Figure 2). The development of the breakdown is shown in Figure 3 as a function of time. It can be seen that the plasma layer is rather wide and the equilibrium concentration curve which corresponds to temperature curve 2, on this scale coincides with the ordinate. However, as was stated above, a thicker absorbing layer had no influence on the size of the breakdown, something which is apparently related to the weak dependence of T_p on the dimension of the system R (see (2) and 3)). The questions discussed in sections 3 and 4 are close to the approach developed in paper [17] for other conditions; the vaporization of the target material, in particular, was not taken into account in [17].

Thus, we have shown that low threshold breakdown close to a target of materials which are not difficultly fusible can be explained by thermal breakdown in the vapors of the material. In this case, the breakdown occurs until the onset of intense vaporization and destruction of the target. A comparison of the theory and calculations with experimental data is necessary for a more detailed study of the reason for the formation of the plasma close to the target.

BIBLIOGRAPHY

1. Ya. N. Gnoyevoy, A.N. Petrukhin, Yu.Ye. Pleshakov, V.A. Sulyayev, PIS'MA V ZhETF [LETTERS TO THE JOURNAL OF EXPERIMENTAL AND THEORETICAL PHYSICS], 11, 440 (1970).

2. E. Locke, E. Hoag, R. Hella, IEEE J., QE-8, 132 (1972).

3. A.I. Barchukov, F.V. Bunkin, V.I. Konov, A.M. Prokhorov, PIS'MA V ZhETF, 17, 413, (1973).

4. N.N. Rykalin, A.A. Uglov, M.M. Nizametdinov, DAN SSSR [REPORTS OF THE USSR ACADEMY OF SCIENCES], 218, 330 (1974).

5. V.P. Ageyev, A.I. Barchukov, F.V. Bunkin, et al., IZVESTIYA VUZOV SSSR. SER. FIZIKA [PROCEEDINGS OF THE USSR HIGHER EDUCATIONAL INSTITUTES. PHYSICS SERIES], 11, 34 (1977).

6. A.P. Golub', I.V. Nemchinov, KVANTOVAYA ELEKTRONIKA, 7, 209 (1980).

7. A.A. Vedenov, G.G. Gladush, FIZIKA I KHIMIYA OBRABOTKI MATERIALOV [MATERIALS PROCESSING PHYSICS AND CHEMISTRY], No. 1, 142 (1979).

8. Yu.P. Rayzer, "Lazernaya iskra i rasprostraneniye razryadov" ["Laser Spark and Discharge Propagation"], Moscow, Nauka Publishers, 1974.

9. D.A. Frank-Kametskiy, "Diffuziya i teploperedacha v khimicheskoy kinetike" ["Diffusion and Heat Transfer in Chemical Kinetics"], Moscow, Nauka Publishers, 1967.

10. "Tablitsy fizicheskikh velichin: Spravochnik" ["Tables of Physical Quantities: Handbook"], edited by I.K. Kikoin, Moscow, Atomizdat Publishers, 1976.

11. P. Kofsted, "Vysokotemperaturnoye okisleniye metallov" ["High Temperature Oxidation of Metals"], Moscow, Mir Publishers, 1969.

12. "Opticheskiye svoystva goryachego vozdukha" ["Optical Properties of Hot Air"], edited by L.M. Biberman, Moscow, Nauka Publishers, 1970.

13. A.V. Bondarenko, Ye.V. Dan'shchikov, V.S. Golubev, F.V. Lebedev, A.F. Nastoyashchiy, A.V. Ryazanov, PIS'MA V ZhTF [LETTERS TO THE JOURNAL OF TECHNICAL PHYSICS], 5, 221 (1979).

14. A.F. Nastoyashchiy, KVANTOVAYA ELEKTRONIKA, 7, 170 (1980).

15. D. Sutton, A. Sherman, "Osnovy tekhnicheskoy magnitnoy gidrodinamiki" ["Principles of Applied Magnetic Hydrodynamics"], Moscow, Mir Publishers, 1968.

16. B.M. Smirnov, "Iony i vozbuzhdennyye atomy v plazme" ["Ions and Excited Atoms in a Plasma"], Moscow, Atomizdat Publishers, 1974.

17. V.I. Mazhukin, A.A. Uglov, B.N. Chetverushkin, DAN SSSR, 246, 1338 (1979).

8225
CSO: 1862/252

OPTICS AND SPECTROSCOPY

UDC 535.338:539.194

ANALYSIS OF ABSORPTION SPECTRUM FOR D_2O, HDO AND H_2O VAPOR IN 1.06 μm REGION

Moscow DOKLADY AKADEMII NAUK SSSR in Russian Vol 258, No 4, 1981 (manuscript received 22 Dec 80) pp 854-858

[Article by A. D. Bykov, Associate Member of USSR Academy of Sciences V. Ye. Zuyev, V. P. Lopasov, Yu. S. Makushkin, L. N. Sinitsa and O. N. Ulenikov, Tomsk Affiliate, Institute of Optics of the Atmosphere, Siberian Department, USSR Academy of Sciences]

[Text] Vibrational-rotational spectra of molecules are a unique source of complete and reliable data on the nature of intermolecular interaction, internal states and physicochemical properties of molecules in a variety of external conditions. Of special interest is the investigation of spectra of different isotopic varieties of a given type of molecule since this gives significant supplementary information on the same or similar parameters and properties of molecules.

This paper gives some results of the first laboratory recording of the absorption spectrum of D_2O and HDO vapor in the 9160-9400 cm^{-1} region together with a theoretical analysis. The measurements (P = 1 kPa) were done on a neodymium laser spectrometer on the basis of the method of intracavity absorption [Ref. 1]. The spectral range of operation of the spectrometer is 9100-9520 cm^{-1}, resolution 0.08 cm^{-1}, threshold sensitivity to absorption 10^{-7} cm^{-1}, which corresponds to using 10 km of absorbing layer in classical spectroscopy. The positions of line centers were measured with accuracy of 0.08 cm^{-1} relative to the absorption lines of H_2O measured in Ref. 2.

A mixture of H_2O, D_2O and HDO vapors was used as the investigated medium. The width of the laser emission spectrum over a pulse is 7-10 cm^{-1}. Registration of the absorption spectrum throughout the spectral interval of 9160-9400 cm^{-1} was by wavelength tuning from pulse to pulse with overlapping of adjacent regions of the spectrum.

In the above-mentioned section of the spectrum a total of more than 300 absorption lines was registered, belonging to bands (111) and (012) of H_2O, (112) and (013) of D_2O, (310) and (121) of HDO. As an example, Fig. 1 shows a section of the obtained spectrum. Theoretical analysis of the experimental results included interpretation of the lines, determination of vibrational-rotational energies in upper vibrational states, determination of rotational and centrifugal constants (in the interpretation a preliminary theoretical estimate was made of the positions of the centers of vibrational-rotational bands of the D_2O and HDO molecules).

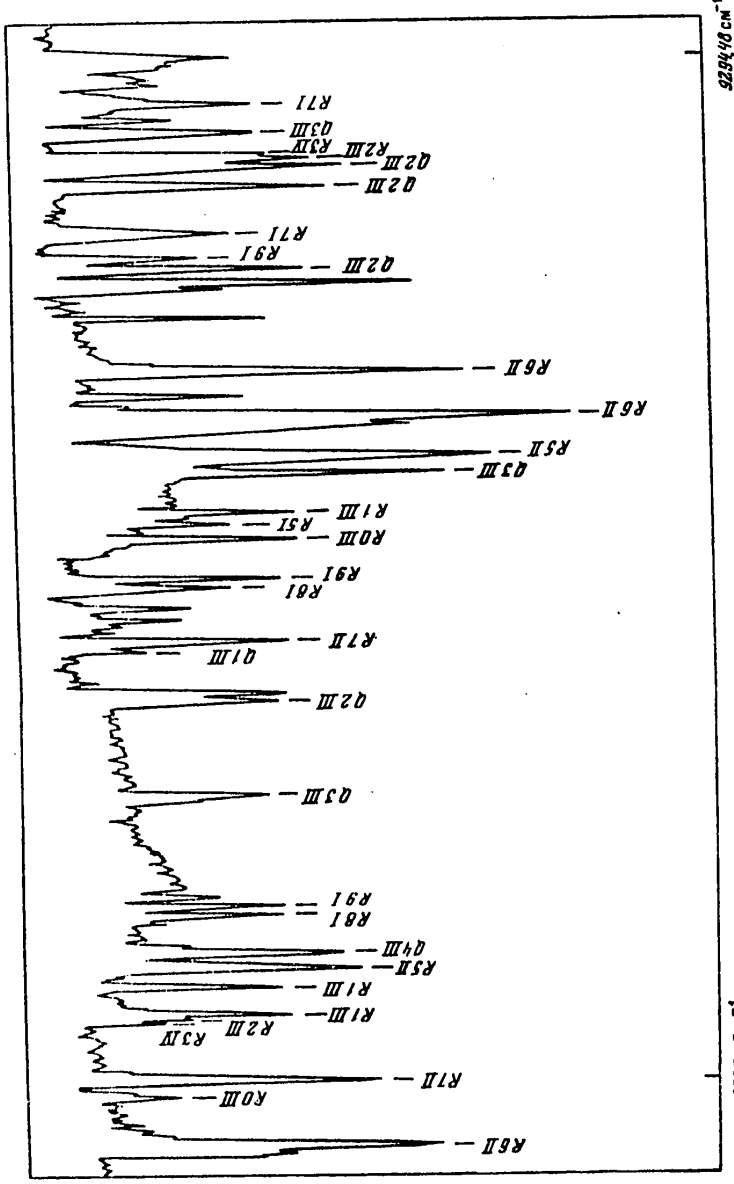

Fig. 1. Absorption spectrum of mixture of H_2O, D_2O and HDO vapor in 9294-9325 cm^{-1} region. Indices I, II, III, IV refer to bands (111) of H_2O, (012) of H_2O, (310) bf HDO and (112) of D_2O respectively.

In analyzing the spectra of the water molecule and its isotopic modifications it is necessary to take into consideration the presence of resonant interaction between different vibrational states. In our case it is difficult to use the traditional approach (see for example Ref. 3) to the determination of rotational and centrifugal constants in connection with the necessity of simultaneously accounting for a large number of resonating states. For example, for states (112) and (013) of D_2O in accordance with the traditional method it is necessary in addition to these two states to account for eight others that interact with them. In this connection, the resultant spectrum was interpreted by using a technique developed by the authors and described in Ref. 4, 5, enabling a reduction in the total number of vibrational states taken into consideration in solving the inverse problem with regard to resonant interactions. Analysis showed that in the case of interest to us, states (112), (013) of D_2O and (310), (121) of HDO can be treated with a fair degree of validity as isolated, at least for small values of quantum number J.

Another important point in solving the inverse problem is choosing the zero-order approximation. The following procedure was carried out to calculate the initial approximation of rotational and centrifugal constants of D_2O and HDO molecules and also to check the validity of line interpretation. The authors had previously developed a method of analyzing the influence of isotope substitution on the parameters of molecules [Ref. 6, 7]. In particular, isotope ratios were found for some spectroscopic constants of X_2Y molecules of C_{2V} symmetry (the formulas were derived within the framework of the harmonic oscillator approximation). In this research it was shown that similar expressions

$$(1) \quad A' = f(m, m', \omega, \omega')\, A + \Delta A$$

can be obtained with isotope substitution in the anharmonic oscillator approximation as well. In (1), A and A' are the spectroscopic constants of the fundamental modification and the isotope respectively, f(m, m', ω, ω') are known functions of the masses of the nuclei; ΔA represents small corrections to the first term.

To estimate the rotational and Δ constants of bands of the D_2O molecule that we require, the corresponding constants of bands (112) and (013) of the H_2O molecule were determined. To do this, an analysis was made of the H_2O absorption spectrum in the vicinity of 0.80 μm. As the initial data, we used the experimental results in the solar spectrum atlas of Ref. 9 with theoretical processing to determine the rotational and centrifugal constants of the above-mentioned bands of the H_2O molecule. The resultant parameters were used in formula (1) for estimates of rotational and Δ constants of vibrational states (112) and (013) of D_2O.

Concomitantly, formulas were obtained enabling evaluation in the anharmonic oscillator approximation of rotational constants for individual vibrational states (in particular for states (112) and (013)), based on the structural and force constants of D_2O. It is shown that in the case of paired Darling-Dennison vibrational resonance the rotational constants $B_\beta^{V_1V_2V_3}$ can be calculated from the formula

$$(2) \quad B_\beta^{V_1, V_2, V_3} = B_\beta^e - \gamma^2_{V_1, V_2, V_3,\ V_1, V_2, V_3} \sum_{\lambda=1}^{3} \alpha_\beta^\lambda (V_\lambda + \tfrac{1}{2}) -$$

$$- \gamma^2_{V_1 \pm 2, V_2, V_3 \mp 2,\ V_1, V_2, V_3} \{\alpha_\beta^1 (V_1 \pm 2 + \tfrac{1}{2}) + \alpha_\beta^2 (V_2 + \tfrac{1}{2}) + \alpha_\beta^3 (V_3 \mp 2 + \tfrac{1}{2})\} +$$

$$+ \Delta B_\beta^{V_1, V_2, V_3}.$$

where $\Delta B_x = \Delta B_z = 0$ (B_x and B_z are the greater and average of the rotational constants); B_β^e are the equilibrium values of these constants; α_β^λ are vibrational-rotational constants (see for example Ref. 8); $\gamma^2 V_1 V_2 V_3$, $V_1' V_2' V_3'$ are the weights with which harmonic functions $|V_1 V_2 V_3>$ and $|V_1' V_2' V_3'>$ participating in the Darling-Dennison resonance enter into the total vibrational wave function.

Formulas were derived in a similar way for HDO molecules, enabling estimation of rotational and Δ constants based on structural and force constants of HDO, and also by using isotope ratios.

TABLE 1

Rotational and centrifugal constants of states (112) of D_2O and (310) of HDO (cm^{-1})

Parameter	(112) D_2O			(310) HDO	
	Est. by Formula (1)	Est. by Formula (2)	Exp. data processing	Calculation	Exp. data processing
E	9207*		9205,86	9279*	9292,90
A	15,3	15,2	15,56	25,0	24,89
B	7,2	7,1	7,43	8,8	8,71
C	4,6	4,6	4,70	6,0	5,99
$\Delta_K 10^3$	11,0	7,5	8,5	26,2	21,3
$\Delta_{JK} 10^3$	-1,6		-2,5	1,6	3,1
$\Delta_J 10^4$	4,0		4,2	6,0	5,1

*Theoretically calculated with consideration of vibrational resonances

TABLE 2

Vibrational-rotational energies of excited states (112) of D_2O and (310) of HDO (cm^{-1})

J	KA	KC	(112) D_2O	(310) HDO	J	KA	KC	(112) D_2O	(310) HDO
0	0	0	9205,81	9292,94	3	2	1	9319,31	9452,19
1	0	1	9217,99	9307,67	3	3	1	9363,97	9537,04
1	1	1	9226,12	9323,73	3	3	0	9364,00	9537,06
1	1	0	9228,88	9326,41	4	0	4	-	9435,38
2	0	2	9241,68	9336,74	4	1	4	9321,60	9442,97
2	1	2	9247,68	9350,35	4	1	3	-	9469,83
2	1	1	9255,77	9358,48	4	2	3	-	9509,04
2	2	1	9280,20	9406,78	4	2	2	9371,88	-
2	2	0	9280,64	9407,05	4	3	2	-	9596,03
3	0	3	9275,85	9379,57	4	3	1	-	9596,19
3	1	3	9279,53	9390,18	4	4	1	9478,17	9714,38
3	1	2		9406,40	4	4	0	9478,17	9714,38
3	2	2	-	9450,75					

The parameters obtained in this way were then used as a zero-order approximation for determining rotational and centrifugal constants of states (112), (013) of D_2O, and (310), (121) of HDO from experimental data. As an example, tables 1 and 2 summarize some results of theoretical processing of the recorded spectrum.

Table 1 shows estimates of the values of rotational and centrifugal constants of states (112) of D_2O and (310) of HDO, and for comparison the values of these parameters obtained by formulas (1), (2) and used as a first approximation for D_2O. Table 2 contains some vibrational-rotational energy levels obtained for two of the above-mentioned bands of D_2O and HDO molecules. Interpretation of the spectrum was done simultaneously with determination of spectroscopic constants. The results of the analysis enabled interpretation of more than 75% of the recorded absorption lines. By way of illustration of the results of this interpretation, Fig. 1 shows lines corresponding to Q- and R-branches of absorption bands of H_2O, D_2O and HDO.

The results provide additional information that can be used for example in studying the physical and chemical properties of the H_2O molecule. They may also be of independent interest, for example for atmospheric optics or physics of the interstellar medium.

REFERENCES

1. Sinitsa, L. N., KVANTOVAYA ELEKTRONIKA, Vol 4, 1978, p 148.

2. Flaud, J. M., Camy-Peyret, C. et al., J. MOL. SPECTROSC., Vol 75, 1979, p 339.

3. Kwan, Y. Y., Ibid., Vol 71, 1978, p 260.

4. Antipov, A. B., Bykov, A. D. et al., Preprint, Institute of Optics of the Atmosphere, Siberian Department, USSR Academy of Sciences, IOA SO AN SSSR No 28, Tomsk, 1979.

5. Antipov, A. B., Bykov, A. D. et al., DOKLADY AKADEMII NAUK SSSR, Vol 251, 1980, p 267.

6. Bykov, A. D., Makushkin, Yu. S., Ulenikov, O. N., OPTIKA I SPEKTROSKOPIYA, Vol 46, 1979, p 673.

7. Makushkin, Yu. S., Terent'yev, V. A., Ulenikov, O. N., in: "Molekulyarnaya spektroskopiya vysokogo i sverkhvysokogo razresheniya" [High- and Ultrahigh-Resolution Molecular Spectroscopy], Novosibirsk, "Nauka", 1976, p 3.

8. Kuchitsu, K., Morino, Y., BULL. CHEM. SOC. JAPAN, Vol 38, 1965, p 814.

9. Moore, C. E., Minnaert, M. G. J., Houtgast, J., "The Solar Spectrum 2935 Å to 8770 Å", NAT. BUR. STAND. USA, 1966.

6610
CSO: 8144/063

UDC 551.501.7:621.373.826

POWERFUL LASER PROBING OF PHYSICOCHEMICAL PARAMETERS OF ATMOSPHERE

Tomsk ZONDIROVANIYE FIZIKO-KHIMICHESKIKH PARAMETROV ATMOSFERY S ISPOL'ZOVANIYEM MOSHCHNYKH LAZEROV in Russian 1979 (signed to press 29 Dec 79) pp 2, 98-102, 220-221

[Annotation, paper "Method of Measuring Absolute Intensity of Intense Laser Beam From Dynamics of Scattered Radiation", by G. A. Mal'tseva, and table of contents from book "Power Laser Probing of Physicochemical Parameters of Atmosphere", edited by V. Ye. Zuyev, associate member, USSR Academy of Sciences, Institute of Optics of the Atmosphere, Siberian Department, USSR Academy of Sciences, 221 pages]

[Text] The collection is devoted to problems of the application of high-intensity laser sources to purposes of remote probing of physicochemical parameters of the atmosphere. Some papers deal with development of the physical principles of new probing methods based on using a particular class of interactions of intense radiation with matter--nonlinear optical effects. An examination is made of problems of self-stress of laser beams on direct and lidar paths, and also the particulars of construction of systems of adaptive optics under conditions where nonlinear effects show up.

The collection is written for scientific workers and graduate students specializing in the field of atmospheric optics research, and also for specialists in related fields developing and using laser equipment for studying and monitoring the state of the atmosphere.

METHOD OF MEASURING ABSOLUTE INTENSITY OF INTENSE LASER BEAMS FROM DYNAMICS OF SCATTERED RADIATION

[Article by G. A. Mal'tseva]

[Text] An interesting question in propagation of intense laser emission in the atmosphere is the capability of determining absolute intensity of the laser beam along its path.

This paper suggests a method of determining the absolute intensity of a laser beam in water haze from the dynamics of the scattered radiation.

For radiation $I_\theta(x,t)$ scattered at angle θ, we can write from the lidar equation:

$$I_\theta(x,t) = \frac{c I_0 (\sigma_{\theta a} + \sigma_{\theta M})}{x^2} \exp(-\tau_0 - \tau^N); \quad I_0' = \frac{I_0 \exp(-\tau_0)}{\left(1 - x\frac{\theta_0}{R_0}\right)}, \qquad (1)$$

where

$$\sigma_{\theta a} = \frac{16\pi^4 a^6 N a}{\lambda^4}\left|\frac{m^2-1}{m^2+2}\right|^2 (1-\sin^2\theta), \quad \sigma_{\theta M} = \frac{2\pi^2(n-1)^2}{\lambda^4 N_M}(1+\cos^2\theta),$$

$\sigma_{\theta a}$, $\sigma_{\theta M}$ are the coefficient of aerosolic and molecular scattering [Ref. 1]; x is the distance to the space to be probed; θ_0 is beam divergence; R_0 is the initial beam radius; I_0 is the initial power density of the laser radiation; $\tau_0 = (\alpha_{oa} + \alpha_{oM})x$; α_{oa}, α_{oM}, α^N are coefficients of aerosolic, molecular and nonlinear attenuation respectively; N_M, N_a are the concentration of molecules and of aerosols; a is the size of an aerosol particle; n is the index of refraction; $m = n - i\kappa_a$ is the complex index of refraction,

$$\tau^N = \int_0^x \alpha^N(I_0'(x),t)\,dx = \pi N_a a_0^2 \sum_{\kappa=1}^{5} \rho^\kappa P_\kappa D_\kappa,$$

where a_0 is the initial size of aerosol particles, P_K are coefficients in the asymptotic formula for the coefficient of attenuation of haze [Ref. 2],

$$D_\kappa = \frac{\sqrt{B_\kappa}}{C}\left[\frac{1}{\sqrt{B_\kappa}} e^{\frac{-B_\kappa}{(1-xC)^2}}\left(e^{(1-xC)^2} + xC - 1\right) - \sqrt{\pi}\left(\Phi\left(\frac{\sqrt{B_\kappa}}{1-xC}\right) - \Phi(\sqrt{B_\kappa})\right)\right];$$

$$C = \frac{\theta_0}{R_0}; \quad B_\kappa = (\kappa+2)\exp(-0.2[n^2 + \varkappa_a^2 - 2n - 1])^{1/2}\frac{8\pi\varkappa_a}{\lambda} A_2 I_0 t; \quad \rho = \frac{2\pi a_0}{\lambda}.$$

Φ is the probability integral; $P_2 = 0$; $D_K = 0$; γ is the density of water; L_T is the specific heat of vaporization; C_p, T^ℓ are the specific heat and temperature of the vapor-gas mixture; T_∞, P_∞ are the temperature and pressure of the medium; λ^ℓ is the coefficient of thermal conductivity of the mixture; R is the gas constant; D is the coefficient of diffusion; μ is molecular weight.

For vaporization of a droplet in the state of slight superheating $\Delta T/T_K \ll 1$ (T_K is the boiling point),

$$A_2 = \frac{1}{4\gamma[L_T + C_p T_\infty + \lambda^\ell R^2 T_\infty^3 / D\mu L P_\infty]},$$

if the condition of weak superheating is not met, then

$$A_2 = 1/4\gamma[L_T + C_p D/(D/T^\ell))] \text{ [Ref. 3].}$$

Fig. 1 and 2 show the dynamics of the backscattered radiation calculated by formula (1) for the following parameters: $R_0 = 12$ cm, $\theta_0 = 9\cdot10^{-4}$ rad, $N_a = 10^3$ cm^{-3}, $L = 100$ m and $t = 0.2\cdot10^{-6}$ s.

On Fig. 1, curves 1, 2, 3 are for particles with dimensions of 0.5, 1 and 1.5 μm respectively. The prime indicates curves for radiation divergent at the same angle. To determine the absolute intensity of a powerful laser beam from the dynamics of radiation scattered at angle θ we find the relation for the time derivative of the scattered signal. For the case τ_0, $\tau^N \ll 1$, and $\sigma_{\theta a} > \sigma_{\theta M}$

$$I_0'(x) = \eta\left(\frac{dI_\theta/dt}{I_\theta}\right),$$

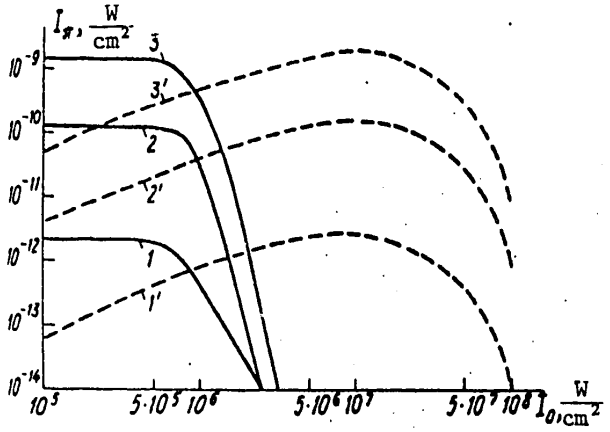

Fig. 1. Backscattering signal as a function of intensity of incident radiation

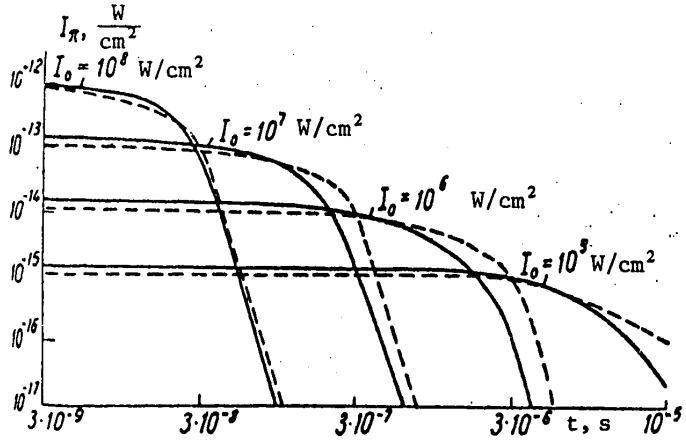

Fig. 2. Backscattering signal as a function of time

where

$$\eta = \left(6\exp\left(-0.2\left[n^2+\varkappa_a^2-2n-1\right]^{1/2}\frac{8\pi\varkappa_a}{\lambda}A_2\right)\right)^{-1}.$$

The dependence of η on λ is shown in Fig. 3, and can be used as a calibration curve for determining the intensity of a laser beam in absolute units over a path for different wavelengths.

In conclusion I thank Yu. D. Kopytin for formulating the problem and constructive discussion of the results of the work.

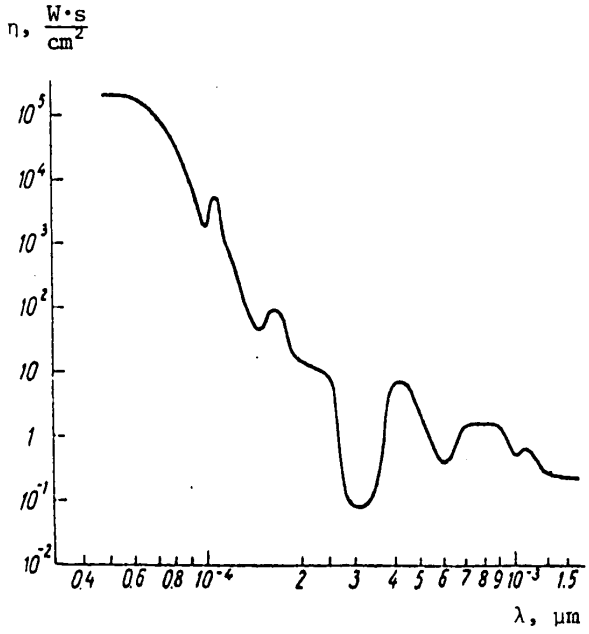

Fig. 3. Dependence of η on wavelength λ

REFERENCES

1. Shifrin, K. S., "Rasseyaniye sveta v mutnoy srede" [Scattering of Light in a Turbid Medium], Moscow-Leningrad, Gostekhizdat, 1951.

2. Zuyev, V. Ye., "Prozrachnost' atmosfery dlya vidimykh i infrakrasnykh luchey" [Transparency of the Atmosphere for Visible and Infrared Rays], Moscow, "Sovetskoye radio", 1966.

3. Zuyev, V. Ye., Luzikovskiy, A. V., Pogodayev, V. A., Khmelevtsov, S. S., Chistyakova, L. K., "Thermal Effect of Optical Radiation on Water Droplets of Small Diameter", DOKLADY AKADEMII NAUK SSSR, Vol 205, No 5, 1972, p 1069.

Contents page

6610
CSO: 1862/263

OPTOELECTRONICS

UDC 621.373.8.029.71:535.37

CHARACTERISTICS OF TEMPERATURE-SENSITIVE PHOSPHOR SCREENS FOR IR PHOTOREGISTRATION

Moscow KVANTOVAYA ELEKTRONIKA in Russian Vol 8, No 8(110), Aug 81
(manuscript received 10 Dec 80) pp 1754-1759

[Article by L. M. Klyukin, Ye. N. Koroleva and M. V. Senashenko, All-Union Scientific Research Institute of Opticophysical Measurements, Moscow]

[Text] An analysis is made of the fundamental and actual threshold energy sensitivity of thermographic phosphor screens for registration of IR radiation. A technique is proposed for determining frequency-contrast characteristics by reconstructing them from the function of response to a step signal. The limiting resolution of the phosphorescent converter is determined.

1. Introduction

The thermographic phosphor screen is one of the most effective visualizers of IR radiation due to stability of its characteristics, simplicity of manufacture and high reproducibility of properties. The use of phosphor crystals for visualizing radiation in the intermediate and far IR bands ($\lambda \geqslant 2$ μm) has been discussed in Ref. 1-4; however, the capabilities for metrology of IR radiation by such screens were not adequately covered [Ref. 5-7] because of difficulties that arise with work in this band. In particular, it is quite complicated to make test patterns for the intermediate and far IR band, and the use of a δ-signal to determine the frequency-contrast characteristics is difficult because of diffraction limitations [Ref. 8].

In this paper an analysis is made of the extremum values of major characteristics of temperature-sensitive phosphor screens in registration of IR radiation: threshold energy sensitivity, frequency-contrast characteristics and spatial resolution. Some new experimental techniques are proposed for determining these characteristics with consideration of their mutual relation to the temperature properties of phosphors, as well as to the parameters of the screen and the conditions of use. A theoretical basis is given for the proposed techniques.

2. Fundamental and Actual Threshold Sensitivities of Phosphor Screens

The fundamental value of threshold sensitivity is determined primarily by the thermal mechanism of recording information on the phosphor screen. In any system under

conditions of heat exchange with the ambient medium, the field of temperature fluctuations $\delta(T)$ corresponds to the field of heat flows of the system

$$\delta(Q)=C\delta(T), \tag{1}$$

where C is its specific heat. Introducing the time constant

$$\tau=C/2\eta \quad \text{[Ref. 9]} \tag{2}$$

that characterizes heat exchange with coefficient η on both sides of the screen, and considering that by definition the fundamental threshold sensitivity is

$$P^f_{th}=\overline{\delta(Q)}\,|_S/\tau|_S S, \tag{3}$$

where S is screen area, we get

$$P^f_{th}=2\eta\overline{\delta(T)}\,|_S. \tag{4}$$

Since the screen has a finite time lag, estimation of the temperature fluctuation by formula [Ref. 10] $\delta(T)=\sqrt{(k/C)T}$, where k is Boltzmann's constant, would give overstated results for P^f_{th}. An explicit form of the function $\delta(T)$ can be found by using the fluctuation-dissipation theorem [Ref. 11] for thermal impedance of the system:

$$P^f_{th}=4\pi T\,(S^2Kdc^2\rho^2\eta^{-5})^{-1/4}, \tag{5}$$

where K is the heat-transfer coefficient, d is thickness, c is the specific heat of the screen, ρ is density. Substituting in (5) the tabular values of K, c, η, ρ, d = 20 μm and S = 300 cm^2, we find the fundamental value of the threshold sensitivity of such a phosphor screen: $P^f_{th} \approx 0.1$ nW/cm^2.

The actual value of threshold sensitivity P^{ac}_{th} is naturally higher than the fundamental value, not only because of the random scatter of physical geometric parameters caused by the screen manufacturing process or variance of other parameters (for example fluctuation of screen luminescence intensity I), but mainly, as shown in Ref. 12, because of the conversion coefficient $R_T = dI/IdT$ that is characteristic of the given material and plays the role of a transition characteristic from the thermal to the optical field of screen luminescence. In this case

$$P^{ac}_{th} = \eta\Delta T, \tag{6}$$

where ΔT is the threshold temperature change.

The quantity ΔT can be found by using the experimental temperature dependence of luminescence of temperature-quenched phosphors ZnSCdS-Ag, Ni [Ref. 2]:

$$I=I_0\exp(-R_{T\max}\Delta T), \tag{7}$$

where $R_{T\max}$ is the maximum value of the conversion coefficient of phosphor $ZnS_{50}CdS_{50}$-Ag $3\cdot10^{-4}$, Ni $3\cdot10^{-6}$ at the selected level of UV pre-illumination of ~50 $\mu W/cm^2$. The limiting value of P^{ac}_{th} is realized for a screen in vacuum, where $\eta = 4(\varepsilon_1+\varepsilon_2)\sigma T_0^3$, where ε_1 and ε_2 are the degrees of blackness of the two faces

of the screen, σ is the Stefan-Boltzmann constant, T_0 is ambient temperature. At threshold perception of the change of intensity $\Delta I/I = K_{th}$, we get the actual value of threshold sensitivity

$$P_{th}^{ac} = 4(\varepsilon_1 + \varepsilon_2)\sigma T_0^3 \ln(1 + K_{th}) R_{T\max}^{-1}; \quad (8)$$

after substituting appropriate values, we get $P_{th}^{ac} = 281\ \mu W/cm^2$.

3. Experimental Estimate of Threshold Sensitivity

As experimental specimens, we used phosphor screens of composition $ZnS_{50}CdS_{50}$ $Ag3\cdot10^{-4}$, $Ni3\cdot10^{-6}$ applied on mylar film with absorptive layer. The processes of phosphor preparation and screen manufacture are described in Ref. 6. Threshold screen sensitivity was measured in the continuous mode, using an incandescent lamp as the source of IR radiation with filament stabilized at a definite temperature. The purpose of the absorbing layer was to convert the radiant energy to a temperature relief. The wavelength of the registered emission has no appreciable significance here; the coefficient of absorption of the given screen retains a constant value over a wide range [Ref. 6]. The phosphor screens were excited by monochromatic radiation ($\lambda = 365$ nm) of a stabilized mercury vapor lamp with power density of 50 $\mu W/cm^2$. The spatial distribution of power density in the IR beam was determined by an IMO power meter through a diaphragm with diameter of 0.1 mm. The pattern on the phosphor screen was photographed by the Kiev-15 camera, and the negative was analyzed on an IFO-451 microphotometer.

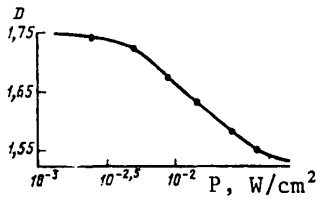

Fig. 1. Characteristic curve of phosphor screen

Since the threshold sensitivity is the signal whose effect produces the same change in density of blackening of the negative as noise δD [Ref. 6], it can be determined by using a characteristic curve with consideration of the inherent steady-state noise of the screen. Frames produced when signals with different radiation power densities act on the screen are used to plot a characteristic curve of the screen (Fig. 1) as the dependence of blackening density on the power density of the registered radiation (the relation between the screen luminescence intensity and the corresponding blackening density on the negative in the experiment was taken as linear).

Since the inherent noise of the photographic film is much lower than for the screen, the steady-state noise of the latter can be judged from the result of microphotometry of the negative taken immediately before exposure of the screen. The value of the mean-square noise δD was determined by microphotometry in two perpendicular directions passing through the center of the screen, giving $\delta D = 0.062 \pm 0.001$.

The graphic method of determining threshold sensitivity from the intersection of δD plotted from initial level D_0 with the characteristic curve leads to an error due to the inaccuracy of the graphic plot, which is especially large on the initial section of the curve. For more exact determination of the threshold sensitivity of phosphor screens, we approximated the characteristic curve on the initial section by a polynomial of the form

$$P=\alpha+\beta D+\gamma D^2, \tag{9}$$

in which the coefficients were obtained with respect to points (D,P) near this section. The working relation obtained for points (1.74, 2.55 mW/cm^2), (1.73, 5.1 mW/cm^2) and (1.66, 15.3 mW/cm^2) had the form $P = -3.6298 + 4.442D - 1.3537D$ [W/cm^2].

At a mean level of the initial background equal to $\overline{D}_0 = 1.75$, the measured value of δD corresponded to a threshold power density $P_{th} = 1.17$ mW/cm^2. If the rms noise had been reduced by an order of magnitude, P_{th} would have been down to 0.37 mW/cm^2, i. e. it would have been close to the extremum value obtained above.

4. Resolution and Frequency-Contrast Characteristics

As pointed out above, the main difficulty in estimating these parameters of the screen, especially in the intermediate and far IR wavelength bands, is production of the appropriate test patterns. The method proposed in Ref. 13 for reconstruction of frequency-contrast characteristics from the response to an output signal in the form of a δ-function is not suitable under conditions of the far IR band, where diffraction by the slit cannot be disregarded.

We have attempted to reconstruct the frequency-contrast characteristics by using the response to the image of the edge of a step; as will be shown below, this reconstruction is possible in the thermal method of registration since we can get an analytical expression for the response of the screen to a step signal, and experimentally verify the resultant function. Such a technique can be used if two principal conditions are observed: the screen must be isotropic with respect to its space-frequency properties, and the response must depend linearly on the input signal. The first condition is met for phosphor screens; the condition of linearity imposes constraints on the section of the characteristic curve of the screen [Ref. 6] on which an experimental estimate can be made.

To measure the frequency-contrast characteristics, a facility was put together where the signal shaping system included an incandescent lamp, an IKS-7 light filter, a lens for producing a wide uniform spot about 50 mm in diameter, and a steel razor covering half the spot on the blackened backing of the screen (the edge of the razor was indicated by a taut fine filament on the phosphor side), and the information extraction system was made up of the phosphor screen excited by UV radiation, and a camera to record the steady-state pattern at the output.

Fig. 2 shows the arrangement for getting the response of the phosphor screen to the edge of a step. The registered signal acting in zone A under steady-state conditions leads to heating of the screen so that its temperature $\theta(x)$ is constant in the region $x \to -\infty$ (as will be shown below, the small dimensions of the transition zone allow us to assume this). In the vicinity of $x \to 0$, a transition temperature is formed that is equal to zero at $x \to \infty$. The stepwise nature of temperature distribution corresponds to stepwise distribution of phosphor luminescence brightness $I(\theta)$ and density $D(x)$ of the investigated negative.

By definition [Ref. 8], the frequency-contrast characteristic is the ratio of the Fourier transform of the output signal to the Fourier transform of the input signal:

$$F(\omega)=F(U_{out})/F(U_{in}).$$

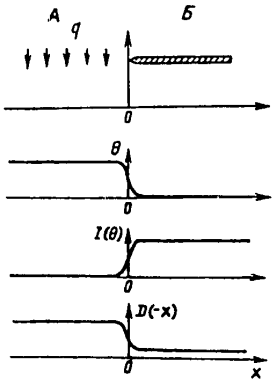

Fig. 2. Scheme for getting response of phosphor screen to step edge

Since I is exponentially dependent on θ, and D in turn is logarithmically dependent on I, the output signal can be approximated with accuracy to a constant term by the function θ(x) that we get by solving the corresponding thermal problem.

The initial heat conduction equation is determined by the following conditions: a) steady-state operation $\partial\theta/\partial t = 0$; b) $\eta = \text{const}$, which is dictated by heat exchange conditions at small θ; c) flux q is formed as a step function $q(x) = q_0|Y(x)|$. Then for zones A and Б (see Fig. 2) with consideration of the boundary conditions that relate these zones, the solution of the corresponding heat conduction equation takes the form

$$\theta_A = B(1-{}^1/_2 e^{nx}), \quad (10a)$$

$$\theta_Б = {}^1/_2 Be^{-nx}, \quad (10b)$$

where $B = q/2\eta$, $n = \sqrt{2\eta/kd}$. The behavior of θ(x) as plotted with consideration of the parameters of the phosphor screen ($\eta = 5$ mW/(cm²·deg), $K = 24$ mW/(cm·deg), $d = 2\cdot10^{-3}$ and $B = 9.8$°C) is shown in Fig. 3, which also shows the experimentally measured characteristic D(-x) (both curves are normalized to facilitate comparison).

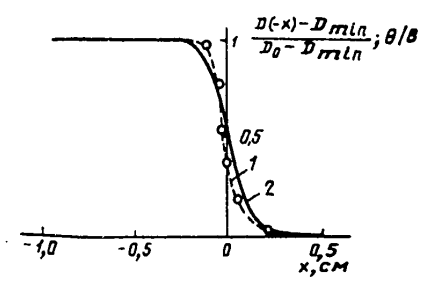

Fig. 3. Spatial distribution of negative blackening density (1) and temperature (2) along step edge on phosphor screen

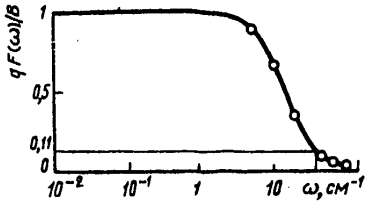

Fig. 4. Frequency-contrast characteristic of phosphor screen

We might, as suggested previously [Ref. 13], have used any function, for example $D(x) = Ee^{-\alpha x^2}$, $x > 0$, to approximate the output signal D(x). However, passage to the frequency region gives rise to distortions of frequency-contrast characteristics associated with discontinuity of the derivative of D(x), and therefore it is advisable to use the physical model of the response function (13), for which the Fourier transform is constructed; then

$$F[\theta(x)] \sim BF[-Y(x)] + BF[(e^{nx})], \quad (11)$$

where Y(x) is the function of a unit step, and after Fourier transformation, we have [Ref. 14]

$$F(\omega) \doteq \frac{B}{q}\left(1 - \frac{\omega^2}{\omega^2 + \omega^2 + 2\pi\omega\delta(\omega)}\right). \quad (12)$$

Considering the fact that $2\pi\omega\delta(\omega) = 0$, we finally get

$$F(\omega) = \frac{B}{q}\left(1 - \frac{\omega^2}{n^2 + \omega^2}\right). \quad (13)$$

Fig. 4 shows the frequency-contrast characteristic of a screen as reconstructed by formula (13). The limiting resolution as found from this graph in accordance with the Rayleigh test is 30 cm^{-1}, which agrees with previous experimental data [Ref. 4].

5. Conclusions

1. Our analysis has shown that the fundamental threshold sensitivity of a phosphor screen based on heat-sensitive ZnSCdS-Ag, Ni phosphor, as determined only by the thermal mechanism of data recording, is many orders of magnitude lower than the actual value dictated by the mechanism of conversion of the heat field to the field of screen luminescence. We found that the limiting threshold sensitivity of a luminescent receiver of IR emission may reach 0.1 mW/cm^2 with improved manufacturing techniques and reduction of noise through homogeneity of UV pre-exposure.

2. A physical model has been derived for the response function of a thermographic phosphor screen that provides a most convenient method of reconstructing its frequency-contrast characteristic. The curve is reconstructed for a screen receiving a step-function signal, and the limiting resolution is determined.

The given methods of reconstructing frequency-contrast characteristics and determining threshold sensitivity can be applied to any other media that are intended for imaging signals in the IR region as well.

REFERENCES

1. Urbach, F., Nail, N. R., Pearlman, D., J. OPT. SOC. AMER., Vol 39, 1949, p 690.

2. Levshin, V. L., Mitrofanova, N. V., Timofeyev, Yu. P. et al., TRUDY FIZICHESKOGO INSTITUTA IMENI P. N. LEBEDEVA AKADEMII NAUK SSSR, Vol 59, 1972, p 64.

3. Timofeyev, Yu. P., Fridman, S. A., IZVESTIYA AKADEMII NAUK SSSR: SERIYA FIZICHESKAYA, Vol 43, 1979, p 1303.

4. Timofeyev, Yu. P., Fok, M. V., TRUDY FIZICHESKOGO INSTITUTA IMENI P. N. LEBEDEVA AKADEMII NAUK SSSR, Vol 117, 1980, p 3.

5. Bazhulin, A. P., Vinogradov, Ye. A., Irisova, N. A. et al., TRUDY FIZICHESKOGO INSTITUTA IMENI P. N. LEBEDEVA AKADEMII NAUK SSSR, Vol 117, 1980, p 122.

6. Klyukin, L. M., Klyuchnikov, V. M., KVANTOVAYA ELEKTRONIKA, Vol 3, 1976, p 1095.

7. Zaytsev, L. M., Zysina, L. Yu., Senashenko, M. V., Tsarapayeva, Ye. I., PRIBORY I TEKHNIKA EKSPERIMENTA, No 5, 1978, p 253.

8. Collier, R. J., Burckhardt, C. B., Lin, L. B., "Opticheskaya golografiya" [Optical Holography], Moscow, Mir, 1973.

9. Kondrat'yev, M. G., "Teplovyye izmereniya" [Thermal Measurements], Moscow-Leningrad, Mashgiz, 1957.

10. Landau, L. D., Lifshits, Ye. M., "Staticheskaya fizika, ch. I" [Statistical Physics, Part I], Moscow, Nauka, 1976.

11. Callen, H. B., Welton, T. A., PHYS. REV., Vol 83, 1951, p 34.

12. Klyukin, L. M., Stepanov, B. M., ZHURNAL NAUCHNOY I PRIKLADNOY FOTOGRAFII I KINEMATOGRAFII, No 2, 1979, p 153.

13. Klyukin, L. M., Namiot, V. A., Senashenko, M. V., PRIBORY I TEKHNIKA EKSPERIMENTA, No 1, 1981, p 53.

14. Soroko, L. M., "Osnovy golografii i kogerentnoy optiki" [Principles of Holography and Coherent Optics], Moscow, Nauka, 1971.

6610
CSO: 1862/14

UDC 531.715.1.(0.88.8)

PROPERTIES OF INCOHERENT FOURIER-TRANSFORMING OPTICAL SYSTEMS

Leningrad OPTIKO-MEKHANICHESKAYA PROMYSHLENNOST' in Russian No 8, Aug 81 (manuscript received 25 Sep 80) pp 7-9

[Article by I. N. Matveyev, N. D. Ustinov and B. A. Shiryayev]

[Text] The process of imaging a spatially incoherent radiation source consists in double conversion of the Fourier distribution of intensity over the source. This conversion is done by using an objective lens. In this case, the image is registered immediately at the output. Holographic devices enable a two-stage process of image formation; the first stage is direct Fourier transformation with registration of the spatial spectrum of the object, and the second is inverse Fourier transformation and reconstruction of the image of the object. Measurement and registration of the spatial spectra of objects rather than their images is of both theoretical and practical interest for solving a number of applied problems. The principle of measurements is based on spatial coherence that arises in the process of propagation of initially incoherent radiation. In accordance with the well known Van Zitter-Zernike theorem, the correlation function of the field in the far zone is related by Fourier transformation to the intensity distribution over the source. Thus the problem of obtaining the spatial spectrum consists in measuring the correlation function of the field.

This paper analyzes two-dimensional Fourier-transforming interferometers for measurements of this type.

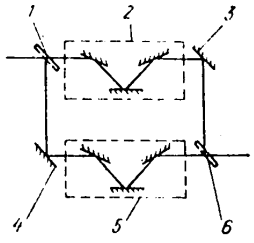

Fig. 1. Optical diagram of interferometer in Mach-Zehnder arrangement: 1, 6--beam-splitter mirrors; 2, 5--Dove mirror prisms; 3, 4--swivel mirrors

Let us consider the interferometer [Ref. 1] shown in Fig. 1. The light flux arriving at the input of the device is divided in half by a beam-splitter mirror. the fluxes are then directed to the interferometer arms, each containing Dove mirror prisms that rotate the wavefront through 180° relative to the edge of the prism. Let us rotate one of the prisms about the optical axis through an angle $\pi + \alpha/2$, and the other through angle $\pi - \alpha/2$; the corresponding wavefronts are turned through twice the angle, and two waves are formed at the output of the interferometer with relative rotation of wavefronts through angle 2α.

Let us find the intensity distribution at the interferometer output. Let the field on the output aperture of the interferometer be a set of quasimonochromatic waves from a remote source that are plane-polarized with polarization vector $\vec{P}$. The polar coordinates in the plane of the source are designated by r_1, θ_1, and in the plane of the output aperture of the interferometer--by r_2, θ_2, and the distance from the source to the output aperture is designated by z. We write the complex amplitudes of the field in the arms of the interferometer in the form

$$\begin{aligned} E_1\left(r_2\theta_2+\frac{\pi+\alpha}{2}\right) &= e_1\int_\sigma E(r_1\theta_1)\exp\left[\frac{ikr_1r_2}{z}\cos\left(\theta_1-\theta_2+\frac{\pi+\alpha}{2}\right)\right]r_1dr_1d\theta_1, \\ E_2\left(r_2\theta_2+\frac{\pi-\alpha}{2}\right) &= e_2\int_\sigma E(r_2\theta_1\exp\left[\frac{ikr_1r_2}{z}\cos\left(\theta_1-\theta_2+\frac{\pi-\alpha}{2}\right)\right]r_1dr_1d\theta_1. \end{aligned} \tag{1}$$

In expression (1), integration is carried out over the surface of the object. The intensity at the output of the interferometer, considering that the waveforms are independent of the various elements of the source, is equal to

$$I=\int_\sigma I(r_1\theta_1)\,r_1dr_1d\theta_1+V(\alpha)\int_\sigma I(r_1\theta_1)\cos\left[\frac{2kr_1r_2}{z}\cos(\theta_1-\theta_2)\sin\alpha\right]r_1dr_1d\theta_1,$$

where

$$V(\alpha)=e_1e_2=\cos 2\alpha.$$

Converting to cartesian coordinates with radii-vectors in the planes of the object and the output mirror of the interferometer $\vec{r}_1$ and $\vec{r}_2$ respectively, we get

$$I(r_2)=\int_\sigma I(r_1)\,dr_1+V(\alpha)\int_\sigma I(r_1)\cos\left(\frac{2kr_1r_2}{z}\right)dr_1. \tag{2}$$

The second term of this expression is the Fourier transform of the intensity distribution over the object. The scale of conversion is determined by the exponential factor $2\sin\alpha$.

Thus the given interferometer is a lensless Fourier-transforming optical system. A similar result is obtained when a Michelson interferometer is used with the mirrors in the arms replaced by rectangular prisms (Fig. 2) [photo not reproduced].

Expression (2) can be written in a more convenient form that gives a clear idea of how the intensity is distributed on the interference pattern. To do this, the direction to some fixed point of the object is assigned by a unit vector drawn from the center of the input aperture of the interferometer to the given point. We denote the component of this vector in the plane of the aperture by $\vec{\rho}_0$. Obviously the vector $\vec{\rho}_0$ characterizes the angular displacement of the object from the optical axis. The position of an arbitrary point of the object is determined by the vector $\vec{\rho}_0+\vec{\rho}$, which is also the projection of the corresponding unit vector. We will carry out integration with respect to the solid angle from which radiation arrives:

$$I(r)=\int_\Omega I(\vec{\rho})\,d\vec{\rho}+V(\alpha)\,\mathrm{Re}\exp(i2k\vec{\rho}_0r\sin\alpha)\int_\Omega I(\vec{\rho})\exp(2ik\vec{\rho}r\sin\alpha)\,d\vec{\rho}. \tag{3}$$

As we can see from (3), displacement of the object from the optical axis leads to a rapidly oscillating carrier in the interferogram, modulated by the spatial spectrum of the object.

Inverse Fourier transformation of interference pattern (3), carried out for example with the same kind of interferometer, results in reconstruction of the image of the object:

$$I(\bar{x}) = S\int_{\Omega} I(\bar{\rho})\,d\bar{\rho} + SV(\alpha)\left[H(2\bar{x}\sin\alpha)\int_{\Omega} I(\bar{\rho})\,d\bar{\rho} + S\int_{\Omega} I(\bar{\rho})\,H[2(\bar{x}\pm\bar{\rho}\pm\bar{\rho}_0)\sin\alpha]\,d\bar{\rho}\right], \tag{4}$$

Here S is the area of the input aperture of the interferometer. The first term of expression (4) gives the fixed background, the second is the peak of intensity on the optical axis, and the third term describes two symmetrically located images of the object, one of which coincides with the object itself. The function

$$H(2\bar{x}\sin\alpha) = \frac{1}{S}\int_{S} \exp(2ik\bar{x}\bar{r}_2\sin\alpha)\,dr_2 \tag{5}$$

determines the resolution of the system, which ranges from 0 to the diffraction limit, depending on angle α. As can be seen from formula (5), maximum resolution is reached at $\alpha = \pi/2$, and at diameter D of the input aperture is $w = \lambda/2D$, which is twice the diffraction resolution of lens optics. It should be pointed out that the interferometer is apparently the only optical device with ideal resolution that can be varied with a fixed aperture.

Thus the interferometric Fourier-transforming optical system can be considered a two-stage imaging system. In essence, the production and processing of interference patterns is a holographic process of image reconstruction with spatially incoherent illumination of the object. This is what dictates the capability of using Fourier-transforming interferometers in holography. But since the intensity spectrum is recorded in the given case, the reconstructed image, like an ordinary photographic image, is not three-dimensional.

Another most interesting example of use of these devices is their application for astronomical measurements of the angular dimensions of planets and stars, distances between binary and ternary stars and the like. As pointed out previously, at an angle of $\alpha = \pi/2$, sections of the wavefront interact at the output of the interferometer that are symmetric relative to its optical axis. Thus the two-dimensional interferometer is equivalent to a set of two-slit stellar Michelson interferometers with bases that change from zero to the dimensions of the aperture of the two-dimensional interferometer and have all possible orientations from 0 to 2π.

It can be seen from formula (2) that the normalized function that describes intensity distribution in the interference pattern coincides with the real part of the complex degree of coherence of the field. For a source in the form of a circular uniformly illuminated disk, the intensity is equal to

$$I(r) = \int I(\bar{\rho})\,d\bar{\rho}\,[1 + 2\cos(2k\bar{\rho}_0 r)\frac{J_1(2k\theta_r)}{2k\theta r}.$$

In view of the symmetry of the object, the envelope of the interference pattern depends only on the absolute value of the radius-vector $\vec{r}$ and the angular size of the object θ, and coincides with band luminosity in the stellar interferometer.

Magnification of the input aperture of the two-dimensional interferometers can be achieved when they are used jointly with large-diameter telescopes.

Interferometers based on the Mach-Zehnder scheme can be set up in both convergent and parallel beams, while interferometers based on the Michelson arrangement operate only in parallel beams. Symmetry of the beam path in the arms of the interferometers makes optical matching with telescopes simple. Simultaneous registration of the two-dimensional correlation function considerably shortens measurement time and enables analysis of the shape of complex objects, which is practically impossible when using the Michelson stellar interferometer. This leads us to believe that including two-dimensional interferometers in the instrumentation of present-day large-diameter telescopes will appreciably improve measurement efficiency, and thus extend the capabilities of the telescopes themselves.

Let us recall that the basic property of interference patterns is that the interference bands are displaced in the presence of phase distortions, while their envelope and the band luminosity are retained. The size and shape of the investigated object is determined from the luminosity of the interference bands. The size of the object is determined from the zeros of the luminosity function. The shape of the object can be determined from convolution of the image with itself. To form the convolution of the image, it is necessary to carry out Fourier transformation of the luminosity function and square the result. Fig. 3 [photo not reproduced] shows the interference pattern of an object simulating a binary star obtained under actual atmospheric conditions using a telescope with aperture of 0.5 m. As we can see from this picture, the interference bands are distorted by fluctuations of the atmosphere; nonetheless, bands of zero and maximum contrasts can be clearly distinguished on the interference pattern. The distance between adjacent maxima or minima can be used to measure the angular distance between sources.

Let us briefly consider the aberrational characteristics of the optical system with interferometer, and show that partial compensation of aberrations occurs in such a system.

We write the equation of the spherical surface corresponding to the reception objective in the form

$$(z-r)^2+\xi^2+\eta=r^2.$$

Expanding z with respect to powers of $\frac{\xi^2+\eta^2}{r}$, we get

$$z=\frac{\xi^2+\eta^2}{2r}+\frac{\xi^2+\eta^2}{8r^3}+\dots$$

The phase of a wave propagating in direction z is determined by this expression. The first term leads to focusing of the wave, while subsequent terms lead to distortions, i. e. to aberrations of the optical system. In the more general case [Ref. 2], the Seidel eikonal is used to describe optical systems with representation by the sum

$$S=S_0+S_3+S_4+S_6.$$

Term S_2 characterizes the ideal optical system, sum S_4 characterizes third-order aberrations, and is expressed through the coordinates (x,y) of the image plane and (ξ,η) of the pupil plane as follows:

$$S_4 = 1/4\,A(x^2+y^2) + 1/4\,B(\xi^2+\eta^2) +$$
$$+ 1/4\,C(y\eta + x\xi)^2 + 1/2\,D(x^2+y^2)(\xi^2+\eta^2) +$$
$$+ E(y^2+x^2)(y\eta + x\xi) + F(\eta^2+\xi^2)(y\eta + x\xi),$$

where A, B, C, D E and F are constant coefficients.

Since the fields interact at points that are symmetric relative to the optical axis in formation of the interference pattern, it contains information on the phase difference at these points. Therefore, the aberrational terms that contain even powers of ξ and η will be compensated. Thus the interference pattern has compensation for third-order spherical aberrations and astigmatism, which are characterized by coefficients B and D respectively. It can be shown that spherical aberrations of higher orders will also be compensated. Consequently, in small fields of view where the distortions of lens optics are determined chiefly by spherical aberrations, the optical system with interferometer has high instrumental resolution.

REFERENCES

1. Katorgin, V. F., Shiryayev, B. A., Soviet Patent No 395706, BYULLETEN' IZOBRETENIY, No 35, 1973, p 136.

2. Korolev, F. A., "Teoreticheskaya optika" [Theoretical Optics], Moscow, Vysshaya shkola, 1966.

6610
CSO: 8144/0101-A

LIGHT BEAM AMPLIFICATION BY DYNAMIC HOLOGRAMS IN LZT-La CERAMIC

Leningrad PIS'MA V ZHURNAL TEKHNICHESKOY FIZIKI in Russian Vol 7, No 15, 12 Aug 81 (manuscript received 8 Apr 81) pp 914-917

[Article by M. M. Butusov, A. V. Knyaz'kov, A. E. Krumin', N. V. Kukhtarev and A. S. Saykin, Leningrad Polytechnical Institute imeni M. I. Kalinin]

[Text] One of the most interesting effects that is observed in recording of dynamic phase holograms is energy exchange between interfering beams. The cause of energy exchange between light beams is phase mismatch (displacement) of the hologram and the interference light pattern. As a consequence of interaction of the recording beams with the displaced hologram, one of the beams is intensified at the expense of the other. Phase mismatch may be either steady [Ref. 1, 2] or unsteady [Ref. 1], producing holographic amplification of light beams either after recording or during the recording of the hologram.

Steady-state energy exchange in crystals with linear electro-optic effect takes place with the diffusion mechanism of hologram recording ($LiNbO_3$) or with the drift mechanism of recording in an external or internal field E under conditions of nonfulfillment of quasineutrality ($KNbO_3$) [Ref. 2, 3]. In the latter case, the steady-state energy exchange is controlled by the external field. The gain that characterizes energy exchange in these media does not exceed 10 cm^{-1}. This gain is calculated from the following formula:

$$\Gamma = \frac{1}{z} \ln \left(\frac{I_1}{I_{-1}} \cdot \frac{I_{-10}}{I_{10}} \right), \qquad (1)$$

where z is the thickness of the hologram, I_{10}, I_{-10} and I_1, I_{-1} are the intensities of the recording beams before and after passage through the crystal respectively.

This paper is devoted to theoretical and experimental investigation of steady-state energy exchange in transparent LZT-La-9.2 [$Pb_{0.908}La_{0.092}(Zr_{0.65}Ti_{0.35})O_3$]--a ferroelectric ceramic that has a square-law electro-optic effect ($\Delta n \sim E^2$). The principal mechanism of photorefractive recording in LZT-La is diffusion and drift of photo-excited carriers in the external field [Ref. 4].

Calculation of gain based on the model developed in Ref. 2 for material having a square-law electro-optic effect gives

$$\Gamma \sim E\Lambda^{-1}, \quad \Gamma \neq \Gamma(m) \qquad (2)$$

for the diffusion approximation, and

$$\Gamma \sim E\Lambda, \quad \Gamma \neq \Gamma(m) \tag{3}$$

in the strong-field approximation when the condition of quasineutrality is violated, where Λ is the period of the holographic grating, $m = I_{10}/I_{-10}$.

The holographic gratings were recorded by an He-Cd laser ($\lambda = 0.44$ μm) with power of $5 \cdot 10^{-3}$ W. A conventional symmetric two-beam arrangement was used. Gratings with spatial frequencies from 1 to 6.5 μm were produced by changing the angle of convergence of the beams. The plane of polarization of the light beams coincided with the plane of incidence. Ratio of beam intensities was regulated from 1 to 0.015. The external electric field was applied orthogonally to the bands of the interference pattern, and its magnitude was varied over a range from 0 to 10 kV/cm. The thickness of the LZT-La ceramic specimen was 240 μm.

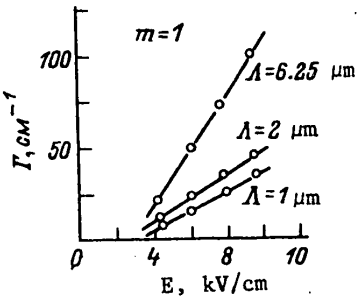

Fig. 1

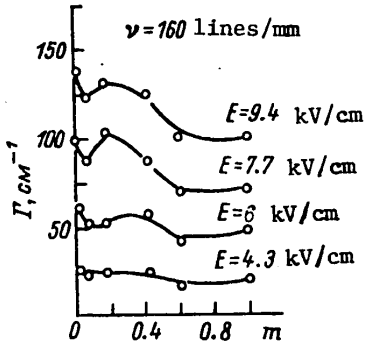

Fig. 2

In recording the holographic grating, the steady-state value of energy exchange was reached in a time of no more than 3 minutes. The direction of energy "transfer" was independent of the ratio of intensities of the recording beams, but was completely determined by the direction of the electric field. The principal result found in the research is an anomalously high gain $\Gamma = 130$ cm^{-3}, which is an order higher than in $LiNbO_3$ and $KNbO_3$ [Ref. 2, 3].

Γ increases with increasing E and as the period Λ of the holographic grating increases (Fig. 1), and changes fairly weakly with ratio of beam intensities m (Fig. 2).

The dependence of steady-state energy exchange on Λ and E is qualitatively described by theory with assumption of violation of the condition of quasineutrality [Ref. 3]. However, use of the given theory for LZT-La is restricted by two circumstances. The theory considers a one-level straight-band model assuming monopolar conductivity in the absence of light scattering processes [Ref. 2]. At the same time, the high concentration of defects in LZT-La accompanied by low dark conduction as well as some other effects show that the bands in LZT-La are modulated, and bipolar conduction takes place here [Ref. 5]. Besides, the recording of holograms in LZT-La is complicated by effects of light scattering, i. e. by the possibility of recording noise gratings [Ref. 5]. Both of these aspects may reduce Γ in the region of small Λ [Ref. 7].

The theory that we have developed correctly reflects the experimentally observed pronounced dependence $\Gamma(E)$ and the weak dependence of Γ on the ratio of beam intensities. At the same time, the question of violation of the condition of quasi-neutrality in LZT-La remains open. To answer this question, future research must take consideration of the possibility of existence of bipolar conduction and scattering of light.

The high gain in LZT-La is due to the fact that at room temperature LZT-La-9.2 is in the region of diffuse ferroelectric phase transition and has high values of the effective linearized electro-optical coefficient. This paper has demonstrated for the first time that the use of a square-law electro-optic effect enables effective control of steady-state energy exchange by means of an external field.

REFERENCES

1. Vinetskiy, V. L. et al., USPEKHI FIZICHESKIKH NAUK, Vol 129, 1979, p 113.

2. Kukhtarev, N. V. et al., FERROELECTRICS, Vol 22, 1979, p 949.

3. Krumins, A., Günter, P., APPL. PHYS., Vol 18, 1979, p 153.

4. Burgess, J. W. et al., APPL. OPT., Vol 15, 1976, p 1550.

5. Dimza, V. I., Krumin', A. E., IZVESTIYA AKADEMII NAUK LATVIYSKOY SSR: SERIYA FIZICHESKIKH I TEKHNICHESKIKH NAUK, No 6, 1979, p 53.

6. Magnusson, R., Gaylord, T. K., APPL. OPT., Vol 13, 1974, p 1545.

7. Orlowski, R., Krätzig, E., SOLID STATE COMMUN., Vol 27, 1978, p 1351.

6610
CSO: 1862/4

CORRECTING IMAGE SHARPNESS IN THE CASE OF UNKNOWN 'SMOOTH' DEFOCUSING

Leningrad PIS'MA V ZHURNAL TEKHNICHESKOY FIZIKI in Russian Vol 7, No 15, 12 Aug 81 (signed to press 21 Jul 81, manuscript received 6 Mar 81, after revision 12 May 81) pp 908-911

[Article by V. N. Karnaukhov and L. P. Yaroslavskiy, Institute of Data Transmission Problems, USSR Academy of Sciences, Moscow]

[Text] Correction for sharpness of a defocused image usually requires knowledge of the pulse response or frequency characteristic of the defocusing system and the noise level on the image. In many practical cases such a priori information is lacking, and the required parameters of distortions and noise must be determined from the distorted image.

However, there is a rather extensive and important class of systems for which correction does not require exact knowledge of their frequency response and noise level. These are systems that do not distort the phase spectrum of the signals. In this class is defocusing due to atmospheric turbulence (see for example Ref. 1, 2), defocusing in systems that produce an image by electron beam and so on. We will call these imaging systems with "smooth" defocusing.

The capability of correcting "smooth" defocusing of images is based on the fact that experiments have shown the sufficiency of only a very rough reconstruction of the amplitude spectrum of an image while retaining the phase spectrum for satisfactory image reproduction. It should be noted that this property of amplitude and phase spectra has been mentioned previously [Ref. 3] and has been used in image coding [Ref. 4, 5].

Such image stability in the face of amplitude distortions prompts us to suggest the following method of correcting "smooth" defocusing: the phase spectrum of the distorted defocused image is determined, and the amplitude spectrum is replaced by one that is standard for the given class of images, after which the image is reconstructed in accordance with such a corrected spectrum.*

---

*One of the authors discussed this method in 1977 with V. N. Dudinov and V. S. Tsvetkova (Astronomical Observatory at Khar'kov State University), who had come to similar conclusions in experiments on optical correction of astronomical images.

The effectiveness of the proposed method is proved by the results of modeling the correction of "smooth" defocusing as shown in the figure [photo not reproduced] (a, b--defocused images; c, d--correction results). Gaussian "smooth" defocusing of these images was by spatial filtration techniques in a digital computer, using fast Fourier transformation algorithms. The frequency response of the defocusing filter was described by the expression

$$H(\xi,\eta) = e^{-\frac{\xi^2+\eta^2}{2\sigma}},$$

where ξ and η are coordinates in the frequency plane. The quantity σ was chosen in such a way that the radius of the circle of confusion in the object plane was equal to 11 elements for the first image (a) and 3 elements for the second image (b). The estimate of the amplitude spectrum of both images was obtained by using the averaged energy spectrum of 29 fragments of the initial image partly overlapping with the fragment being processed (the energy spectrum of the initial fragment was not used in averaging).

Thus the proposed method of correcting image sharpness in "smooth" defocusing does not require exact knowledge of the frequency response of the imaging systems, and realization necessitates only a priori information on the form of amplitude spectrum of the image class to which the image being processed belongs.

The proposed technique can be comparatively simply realized in an adaptive optical system such as proposed in Ref. 6. In this system, a sandwich is placed in the Fourier plane, made up of a nonlinear optical element that changes its transparency in inverse proportion to the square root of the intensity of the incident light, and a filter with spatial distribution of amplitude transmission proportional to the required distribution of the amplitude spectrum that is standard for the given class of images. The nonlinear optical element in such a system effects so-called enhancement of the image spectrum, i. e. it transforms the spectrum of the distorted image to a uniform spectrum, and the spetial filter forms the required standard amplitude spectrum characteristic of the given class of images.

The simplicity of correction of "smooth" defocusing allows us to suggest that in cases where the danger of defocusing is difficult to avoid in designing imaging systems, it would be advisable to select the construction of optical systems and the photographic conditions so that defocusing will be "smooth," i. e. so that the phase of the frequency components of the image is retained.

REFERENCES

1. Pratt, W. K., "Digital Image Processing", New York, Wiley, 1978.

2. Carasso, A. S., Sanderson, J. G., Hyman, J. M., "Digital Removal of Random Media Image Degradations by Solving the Diffusions Backwards in Time", SIAM J. NUMER. ANAL., Vol 15, 1978, pp 344-367.

3. Huang, T. S., Burnet, J. W., Deczky, A. G., "The Importance of Phase in Image Processing Filters", IEEE TRANS. ACOUST., SPEECH, SIGNAL PROCESSING, ASSP-23, 1975, pp 529-542.

4. Perlman, W. A., Gray, R. M., "Source Coding of the Discrete Fourier Transform", IEEE TRANS. INFORM. THEORY, Vol IT-24, 1978, pp 683-692.

5. Rohling, S. C., "Fourier Transform Phase Coding of Image", IEEE TRANS. ACOUST., SPEECH, SIGNAL PROCESSING, Vol ASSP-28, 1980, pp 339-341.

6. Yaroslavskiy, L. P., USSR Patent No 536497, BYULLETEN' IZOBRETENIY, No 43, 1976.

6610
CSO: 1862/4

MATHEMATICS

UDC 517:534

INTEGRAL-TRANSFORM METHOD IN WAVE PROBLEMS OF HYDROACOUSTICS

Kiev METOD INTEGRAL'NYKH PREOBRAZOVANIY V VOLNOVYKH ZADACHAKH GIDROAKUSTIKI in Russian 1981 (signed to press 18 Feb 81) pp 2-4, 283-285

[Annotation, preface and table of contents from book "Integral-Transform Method in Wave Problems of Hydroacoustics", by V. V. Dykhta, Design and Planning Office of Electrohydraulics, UkSSR Academy of Sciences, Izdatel'stvo "Naukova dumka", 288 pages]

[Text] The book outlines theoretical principles of the integral-transform method in coordinate systems allowing separation of variables in a wave equation. Main emphasis is on applications of the method to solving unsteady problems of hydroacoustics. An examination is made of problems of emission and scattering of sound by shells, problems of horns and resonators, and propagation of sound in wedge-shaped, conical and other regions, problems of combined radiators, on interaction of complex fields with solid walls and the like.

The author gives the basic properties of special functions appearing in the kernels of transforms that are in turn the result of expansion of sought functions in integrals or series with respect to eigenfunctions of the corresponding Sturm-Liouville problems.

For scientists, engineers and technicians interested in the mathematical aspects of applied hydroacoustics, theory of emission and diffraction of sound by underwater objects, and for graduate and undergraduate students majoring in corresponding fields in colleges and universities.

Figures, 21, tables 2, references 65.

Preface

In science and practice we are more and more faced with the necessity of calculating hydroacoustic fields, using the most diverse methods and means. Even now it would be difficult to name the field of knowledge where solutions of applied hydroacoustics problems would not be of considerable theoretical and practical interest. This interest shows up especially in areas involving deep ocean research, where we have a veritably infinite treasure trove of food, water, raw materials, minerals, energy resources and so on. Investigation of the propagation of sound in the sea, the study of questions of its generation and scattering by various objects are

problems that are intimately involved with many related fields of science (oceanology, seismology and geology of the ocean floor and so on). Thus in the final analysis applied hydroacoustics can be defined as a branch of geophysics and other sciences associated with the study of the seas, emphasizing the variety of problems that are solvable by hydroacoustic methods.

A common feature of all these problems is the presence of an acoustic medium (more precisely the mathematical model of such a medium)--a continuous medium in which the stress vector is normal to any elementary area, i. e. an acoustic medium is understood as one such that propagation of shear (transverse) forces and waves cannot arise therein. Many media have this property at high temperatures and pressures, which further extends the limits of the concept "hydroacoustics" and enables a unique approach to solution of a large number of applied problems from different fields of science and technology. In this connection there is an increase in the role of exact analytical methods of solving boundary value problems for partial differential equations that describe fundamental properties of acoustic media, since in many cases they enable representation of the final result in a form that is convenient for analysis of a formula, and in the other cases--in a form that is comparatively easily computerized. Among the principal methods, mention should be made of the method of invariant-functional solutions proposed by V. I. Smirnov and S. L. Sobolev, the Wiener-Hopf method, generalized Volterra and Hadamard methods, the Fourier method, the integral-transform method and others.

The purpose of this book is to present and illustrate by specific examples the basic concepts and mathematical aspects of the last of these methods--the integral-transform method--as applied to the wave equation in coordinate systems that allow separation of variables. Since in this case the integral-transform method and the Fourier method have a common basis in the separation of variables, the exposition is illustrated by examples in which both methods are sometimes used simultaneously.

The monographic contains elements of the theory and examples of applications of Fourier, Laplace, Hankel and Legendre transforms to solution of some problems that are encountered in practice, and illustrates the feasibility of using Laplace transforms for describing moving acoustic fields. The first two chapters are introductory and contain information on equations of hydrodynamics and methods of integrating them, and on the basics of the integral-transform method--expansion of the sought functions with respect to systems of eigenfunctions of the corresponding Sturm-Liouville problems. Since there are fundamental papers by both Soviet and non-Soviet scientists on the theory of the integral-transform method [Ref. 7, 25, 36, 57 and others], the presentation of the theory in this book is synoptic, but it does contain the minimum of information required for understanding the essence of the problem.

The book makes no pretense of completeness in presenting problems of applied hydroacoustics that are solvable by the integral-transform method.

Contents page

6610
CSO: 1862/261

UDC 512.25/26+519.3:330.115

PROBLEMS OF ANALYZING RESOURCE DISTRIBUTION

Moscow IGRY, GRAFY, RESURSY in Russian 1981 (signed to press 3 Apr 81) pp 2-4, 113

[Annotation, preface and table of contents from book "Games, Graphs, Resources", by Erik Georgiyevich Davydov, Izdatel'stvo "Radio i svyaz'", 7000 copies, 113 pages]

[Text] The book deals with problems of the distribution of resources on PERT nets and transport grids. Both the deterministic case and the case where there are indeterminate factors or an opponent are considered. In the final analysis, all problems reduce to nonlinear programming problems.

The book will be of use to scientists and engineers dealing with problems of resource distribution.

Figures 6, references 29.

Preface

A great deal has been said about methods and techniques of resource distribution, about their importance for working of economic, ecological, military and other systems. Nevertheless, our understanding of problems of resource distribution is too limited in the area of operations research and the theory of games. This class subsumes mainly problems of the Gibbs lemma type and its generalizations, stipulating however that most linear programming problems (and they are innumerable) also fall into the class of resource distribution problems.

Our understanding of these problems is as follows. In any mathematical descriptions of working systems subject to human action, resource limitations may be imposed on these systems, and the evolution of the systems will depend on the methods of distribution of the limited resources. The systems may be deterministic, operating in the presence of indeterminate factors (including in the presence of an opposing side) and adaptive (with random factors) systems, whose characteristics are known or become known in the process of operation. In the most general description of operation of large systems, obviously all factors will be present. In consideration of such systems, the options for distribution of resources will be scalar or vector variables, vector-functions, and even dimensions, depending on the capabilities of the operating side.

This book examines two types of models: models of distribution of vector resources on PERT nets or transport grids in the presence of indeterminate factors or an opponent, and deterministic models.

Problems of resource distribution on PERT nets and transport grids in the deterministic case reduce quite simply to nonlinear programming problems. On the other hand, if there are indeterminate factors, the search for guaranteed distribution of resources in a direct formulation reduces to a game problem of triple optimization with related constraints, and a certain art is required to reduce these problems to nonlinear programming problems.

The book does not give problem solving algorithms, since there are very many known algorithms for solving nonlinear programming problems. Selection of each algorithm is dictated by the particulars of the problem and the software of available computers. The list of references contains a fair number of handbooks that describe algorithms of local, global and complex optimization, and even have programs for these algorithms in algorithmic language.

At first glance it may seem that the author has narrowed the region of applicability of the problems under consideration by limiting himself to the case of a finite number of values of indeterminate factors. But this limitation in the first place has enabled considerable simplification of the structure of the problems, and in the second place has not been too restrictive since any continuous game on compact sets of player strategies can be approximated by a finite game after choosing sufficiently dense grids on the sets of player strategies. The latter fact was first published in 1973 in a mimeographed version of a book by the author that was put out by this same publishing house [E. G. Davydov, "Metody i modeli teorii antagonisticheskikh igr" (Methods and Models of the Theory of Antagonistic Games)].

In conclusion, the author considers it his pleasant duty to thank L. S. Gurin, whose comments considerably improved the content of the book.

Contents page

6610
CSO: 1862/267 - END -